# Environmental fate and behavior of nanoplastics : Implication of physico-chemical processes

Alice Pradel

UNIVERSITÉ DE RENNES 1

# THESE DE DOCTORAT DE

L'UNIVERSITE DE RENNES 1

ECOLE DOCTORALE N° 600
*Ecole doctorale Ecologie, Géosciences, Agronomie et Alimentation*
Spécialité : *Sciences de la Terre et de l'Environnement*

Par
**Alice PRADEL**

## Comportement et devenir environnemental des nanoplastiques

Quels processus physico-chimiques ?

**Thèse présentée et soutenue à Rennes, le 25 Novembre 2021**
**Unité de recherche : UMR 6118**

**Rapporteurs avant soutenance** :

| | |
|---|---|
| Denise M. Mitrano | Chargé de Recherche, ETH Zürich |
| Mark R. Wiesner | Professeur distingué, Duke University |

**Composition du Jury :**

| | | |
|---|---|---|
| Président : | Mélanie Davranche | Professeur, Université Rennes 1 |
| Examinateurs : | Mélanie Davranche | Professeur, Université Rennes 1 |
| | Mohammed Baalousha | Maitre de Conférence, University of South Carolina |
| | Aline Dia | Directrice de Recherche, CNRS, Géosciences Rennes |
| Rapporteurs: | Denise M. Mitrano | Maitre de Conférence, ETH Zürich |
| | Mark R. Wiesner | Professeur distingué, Duke University |
| Invité: | Hervé Tabuteau | Chargé de recherche (HDR), CNRS, Institut de Physique de Rennes |
| Dir. de thèse : | Julien Gigault | Chargé de recherche (HDR), CNRS, Takuvik |

*Pour Anaëlle N'Guessan*
*Je te souhaite de réaliser tes rêves les plus fous.*

# Comportement et devenir environnemental des nanoplastiques: *Quels processus physico-chimiques ?*

## Environmental fate and behavior of nanoplastics : *Implication of physico-chemical processes*

Thèse pour le grade de: Docteur de l'Université de Rennes 1
Mention : Sciences de la Terre et de l'Environnement
Ecole Doctorale: Ecologie, Géosciences, Agronomie et Alimentation (EGAAL)

Présentée par:

Alice PRADEL

Préparée dans l'unité de recherche Géosciences Rennes (UMR 6118)
Observatoire des Sciences de l'Univers de Rennes (OSUR)

Thèse soutenue à Rennes (France), le 25 Novembre 2021, devant le jury composé de :

Denise M. Mitrano,
*Chargé de Recherche, ETH Zürich, Rapporteur*
Mark R. Wiesner,
*Professeur distingué, Duke University, Rapporteur*
Mélanie Davranche,
*Professeur, Université Rennes 1, Examinateur*
Mohammed Baalousha,
*Professeur, Université Rennes 1, Examinateur*
Aline Dia,
*Directrice de Recherche, CNRS, Géosciences Rennes, Examinateur*
Hervé Tabuteau,
*Chargé de recherche (HDR), CNRS, Institut de Physique de Rennes, Invité*
Julien Gigault,
*Chargé de recherche (HDR), CNRS, Takuvik, Directeur de Thèse*

# Remerciements

Merci Julien Gigault de m'avoir fait découvrir la recherche scientifique, dans toute sa complexité, toutes les possibilités, mais aussi dans sa dimension humaine. Merci de m'avoir formé et de m'avoir fait gagner confiance en moi.

Merci Bruno Grassl et Hervé Tabuteau pour votre encadrement et coaching!

Merci à Nolwenn Delouche qui m'a fait découvrir comment réflechissent les physiciens, et à Maud Gautier qui m'a fait découvrir comment bosser comme une chimiste ! Merci pour tout votre travail. Ça a été un plaisir de bosser avec vous.

Merci à l'équipe Paloise de l'Institut des Sciences Analytiques et de Physico-Chimie pour l'Environnement (IPREM) : Hind el Hadri, Stéphanie Reynaud, Cloé Véclin, Mathilde Puscheu, pour votre accueil dans votre labo et le temps que vous m'avez consacré.

Merci aux chercheurs du European Commission Joint Research Centre (JRC): Cloé Desmet, Andrea Valsesia, Jessica Ponti, Pascal Colpo, de m'avoir donné l'opportunité de venir travailler avec vous. Ça a été une expérience très enrichissante.

Merci à l'équipe (et ex-équipe) de Cordouan : Boris Pedrono, Benoit Maxit, David Jacob pour votre super boulot, et les connaissances techniques que vous m'avez apporté.

Merci à ceux et celles avec qui j'ai pu travailler et qui m'ont permis de faire de la recherche de qualité : Patrice Petitjean, Ludivine Rault, Véronique Vié, Fabienne Gauffre, Aurelien Dupont, Christian Le Carlier. Merci aussi à Julie Borgese qui m'a aidé à communiquer effectivement.

Merci en particulier à Dominique Bavay, pour toute ton aide, ta bienveillance et nos conversations farfelues qui ont bien égayé mes journées au labo.

Merci à l'équipe de Géosciences qui a contribué à ce que soit une belle aventure : Geraldine Gourmil et Chantal Perot-Busnel, Olivier Dauteuil, Charlotte Catrouillet, Rémi Marsac, Anne-Catherine Pierson-Wickmann, Mathieu Pédrot, Aline Dia, Mélanie Davranche, Muqeet Iqbal, Léa Mounier, Kaisa Patterson, Yasaman Tadayon.

Merci à mes co-bureau Zélie Venel, Elaheh Lotfi Kalahroodi, Anthony Beauvois, Phoomipat Jungcharoen, Florent Blancho, Aurélie Wahl et Marawit Tesfa, d'avoir rendu la vie au laboratoire bienveillante et amusante.

Merci à tous les stagiaires, doctorants, post-doctorants et ingénieurs de Géosciences qui rendent la vie au labo joyeuse !

Merci à toutes les initiatives de sciences ouvertes et en libre accès, et à Isabelle Dubigeon pour nous aider à mettre ça en oeuvre.

Merci à la communauté d'escalade ! Comme la thèse, on est peut-être tout seuls sur le mur mais on ne grimpe jamais seuls. Merci Modjo en particulier !

Merci aux amis d'avoir été là.

Merci à mes parents qui m'ont toujours donné de merveilleuses opportunités de découvrir, de m'enrichir et de m'épanouir. Merci d'avoir toujours valorisé mon éducation.

Merci à ma soeur Olivia pour l'inspiration que tu m'apportes et la beauté que tu crées.

Et finalement, Sebastián : les mots ne suffisent pas ici pour te remercier de tout ton soutient, ta patience et ton écoute qui m'ont aidé pour ma thèse... mais, merci !

# Contents

# Introduction

After steel and cement, plastics are the third most-produced material on Earth by mass. With mismanagement of waste and aging of plastic material, a large proportion (>25%) of plastic ends up in the environment. Plastic debris is now an integral part of the biogeochemical cycle (Bank and S. V. Hansson 2019) and has been proposed as a marker of the Anthropocene (Waters et al. 2016). This environmental issue is multi-faceted since plastic debris can have different effects on organisms and ecosystem functions depending on their properties (e.g.: size, shape, composition) and the transformations they undergo in the environment (e.g.: oxidation, adsorption of natural matter). Tracking the sources, transport pathways, and sinks of plastic debris in the environment has proven difficult since the combined actions of abiotic and biotic processes degrades plastic into small particles that are difficult to sample and quantify. Indeed, the degradation of plastic objects produces nanoplastics, defined as plastic particles smaller than 1 $\mu$m that present colloidal behavior. It has been demonstrated that the mass of all plastic debris accumulated at the ocean's surface is orders of magnitude smaller than the yearly input estimated from material flow analysis. The omission of nanoplastics from the sampling effort can explain a significant part of this discrepancy. Indeed, nanoplastics could form a substantial fraction of the global budget of plastic debris. Therefore, it is crucial to elucidate how nanoplastics are transported in the environment and where they may accumulate to resolve environmental plastics' global budget and assess which ecosystems may be more exposed.

The goal of this work is to gain a better understanding of where nanoplastics, dispersed in water, may accumulate in the environment. The approach aims to model the behavior and fate of nanoplastics in the environment by performing lab experiments that mimic environmental systems. A specificity of this work is it focuses on nanoplastics' transport through environmental interfaces. These interfaces are zones where the structure of an environmental system changes abruptly over space and/or time, and therefore, where physicochemical gradients occur. Since physicochemical gradients can modify nanoplastics' journeys in the environment, focusing on environmental interfaces allows us to better locate nanoplastics' potential accumulation zones. Furthermore, special attention has been devoted to using novel nanoplastic model particles produced from fragmenting polystyrene pellets. This fragmental nanoplastic has nonspherical and irregular shapes,

polydisperse sizes, and a moderately negative charge, making it more environmentally relevant than other particles broadly used in literature these last 30 years.

The thesis has been written as a compilation of scientific publications, either published or in preparation. Chapter 1 is a critical review of the environmental fate of nanoplastics with a particular focus on the parameters that impact their aggregation. This process is determinant for nanoplastics' environmental fates since i) colloids are sensitive to aggregation in water, and ii) their aggregation state will impact further downstream processes, such as settling, transfer in soils, or uptake by biota. The following chapters (2, 3, and 4) will present three independent experimental studies. Chapter 2 studies the aggregation potential of nanoplastics in water with varying solution chemistries. After comparing the stability of two nanoplastic models in solutions with increasing ionic strength, this Chapter investigates how two types of natural organic matter (NOM) stabilize nanoplastics. Chapters 3, 4, and 5 focus on two other environmental interfaces: porous media, as a proxy for soils, sediments, and aquifers (in Chapters 3 and 4), and a freezing front of saltwater, as a proxy for the interface betweenseawater and sea ice (in Chapter 5). In Chapter 3, the transport and deposition rates of nanoplastic models in a sand column were compared. Each nanoplastic model presents specific physicochemical properties (size, composition, and shape), which allowed us to elucidate the importance of these properties in controlling deposition. This section will be followed, in Chapter 4, by a new study that investigates the deposition of fragmental nanoplastic particles in synthetic porous media with controlled geometries. This study was designed to elucidate the impacts of size polydispersity and NOM on deposition. Finally, Chapter 5 investigates the possible fate of nanoplastics at the surface of polar seawaters. While microplastics (1 $\mu$m to 5mm) are already identified in sea ice, nanoplastics' fate at this interface has been unexplored to date. Therefore, we explore how micro-and nanoplastic particles respond to sea ice growth using a novel approach.

*Note: This manuscript will have some redundancies since it is a compilation of articles published (or to be published) separately. For example, particles' descriptions and methods to characterize them may change between the articles. These changes reflect both the needs of each topic and the evolution of my investigation and understanding over time.*

# References


Bank, Michael S. and Sophia V. Hansson (June 2019). "The Plastic Cycle: A Novel and Holistic Paradigm for the Anthropocene". en. In: *Environmental Science & Technology*, acs.est.9b02942. ISSN: 0013-936X, 1520-5851. DOI: 10.1021/acs.est.9b02942.

Waters, C. N., J. Zalasiewicz, C. Summerhayes, A. D. Barnosky, C. Poirier, A. Ga uszka, A. Cearreta, M. Edgeworth, E. C. Ellis, M. Ellis, C. Jeandel, R. Leinfelder, J. R. McNeill, D. d. Richter, W. Steffen, J. Syvitski, D. Vidas, M. Wagreich, M. Williams, A. Zhisheng, J. Grinevald, E. Odada, N. Oreskes, and A. P. Wolfe (Jan. 2016). "The Anthropocene Is Functionally and Stratigraphically Distinct from the Holocene". en. In: *Science* 351.6269, aad2622–aad2622. ISSN: 0036-8075, 1095-9203. DOI: 10.1126/science.aad2622.

This Chapter is a critical review that is currently in preparation. It presents the approach used in this work to elucidate which physicochemical processes will impact nanoplastics and how these processes will control their transport and accumulation in the environment. The first part places nanoplastics within the global context of plastic contamination. Then, a second part presents approaches and theoretical frameworks used to assess nanoplastics' fate. The third part discusses nanoplastics' fate in environmental systems, with a particular focus on aggregation. The final part describes environmental interfaces whose physicochemical gradients are likely to impact nanoplastics' environmental fate.

# Chapter 1

# Assessing the environmental fate of nanoplastics: A critical review of aggregation processes

Alice Pradel[a,b], Charlotte Catrouillet[a], Julien Gigault[a,b]

[a]Univ Rennes, CNRS, Géosciences Rennes - UMR 6118, 35000 Rennes, France

[b]TAKUVIK, CNRS/Université Laval, UM I3376, G1V 0A6 Québec, Canada

## 1.1 Nanoplastics: what and where?

### 1.1.1 Plastic debris as environmental contaminants

Plastic debris has contaminated all of Earths' compartments, from freshwater lakes, rivers, and sediments (Klein, Worch, and Knepper 2015; Eriksen et al. 2013), soils (Scheurer and Bigalke 2018; Zubris and Richards 2005), seas and oceans that are close to anthropogenic activity (Thompson 2004), and more remote (Lusher et al. 2015), as well as some of the deepest ocean sediments (Peng et al. 2020), the atmosphere (Allen et al. 2019) and biosphere (L. Li et al. 2020; Provencher et al. 2019 and references therein). Due to this planetary-wide contamination, plastics' environmental fate can now be studied through the lens of a plastic cycle, comparable to the carbon or nitrogen cycle (Bank and S. V. Hansson 2019). Furthermore, plastics are now proposed as a marker of the Anthropocene, a proposed geological era defined by widespread anthropic activity (S. L. Lewis and Maslin 2015; Waters et al. 2016).

Contamination is defined here as the introduction of a foreign object or energy into the environment, whereas pollution is contamination that causes harmful effects to ecosystems and/or human health (GESAMP 1991). As for other environmental contaminants, to define the magnitude of the risk posed by plastics, two sides of an equation must be solved (Albert A. Koelmans et al. 2017b):

1. their concentration in an area, which represents organisms' level of exposure and their probability of coming into contact with environmental processes

2. their hazard to a given organism or environmental process.

Therefore, **to better understand how plastic debris may cause harm, it is essential to study how they are transformed, transported, and accumulated in order to shed some light on their environmental concentrations.** However, understanding plastics' environmental fate is complicated due to i) the numerous sources of plastic debris into the environment, ii) the long-range dispersal of plastic debris by air and water currents caused by plastics' lightweight and relative durability and, iii) the incidental production of plastic particles from larger plastic objects.

### 1.1.2 How a revolutionary material became an environmental concern

Plastics are synthetic water-insoluble materials that are produced by chemically linking the same simple organic molecules called monomers, into polymers with high molecular weight. The development of organic chemistry and industrial processes in the 1940s and

1950s has allowed the development and mass commercialization of plastics with a wide array of modular properties (Andrady and Neal 2009). Plastics generally belong to one of these functional categories:

- thermoplastic polymers, which can be hardened and softened repeatedly by temperature changes;
- thermosetting polymers, which when cured by heat or other means become insoluble and unable to melt;
- elastomers, which can be deformed by mechanical stress and rapidly recover;
- polyurethane (PUR) resins, which can be composed of different monomers linked with urethane. (International Organization for Standardization, 2013).

The following thermoplastic and thermoset polymers: polyethylene (PE), polypropylene (PP), polystyrene (PS), polyvinyl chloride (PVC), polyethylene terephthalate (PET) and fibers of polyester, polyamide, and acrylic (PP&A) constitute 89% of all the plastic polymers produced (Figure 1.1, inner circle). Finally, PUR resins, which are neither thermoplastics nor thermosets, are also produced in high quantities and comprise approximately 7% of the total polymer production (Figure 1.1, inner circle) (Geyer, Jenna R. Jambeck, and Kara Lavender Law 2017). Plastics' properties depend on the monomers and additives that compose the plastic, as well as the production process. Incorporating different additives can confer a wide array of functionalities, such as improved plasticity during manufacturing and, increased rigidity, lightness, and resistance to fire(Hahladakis et al. 2018). Therefore, additives are a non-negligible component of plastics, with variable concentrations according to the plastic composition and use (Geyer, Jenna R. Jambeck, and Kara Lavender Law 2017; Lithner, Larsson, and Dave 2011).


*Figure 1.1: Mass-based distribution of worldwide plastics production (inner circle) and plastic waste generation (outer circle) in 2015, according to polymer type and additive. The inner circle corresponds to a total of 407 million metric tons (Mt) produced, and the outer circle corresponds to 302 Mt discarded. The primary market sector for each polymer is indicated, with C&I = Consumer and Institutional. (Source = Geyer, Jenna R. Jambeck, and Kara Lavender Law 2017). Figure produced with https://rawgraphs.io*

Plastics have become an inherent component of the modern industrial world. They are generally produced from fossil carbon sources at an affordable monetary price. These lightweight and durable materials have brought about significant societal advancements, for example, by increasing access to medical care and technology, by replacing heavier and more fragile alternatives, as well as slowly renewable or rare natural materials(Andrady and Neal 2009). Therefore, by 2015 it was estimated that 8.3 billion metric tons of plastic had been produced, which makes plastics the third most-produced material behind steel and cement (Geyer, Jenna R. Jambeck, and Kara Lavender Law 2017). To place plastics in a planetary context, the mass of plastic produced is estimated to be roughly twice that of all animals on Earth (Elhacham et al. 2020).

The increasing mass of plastic debris generated has been the unforeseen consequence of introducing such vast amounts of plastics in our livelihoods. Plastic debris is defined

here as materials mainly composed of synthetic or semi-synthetic water-insoluble polymers that are present in the natural environment without fulfilling an intended function (GESAMP 2016; Hartmann et al. 2019). Approximately a third of all the plastics that have been produced is currently in use, and the other two-thirds have been discarded (Geyer, Jenna R. Jambeck, and Kara Lavender Law 2017). While the majority of discarded plastics are expected to have been handled appropriately, by either being stored in landfills (21 to 42 %), incinerated (approximately 13%), or recycled (6 to 26%), a significant proportion (>20%) has been mishandled and leaked into the environment (Geyer, Jenna R. Jambeck, and Kara Lavender Law 2017; Alimi, Farner Budarz, et al. 2018). Figure 1.1 (outer circle) presents a breakdown of polymers produced and discarded in 2015 and shows that most of the discarded items come from products with short durations of use (<5 years), such as packaging, consumer and institutional products (C&I Products). While most plastic debris is generated from mismanaged plastic waste, plastic debris is also produced incidentally by the aging of plastic materials in the environment. Examples of this latter source are the production of tire wear particles during driving, the release of fibers when washing synthetic textiles, and the aging of fishing nets and ropes during use (Wik and Dave 2009; Zubris and Richards 2005). Finally, a minimal portion of plastic debris comes from intentionally produced plastic particles lost in the environment. These particles are used in agricultural, cosmetic, or medical applications (e.g.: seed coatings, microbeads, and drug delivery). They are introduced directly into the environment or indirectly through wastewaters (Mitrano and Wohlleben 2020). All plastic pieces that come from the incidental degradation of plastics in the environment are defined as **secondary plastics**, as opposed to **primary plastics** which are produced intentionally.

All plastic debris is subject to degradation by environmental factors such as sunlight, physical stress, heat, biological activity, etc. (GESAMP 2015; M. Wagner and Lambert 2018 and references therein). Although most plastics are designed to be durable, their degradation in the environment is observable on human time scales (Chamas et al. 2020). Rates of plastic degradation and the type of degradation that occur (e.g.: cracking, peeling, solubilizing, etc.) depend upon the interplay between plastic composition and environmental conditions (Hahladakis et al. 2018; Min, Cuiffi, and Mathers 2020; ter Halle et al. 2016). The most efficient pathways for plastic degradation are photo-oxidation by sunlight irradiation and mechanical abrasion by physical stress (e.g.: by the action of waves and wind) (Chamas et al. 2020; Efimova et al. 2018; Gewert, Plassmann, and MacLeod 2015; Karin Mattsson et al. 2021; Min, Cuiffi, and Mathers 2020; Y. K. Song, Hong, Eo, et al. 2020). To a lesser extent, thermo-oxidation, hydrolysis, and biological degradation can also degrade plastic objects (Dawson et al. 2018; Julienne, Delorme, and

Lagarde 2019; Min, Cuiffi, and Mathers 2020; Zettler, Mincer, and Amaral-Zettler 2013). Plastic degradation is an overarching term that includes many environmental transformations, such as fragmentation and surface oxidation, enzymatic degradation, and leaching of additives (Andrady 2011). All of these transformation processes are interconnected. For example, fragmentation can accelerate the leaching of additives. Surface oxidation can increase particle's stiffness and ability to be fragmented. Ultimately, since plastics are carbon-based materials, they can be mineralized into $CO_2$ and the elementary forms of monomers and additives (Lixin Zhu et al. 2019). However, for complete mineralization to occur, optimal conditions are required that are rarely met (Chamas et al. 2020; Harrison et al. 2018). Therefore, as illustrated in Figure 1.2, plastic debris persists in the environment as particulate degradation products (i.e.: non-dissolved and non-elemental).

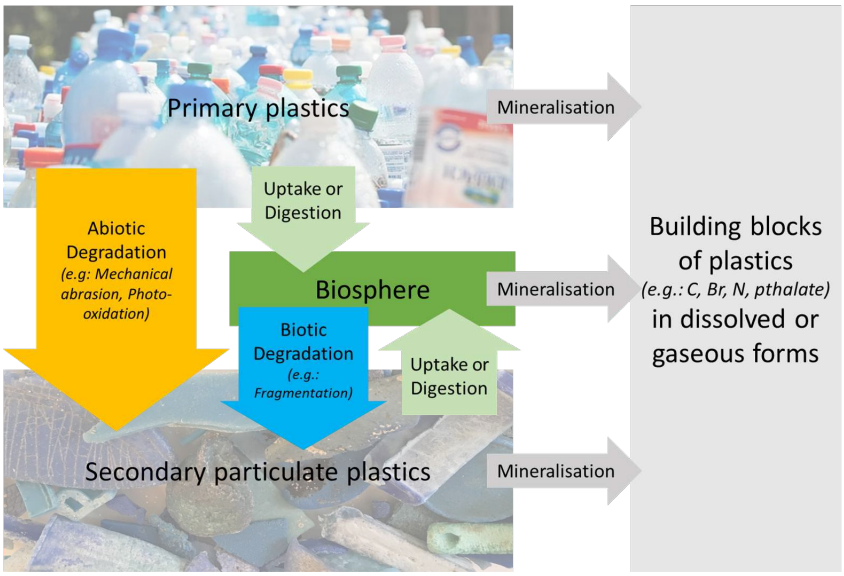


*Figure 1.2: Schematics of plastic stocks and processes that lead to the production and removal of secondary particulate plastics from the environment*

Due to their diversity of sources and degradation pathways, secondary plastic particles can take on an infinite combination of compositions, shapes, surface properties, color, density, hardness, etc. (Kooi, Primpke, et al. 2021; Rochman et al. 2019). The projected increase in secondary particulate plastics and the diverse properties of these contaminants make them a major environmental concern. In particular, secondary plastics with submicrometric size, which have been called nanoplastics (Gigault, Halle, et al. 2018; Hartmann et al. 2019), are a particular concern since they may form a substantial proportion of total stocks of plastic debris but are undetectable with standard instruments and methods (K. Mattsson, L.-A. Hansson, and Cedervall 2015).

### 1.1.3 Transport and transfer of plastic debris

A material flow analysis (MFA) calculated that approximately 4.8 to 12.7 million metric tons (Mt) of plastic debris generated in coastal countries would enter the oceans in 2010 (J. R. Jambeck et al. 2015). This yearly input of plastics into the ocean is expected to increase in the future if there are no significant changes in the quantity of waste generated and the waste infrastructure (J. R. Jambeck et al. 2015). However, the mass of all plastic debris accumulated at the ocean's surface since the invention of plastic is orders of magnitude smaller than the estimated yearly input. To evaluate this mass, models have combined ocean circulation models with direct measurements of plastics debris with sizes ranging from 0.33 to 200 mm. According to the highest estimate, there are only 236 000 metric tons of plastics at the ocean surface, representing significantly less than 1% of the plastic expected to be present (van Sebille, Wilcox, et al. 2015). In ocean gyres (zones where oceanic currents converge), where models predict that most plastic debris accumulates, the measured concentration of plastics has been at a steady state in recent years (the 1980s to 2010s)(F. Galgani et al. 2021). Rapid increases in the concentration of plastic debris at the ocean surface have been recorded either i) close to anthropic sources and at the early stages of mass plastic production (Thompson 2004) or ii) in remote areas and decades after the mass production of plastics has started (F. Galgani et al. 2021).

Several hypotheses have been advanced to explain the discrepancy between the plastic stocks expected to be at the oceans' surface and those measured. While none of the hypotheses can on its own explain two orders of magnitude difference, some hypotheses help the numbers of measured and expected stocks to converge:

Overestimation of the mass of plastic **expected** at the ocean surface:

> Hypothesis 1: The uncertainties in the MFA used to estimate stocks and flows of plastic at the Earth-scale (e.g.: the amount of waste generated, collected through formal and informal methods, and discarded as well as its rate of transfer into oceans) have overestimated inputs of plastic debris into the ocean (van Sebille, Wilcox, et al. 2015; L. Weiss et al. 2021).
>
> Hypothesis 2: The rates at which plastic debris deposits to the shorelines or sink to the ocean floor could have been underestimated, leading to an overestimation of concentrations expected at the ocean surface (van Sebille, Wilcox, et al. 2015)

Underestimation of the mass of plastic **measured** at the ocean surface:

Hypothesis 3: Plastics larger than 200 mm, which were omitted from models of plastic concentrations at the ocean surface, could constitute a significant portion of the total stocks of plastic (van Sebille, Wilcox, et al. 2015).

Hypothesis 4: The depth at which plastics are located at the ocean surface does not coincide with the depth at which plastics were sampled, leading to an underestimation of plastic stocks at the ocean surface (Poulain et al. 2019). Indeed, the depth at which small plastic debris (0.3 to 5 mm) is located can vary due to wind turbulence and biofouling (the covering of surfaces by organisms and their exudates, which dynamically modifies their buoyancy) (Kooi, Nes, et al. 2017).

Hypothesis 5: The missing fraction corresponds to small microplastics (1 to 1000 $\mu$m) and nanoplastics (<1$\mu$m). This smaller plastic debris may have been omitted during sampling since the sampling nets had a minimum mesh size of 330 $\mu$m. Even particles ranging from 330 to 1000 $\mu$m, which are expected to be captured during sampling, are often lacking in the size distribution of plastic debris(A. Cózar et al. 2014). This is attributed to the analytical challenges involved in measuring small carbon-based particles in natural matrices (Mintenig et al. 2018).

The overestimation of plastic waste input into the oceans (Hypothesis 1), as well as the omission of plastics larger than 200 mm (Hypothesis 3) and plastics located at different depths (Hypothesis 4) can explain a certain degree of discrepancy between expected stocks and measured stocks. However, these values are expected to be relatively constant over time and therefore cannot explain how plastic debris at the ocean surface has reached a steady state. To explain how plastic concentration at the ocean surface appears to have reached an apparently constant concentration which is lower than predicted concentrations, rates of plastic debris removal from the ocean surface by sinking, beaching onto shorelines (Hypothesis 2), and fragmentation down to micrometric and submicrometric sizes (Hypothesis 5) are all preferable hypotheses. In particular, small microplastics (1 to 1000 $\mu$m) and nanoplastics (<1 $\mu$m) may form an essential fraction of the plastic budget. This hypothesis has been supported by:

- Scarcity of plastics smaller than 1 mm in size distributions of samples (A. Cózar et al. 2014);
- Experimental studies that observed the formation of nanoplastics by abrasion, photo-oxidation, and digestion (Karin Mattsson et al. 2021; Lambert and M. Wagner 2016; Gigault, Pedrono, et al. 2016; Dawson et al. 2018);

- Identification of increasingly small microplastics (Primpke, Christiansen, et al. 2020; Primpke, Cross, et al. 2020) and nanoplastic signatures (Ter Halle et al. 2017) with improved analytical methods.

### 1.1.4 Focusing on nanoplastics

From the previous hypotheses, it can be assumed that fragmentation of plastics to micrometric and submicrometric sizes is one of the several fates of plastic debris. Based on the diversity of environmental mechanisms that can incidentally produce small microplastics (1 to 1000 $\mu$m) and nanoplastics (<1 $\mu$m) (e.g.: mechanical abrasion, photo-oxidation, etc.), these plastic particles are expected to be present in all environmental compartments. Therefore, it is essential to assess their environmental fate in order to i) resolve the mass balance of plastic debris, ii) determine organisms' level of exposure and iii) determine their potential impact on Earth system processes. However, due to their smaller size, nanoplastics have colloidal properties that make them significantly different from larger particles in several respects and warrants studying them separately.

A colloidal dispersion is a system where one phase (liquid, solid or gas) is dispersed in a different continuous phase. In our case, solid nanoplastics particles are dispersed in liquid (Goodwin 2004; Hiemenz and Rajagopalan 1997). There have been some attempts to give a clear-cut definition of colloidal dispersions, such as the CRC Handbook of Chemistry and Physics definition: *molecules or polymolecular particles dispersed in a medium that have at least in one direction a dimension roughly between 1 nm and 1 $\mu m$*(Haynes, Lide, and Bruno 2015). However, it will become clear that colloidal properties which allow particles to remain dispersed within another medium are highly dependent on the physicochemical properties of the continuous phase.

Due to their colloidal properties, nanoplastics may have a different environmental fate compared to larger particles. Furthermore, studying them requires the use of various analytical methods and theoretical frameworks compared to larger particles. Indeed, as particles' size decreases down to the colloidal size range, they transition away from motion dictated by gravitational forces and towards motion dictated by intermolecular forces (Elimelech 1998; Goodwin 2004; Hiemenz and Rajagopalan 1997) . The particle size at which this transition occurs depends on the relative densities of the dispersed phase (particle) and of the continuous phase (liquid) and the liquid viscosity, as defined by Stokes' law (Stokes 1851), as well as the particle size as defined by the Stokes-Einstein equation (Einstein 1905; Sutherland 1905). Indeed, Stokes' law :

$$V_s = \frac{2}{9}\frac{\rho_p - \rho_f}{\mu} g r_p^2 \tag{1.1}$$

shows that the settling speed of a spherical particle $V_s$ (m $s^{-1}$) is a function of the difference between its density $\rho_p$ and the density of the fluid $\rho_f$ (kg $m^{-3}$), as well as the dynamic viscosity of the fluid $\mu$ (kg $m^{-1}$ $s^{-1}$), the square of the particle radius $r_p$ (m) and gravitational acceleration g (equal to 9.8 m $s^{-2}$ on Earth). Furthermore, the collision of small particles with water and solutes causes their hydrodynamic diffusion, also called Brownian motion. This is illustrated in the Stokes-Einstein equation:

$$D = \frac{k_B T}{6\pi\mu r_p} \tag{1.2}$$

which relates a spherical particles' diffusion coefficient D ($m^2$ $s^{-1}$) to its radius, the fluid's viscosity and the thermal energy of agitation, given by the Boltzmann constant $k_B$ (kg $m^2$ $K^{-1}$ $s^{-2}$) and the temperature T (K).

While Equation 1.1 shows that the settling speed $V_s$ is proportional to the size ($r_p^2$), Equation 1.2 means that the Brownian motion, characterized by D, is inversely proportional to its size. Therefore, when the size decreases D becomes predominant compared to $V_s$. Based on these equations, carbon-based particles in aqueous systems are deemed to be colloidal around 1 $\mu$m, which is why nanoplastics are defined as submicrometric. This Brownian motion is an important consideration when assessing environmental transport as well as during their analysis and theoretical study. For example, due to Brownian motion, nanoplastics cannot be extracted from environmental media with the density-based methods used for microplastics.

Colloids are also characterized by a high specific surface area, defined as the total surface area per particle mass. This renders surface interactions crucial in shaping colloidal behavior and in selecting appropriate methods of analysis. These surface interactions (e.g.: electrostatic repulsion and Lifshitz van der Waals attraction) operate at short distances from the particle's surface (up to approximately 50 nm)(Israelachvili 2015). The section on the Derjaguin-Landau-Verwey-Overbeek (DLVO) theory of colloidal stability (cf : Section 1.2.2) will provide a review of the surface interactions. Given a favorable (attractive) balance of surface interactions and hydrodynamic forces, colloids sorb onto other species (e.g.: other colloids, molecules, surfaces). The properties of species onto which nanoplastics sorb (or that sorb onto nanoplastics) significantly modifies nanoplastics' overall physicochemical properties, such as their dimensions, surface chemistry, etc. Furthermore, nanoplastics' size may be comparable to that of environmental macromolecules. Therefore their sorption onto these molecules may strongly modify nanoplastics' physicochemical properties.

A final consideration that sets nanoplastics are apart from microplastics is that different optical methods must be used when analyzing microplastics and nanoplastics. Indeed,

since nanoplastics' size is similar to the wavelengths of visible light, they cannot be detected by optical instruments which are diffraction-limited (e.g.: light microscopy and infrared spectroscopy) (Gigault, Halle, et al. 2018; Gigault, El Hadri, Nguyen, et al. 2021).

Nanoplastics are a contaminant of emerging concern (CEC) since they are "*new compounds or molecules that were not previously known or that just recently appeared in the scientific literature*" (Sauvé and Desrosiers 2014). The impacts of this emerging contaminant on organisms and environmental processes have become a global concern for the public and policymakers (Allan, Sokull-Kluettgen, and Patri 2020; GESAMP 2015; SAPEA, Science Advice for Policy by European Academies 2019). Therefore, nanoplastics have been the topic of an increasing amount of scientific investigation (Alimi, Farner Budarz, et al. 2018; da Costa et al. 2016; Lehner et al. 2019 and references therein). The focus of this work is to determine nanoplastics' environmental fate to assess their potential risk. However, it is still unclear whether nanoplastics may be a hazard since studies investigating their effects on ecosystem and human health have rarely used nanoplastic particles that are representative of nanoplastics found in the environment. Instead, studies have often used model nanoplastic particles composed of PS and suspended with additives such as preservatives, antimicrobials, or surfactants. Pikuda et al. demonstrated that the (eco)toxicity of nanoplastics was usually caused by the additives added to the liquid dispersion of nanoplastic models rather than the plastic itself (Pikuda et al. 2019). Conversely, nanoplastics are expected to be (eco)toxic in large part due to the leaching of additives added during the manufacturing process (e.g.: brominated flame retardants, phthalate plasticizers, and lead heat stabilizers) and the release of (eco)toxic monomers (e.g.: PUR, and polyacrylonitrile) (Lithner, Larsson, and Dave 2011). However, to date (eco)toxicity studies have mainly focused on pristine polystyrene particles that are free of additives used during manufacturing. Nanoplastics may cause deleterious effects other than (eco)toxicity, for example, by impacting ecosystem processes, such as biogeochemical cycling (L. Galgani and S. A. Loiselle 2020). Therefore, a One Health perspective, combining transdisciplinary studies in the domains of human, animal and environmental health is called for (Prata et al. 2021).

## 1.2 Approaches to assess the environmental fate of nanoplastics

### 1.2.1 The role of experimental approaches

Assessing the transport and accumulation of nanoplastics in the environment benefits from previous approaches developed for engineered nanomaterials (ENM), since these are also colloidal anthropogenic contaminants (Dale et al. 2015; Mitrano, Wick, and Nowack 2021; Gigault, El Hadri, Nguyen, et al. 2021). **A preliminary step consists in conceptualizing the life cycle of nanoplastics.** Sources of nanoplastics are multiple since they can be generated from plastic objects and plastic debris by various mechanisms. **So, to assess the transport and accumulation pathways of nanoplastics in the environment, it is crucial to identify the natural physical and chemical processes that may impact their behavior in all environmental compartments (e.g.: freshwater, seawater, soils, etc.).**

While, rejection of plastic aerosols to the atmosphere can occur (Allen et al. 2019; Bergmann, Mützel, et al. 2019; Wik and Dave 2009), current evidence shows that most plastic debris is water-bound (Horton et al. 2017; Schwarz et al. 2019 and references therein). Therefore, the main transport pathways of nanoplastics in the environment are through aqueous systems. Based on the current understanding of the transport and accumulation pathways of ENM's, the most relevant abiotic processes affecting nanoplastics' fate in the environment are summarized in Figure 1.3. Two key processes are nanoplastics' ability to aggregate with other particles, and their ability to be stabilized by the sorption of dissolved (i.e.: low molecular weight) organic species ((Wang et al. 2015; Yu, Jingfu Liu, et al. 2018) and references therein). Indeed, nanoplastics are more likely to hetero-associate with naturally occurring species than to homo-aggregate with other nanoplastic particles, since the concentration of natural dissolved or particulate species in aqueous environmental systems are in the range of $\mu$g $L^{-1}$ to mg $L^{-1}$ (Benner 2002; Burdige 2002; Sanderman, Baldock, and Amundson 2008; Stumm and Morgan 1996), whereas projected nanoplastic concentrations are in the range of pg $L^{-1}$ to $\mu$g $L^{-1}$ (Lenz, Enders, and Nielsen 2016). Homo-aggregation of a nanoplastic with another nanoplastic could occur at the surface of a disintegrating piece of plastic debris, where surface concentrations of nanoplastics may be high.

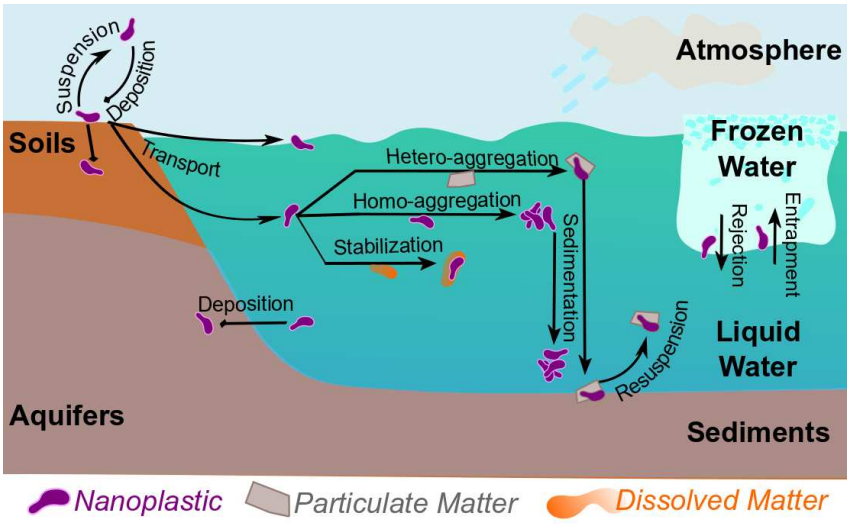


*Figure 1.3: Schematics of major abiotic processes that control nanoplastics' environmental fate*

The impact of hetero-association on nanoplastics' mobility is highly dependent on the species' molecular weight. For simplicity, natural species are classified as either dissolved (e.g.: electrolytes, dissolved organic matter, etc.) or particulate (e.g.: metal oxides, clays, particulate organic matter, etc.) Even though the transition between the two is inherently blurry, it has often been fixed at arbitrary cut-off sizes (mostly 0.2 and 0.45 $\mu$m) due to the widespread use of filters as separation methods. Truly dissolved species are under a few kDa in molecular weight and in thermodynamic equilibrium with the water. Here, for the purpose of this work which aims at understanding plastic colloids' environmental fate, large macromolecules that pass through 200 nm filters and have molecular weights up to approximately $10^6$ g mol$^{-1}$ are considered dissolved. The dimensions of particulate species can be as small as a few nanometers but they are orders of magnitude denser than dissolved species.

Hetero-aggregation of nanoplastics with particulate species can produce aggregates that either remain dispersed, cream (move to the surface) or settle, depending on their size, shape, density, and porosity. Stokes' law (Equation 1.1) presents the effects of particle size and density, assuming particles are spheres. However, aggregates cannot be simply considered as larger spherical particles since they have a nonspherical shape and high porosity, which impacts their buoyancy. For example, colloidal aggregation can give rise to aggregates with a linear structure (i.e.: low fractal dimension ≈1.6) in conditions where colloids immediately adhere to each other when they first come into contact. However, in conditions that are less favorable to adhesion, aggregates have a more compact structure (i.e.: high fractal dimension ≈2) (Hackley and M. A. Anderson 1989). The more linear (less compact) aggregates tend to settle more rapidly due to the reduced drag force of the fluid on the aggregate, compared to a permeable sphere of

equivalent density (C. P. Johnson, X. Li, and Logan 1996). Aggregation not only reduces nanoplastics' colloidal properties but also affects other (downstream) processes, such as deposition in porous media (e.g.: soils, aquifers, sediments, etc.)(S. Lin and Wiesner 2012a) and bioavailability (Lebordais et al. 2021), etc.

Another critical process is nanoplastics' ability to sorb dissolved matter onto their surface. This layer of sorbed materials, called eco-corona, provides nanoplastics a new type of identity (i.e.: surface charge composition, optical property, etc.) (Wheeler et al. 2021). The eco-corona can be composed of naturally occurring molecules in solution, such as dissolved organic matter, exudates from microorganisms, or even dissolved contaminants. The formation of this eco-corona and its ability to stabilize nanoplastics against aggregation depends on the water's electrolytic composition, as well as the chemical composition of the molecules and of the nanoplastic (Buffle et al. 1998; Yu, Jingfu Liu, et al. 2018).

Once the abiotic processes that control nanoplastics' fate have been identified, assessing nanoplastics' environmental fate requires the iterative use of **three complementary approaches**, as depicted in Figure 1.4:

- **One approach consists in undertaking experiments that model nanoplastics' transport pathways in environmental systems to identify and quantify the processes that control nanoplastics' environmental fate.** Two complementary types of experimental systems exist. First, there are those that attempt to elucidate possible outcomes by measuring probabilities that specific processes occur or the rates at which these occur. In this case, experiments rapidly and empirically define transport rates and can give insights into probable mechanisms. For example, colloids are observed to be retained in soils. This is potentially due to different processes (e.g.: physical entrapment in soils or chemical affinity for surfaces), but these processes are not identified (Hendren et al. 2015). The second type of experimental systems attempt to elucidate the mechanisms behind a given behavior. This consists in simplifying the system until a given parameter is isolated and a mechanism identified. For example, this could ascertain that colloids are retained due to chemical affinity for soil surfaces.

- **Another approach consists in numerically modeling nanoplastics fate and behavior** by combining the rates and probabilities obtained experimentally with data on nanoplastics' presence and/or concentration. For nanoplastics, this data can be estimated by MFA, plastic degradation rates, and extrapolated from microplastic concentrations (Albert A Koelmans et al. 2017a; Lenz, Enders, and Nielsen 2016). Numerical simulations can either predict the environmental fate

of nanoplastics (Besseling et al. 2017) or model all possible outcomes to determine the key processes controlling nanoplastics' fate (Clavier, Praetorius, and Stoll 2019).

- **Finally, numerical simulations and experimental results can be confronted with data on environmental presence or concentrations of nanoplastics obtained from the characterization of field samples to assess their validity.** Inversely, results from the characterization of field samples can give informations on the processes that must be investigated by experimentation and numerical simulations. For example, if high concentrations of nanoplastics are quantified in soils, numerical and experimental models should focus on quantifying deposition rates as a function of soil properties to quantify exposure to soil-dwelling organisms and potential impacts on soil properties.

This tiered approach is an iterative approach that has been used successfully to study natural, engineered, and incidental particles. However, different challenges arise depending on the nature of the particle.

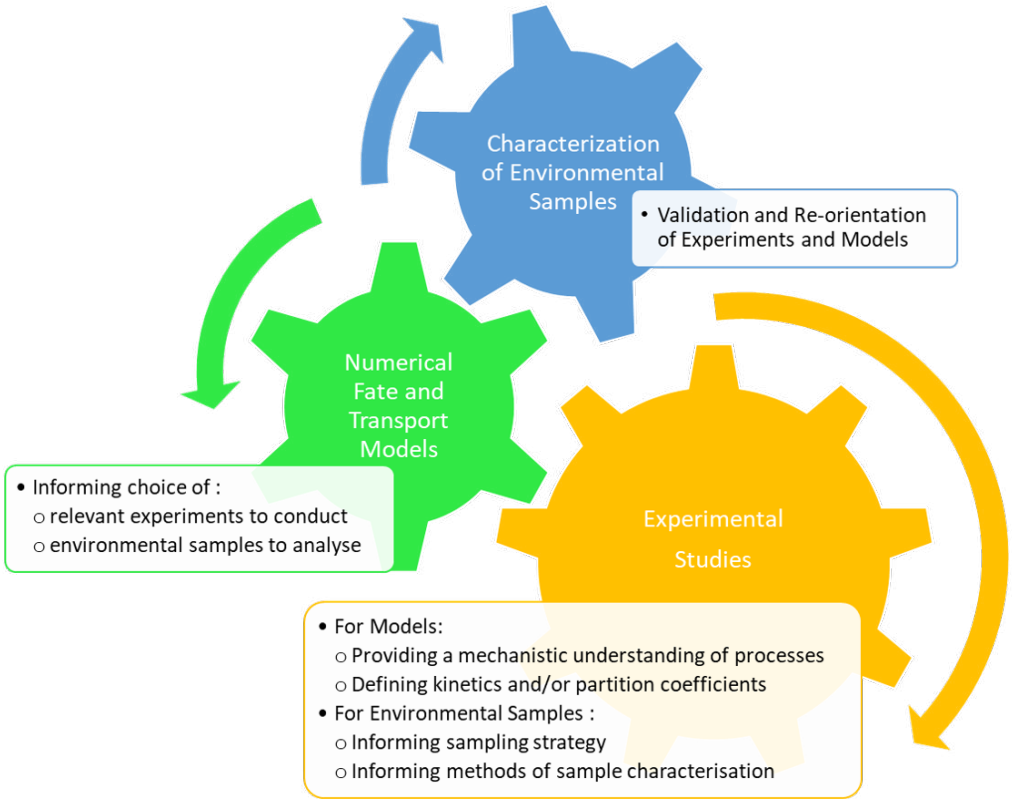


*Figure 1.4: Schematics of the different approaches to study nanoplastics' fate and how they are interrelated*

When studying natural colloids, information about colloidal fate can be obtained from appropriate sampling and characterization of field samples, complemented by experimen-

tal and numerical modeling studies (Buffle et al. 1998; Filella 2007 and references therein). Field sampling is not always the most suited approach for engineered colloids, such as ENM, since their release in the environment occurs as occasional point-source contamination events or diffuse contamination in low concentrations(Bystrzejewska-Piotrowska, Golimowski, and Urban 2009). Therefore, the goal has been to design environmentally relevant laboratory experiments to study the different ENM transport and transformation pathways they can undergo in the environment (Peijnenburg et al. 2015). Other challenges occur for incidentally produced colloids, such as nanoplastics, depending on the nature of the colloid and their location. If present in high concentrations (e.g.: from point sources) and/or easily distinguishable from the biogeochemical background (e.g.: mineral oxides in mines and soot), characterization of field samples can be a suited approach. However, this approach is technically unfeasible for nanoplastics since they are both carbon-based particles and present in low concentrations compared to background concentrations of carbon contained in natural organic matter (NOM). Therefore, since nanoplastics are challenging to detect in natural samples, studying their environmental fate in laboratory experiments is the most appropriate approach.

Contrary to ENM that are manufactured to have specific properties, nanoplastic particles are expected to have heterogeneous properties (i.e.: a variety of shapes, compositions, surface properties, etc.)(Gigault, El Hadri, Nguyen, et al. 2021). **Therefore, to properly assess nanoplastics environmental fate, another challenge, besides choosing environmentally relevant experimental conditions, is to study environmentally relevant nanoplastic models. In conclusion, evaluating nanoplastics' fate in the environment today must rely on numerical models of nanoplastic transport underpinned by experimental research. In parallel, analytical techniques to characterize them in environmental samples must be developed.**

### 1.2.2 Global theoretical frameworks

Theoretical frameworks are necessary to interpret experimental results and to implement numerical models. In the following section, two theoretical frameworks commonly used to assess the fate of colloids will be described: 1) particle collision rates and attachment efficiencies, and 2) the Derjaguin-Landau-Verwey-Overbeek (DLVO) theory of colloidal stability and its extended versions.

#### *Particle collision rate ($\beta$) and attachment efficiency ($\alpha$)*

To elucidate the environmental fate of colloids such as nanoplastics, it is necessary to break down their behavior into two independent steps: 1) the rate of colloids' collision

with a surface (of another particle or a larger object) and 2) the probability that this collision results in attachment. These two steps can be treated independently since the forces of colloidal attraction that lead to attachment are of a shorter range than the particle size. Therefore they do not affect collision rate. Figure 1.5 illustrates the major processes and parameters of the solution that impact particle collision rate and attachment efficiency. They are summarized in the empirical predictors $\beta$: particles' collision rate with other particles or surfaces and $\alpha$: particles' attachment efficiency (Elimelech 1998; Xing, Vecitis, and Senesi 2016).

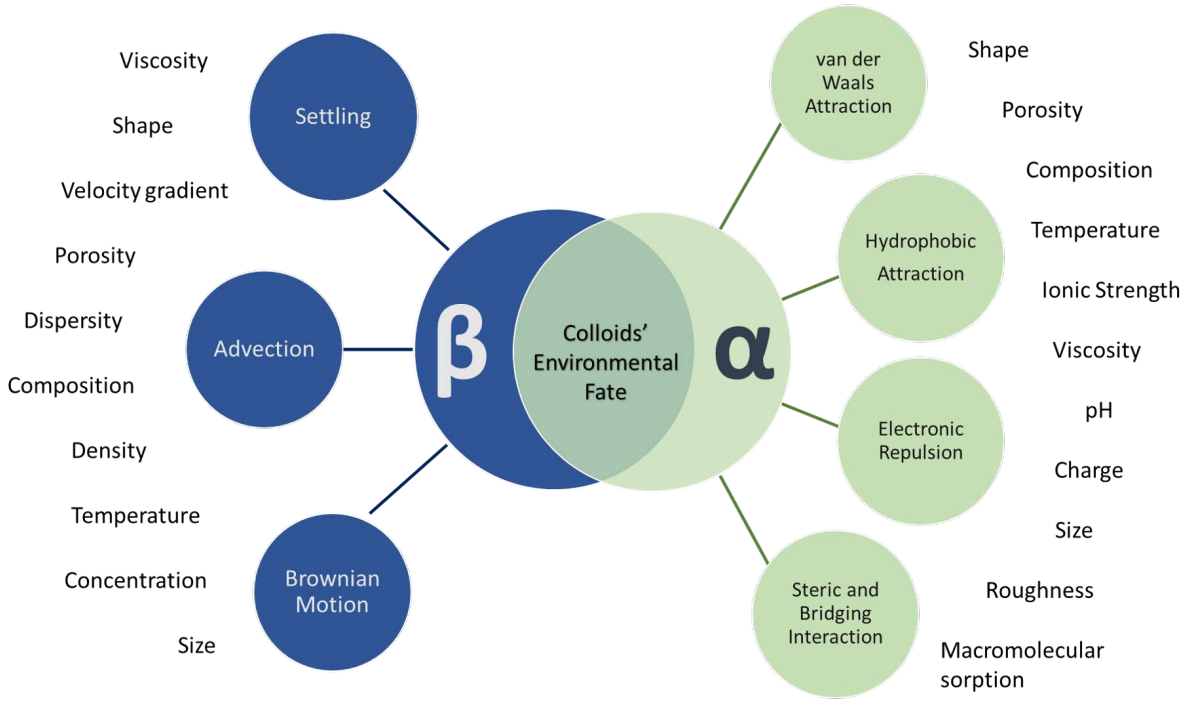


*Figure 1.5: Schematics showing the processes (circles) and parameters (left and right edges) that can affect collision rate ($\beta$) and attachment efficiency ($\alpha$).*

**Collision rate $\beta$**

Three main mechanisms cause particle motion and consequently, particle collision: Brownian motion, settling due to gravity, and advection by fluid flow. For colloidal particles, Brownian motion is the dominant mechanism. Collision rates between particles and surfaces have been calculated for aggregation and deposition during transport in porous media (Elimelech 1998; Xiao et al. 2017).

Concerning aggregation, the rate of collision ($k_{agg,ij}$) of Brownian particles (named i and j) in the absence of agitation is based on the Stokes' Law and is given by the Smoluchowski equation:

$$k_{agg,ij} = \frac{2k_B T}{3\mu} \frac{(r_{pi} + r_{pj})^2}{r_{pi} r_{pj}} \tag{1.3}$$

for particles i and j. Interestingly for particles of equal size, this equation can be simplified to yield:

$$k_{agg,ij} = \frac{8k_BT}{3\mu} \tag{1.4}$$

Equations1.3 and 1.4 reveal that temperature and liquid viscosity have opposite effects on particle collision rate, with temperature increasing collision and liquid viscosity that decreasing collision. However, this equation does not show that the collision rate is also dependent on the concentration of particles (as will be seen later in Equation 1.7).

For particle deposition in porous media, correlation equations are used to calculate the single-collector contact efficiency ($\eta_0$), which is the highest probability of contact with the collectors (i.e.: spherical solid surfaces of the porous media). These calculations have been extensively presented elsewhere (Elimelech 1998 as well as Molnar et al. 2015; Petosa et al. 2010 and references therein) and will be briefly discussed below. Most correlation equations are based on the assumption that the flow in a porous medium can be conceptualized as the flow around a spherical collector, such as the Happel sphere-in-cell described in Figure 1.6 (Happel 1958). In this model, a collector is surrounded by an envelope of fluid. It is in this envelope that particles can interact with the collector. The flow rate and particle concentrations are null at the surface of the collector and maximal at the outer boundary.

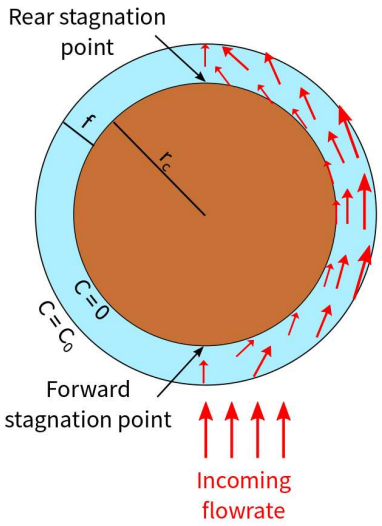


*Figure 1.6: Schematic of a Happel sphere-in-cell flow field geometry, showing the collector radius $r_c$, the thickness of the fluid envelope (f), the flow rates which are proportional to the arrow dimensions and, the concentrations (C) of colloids at the collector surface and at the outer boundary of the fluid envelope. (Adapted from Molnar et al. 2015)*

Correlation equations are developed using this geometry (or similar geometries) and solving the advective diffusive equation while assuming that particles can be deposited

by diffusion (D), interception (I) or gravitational settling (G)(Molnar et al. 2015), as described in equation 1.5

$$\eta_0 = \eta_D + \eta_I + \eta_G \tag{1.5}$$

Each component of the single-collector contact efficiency ($\eta_0$) is calculated using different dimensionless parameters, as illustrated in equation 1.6, which shows the correlation equation developed by Tufenkji and Elimelech 2004:

$$\eta_0 = 2.4A_S^{1/3}N_R^{-0.081}N_{Pe}^{-0.715}N_{LW}^{0.052} + 0.55A_S N_R^{1.675}N_A^{0.125} + 0.22N_R^{-0.24}N_G^{1.11}N_{LW}^{0.053} \tag{1.6}$$

with, $A_S$ a porosity dependent parameter, $N_R$ the ratio of colloid and collector dimensions, $N_P$ the ratio of convective to diffusive transport (Péclet number), $N_{LW}$ the ratio of Lifshitz van der Waals attraction to thermal energy, $N_A$ which represents influence of van der Waals attraction forces and fluid velocity and $N_G$ the ratio of settling velocities and approach velocity of the flow. This correlation equation assumes a Happel sphere-in-cell geometry. It takes into account many processes such as the null flow at the surface of the collector (hydrodynamic retardation effect), lower diffusion of particles at the surface of the collector (anisotropic diffusion) as well as Lifshitz van der Waals attraction (described later). However, other equations exist, with different porous media geometries, boundary conditions and equations governing transport, etc. (Molnar et al. 2015).

Calculating collision rates requires the use of some simplifying assumptions for both aggregation and deposition. Common simplifications are that particles have well-defined shapes (spherical, rod-like, spheroidal, etc.), size distributions (monodisperse and monomodal) and smooth surfaces. Concerning deposition, the porous media is generally conceptualized as monodisperse grains packed without touching each other. The flow velocity profiles are assumed to be uniform around each grain with no possibility of physical entrapment in confined zones. Finally, most theoretical frameworks concerned with deposition assume that soils, aquifers, and sediments can be conceptualized as porous media. However, this is only true in some cases (e.g.: sandstone aquifers and loamy soils) and many underground terrestrial systems present different types of porosities (e.g.: fractured granite or clayey soils presenting preferential infiltration zones).

**Attachment efficiency** $\alpha$

Attachment efficiency ($\alpha$) reflects particles' affinity for a surface (of a particle or a larger object). The empirical predictor $\alpha$ varies from 0 to 1, with $\alpha = 1$ corresponding to conditions where each collision results in attachment and $\alpha = 0$ corresponding to the least favorable conditions, where no attachment occurs during collision. This surface affinity depends on the energy barrier between particles, which results from the balance between attractive and repulsive forces. For nanoplastics, the main forces are Lifshitz van

der Waals attraction, electronic repulsion, hydrophobic attraction, and steric repulsion (Figure 1.5). These processes can be modeled to a certain extent by the Derjaguin-Landau-Verwey-Overbeek (DLVO) theory of colloidal stability (cf: Section 1.2.2). Many parameters that control these interaction forces: such as particles' core composition and surface coating for attractive forces, and the chemical moieties on a particles' surface (e.g.: carboxylic sites), their acid dissociation constant (pKa) and the solutions' pH for repulsive forces (Hotze, Phenrat, and Lowry 2010; Peijnenburg et al. 2015; Petosa et al. 2010).

To date, two methods can be used to evaluate attachment efficiency. The rate of aggregation (or deposition) is either normalized by the rate of collisions determined from calculations (equations 1.3, 1.4, 1.5, 1.6) or by the maximal rate of aggregation (or deposition). This maximum rate corresponds to that obtained in favorable conditions: when all repulsion between particles is removed. These favorable conditions can be obtained experimentally by removing all electrostatic repulsion between particles and surfaces. This is achieved by adding a range of concentrations of indifferent electrolytes (i.e.: electrolytes that do not form covalent bonds) and measuring the aggregation (or deposition) rate until a plateau is reached. For example, the aggregation rate is determined through the evolution of particles' size over time according to the equation:

$$\left(\frac{\partial d_H(t)}{\partial t}\right)_{\lim_{t\to 0}} \propto k_{agg} N_0 \tag{1.7}$$

where $d_H$ is the hydrodynamic diameter of particles or aggregates as a function of time t and $N_0$ is the initial number-based particle concentration. At low ionic strengths, colloids aggregate according to the reaction-limited aggregation (RLA) regime with a rate $k_{agg}$. In this regime, aggregates formed have a relatively compact structure (high fractal dimension). Then, the electrostatic energy barrier decreases as ionic strength increases until particles' surface charges are entirely screened. The ionic strength at which the energy barrier is annihilated corresponds to ions' critical coagulation concentration (CCC) and to a maximum aggregation rate ($k_{agg,fast}$).In these conditions, colloids are in the diffusion-limited aggregation (DLA) regime and the structure of aggregates is more linear.

The attachment efficiency $\alpha$ can be obtained for aggregation kinetics by normalizing aggregation rates under the RLA regime ($k_{agg}$) by the rate in the DLA regime ($k_{agg,fast}$),

at the same number-based concentration ($N_0$):

$$\alpha = \frac{k_{agg}}{k_{agg,fast}} = \frac{\left(\frac{\partial d_H(t)}{\partial t}\right)_{\lim_{t\to 0}}}{\left(\frac{\partial d_H(t)}{\partial t}\right)_{\lim_{t\to 0,fast}}} \tag{1.8}$$

For transport experiments, attachment efficiency can also be determined by normalizing deposition rates by the rates of the most favorable conditions for deposition (Geitner et al. 2017). Furthermore, the attachment rate can be extrapolated from the calculated collision rate (using correlation equations such as Equation 1.6) and the observed deposition rate (Petosa et al. 2010; Tufenkji and Elimelech 2004). The advantages and disadvantages of both methods are summarized in Table 1.1.

*Table 1.1: Comparison of two standard methods to obtain attachment efficiencies from experiments studying colloid deposition in porous media*

| Method | Equation | Advantage | Disadvantage |
|---|---|---|---|
| Deposition rate is normalized by favorable deposition* | $\alpha = \frac{k_{dep}}{k_{dep,fast}}$ | No need for *a priori* knowledge of particle or porous media characteristics | Experiments need to be performed over an extensive range of ionic strengths to attain $k_{dep,fast}$. Difficult if repulsion between particles and porous media is stronger than repulsion between particles, since $k_{agg,fast} > k_{dep,fast}$. |
| Deposition rate is normalized by collision rate calculated from colloid filtration theory+ | $\alpha = -\frac{2d_{50}}{3(1-\epsilon)\eta_0 L} \cdot ln\left(\frac{C}{C_0}\right)$ | Experiments do not need to be performed over a large range of ionic strengths | Assumptions about porous media properties (spherical, smooth, and separate) collectors introduce errors. |

* *(Geitner et al. 2017),* + *(Tufenkji and Elimelech 2004).*

A theoretical framework that can help predict or evaluate colloids' surface affinity for other colloids or surfaces), is the Derjaguin-Landau-Verwey-Overbeek (DLVO) theory of colloidal stability and its extended versions (XDLVO theories).

### *Classical and extended DLVO theories of colloidal stability*

Colloidal stability must be distinguished from thermodynamic stability. While the latter describes a system in equilibrium, colloidal stability describes dispersions that "do not aggregate at a significant rate" (IUPAC 1997). Stable colloids have a low attachment efficiency, remain in liquids and persist longer in a water column or soil water. Such stability helps colloids be transported over long distances by water currents (Stumm and

Morgan 1996; Filella 2007). On the contrary, destabilized particles have a gravity-driven behavior (e.g.: floating or settling).

The short-range interactions that control colloids' attachment efficiency can be conceptualized and modeled with the Derjaguin-Landau-Verwey-Overbeek (DLVO) theory of colloidal stability which takes into account electrostatic repulsion and Lifshitz van der Waals attraction. This theory is named after scientists who have developed it in the 1940s (Verwey, Overbeek, and Van Nes 1948; Derjaguin and Landau 1993). The following section first presents the hypothesis underlying (X)DLVO theories. Then, typical energy profiles are described (page 27). The types of forces relevant to nanoplastics and the method used to calculate these as a function of particle/surface geometries are then presented(page 27)). Finally, some limitations of the (X)DLVO theories are discussed (page 38).

The (X)DLVO theory is concerned with physical interactions between particles and between particles and plane surfaces. The interaction energy is calculated as a function of the distance separating these elements. This theory does not consider chemical interactions by covalent bonding, which are specific, stoichiometric, and directional. Compared to chemical interactions, physical interactions have a longer range, and can be perturbed or restored more dynamically (Israelachvili 2015).

**Hypothesis**

Important hypotheses are the following:

- Particles have a homogenous charge density;
- The counterions (ions that have an opposite charge to that of the particle) are conceptualized as points charges following the Boltzmann distribution around particle and plane surfaces;
- None of the interaction forces interact with each other;
- Traditionally, particles are modeled as spheres, and surfaces are modeled as plates of infinite length, and both are considered to have a smooth surface (Hiemenz and Rajagopalan 1997; Israelachvili 2015).

However, some more recent DLVO models have overcome these simplifying assumptions. Heterogeneity of charges and surface roughness have been modeled by modified DLVO theories by linear combinations of different charges and surface heights(Bradford, H. Kim, et al. 2017). Furthermore, methods to calculate the DLVO interaction profiles in the case of non-spherical and non-smooth particles or surfaces have also been developed and will be described below (Bhattacharjee, J. Y. Chen, and Elimelech 2000; Bhattacharjee and Elimelech 1997; E. M. Hoek and Agarwal 2006; Huang, Bhattacharjee, and E. M. V. Hoek 2010).

### Energy profiles

Figure 1.7 presents two typical interaction energy profiles: negative and favorable to particle attachment in blue and positive and unfavorable to attachment in orange. In the case of the favorable interaction energies, at a distance of approximately, 20 nm the particles are subject to attractive energy, which is highly superior to their thermal energy of agitation ($\approx$1.5 $k_BT$) and called a primary energetic minimum ($\Delta G^{tot}_{min1}$). In the case of unfavorable interactions, the particle first arrives in a weakly negative zone at 50 nm (inset) called the secondary energetic minimum ($\Delta G^{tot}_{min2}$). Given sufficient thermal or hydrodynamic energy, particles can be expulsed from this weak minimum. As the particle moves closer to the surface, it is confronted to the highest magnitude of positive interaction energy, around 5 nm, called the energy barrier ($\Delta G^{tot}_{max}$). The probability that a particle overcomes this energy barrier and enters the primary energetic minimum is given by the Boltzmann distribution (Israelachvili 2015).

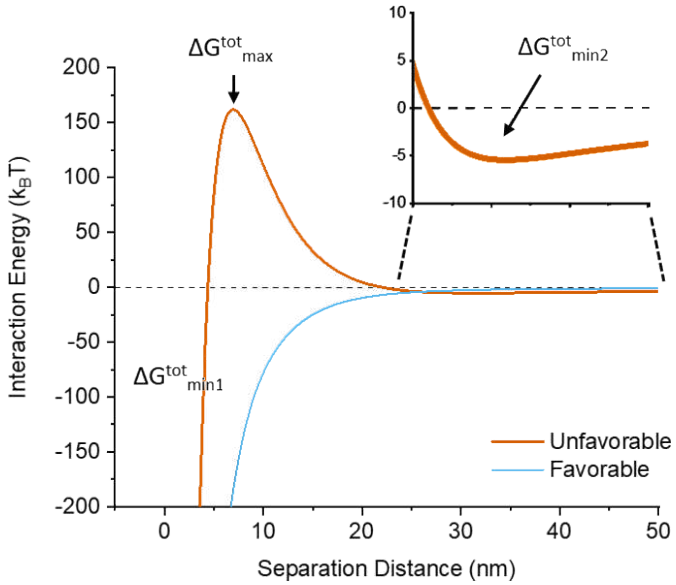


*Figure 1.7: Interaction energy (J scaled to $k_BT$) between a particle and a surface, according to XDLVO. Details can be found in Chapter 3 with parameters corresponding to those of the NPT-P particle with the diameter modified to 900 nm and surface potential set to + 33 mV for the favorable conditions.*

### Surface interactions that are relevant to nanoplastics

The interaction energy profiles presented in Figure 1.7 can be composed of various interaction energies as detailed in Table 1.2 and illustrated in Figure 1.8. Table 1.2 presents surface interactions that are relevant to nanoplastics, their origin, typical range and repulsive or attractive nature. DLVO theory only models electrostatic and Lifshitz van der Waals energies (**in bold**), while the (X)DLVO can additionally model steric, Lewis Acid-Base (hydrophobic), Born and hydration forces (*in italic*).

*Table 1.2: Colloidal forces their origin, range and nature showing DLVO forces in bold and XDLVO forces in italics. (Adapted from Saleh, Afrooz, et al. 2016)*

| Interaction | Origin | Typical range (nm) | Nature of Force |
|---|---|---|---|
| **Electrostatic** | Surface charge | 1-20 | Generally repulsive |
| **van der Waals** | Electromagnetic interactions | 5-10 | Generally attractive |
| *Lewis Acid-Base* | Changes in hydrogen bonding | 20-60 | Attractive |
| *Steric* | Adsorbed polymers or surfactants | 1-5 | Repulsive |
| *Bridging* | Adsorbed polymers or particles | 5-20 | Attractive |
| *Born repulsion* | Interpenetrating electron clouds | 0.3- 2 | Repulsive |
| *Hydration* | Surface/solvent interaction | 1.5 | Repulsive |

### Classical DLVO theory

Figure 1.8 compares the interaction energy profile modeled by DLVO theory, which includes Lifshitz van der Waals and electrostatic components and an XDLVO theory interaction energy profile, which additionally includes Lewis Acid-Base (hydrophobic) component. It shows that the XDLVO interaction energy profile is significantly reduced by including the positive hydrophobic forces, with an energy barrier lowering from 600 $k_BT$ to less than 200 $k_BT$.

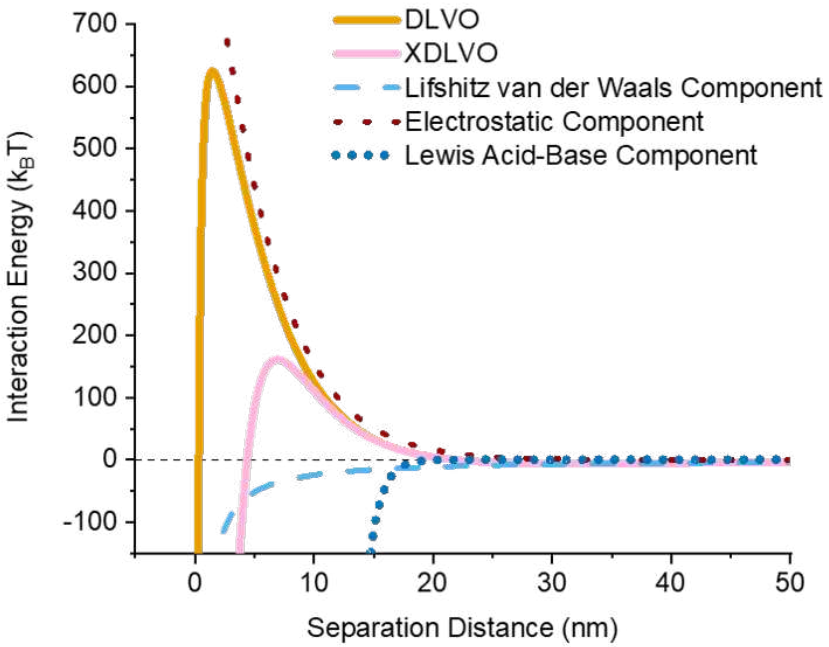


*Figure 1.8: Interaction energy between a particle a surface, according to DLVO and XDLVO theories. Details can be found in Chapter 3 with parameters corresponding to the NPT-P particle's size modified to 900 nm diameter.*

**Lifshitz van der Waals forces**

The Lifshitz van der Waals forces originate from the polarizability of the interacting elements: particles, surfaces, and fluid separating them. At the microscopic scale, this attraction results from induced and permanent magnetic dipoles interacting with each other. These forces are ubiquitous but relatively weak, as seen from the lower Lifshitz van der Waals energies compared to Lewis Acid-Base or electrostatic energies (Figure 1.8). Furthermore, they operate at a shorter distance than electrostatic energies and especially compared to Lewis Acid-Base energies. Finally, as shown in Figure 1.8 (and as will be evident from Equations 1.11,1.14, and 1.15 used to calculate interaction energies), Lifshitz van der Waals energies decay more slowly than electrostatic and Lewis Acid-Base energies.

These attractive forces are calculated by combining Hamaker constants (A) of the elements and the fluid separating them (Israelachvili 2015). To estimate the attraction of two similar materials of composition 1 in a fluid of composition 2 (e.g.: in the case of homo-aggregation), the overall Hamaker interaction parameter is calculated as:

$$A_{121} = \left(\sqrt{A_{22}} - \sqrt{A_{11}}\right) \tag{1.9}$$

with $A_{22}$ the Hamaker constant of material 2 and $A_{11}$ the Hamaker constant of materials 1. Similarly, in the case of hetero-aggregation or particle deposition, the overall Hamaker interaction parameter of two materials of composition 1 and 3 in a fluid of composition 2, is calculated as:

$$A_{123} = \left(\sqrt{A_{33}} - \sqrt{A_{22}}\right)\left(\sqrt{A_{11}} - \sqrt{A_{22}}\right) \tag{1.10}$$

The Hamaker constants can be calculated using quantum field theory and knowledge of the materials refractive index and dielectric constants (Table 13.2 of Israelachvili 2015. As seen in equations 1.9 and 1.10, the strength of Lifshitz van der Waals forces between two elements increases as the Hamaker constant of these elements increases and as the Hamaker constant of the fluid decreases. For example, in water, polystyrene colloids, with a Hamaker constant of 6.5 $10^{-20}$ J, are less attracted to each other than colloidal metals with Hamaker constants of 25 $10^{-20}$ to 40 $10^{-20}$ J (Israelachvili 2015).

Due to the electromagnetic character of Lifshitz van der Waals interaction energy, retardation effects can occur and reduce the overall attraction. This effect becomes significant at a distance approximately equal to that of the characteristic wavelength ($\lambda$), which is generally around 100nm ($\lambda = 2\ \pi c/\omega_v$ with c the velocity of light and $\omega_v$ the dispersion frequency). A typical retarded Lifshitz van der Waals interaction energy for two particles is proposed by Gregory 1981:

$$G^{LW} = -\frac{Ar_{p1}r_{p3}}{6\left(r_{p1}+r_{p3}\right)h} \cdot \left[1 - \frac{bh}{\lambda} ln\left(1+\frac{\lambda}{bh}\right)\right] \tag{1.11}$$

where $r_{p1}$ and $r_{p3}$ are the radii of particles 1 and 3, respectively; b an empirically defined constant, b = 5.32; and h the distance separating the particles in nm.

**Electrostatic interaction energy**

Electrostatic forces originate because charged particles in an electrolytic solution are surrounded by a "cloud" of ions, named the electronic double layer (EDL). As illustrated in Figure 1.9, these ions are attracted to the charged particles. They form an inner layer of strongly attracted ions, which are mostly oppositely charged (Stern layer, in dark grey). Further away from the particle, ions form an outer layer that is more hydrated, less firmly bound and whose concentration decreases until the bulk ionic composition is attained (diffuse layer, in light gray).

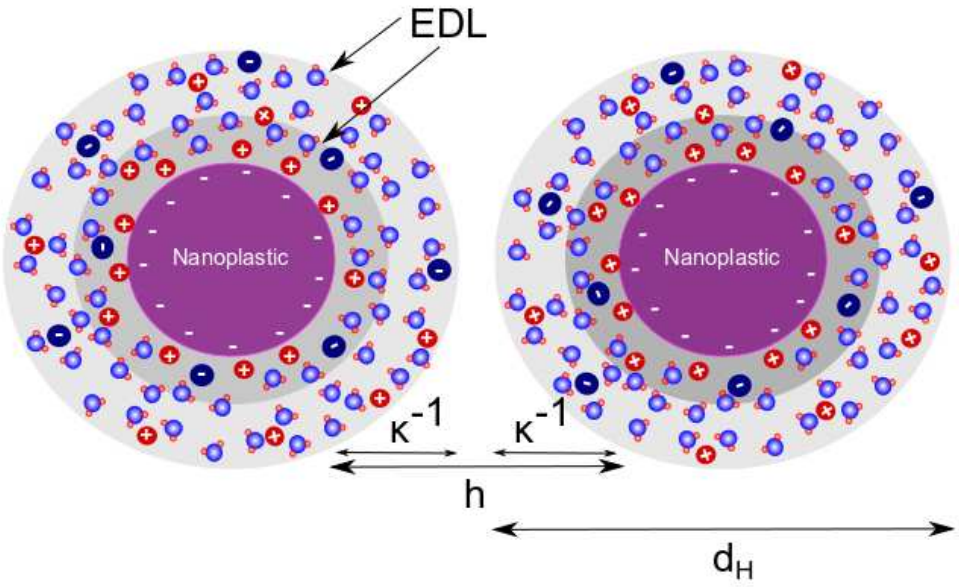


*Figure 1.9: Schematics of electronic double layers of lengths $\kappa^{-1}$ surrounding negatively charged nanoplastics, showing the Stern layer in dark gray and the diffuse layer in light gray (not to scale). (Adapted from Saleh, Afrooz, et al. 2016)*

The inverse of the EDL thickness (Debye-Hückel reciprocal length, $\kappa$) is given by the following equation for symmetrical electrolytes:

$$\kappa = \left( \frac{e^2}{\epsilon k_B T} \sum_{i=1}^{n} z_i^2 n_i \right)^{1/2} \tag{1.12}$$

with e the charge of the electron in C, $\epsilon$ the permittivity of the medium ($C^2\ J^{-1}\ m^{-1}$), $z_i$ the valency of the ions i, and $n_i$ the number of ions i per unit volume. The second part of the function represents the effect of the ionic strength I (in mol $L^{-1}$):

$$I = \frac{1}{2} \sum_{i=1}^{n} z_i^2 n_i \tag{1.13}$$

From this equation, we can see that length of the EDL is inversely proportional to the ionic strength since the addition of ions compresses the counterions closer to the particle surface (Elimelech 1998; Israelachvili 2015; Saleh, Afrooz, et al. 2016). The sum of particles' geometric radius and the EDL thickness is defined as the particles hydrodynamic diameter ($d_H$)(Figure 1.9). As illustrated in Figure 1.9, upon close approach ($h < 2\ \kappa^{-1}$), the EDLs can overlap. This provokes electronic repulsion caused by particles' same charge and also driven by an osmotic effect as water moves into the zone of close contact which is concentrated in electrolytes (S. Lin and Wiesner 2012b). The electrical double layer repulsion $G^{el}(h)$ between two particles can be calculated using the expression proposed by Hogg, Healy, and Fuerstenau 1966:

$$G^{el} = \pi\epsilon \frac{r_{p1} r_{p3}}{r_{p1} + r_{p3}} \left[ 2\psi_{p1}\psi_{p3} ln \left( \frac{1 + \exp^{(-\kappa h)}}{1 - \exp^{(-\kappa h)}} \right) + \left( \psi_{p1}^2 \psi_{p3}^2 \right) \cdot \ln \left( 1 - exp^{\left(-2\kappa h\right)} \right) \right] \tag{1.14}$$

with $\psi_{p1}$, and $\psi_{p3}$ the surface potential (mV) of particles 1 and 3 respectively.

As can be seen in equation 1.14, correct determination of ionic strength and surface potential is essential. While ionic strength can be easily measured or calculated, the measurement of surface potential is impossible. Therefore, the most practical option is to measure particles' zeta potential, which is the electric potential at the shear plane of the EDL (roughly at the beginning of the diffuse layer) (light grey in Figure 1.9). The zeta potential is determined from measurements of particles' electrophoretic mobility (EPM) (cf: Section 1.3.4). Surface potential can then be estimated from zeta potential by

knowing the ionic strength of the solution and by making a hypothesis about the geometry of the EDL (e.g.: a linear decrease with distance, e.g.: constant capacitance model) or an exponential decrease with distance, e.g.: Gouy-Chapman model) (Hiemenz and Rajagopalan 1997). The surface potential can also be determined by combining surface charge measurements and knowing the solution's ionic strength. A final consideration when modeling the EDL, is that equations can either assume the particles have a constant charge, which overestimates repulsion, or a constant potential, which underestimates repulsion, as is the case for equation 1.14. An alternative assumption exists, called the linear superposition approximation, which effectively averages constant potential and constant charge interaction energies (Elimelech 1998).

Before describing interaction energies used in XDLVO theory, this section explains the method used to calculate interaction energies between objects with different geometries. Two methods exist: the Derjaguin integration method (or Derjaguin approximation), which is the most common and tractable method (used in Equations 1.11, 1.14, and 1.15), and the surface element integration method (SEI). The Derjaguin integration method calculates sphere-sphere or sphere-plate energy from the corresponding plate-plate expression. As such, it is an approximation which is applicable to cases where the particle curvature is not too pronounced, as illustrated in Figure 1.10. Specifically, it is applicable if the particle radius is significantly larger than the distance separating them ($r_p >> h$) and significantly larger than the thickness of the EDL ($r_p >> \kappa^{-1}$)

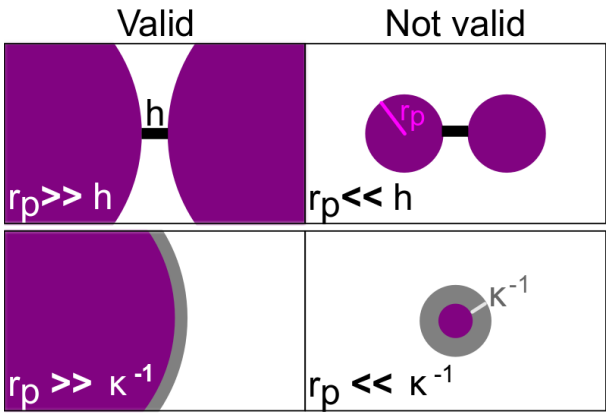


*Figure 1.10: Domains of validity of the Derjaguin Integration method depending on particle radius ($r_p$ in purple), separation distance (h in black) and thickness of the EDL ($\kappa^{-1}$ in grey).*

Alternatively, the SEI method calculates interaction energy by integrating forces oriented normal to the particle or plane surface, over the exact surface geometry. Using this method, the DLVO theory can model interaction energies for nonspherical particles (e.g.: spheroidal and rod-like) at different angles, and a variety of surface roughnesses generally modeled as protrusions and depressions of a certain magnitude and frequency

(Bhattacharjee and Elimelech 1997; Bhattacharjee, J. Y. Chen, and Elimelech 2000; Bhattacharjee, Ko, and Elimelech 1998; E. M. Hoek and Agarwal 2006; Huang, Bhattacharjee, and E. M. V. Hoek 2010; L. Wu et al. 2013). An alternative, the surface integration approach, does not restrict forces to being oriented normal to the surface. However, this additional consideration has not been found to significantly modify interaction energies (Wood and Rehmann 2014).

**Extended DLVO theory**

When studying nanoplastics' behavior in the environment, three other essential interaction energies are relevant to explore and require an extended version of the DLVO theory. It is expected that nanoplastics display different degrees of hydrophobicity since pristine plastics are most hydrophobic, and aging processes, also called weathering, decrease hydrophobicity (Gewert, Plassmann, and MacLeod 2015). This hydrophobicity can be modeled with the hydrogen bonding component of the interaction energy, often called the Lewis Acid-Base component. Also, the sorption of NOM onto nanoplastics can impact interaction energies by forming either steric and/or bridging interactions. Furthermore, Born repulsion, which originates from the interpenetration of electron clouds and hydration forces, which results from interactions between surfaces and solvents, are also relevant to consider. They occur at close separation distances <2 nm and reduce the primary energetic minimum from infinity to a finite value (D. Grasso et al. 2002). These short-distance forces are not covered here. Instead, the longer-range Lewis Acid-Base, steric and bridging interaction energies are described, since these determine the height of the energy barrier to attachment.

**Lewis Acid-Base interaction energy**

The Lewis Acid-Base interaction energy originates from the polarity of water. The positive hydrogen moieties of water behave as Lewis Acids (proton donors $\gamma^+$) while the oxygen moiety acts as Lewis Bases (proton acceptor $\gamma^-$)(van Oss 1993). As such, water bonds with itself and with other hydrophilic elements (e.g.: carboxylic acids and phenolic groups in the range of a few mmol $g^{-1}$ in NOM)(D. Grasso et al. 2002). When a hydrophobic element is introduced in water, the water molecules reorient themselves to reduce its interaction with the non-polar surface (Figure 1.11). This restructuring decreases entropy compared to bulk conditions. Therefore, it is thermodynamically favorable to reduce the surface area of hydrophobic elements by aggregation or adsorption (D. Grasso et al. 2002).

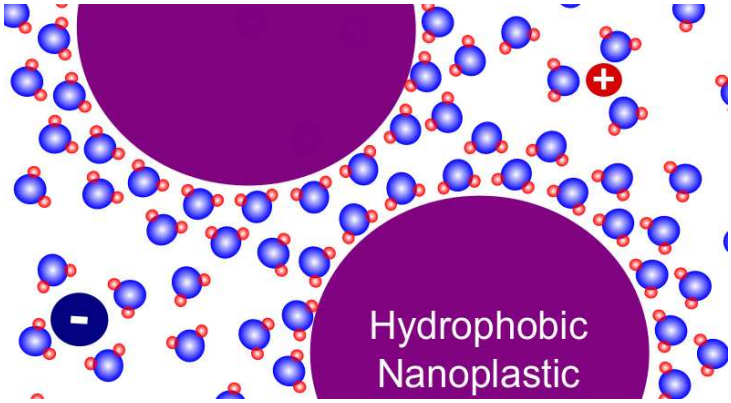


*Figure 1.11: Schematics of water molecules' orientation around hydrophobic nanoplastics. Water is depicted with oxygen in blue and hydrogen in red. A cation and anion, are shown as red and blue circles, respectively (not to scale). (Adapted from D. Grasso et al. 2002)*

The Lewis Acid-Base energy of interaction $G^{AB}(h)$ between two particles can be modeled using the expression proposed by van Oss (1993)(van Oss, 1993):

$$G^{AB} = 2\pi \frac{r_{p1} r_{p3}}{r_{p1} + r_{p3}} \lambda_{AB} \Delta G^{AB}_{h=h_0} \exp^{\left(\frac{h_0 - h}{\lambda_{AB}}\right)} \tag{1.15}$$

with $\lambda_{AB}$ the correlation length, which corresponds to the decay length of molecules in the liquid medium, approximately equal to 1 nm for pure water (van Oss 1993), $h_0$ the minimum distance of separation between the particle and the surface, taken as 0.158 nm. The Lewis Acid-Base potential $\Delta G^{AB}{}_{h=h_0}$ GABh=h0 is expressed as:

$$\Delta G^{AB}_{h=h_0} = -2\left(\gamma^{AB}_{p1} + \gamma^{AB}_{p3} - 2\sqrt{\gamma^{AB}_{p1}\gamma^{AB}_{p3}}\right) \tag{1.16}$$

with $\gamma^{AB}_{p1}$ and $\gamma^{AB}_{p3}$ the polar component of the surface free energy for particles 1 and 2, respectively. Equations 1.15 and 1.16 reveal that a correct determination of the Lewis Acid-Base potential is essential in order to assess particles' hydrophobic affinity. However, methods to quantify this potential in colloidal systems are still being developed.

Indeed, traditional hydrophobicity measurements, which are applicable to large objects or dissolved species, do not apply to colloids. For example, the hydrophobicity of solid materials was determined by the sessile drop (YoungLaplace) method, which measures the angle formed by a drop of liquid (with known hydrophobicity) deposited on a materials' surface. This method is not directly applicable to colloids due to their small size and strong surface curvature. An alternative has been used to overcome this limitation and consists in spreading colloids onto a surface to create a coating and measuring contact angle method with this coated surface. However, the coatings are generally uneven,

affecting the liquid drop's behavior and distorting contact angles (Fu 2018). Another method that was traditionally applied to dissolved species is the measurement of their partition between a hydrophobic (octanol) phase and a hydrophilic (water) phase, called the octanol-water partition coefficient ($K_{ow}$). However, this is inapplicable to colloids since its theoretical underpinning is that the species probed (i.e.: molecule or colloid) should be in thermodynamic equilibrium between the two phases. This is not the case for colloids since they require energy input to become suspended in another phase (Praetorius et al. 2014).

Since then, several alternative methods have been proposed. For example, the degree to which hydrophobic dies adsorb onto the particles can be measured to assess hydrophobicity (Crandon et al. 2020). Some limitations of this method are i) the need to separate the colloids from the dye in order to quantify the unadsorbed dye by absorbance, ii) the fact that the dye can cause particle aggregation, and iii) the need to test dyes with different degrees of hydrophobicity when the particles' hydrophobicity is entirely unknown (and cannot be previously estimated). Recently, methods have been developed to measure colloid hydrophobicity directly. Fu and Zhang (2018) have developed a method relying on the measurement of adhesion forces between particles that were deposited on a surface by atomic force microscopy (AFM) probes with different surface functionalizations (Fu 2018). While this also relies on depositing and drying colloids onto a surface, the AFM probes have a sufficient resolution to overcome the limitations of the sessile drop methods. Valesia et al. (2018) have developed a method to measure the hydrophobicity of dispersed colloids by tracking their deposition onto 3 surfaces with different surface energies (Valsesia et al. 2018) . As described in Figure 1.12 negatively charged particles are dispersed in the same medium and then injected onto one positively charged surface and two surfaces with the same negative surface charge but two different degrees of hydrophobicity (Figure 1.12a). Knowing the charge and hydrophobicity of each surface, the XDLVO is modeled for each of the three scenarios, with the particles' LewisAcid-Base potential as the only unknown in the equations (Figure 1.12b). Solving a system of equations that relates the energy barrier to the deposition speed allows the determination of particle hydrophobicity (Figure 1.12c).

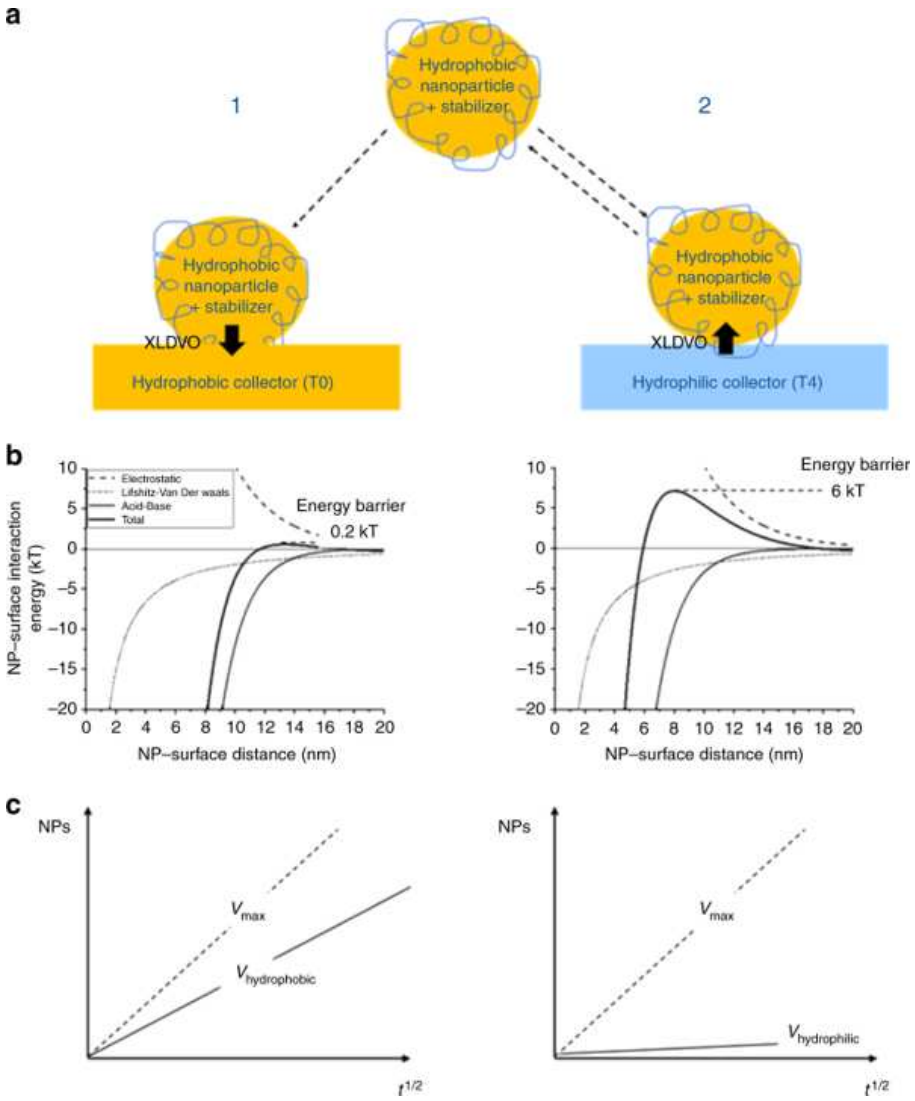


*Figure 1.12: Schematics of a method for quantification of colloid hydrophobicity. a) Colloidal dispersions are incubated with collectors that have the same surface charge but different hydrophobicity to calculate adsorption rates. b) The XDLVO energy is modeled, showing a low energy barrier for the hydrophobic collector and a high energy barrier for the hydrophilic collector. c) The rates of adsorption for the positively charged surface provides Vmax and for the two negatively charged surfaces provide $V_{hydrophobic}$ and $V_{hydrophilic}$ (Reproduced from Valsesia et al. 2018,Creative Commons Attribution 4.0 License)*

Both methods assume that adsorption can be entirely modeled by Lifshitz van der Waals, EDL, and Lewis Acid-Base interaction energies. However, the latter approach (Valsesia et al. 2018) has the advantage of studying particles in their dispersed state, while the former requires depositing them on a surface by drying (Fu 2018).

**Steric and bridging interaction energies**

Finally, steric and bridging interaction energies must be considered when studying nanoplastics since they originate from the adsorption of NOM onto particles' surfaces. As illustrated in Figure 13, this adsorption can result in opposite effects: steric repulsion or destabilization by bridging (Napper 1977; Fritz et al. 2002).

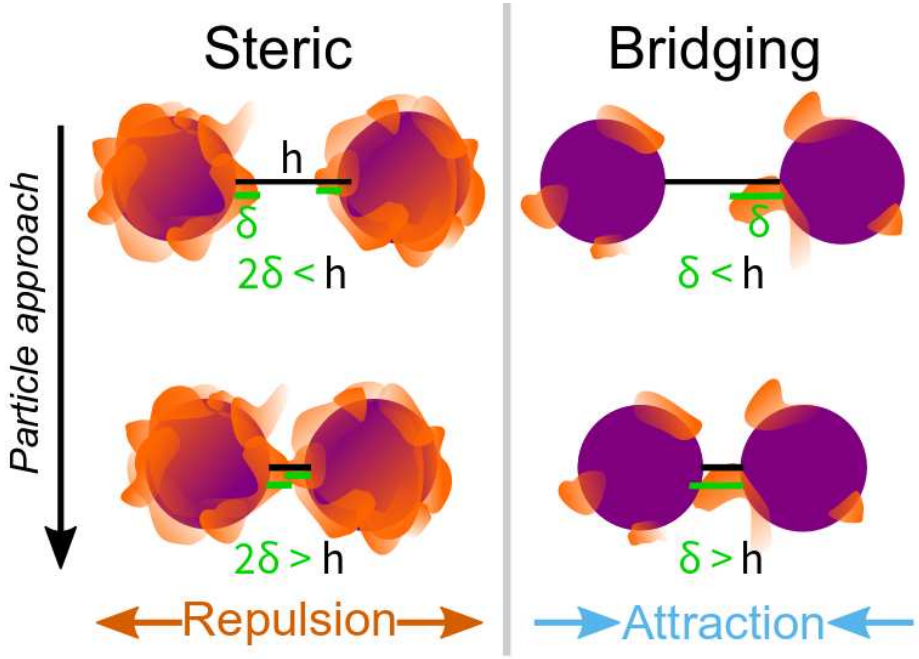


*Figure 1.13: Schematic of how steric and bridging interactions cause repulsion and attraction, respectively, as particles approach each other. NOM and particles are represented in orange and purple, respectively. The thickness of the NOM coating is δ(in green) and the distance of separation is h (in black).*

When low molecular weight (i.e.: dissolved) NOM adsorbs onto the entire surface of a particle, they form a coating of thickness $\delta$. As two particles approach each other, the coatings start interacting at a separation distance of h<2$\delta$ (left side of Figure 1.13. Particles are repulsed from each other since there is a decrease in entropy when NOM molecules from both particles overlap and mix. Furthermore, the close approach of coated particles causes osmotic pressure as the liquid is drawn to this area to dilute the molecules. Therefore, for effective repulsion, the NOM coating should be sufficiently thick. Indeed, in the case of a favorable profile of interaction energy (blue in Figure 1.7), to prohibit particles from reaching the primary energetic minimum ($\Delta G^{tot}_{min1}$), which starts being significantly negative at 25 nm away from the particle, the steric repulsion energy must be significantly positive at this distance (25 nm = $h_{max}(\Delta G^{tot}_{min1})< 2\delta$). In the case represented in Figure 1.7, the thickness should be at least approximately 20 to 30 nms.

The thickness of the coating ($\delta$) depends on the molecules' solubility in a given solution. For example, the molecules of NOM become compressed at high ionic strength due to the reduced electrostatic repulsion and at pH close to the NOM's point of electroneutrality ($pH_{zpc}$). Furthermore, for effective repulsion, the NOM should be adsorbed onto the entire surface of the particle. If sorption is patchy, then at h $<$ $\delta$the macromolecules on one particle can sorb onto the surface of the other particles, resulting in bridging, which is a form of flocculation (right side of Figure 1.13). Finally, the coating should be tightly adsorbed onto the particle surface for steric repulsion to be effective in environmental systems. This is due to the fact that other species in environmental systems can also sorb NOM (e.g.: ligands, metal oxides, etc.)(D. Grasso et al. 2002). Therefore, NOM coatings on particles must be viewed as dynamic systems. Indeed, the nature of this eco-corona (charge, composition, etc.) is continually evolving according to the properties of the environmental system: biological activity, fluxes of natural species, variations in salinity, etc. (Wheeler et al. 2021). To include steric interaction in XDLVO theory, the solvency of molecules and the thickness of the coating ($\delta$) are the two key parameters to include (Fritz et al. 2002). These are often difficult to determine for natural molecules which are inherently heterogeneous.

**Limitations**

As is evident from the hypothesis underlying the DLVO and XDLVO theories, these theories are not adapted to complex (natural) systems:

- Irregular particle shapes or surfaces are not easily modeled, neither is polydispersity of different particle parameters (e.g.: size, charge, etc.), as has been extensively reviewed for nanomaterials (Hotze, Phenrat, and Lowry 2010).
- (X)DLVO theory does not include chemical forces (e.g.: complexation of ions onto surfaces)(Israelachvili 2015). This makes its' applicability to environmentally realistic scenarios very limited since natural waters always contain multivalent ions, which can chemically interact with chemical moieties on nanoplastics' surfaces. In particular, multivalent cations can create bridges between nanoplastics with negative surface charges, which causes a destabilization by flocculation (cf: Section 1.3.2).
- Forces do not seem to be always strictly additive. For example, in theory, identical particles should have equal EDL repulsion in two solutions containing different ions with the same valency and concentration, since these ions are assumed to follow the same Boltzmann distribution around the particles. However, different ions can have different structuring effects on water molecules (López-León et al. 2003). Therefore, electrostatic repulsion cannot be considered separately from Lewis Acid-

Base interactions(W. Wu, Giese, and van Oss 1999). Similarly, steric forces interact with electrostatic and Lifshitz van der Waals forces. Indeed, different ions can change the solvency and length of adsorbed macromolecules (D. Grasso et al. 2002; Napper 1977). Furthermore, surface coating of NOM has been shown to decrease the Hamaker constant of silver and iron colloids (Mohammed Baalousha 2017 and references therein). It has also been suggested that Lifshitz van der Waals and EDL interactions should not be considered separately since some electromagnetic interactions may occur between dissolved ions and colloids (D. Grasso et al. 2002; Ninham 2006). This could be solved by including the Lewis Acid-Base interaction energy for each particle/surface/medium scenario.

- A drawback of (X)DLVO, which also holds for attachment efficiency ($\alpha$) and collision rate ($\beta$), is that it is calculated using parameters that are average values, generally obtained by ensemble methods (e.g.: $d_H$ and zeta potential). This assumes that particle and surface properties are homogenous and conceals the presence of heterogeneity and dispersity (Hotze, Phenrat, and Lowry 2010; Bradford and Torkzaban 2013).

The two previous sections have presented the global issue of contamination by nanoplastics, as well as the approaches and theoretical frameworks that can help understand the transport of these contaminants. The following sections discuss nanoplastics' fate in different environmental systems. The primary process investigated is nanoplastics' aggregation in water since it is one of the first transformations of nanoplastics in the environment, and one that impacts their fate in open waters as well as other downstream processes. The next section is a critical review of literature with the primary aim of elucidating how the properties of model nanoplastic particles impact their aggregation in experimental systems and consequentially interpretations about nanoplastics' environmental fate. A secondary focus will be on how experimental conditions and instrumental methods affect results and interpretation of nanoplastics environmental fate. The final and fourth section of this chapter will explain how the study of nanoplastics' transport through environmental interfaces can aid in assessing nanoplastics' transport and accumulation zones.

## 1.3 Nanoplastic stability in water

The following method was used to collect articles for the literature review. All original research articles present in the search engine Web of Science on August $16^{th}$ 2021, and containing the words nanoplastic* and stability, or nanoplastic* and aggregation, or nanoplastic* and agglomeration in either the article's title, abstract or keywords were collected. This resulted in 88 articles, of which 32 were randomly selected and reviewed in this section. 60 particles types were studied (either different particles or different batches of identical commercial particles). 55% of particles were studied to investigate the effects of nanoplastic stability, transport and deposition, while the remaining 45% of particles were studied to explore how they affect (eco)toxicity or geochemical functions. A summary of the 32 articles studied is presented at the end of this Chapter (page 92).

As mentioned in previous sections and illustrated in Figure 1.5, the aggregation rate depends on the dispersed (colloid) and continuous (fluid) phases, such as the composition of the continuous and dispersed phases, concentration, shape, and size of the dispersed phase, pH, temperature, and velocity gradients of the system. For a thorough review of these parameters, readers are referred to previous works (Mohammed Baalousha 2017; Dwivedi et al. 2015; Hotze, Phenrat, and Lowry 2010; Xing, Vecitis, and Senesi 2016; Peijnenburg et al. 2015). In the aqueous environment, nanoplastics' stability is strongly impacted by the nature and concentration of electrolytes and naturally occurring species (e.g.: dissolved or particulate, organic or mineral, etc.) (Buffle et al. 1998; Quik et al. 2014; Stumm and Morgan 1996), but conclusions about nanoplastics stability also depend on the properties of the particles used as nanoplastic models.

### 1.3.1 Nanoplastic models

By using the keyword nanoplastic, results are reduced to articles published after 2012, that are concerned with the environmental impact of plastic debris. While this approach allows us to focus on what constitutes model nanoplastics particles today, it excludes decades of research focusing on similar model polymeric nanoparticles named latex spheres and not nanoplastic models. To explore this literature, the reader is invited to read the critical review of Alimi, Farner Budarz, et al. 2018, which explores an extensive array of literature on stability and transport of PS latex (*PSL*) spheres in the environment. The main parameters that distinguished the 60 nanoplastic models reviewed in the literature survey were: how the models were produced or synthetized, their composition, their surface chemistry, as well as the presence of surfactants in dispersions (Figure 1.14).

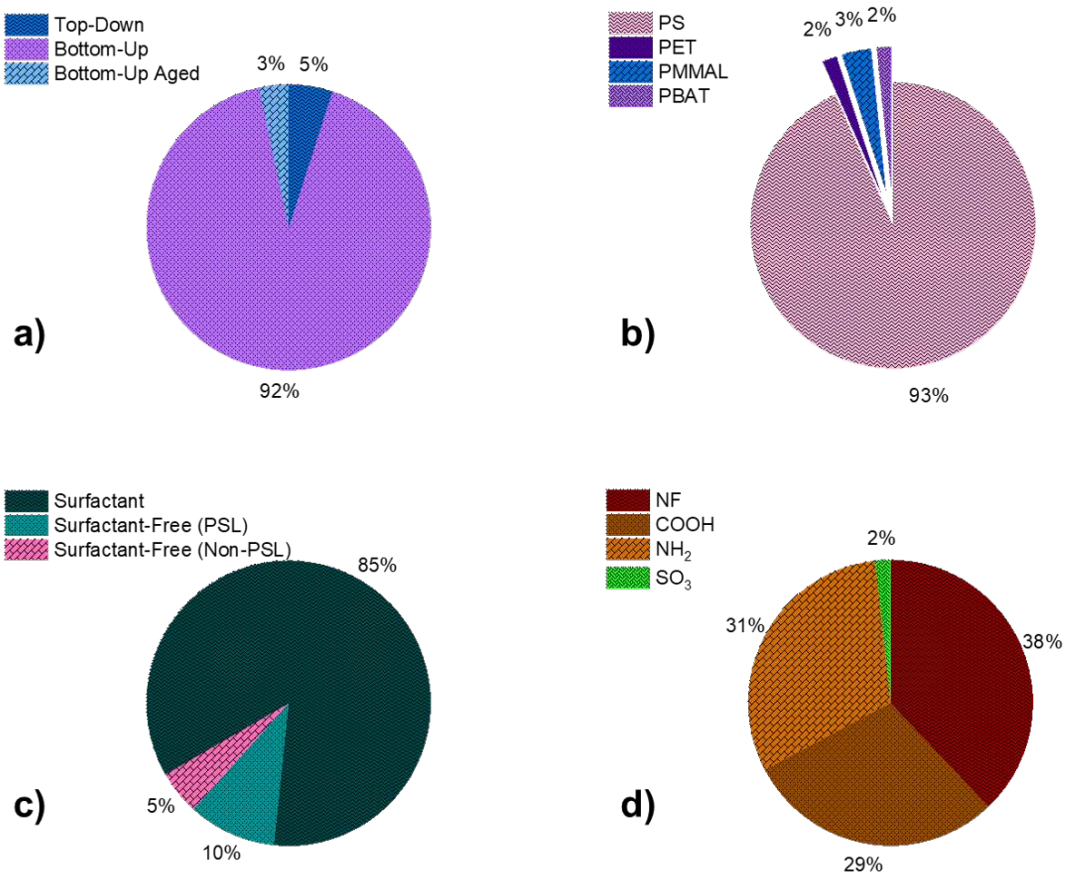


*Figure 1.14: Share of nanoplastic models studied according to a) production/synthesis method, b) composition with PS = polystyrene, PET = polyethylene terephthalate, PMMA = polymethylmethacrylate and PBAT = polybutyrate adipate-co-terephthalate, c) presence of surfactant and d) presence and type of surface functional group with NF = non-functionalized, COOH = carboxylate, $NH_2$= amine, and $SO_3$ = sulfonate. (number of particles=60)*

The vast majority (95%) of the studies use polymeric nanoparticles, also called polymer latex spheres, as models for nanoplastics(Figure 1.14a). These are synthesized from a bottom-up process of emulsion-polymerization, conferring them highly monodisperse sizes. However, as recently explained by Gigault, El Hadri, Nguyen, et al. 2021, environmental nanoplastics are expected to have very irregular and diverse morphologies since they are degradation products of larger plastics by mechanical abrasion, photodegradation, thermo-degradation, oxidation, as well as ingestion. Therefore, due to their sphericity, latex spheres are not resemblant to environmental nanoplastics. Two *PSL* particles were artificially aged by photo-oxidation to increase environmental relevance (Y. Liu et al. 2019; Mao et al. 2020). While these particles were increasingly hydrophobic and had a rougher surface, they generally remained spherical.

Only 5% of nanoplastic models (3 particles) were produced from top-down processes.

Two particles were produced from laser ablation of PET and PS plastic objects (Magrì et al. 2018; Yu, Shen, et al. 2019). One particle was produced from the mechanical abrasion of a biodegradable agricultural mulch composed of polybutyrate adipate-co-terephthalate (PBAT) (A. F. Astner et al. 2020; A. Astner et al. 2019). In-depth characterization of non-standardized nanoplastic models is necessary since these particles are new and more complex than latex spheres. For example, PBAT nanoplastics had a surface roughness of 12 nm. This is significantly rougher than *PSL*'s surface which have a roughness approximately equal to 1 nm (Zimmermann, Mead, and von Kleist-Retzow 2020). Also, environmentally relevant nanoplastic models produced from top-down processes present the drawback of having size distributions that are complex to characterize (as illustrated in Figure 1.15). Without a rigorous analysis of size distribution, converting the mass of particles to the number of particles is impossible. To overcome this issue, nanoplastics' mass concentration was used, although it is not representative of particle number when the size distribution is polydisperse or polymodal.

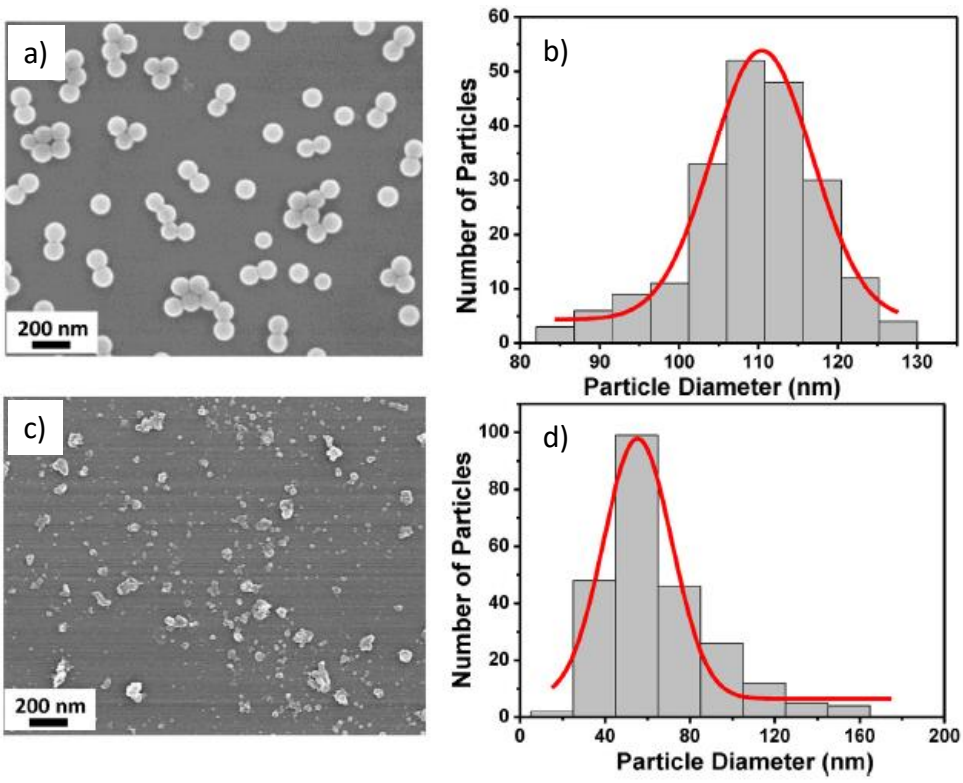


*Figure 1.15: Scanning electron microscopy images (left) and corresponding distributions of $d_{zH}$ (right) for PSL-NF(-), a) and b) and laser-ablated PS c) and d). The x-axis of the size distributions are different, showing that laser-ablated PS are more polydisperse than PSL-NF(-). (Reproduced, with permission, from Yu, Shen, et al. 2019).*

Most of the nanoplastic models were smaller than 100 nm, as illustrated in Figure 1.16. This may be due to the fact that a maximum size limit of 100 nm was used

for nanoplastics, based on the size limit for nanomaterials (Gigault, Halle, et al. 2018; Hartmann et al. 2019). Only two articles noted a size effect on aggregation dynamics. Kihara et al. 2019 observed that human serum albumin (HSA) protein had a softer interaction with 135 nm particles compared to 20 nm particles of the same composition. In agreement with theory (cf: Equation 1.7), Silva et al. 2020 noted that at equal mass concentration smaller particles aggregate more quickly than larger once, since they are more numerous and consequently, have a higher collision rate.

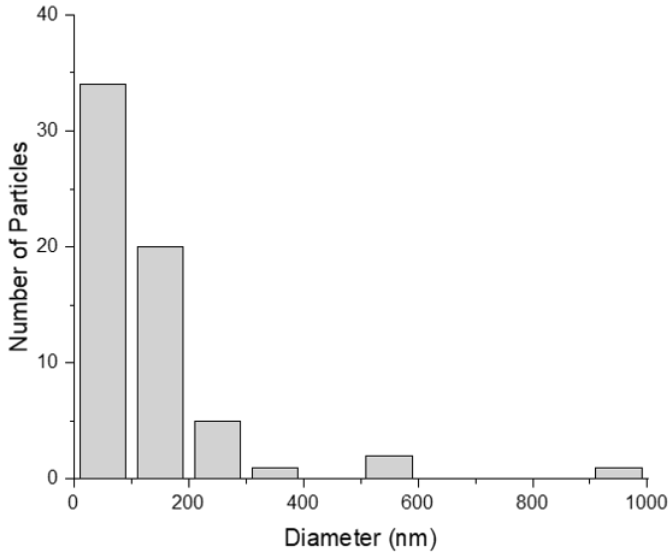


*Figure 1.16: Number of particles studied in the literature belonging to different size classes. Each size class includes the lower boundary and excludes the upper boundary (e.g.: the first bar represents particles ranging from 0 to 99 nm and the second bar, from 100 to 199 nm)*

Nanoplastic models often have limited relevance in terms of composition. 93% of nanoplastics models are composed of PS (Figure 1.14b) despite it only representing 7% of all plastic polymers produced. Conversely, no nanoplastic model was composed of PE or PP although these almost constitute half of the plastic waste generated (Geyer, Jenna R. Jambeck, and Kara Lavender Law 2017)(Figure 1.1)). Furthermore, 89% of the latex sphere models contain surfactants (Figure 1.14c). Since these commercialized dispersions are produced for other purposes (e.g.: calibrating machines), the use of additives, such as surfactants, preservatives, and biocides, increases their shelf life. However, surfactants reduce particles' affinity ($\alpha$) for other particles or surfaces by masking surface charges and/or causing steric repulsion (Fan et al. 2015; Goodwin 2004; Tufenkji and Elimelech 2004). Therefore, the presence of additives in dispersions reduces the environmental relevance of studies.

In an effort to increase the environmental relevance of latex spheres, studies have chosen particles grafted with chemical moieties such as carboxylic, amine and sulfonate (Figure 1.14d). In the present work, to differentiate latex spheres, they are named according to their composition - either polystyrene latex (*PSL*) or polymethylmethacrylate latex (PMMAL) followed by the functional group that they contain and their charge. For example, *PSL-COOH(-)* is a negatively charged *PSL* with carboxylic function groups on its surface, and *PMMAL-NF(-)* is a negatively charged non-functionalized *PMMAL*. The surface functionalization must be environmentally relevant since its charge and chemical affinity with dissolved or particulate species controls particles' attachment efficiency. 58% of latex spheres used in the literaturewere functionalized. Carboxylic and amine functional groups were the most common (29% and 31%, respectively), while only one particle contained a sulfonate functional group. Carboxylate functional groups approach environmental relevance since weathered (i.e.: aged) plastics have oxidized surfaces (Gewert, Plassmann, and MacLeod 2015). With a pKa of approximately 5, they are negatively charged in most natural waters whose pH generally range from 5 to 9 (Stumm and Morgan 1996). However, amine and sulfonate functional groups have limited environmental relevance since most plastics contain no nitrogen or sulfur, and environmental degradation does not generate these species. While sulfonate is negatively charged in the pH range of natural waters (Y. Li et al. 2019), amine is positively charged up to approximately pH 10 (Ramirez et al. 2019). However, a few studies found negatively charged *PSL-$NH_2$* (F. Zhang et al. 2019; Seoane et al. 2019), and one found both positively and negatively charged *PSL-$NH_2$* (J. Wu et al. 2019).

Nanoplastic models produced from top-down methods are not functionalized by grafting chemical moieties on their surface. However, they may contain functional groups, which originate from the production process. Indeed, using X-ray photoelectron spectroscopy (XPS) analysis (Magrì et al. 2018) observed carboxylic functional groups on the surface of nanoplastic models produced from laser ablation of PET.

### 1.3.2 Solution composition

Most of the particles (75%) were studied in synthetic solutions, produced from mixing purified salts and other dissolved or particulate species (e.g.: organic matter, extracted sediments, etc.). In these solutions, homo-aggregation of nanoplastic models is generally studied, for example by determining the CCC of different particles in different salts (Y. Liu et al. 2019; Mao et al. 2020; Singh et al. 2019; Yu, Shen, et al. 2019). This allows systematically varying parameters to get insight into mechanisms of aggregation. However, the CCC does not indicate nanoplastics' fate in the environment since it is more likely that nanoplastics hetero-aggregate with other particles.

The relative proportion of different electrolytes and the relative proportion of different dissolved and particulate species used to evaluate nanoplastic behavior are shown in Figures 1.17 and 1.19, respectively. Since the particle could be studied in different solution compositions, there are more electrolytes (n = 93) than particles (n = 60). However, it was less common to study particles in the presence of other species, such as dissolved or particulate matter (n = 39 particles).

The systematic analysis of nanoplastics' stability in different solutions revealed that:

- **Nanoplastic models produced from top-down processes have more variable behaviors and are generally less stable.**
- **The addition of NOM can either stabilize particles or destabilize them by bridging, depending on the valence of ions in solution and on the relative concentration of NOM, nanoplastics and electrolytes.**
- **The addition of natural particulate matter always destabilized particles.**
- ***PSL-NH*$_2$ are globally more stable than *PSL-COOH* or *PSL-NF*.**

Concerning the environmentally relevant nanoplastic models Magrì et al. 2018 noted that PET produced from laser ablation was significantly oxidated and stable in monovalent salts (CCC = 700 mmol $L^{-1}$ NaCl). Amongst the particles produced from top-down methods, these were the most stable against attachment caused by the screening of the EDL. Yu, Shen, et al. 2019 observed strong aggregation of laser-ablated PS at 300 mmol $L^{-1}$ NaCl and A. F. Astner et al. 2020 noticed homo-aggregation of nanoplastics produced from the mechanical abrasion of PBAT with slight agitation in deionized water. The aggregation of these types of nanoplastics models in deionized water or low concentrations of monovalent salts can be attributed to the absence of surfactants and to the non-spherical shape of the particles. Indeed, Singh et al. 2019 observed a CCC of 140 mmol $L^{-1}$ NaCl for *PSL-NF(-)* whose surfactants were removed. This was lower than the CCC of polymer latex spheres containing surfactants. Particles may also have higher collision rates ($\beta$) when they are polydisperse and non-spherical. When the collision is solely induced by Brownian motion, the collision rate is higher for dispersions with higher size polydispersity (cf: Equations 1.3 and 1.4)(Elimelech 1998). Also, the collision of irregular particles is likely to occur between particle protrusions and edges, and electronic repulsion is less pronounced at smaller contact points since it scales proportionally to particle size (cf: Equation 1.14) (Elimelech 1998; W. Wu, Giese, and van Oss 1999). Finally, at a close approach, particles with elongated shapes have stronger Lifshitz van der Waals attraction when longer side face each other (Vold 1954).

***Electrolytes***

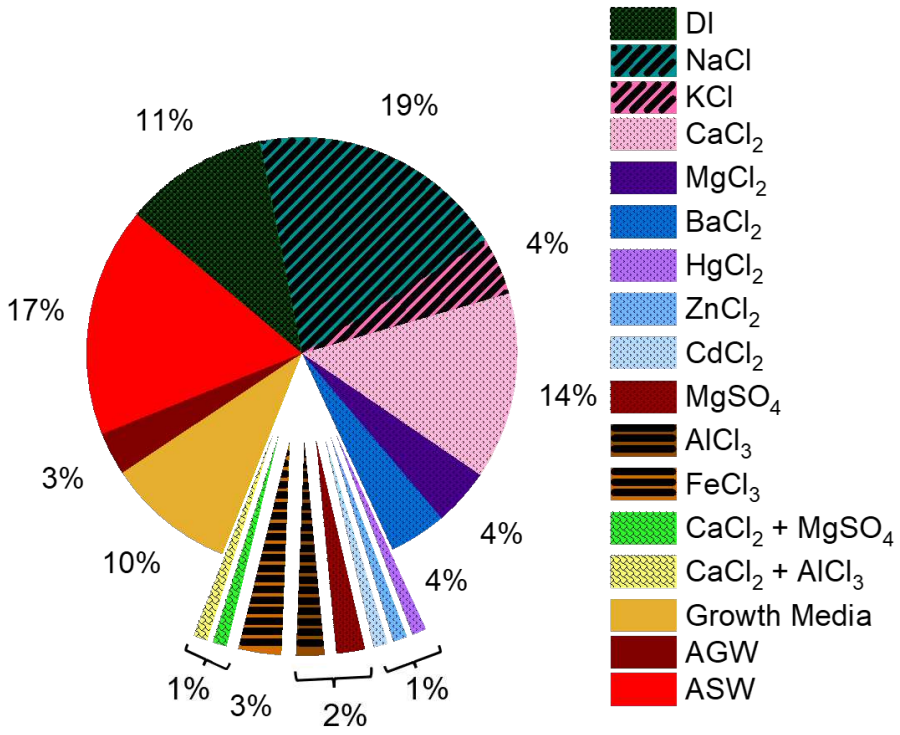


*Figure 1.17: Relative proportion of synthetic electrolytic solutions (n= 93) used to study particles in. ASW = Artificial Seawater; AGW = Artificial groundwater. Growth media mostly contains electrolytes but also has low concentrations of organic species such as vitamins.*

Latex spheres are highly stable in **monovalent solutions** in the pH range of natural waters (Cai et al. 2018; Y. Li et al. 2019). The behavior of latex spheres in monovalent salts is generally in agreement with the DLVO theory of colloidal stability. Indeed, Mao et al. 2020 and (Y. Liu et al. 2019) observed that the stability of photo-oxidized *PSL-NF(-)* increased proportionally to their electronegativity in monovalent salts. However, the stability of *PSL* at NaCl concentrations $> 1000$ mmol $L^{-1}$, when the EDL is entirely screened, points to the role of surfactants in enhancing stability. (González-Fernández et al. 2019; Mao et al. 2020; Yu, Shen, et al. 2019).

**Multivalent ions** destabilized nanoplastics whose charge was opposite that of the particles. This was either due to the fact that i) as the valence of ions increases, they are more effective at screening the EDL in the case of non-functionalized particles or ii) divalent or trivalent ions can bridge particles by creating surface complexes between the surface charge of two different particles.

i) Globally, divalent and trivalent cations destabilized non-functionalized, negatively-charged *PSL-NF(-)* in similar magnitudes. For example, in $CaCl_2$, $BaCl_2$, and

$MgCl_2$ *PSL-NF(-)* had CCCs ranging from ≈ 30 to 40 mmol $L^{-1}$ according to Y. Liu et al. 2019 and ≈ 60 to 70 mmol $L^{-1}$ according to Mao et al. 2020. Similarly, Singh et al. 2019 noted that *PSL-NF(-)* had similar aggregation rates in equal concentrations of $ZnCl_2$, $CdCl_2$, and $CaCl_2$. In trivalent cations, the destabilization was significantly stronger. For example, using $AlCl_3$ and $FeCl_3$ salts, the CCC of *PSL-NF(-)* was 2.12 and 1.4 mmol $L^{-1}$, respectively (Mao et al. 2020). As described by the Schulze-Hardy rule, the valence of counterions has the most effect on destabilization of non-functionalized particles (Hiemenz and Rajagopalan 1997). This rule assumes that only electrostatic and Lifshitz van der Waals interactions take place and that particles aggregate when the energy barrier is null. Using these assumptions, and calculating the Debye-Hückel length of the EDL (which is a power function of the ion valence) reveals that the CCC varies inversely with the sixth power of the valence of counterions in solution (CCC prop to $z^{-6}$). Both Y. Liu et al. 2019 and Mao et al. 2020 found this relationship between counterion valence and CCC.

ii) Destabilization of *PSL-COOH(-)* in the presence of divalent cations is also attributed to cationic bridging (Singh et al. 2019; Yu, Shen, et al. 2019). Y. Liu et al. 2019 even noted that the decrease in stability in $CaCl_2$ was linearly proportional to the degree of surface oxidation of UV-aged *PSL-NF(-)*. This suggests that $Ca^{2+}$ had higher probabilities of creating bridges thanks to the increase in carboxylic functional groups produced by oxidation. However, F. Zhang et al. 2019 noticed that regardless of the type of surface functionalization (NF, $NH_2$or COOH), negatively charged *PSL* were all destabilized at > 2.5 mmol $L^{-1}$ $CaCl_2$ and $MgSO_4$ with a molar ratio of 4:1, respectively. This suggests that the screening of the EDL and surface complexation may be equally effective processes.

Divalent cations do not destabilize positively charged particles due to EDL screening. Indeed, *PSL-$NH_2$(+)* remained stable in solutions with up to 150 mmol $L^{-1}$ $CaCl_2$ which can be explained by short-range repulsive interactions between positively-charged surfaces and ions (Yu, Shen, et al. 2019).

Artificial seawater contains high ionic strength, many multivalent ions, and no added organic matter. This solution generally caused strong aggregation of *PSL-NF(-)* and *PSL-COOH(-)* (Manfra et al. 2017; Sendra et al. 2019; Silva et al. 2020; Tallec et al. 2019). However, *PSL-$NH_2$(+)* either remained stable (Tallec et al. 2019; Z. Dong, W. Zhang, et al. 2019), or were less aggregated than *PSL* COOH(-) (Manfra et al. 2017; Okshevsky et al. 2020). In some cases, *PSL-$NH_2$(+)* was observed to become negatively charged due to the adsorption of anions in artificial seawater and zooplankton growth

media. In both cases, their aggregation was significant(C.-S. Chen et al. 2018; Saavedra, Stoll, and Slaveykova 2019).

Nanoplastic models produced from top-down processes also aggregate in divalent or multivalent electrolytes. PET particles which have carboxyl functional groups rapidly aggregated in a growth medium containing multivalent salts (Magrì et al. 2018). Similarly, Yu, Shen, et al. 2019 observed strong aggregation of laser-ablated PS at 5 mmol $L^{-1}$ $CaCl_2$ and a lower CCC in trivalent salts.

### *Determination of ion speciation*

An essential oversight in all studies using multivalent salts is that the speciation of ions is rarely studied. When performing aggregation experiments, it is imperative to consider metal speciation in solution since ions can form different aqueous complexes, as a function of solution pH, ionic composition and concentration. This modifies ionic strength as well as species' reactivity and solubility.

**Ionic strength**

The speciation of all electrolytes in solution must be calculated to determine the ionic strength of solutions, that is the concentrations of cations and anions present in the solution and their respective charge (Equation 1.17). Due to covalent bonding, aqueous complexes have smaller charges than the free ions, which decreases the values of ionic strength. As an example, an electrolyte composed of $Na_2SO_4$ can dissociate into the following species: $Na^+$, $SO_4^{2-}$, NaOH, $NaSO_4^-$, $HSO_4^-$ and $H_2SO_4$. Therefore, when taking into account the aqueous complexes, the ionic strength is calculated as:

$$I = 0.5\left([Na^+] + [SO_4^{2-}] \cdot 2^2 + [NaSO_4] + [HSO_4^-]\right) \tag{1.17}$$

Whereas without considering ion speciation, ionic strength is calculated as:

$$I = 0.5\left([Na^+] + [SO_4^{2-}] \cdot 2^2\right) \tag{1.18}$$

Comparing equations 1.17 and 1.18 shows that forgetting to account for aqueous complexes overestimates ionic strength values. Furthermore, the presence of $HSO_4$ shows that the solution pH is an essential parameter of speciation. For example, as can be seen in equations 1.19 and 1.20 the proportion of $HSO_4^-$ and NaOH ions is pH-dependent:

$$Na^+ + OH^- \rightleftharpoons NaOH \tag{1.19}$$

$$HSO_4{}^- \rightleftharpoons H^+ + SO_4{}^{2-} \tag{1.20}$$

Geochemical speciation softwares can easily calculate the ionic strength of a solution considering the formation of complexes. However, two main challenges must be considered. i) To calculate aqueous complexes, the software databases must contain the equilibrium constants of all complexes considered. Obtaining a complete database can be a challenge when studying natural waters, which contains numerous cations and anions. ii) To correctly calculate electrolytes' speciation at high ionic strength, it is necessary to calculate the ions' activities:

$$a(i) = f \cdot n_i \tag{1.21}$$

with a the activity of the ion i, f the activity coefficient and $n_i$ the concentration of i. If at low ionic strengths ($< 0.1$ mol $L^{-1}$), the Debye-Hückel equation is used to calculate activity coefficients, Davies equation is needed at larger ionic strength ($<0.5$ mol $L^{-1}$). It is therefore essential to verify if the correct equation is specified in the database of the speciation software.

**Cationic bridges**

It is crucial to determine the speciation of divalent and trivalent ions since EDL screening is a sixth power of ions' valence (cf: Section 1.3.2), but also since they can form ionic bridges between particles. Cationic bridges can only form when the cation is present in the free form (e.g.: [+II] for divalent cations). In fact, (Catrouillet et al. 2021 (Submitted)) showed that *PSL-COOH(-)* had a higher CCC in $MgSO_4$ compared to in $MgCl_2$ and $Mg(NO_3)_2$. This was explained by the formation of aqueous complexes of $MgSO_4$ that cannot form cationic bridges between particles, whereas $MgCl_2$ and $Mg(NO_3)_2$ were practically entirely dissociated into $Cl^-$ and $NO_3^-$ and $Mg^{2+}$, the latter being available for cationic bridges. When, considering only the free $Mg^{2+}$ concentrations, all CCC values were equal (Catrouillet et al. 2021 (Submitted)).

**Solubility**

Another essential mechanism concerning trivalent and divalent cations, is their propensity to precipitate as hydroxides at intermediate and high natural pHs (Brown and Ekberg 2016). For most of the experiments performed using trivalent cations it is impossible to conclude about the rate of homo-aggregation. Indeed, since aggregation was assessed by measuring increases in particle size, the precipitation of trivalent cations into hydroxides (as individual particles or as a coating of nanoplastics' surfaces) cannot be distinguished from the aggregation of nanoplastics. For example, Mao et al. 2020 performed their experiments at pH 7.5 with Al concentrations ranging from 0.25 to 10 mmol $L^{-1}$ and Fe concentrations from 0.1 to 10 mmol $L^{-1}$ using DLS measurements. From geochemical modeling and without considering the potential Al and Fe complexation onto *PSL*, it can be estimated that >95% and 100% of Al and Fe, are present in solid forms boehmite and ferrihydrite, respectively. Similarly, Cai et al. 2018 assessed aggregation by mea-

suring *PSL* size in $FeCl_3$ with concentrations between 0.01 and 1 mmol $L^{-1}$ at pH 5.4. Geochemical modeling also predicts that all Fe is present as the solid ferrihydrite. Such precipitation of divalent and trivalent cations as hydroxides is used in treatment processes. Indeed, Z. Chen et al. 2020 have used solutions of Al and Ca as flocculants. As evidenced from analysis of aggregate crystallinity and from scanning electron microscopy (SEM) images (Figure 1.18), the salts precipitated into solid form at higher pHs. These precipitates were more effective at capturing *PSL-NF(-)* than aggregation by EDL screening (Z. Chen et al. 2020). It is thus crucial when performing aggregation experiments in the presence of trivalent (and to some extent divalent) cations to consider the potential precipitation of cations as hydroxides, in addition to the formation of hydroxide aqueous complexes.

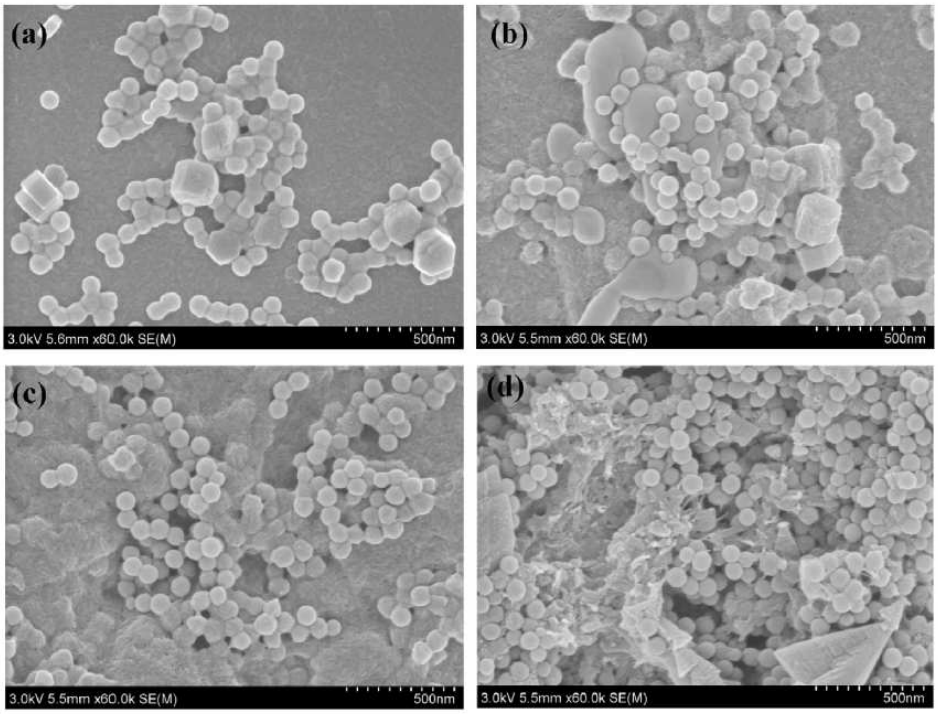


*Figure 1.18: SEM images of PSL-NF(-) spheres flocculated with $Ca^{2+}$ and $Al^{3+}$ at pHs a) 4, b) 6, c) 8, and d) 10. While the crystalline shapes in (a) are salts that crystalised during drying, the crystalline shape at the bottom right of (d) shows ions of $Ca^{2+}$ and $Al^{3+}$ that precipitated in solution. (Reproduced, with permission, from Z. Chen et al. 2020.)*

***Other dissolved or particulate species***

Naturally occurring organic and mineral species play an essential role due to their ubiquity. Concerning organic species, NOM may either originate from the decomposition of living organisms (e.g.: humic and fulvic substances and biopolymers) or secretion by living organisms (e.g.: extracellular polymeric substances (EPS)). Other organic species such as proteins and sugars are essential for living organisms but are very short-lived outside of living systems. Therefore, such macromolecules are less relevant to environmental fate studies (Buffle et al. 1998; Stumm and Morgan 1996; Flemming and Wingender 2010). Organic matter is generally negatively charged, although some species, such as proteins, contain negatively and positively charged zones. Mineral colloids are found in a variety of forms, originating from a multitude of processes. For example, aluminosilicates (i.e.: clays) are produced from extensive bedrock weathering. Metal oxides originate from solubilization and precipitation, and, in some cases, reduction-oxidation processes. Carbonates and siliceous particles are an important source of particulate matter in lakes and oceans, originating from phyto- and zooplankton growth. Finally, suspended sediments, which can occur from surface run-off waters or resuspension of bottom sediments by turbulences, are an essential component of terrestrial and coastal water systems and shallow waters (terrestrial or oceanic) (Stumm and Morgan 1996). Different classifications of naturally occurring species have been proposed to subsume these properties (Buffle et al. 1998). Of all the synthetic solutions studied (n = 93), 42% (n = 39) studied the impact of naturally occurring species. The types of species used are summarized in Figure 1.19. Most of the naturally occurring species studied were of terrestrial origin (33% humic acids and 21% fulvic acids). Alginate, a purified extract of algae that is a proxy for NOM of bacterial or oceanic origin, was studied in 8% of the cases. Bacterial and algal exudates were studied in 8% and 10% of the cases, respectively. 11% of studies, concerned with the (eco)toxicity of nanoplastics, studied particles in protein-rich solutions (hemolymph serum, fetal bovine serum and human serum albumin). Only 6% studied the effect of particulate species.

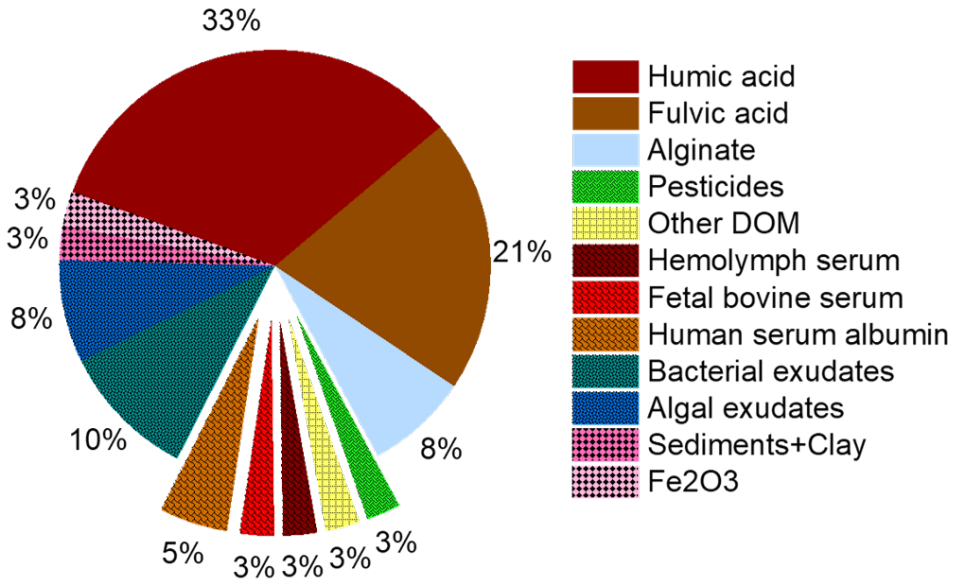


*Figure 1.19: Relative proportion of the different dissolved or particulate species in which particles were studied (n= 39)*

In **monovalent electrolytes**, NOM such as humic, fulvic, and alginic acids, EPS as well as proteins have a stabilizing effect on nanoplastics attributed to the increase in electronegativity and increase in steric repulsion (Y. Li et al. 2019; Mao et al. 2020; Singh et al. 2019). Similarly, the dissolved organic matter produced from the UV-irradiation of *PSL* spheres stabilized *PSL-NF(-)* in NaCl (Y. Li et al. 2019).

In **multivalent electrolytes**, organic matter stabilized nanoplastic models in some cases and destabilized them in other cases. In some situations, the sorption of organic species on the surface of nanoplastics and/or their presence in solution was sufficient to provide steric and/or electrostatic repulsion, respectively. For example, while *PSL-COOH(-)* and *PSL-NH$_2$(+)* were aggregated in artificial seawater and marine broth, they were less aggregated in marine broth due to the sorption of organic constituents of this growth medium onto particles (Okshevsky et al. 2020). Some other organic species, such as the glyphosate molecule, an active ingredient for herbicides, had a stabilizing effect in growth medium (Q. Zhang et al. 2018). In other cases, multivalent cations and NOM flocculate nanoplastics by bridging them instead of stabilizing them (Figure 1.13, bottom right). For example, (Singh et al. 2019) noted that humic acid had a destabilizing effect on *PSL-NF(-)*. Indeed, their CCC was 25 mmol L$^{-1}$ $CaCl_2$ and decreased to 6 mmol L$^{-1}$ $CaCl_2$ in the presence of 5mg L$^{-1}$ humic acid (Singh et al. 2019). Similarly, artificial groundwater caused aggregation of both negatively and positively charged *PSL* due to bridging by NOM and $Ca^{2+}$(Song et al., 2019). No study observed cationic bridges in

the presence of proteins, which could be attributed to the fact that despite their overall negative charge, they generally contain a mixture of negatively and positively charged amino acids (Kihara et al. 2019).

It appears that these differences in stability depend, at least in part, on the relative proportions of nanoplastics, organic matter, and electrolytes, as summarized in Figure 1.20. For high concentrations of monovalent salts, relatively low concentrations of organic matter are sufficient to stabilize nanoplastics (cf: upper section of Figure 1.20). However, nanoplastics models with negatively functional groups (as expected in the environment) dispersed in divalent cations, are only stable with both low concentrations of divalent cations and complete NOM coating (cf: lower section Figure 1.20).

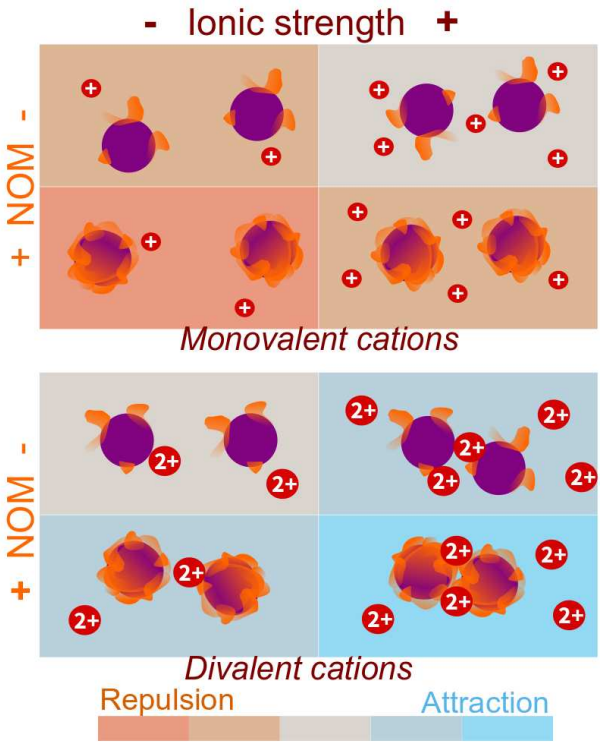


*Figure 1.20: Schematics of how ion valency, ionic strength and NOM concentrations either induce repulsion or aggregation of nanoplastics with negative surface functional groups, based on the results from the current literature review. While the thickness of $\delta$ should vary with ionic strength and ion valency it was kept constant for illustrative simplicity.*

Concerning nanoplastic models produced from top-down methods, humic acid decreased aggregation of laser-ablated PS particles in low concentrations of $CaCl_2$ (5 mmol $L^{-1}$) and provoked aggregation in 20 and 50 mmol $L^{-1}$ $CaCl_2$ (Yu, Shen, et al. 2019). However, laser ablated PET particles were stabilized by forming a protein corona from fetal bovine serum when the latter was more abundant than the nanoplastic (Magrì et al. 2018).

Numerous experiments with *PSL* observe concentration-dependent effect of NOM and multivalent cations (Kihara et al. 2019; Saavedra, Stoll, and Slaveykova 2019; Yu, Shen, et al. 2019). For example, 30 mg $L^{-1}$ of humic acid did not significantly increase the stability of 100 mg $L^{-1}$ *PSL-COOH(-)* or *PSL-NF(-)* in artificial seawater (Tallec et al. 2019). Yu, Shen, et al. 2019 showed that in $CaCl_2$ low concentrations of humic acid (<5 mgC $L^{-1}$) enhanced the stability of 10 mg $L^{-1}$ *PSL-COOH(-)* and *PSL-NF(-)*. However, at higher concentrations (>5 mgC $L^{-1}$), humic acid decreased stability due to interparticle bridging (Yu, Shen, et al. 2019). Similarly, NOM and multivalent cations in natural groundwater destabilized *PSL-COOH(-)* by cationic bridging in conditions where NOM was more abundant than nanoplastic models (Z. Song et al. 2019). Low concentrations of EPS from a bacterial culture had a dispersant effect on *PSL-NF(-)* in artificial seawater, and higher concentrations had a flocculating effect (Summers, Henry, and Gutierrez 2018). For *PSL-$NH_2$(+)*, NOM such as humic acid or alginate can reverse the charge proportionally to the quantity added in various solutions (Oriekhova and Stoll 2018; Saavedra, Stoll, and Slaveykova 2019; J. Wu et al. 2019).

Despite the critical effect of relative NOM and particle concentrations, the majority of particles were studied with mass concentrations of NOM that were lower (40%) or equal (20%) to nanoplastic concentrations. Using nanoplastic concentrations that are larger than NOM concentrations has little environmental relevance since NOM is ubiquitous and more abundant than nanoplastics (cf: Section 1.2.1. Another limitation is that 40% of the particles were studied with filtered NOM (either at 0.22 or 0.45 $\mu$m), which is likely to reduce steric repulsion and aggregation by bridging, due to the reduced size of the molecules. However, even unfiltered NOM, was mostly composed of low molecular weight species, thereby not particulate. Also, the stability of NOM itself with multivalent ions is rarely discussed, although these ions can cause aggregation and folding of NOM, which would reduce their stabilizing effect.

Finally, despite their destabilizing effects, particulate matter has rarely been studied. Y. Li et al. 2019 noted that negatively charged *PSL-$SO_3$(-)* hetero-aggregated with suspended sediments extracted from a river bottom, causing significant settling. Singh et al. 2019 noted that *PSL-NF(-)* hetero-aggregated with bentonite clay in NaCl. (A. F. Astner et al. 2020) even noted hetero-aggregation of vermiculite with fragmental nanoplastic models produced from PBAT in the absence of electrolytes. There is a lack of data concerning the interaction of nanoplastics with both particulate matter and NOM. Within the literature reviewed, only Y. Li et al. 2019 studied both particulate matter, NOM and nanoplastics. They noted that humic acid decreased the hetero-aggregation of suspended sediments with *PSL-$SO_3$(-)* due to steric repulsion.

***Environmental samples***

Approximately 25% of the particles were studied in natural water. Two-thirds were studied in seawater, while the rest were studied in freshwater from rivers, lakes, aquifers, bottled water, or drinking water (Figure 1.21).

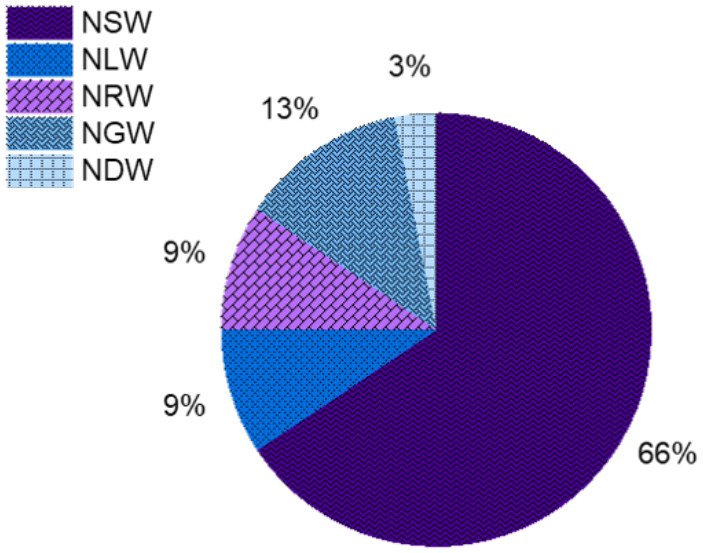


*Figure 1.21: Relative proportion of different natural water types in which nanoplastic models were studied. NSW = natural seawater; NLW = natural lake water; NRW = natural river water; NGW = natural groundwater; NDW = natural drinking water.*

Natural seawaters generally induce strong aggregation compared to freshwaters, due to stronger electrostatic screening, in agreement with DLVO theory (Singh et al. 2019). Manfra et al. 2017 noted the rapid formation of large aggregates for both *PSL-COOH(-)* and *PSL-$NH_2$(+)* in natural seawater. While all negatively charged *PSL* were significantly destabilized in natural sea water, some authors found that *PSL-$NH_2$(+)* were stable in natural sea water (González-Fernández et al. 2019; Tallec et al. 2019). Della Torre et al. 2014 also found *PSL-$NH_2$(+)* were more stable than *PSL-COOH(-)* in natural sea water. However, the addition of exopolysaccharides from algal cultures destabilized *PSL-$NH_2$(+)* (González-Fernández et al. 2019). Not only is the amine functional group not environmentally relevant, but also they are generally positively charged, whereas nanoplastics are expected to be negatively charged. Furthermore, they are often the most stable nanoplastic model, making it irrelevant to draw conclusions on nanoplastics' environmental fate using latex spheres functionalized with amine ($NH_2$) (Bergami et al. 2019; Della Torre et al. 2014; Manfra et al. 2017; Tallec et al. 2019; Yu, Shen, et al. 2019).

Concerning freshwater, Singh et al. 2019 found that *PSL-NF(-)* was more stable in

a groundwater than in a river water. While the groundwater contained approximately twice the total dissolved solids (which is roughly proportional to ionic strength) compared to the river water, it also contained approximately twice as much organic carbon, which provided a stabilizing effect.

Finally, an important consideration when studying natural waters, was their level of filtration. Practically all natural waters (98%) were filtered, whereas it was demonstrated that only dissolved organic matter had a stabilizing effect in groundwater (Z. Song et al. 2019). In contrast, the unfiltered groundwater containing particulate organic matter destabilized nanoplastics, which is in agreement with observations using purified particulate species.

### 1.3.3 Sample preparation methods

Small differences in how samples are prepared can also lead to significantly different results, and therefore different conclusions about nanoplastics' environmental fate.

i) The order in which electrolytes, NOM, and nanoplastics are mixed and the concentrations of the stock solutions may impact aggregation. For example, when a stock dispersion of nanoplastics is added to electrolytes, the ionic strength of the mixture is initially high, and then decreases. Therefore, the first particles added are more likely to aggregate. Inversely, if the electrolytes are added to the nanoplastic dispersion, the ionic strength is always lower than the final ionic strength, which will not enhance the probability of aggregation. However, this information is often omitted in the materials and methods sections of studies.

ii) Natural waters are sensitive to storage conditions (e.g.: growth of biofilm, flocculation of NOM, etc.). Despite the importance of proper storage conditions, few articles thoroughly describe storage parameters, such as storage duration, temperature, and whether or not samples were stored in obscurity, filtered, treated with biocide, etc.

iii) Nanoplastic dispersions were treated very differently before analysis. While most of them receive no particular treatment, some samples are vortexed prior to use (Bergami et al. 2019; Canesi et al. 2016; Della Torre et al. 2014; Y. Liu et al. 2019; Mao et al. 2020; Okshevsky et al. 2020; Saavedra, Stoll, and Slaveykova 2019; Singh et al. 2019), or ultra-sonicated before dispersion and/or characterization (C.-S. Chen et al. 2018; Z. Dong, W. Zhang, et al. 2019).

Most (78%) aggregation studies focus on perikinetic aggregation (i.e.: the fluid is not agitated and collisions occur only by Brownian motion). While this allows the analysis of parameters affecting attachment efficiency without the added complexity of shear

stress, it has limited environmental relevance since natural waters generally have some degree of advection. In fact different results were observed during orthokinetic aggregation (i.e.: the fluid is agitated) (Ramirez et al. 2019; J. Wu et al. 2019; Y. Li et al. 2019; C.-S. Chen et al. 2018; Summers, Henry, and Gutierrez 2018). Summers, Henry, and Gutierrez 2018 incubated *PSL-NF(-)* nanoplastics in unfiltered natural seawater using roller-bottle designs which mimic gentle waves. They found that nanoplastics did not affect the rate of formation of marine snow aggregates whereas, without agitation, polymer latex spheres accelerated the aggregation of dissolved organic matter from seawater, lake water and river water (C.-S. Chen et al. 2018; Shiu et al. 2020). The fact that nanoplastics only impact the aggregation of organic matter in the absence of agitation, is attributed to the shear stress of agitation which breaks aggregates and masks the aggregating effect of nanoplastics. These experimental designs with environmentally relevant solution chemistries suggest that nanoplastics are likely to be included in natural marine and freshwater aggregates. In the presence of turbulence, nanoplastics may not significantly impact the rate of formation or settling of these aggregates.

### 1.3.4 Instruments and methods to assess the stability

Finally, the major instruments and methods used to study nanoplastic stability are briefly discussed. All methods used are presented in Figure 1.22.

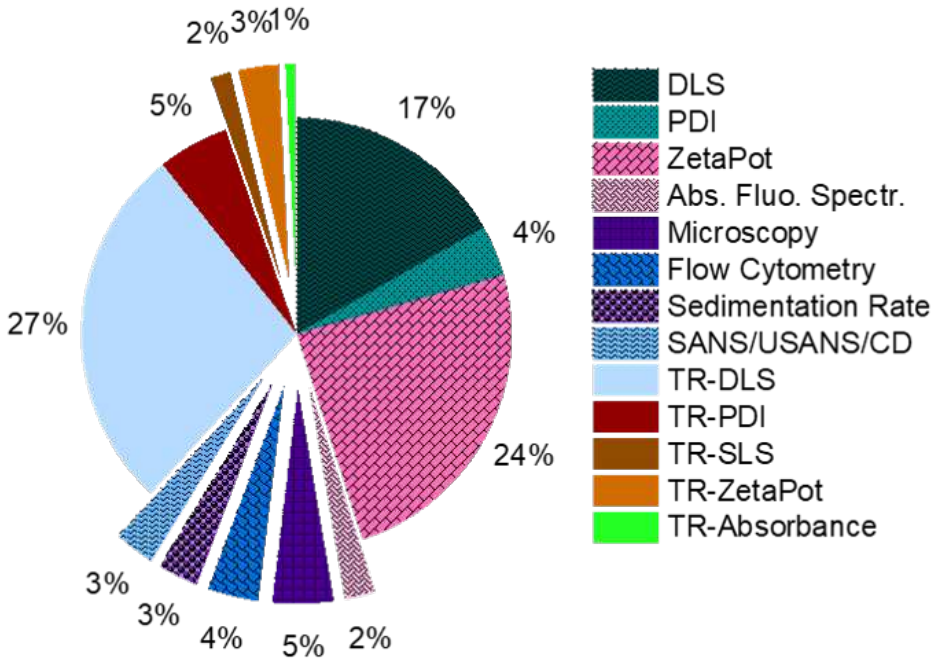


*Figure 1.22: Relative proportion of methods used to characterize nanoplastic particles. DLS = Dynamic Light Scattering; PDI = Polydispersity Index; ZetaPot = zeta potential; Abs. Fluo. Spectr. = Absorbance and/or Fluorescence Spectroscopy, SANS/USANS/CD = Small-angle ,Neutron Scattering /Ultra SANS/ Circular Dichroism; SLS = Static Light Scattering and TR = time-resolved (defined as at least 3 different measurements as a function of time).*

The majority of methods used dynamic light scattering (DLS), either as punctual (17%) or time-resolved (TR) measurements (27%) to assess hydrodynamic diameters ($d_H$)(Figure 1.22). Although DLS is a commonly-used method, results must be interpreted carefully since they tend to overestimate actual sizes (M. Baalousha and Lead 2012). As illustrated in Figure 1.23, DLS is an ensemble method that deconvolutes a global signal. The intensity of light scattering is a power function of particle radius. So, a single large particle can overshadow the signal from all small particles. The most commonly used algorithm to interpret raw data is the Cumulant algorithm which finds z-average hydrodynamic diameter ($d_{zH}$) by fitting a Gaussian size distribution to the raw data (ISO22412:2008). $d_{zH}$ should be interpreted with caution since it is sensitive to i) to size dispersity and ii) the duration of measurements.

i) The polydispersity index (PDI), defined as the variance of this Gaussian-fitted size

distribution, ranges between 0 and 1, with values considered monodisperse up to 0.01 and nearly monodisperse up to 0.1 (Goodwin 2004). When PDI > 0.1, the $d_{zH}$ is an average of several size populations or a wide distribution of sizes. Therefore, this single value cannot represent the true size distribution. When nanoplastic dispersions have a high PDI, alternative algorithms to the Cumulant are better suited, such as CONTIN and Sparse Bayesian Learning algorithms (Hassan, Rana, and Verma 2015; Stetefeld, McKenna, and Patel 2016; R. Xu 2006). Alternatively, the intensity-based hydrodynamic diameter ($d_H$) defined as an intensity-based peak containing 90% of the population, can be used instead of $d_{zH}$, for samples with PDI > 0.5 (Alimi, Farner, and Tufenkji 2021). Despite the importance of PDI, it was only determined for approximately 10% of particles analyzed by DLS. The PDI has also been used as an indicator of stability since a colloidal dispersion contains different particle sizes when aggregation is underway. Authors have defined different PDI thresholds at which they consider dispersions to be aggregated, such as PDI > 0.25 (Yu, Shen, et al. 2019), PDI > 0.2 (González-Fernández et al. 2019; Y. Li et al. 2019; Tallec et al. 2019; Seoane et al. 2019) or PDI > 0.36 (Alimi, Farner, and Tufenkji 2021).

ii) Furthermore, the duration of acquisition of a measurement can affect the $d_{zH}$ since. There is a higher probability that large particles (which have a slow rate of Brownian diffusion, cf: Equation 1.2) cross the detection zone as the measurement lasts longer. So, it is relevant to specify the acquisition time, especially since it can vary from as low as 10 seconds (Bergami et al. 2019; Canesi et al. 2016; Della Torre et al. 2014; Kihara et al. 2019; Manfra et al. 2017; Seoane et al. 2019; Tallec et al. 2019; Yu, Shen, et al. 2019) to 12 minutes (C.-S. Chen et al. 2018; Shiu et al. 2020).

Another consideration when comparing TR-DLS results is that, it is more likely to observe slow aggregation rates as a measurement lasts longer. TR-DLS studies have been found to vary from 10 minutes (Cai et al. 2018; Singh et al. 2019) to as long as 100 minutes (Y. Liu et al. 2019), 24 hours (C.-S. Chen et al. 2018) and 72 hours (Magrì et al. 2018). Finally, the effect of NOM on DLS detection is not always discussed, even though colored NOM, such as humic and fulvic acids, can absorb the laser light and reduce signal.

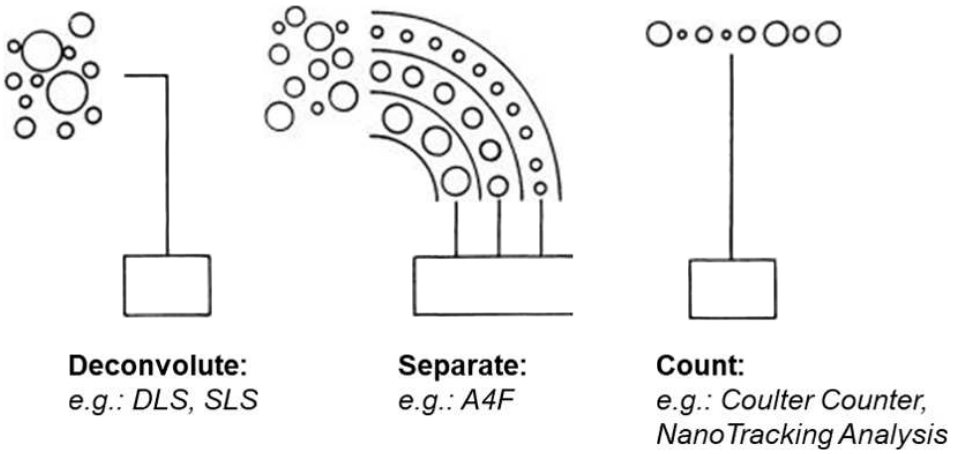


*Figure 1.23: Schematics of different approaches to determine the sizes of particle dispersions. (Adapted from Scarlett 1992).*

Determining the fate of nanoplastic models benefits from the use of complementary methods since each method has its limitations and advantages. For example, to assess size, practical techniques include static light scattering (SLS) preceded by a separation step, counting methods, as well as microscopy to assess the morphologies and aspects of particles or aggregates (Figure 1.23). Measurement of zeta potential is used to evaluate electrostatic repulsion; absorbance spectroscopy is useful to observe changes in concentration, and scattering spectroscopy to monitor interactions between particles and other species.

**Static light scattering** can provide information on particles' or aggregates' radius of gyration. This method is also suited to large aggregates which have lost Brownian motion. Indeed, *PSL-NF(-)* was so aggregated in artificial seawater (PDI $> 0.88$) that DLS measurements were complemented with measurements of particles' radius of gyration (Sendra et al. 2019). To avoid the common bias of light scattering techniques towards larger sizes, it must be preceded by a well-designed size-fractionation step that separates samples according to size, such as asymmetrical flow field flow fractionation (A4F) (Figure 1.23) (Gigault, El Hadri, Reynaud, et al. 2017; Messaud et al. 2009).

**Counting methods** can be useful for polydisperse nanoplastic dispersion since they avoid both biases of having to deconvolute a signal or to separate a sample. Examples of such methods are NanoTracking Analysis which tracks separate particles in dispersion and determines their diffusion coefficient to obtain their $d_H$. Other methods are better suited to larger particles or aggregates ($> 700$ nm), such as Coulter Counter (also called electrosensing zone), which uses electrical signal caused by a particles' displacement of an electrolyte as it passes through an aperture (Barnard, Rhyner, and J. F. Carpenter 2012) and flow cytometry, which also flows particles and aggregates through a detection

zone and then combines the use of fluorescence emissions and light scattering to measure particle size (Shiu et al. 2020; Summers, Henry, and Gutierrez 2018). Important considerations are whether the physicochemical conditions in which dispersions are analyzed (e.g.: salinity, flow rate) modify the dispersion state and whether sufficient particles are analyzed to have statistically representative results.

**Microscopy techniques** such as transmission and scanning electron microscopy (TEM and SEM, respectively) and atomic force microscopy (AFM) can only analyze a small portion of the entire nanoplastic dispersion. Therefore, they do not provide statistically representative data about particle dimensions. The fact that samples must be dried before analysis can introduce artifacts (e.g.: salt crystals and aggregation of particles due to capillary effects during drying). However, these techniques provide detailed information about particles' morphologies and aspects as well as dimensions without the need to deconvolute data with algorithms.

**Electrophoretic mobility**, measures particles motion under the effect of an electric current, to probe its zeta potential. This is the second most used method, since zeta potential was measured for 24% of particles punctually and for 3% of particles as a function of time. Zeta potential measurement can assess the degree of electrostatic repulsion between particles and charge reversal caused by the sorption of ions or other species onto the particle. Indeed, as the ionic strength of monovalent ions increases, the electrophoretic mobility reaches a plateau close to electroneutrality, reflecting the strong compression of the EDL and the inability of particle's charge to cause motion in an electric current (C.-S. Chen et al. 2018; Y. Liu et al. 2019; Mao et al. 2020; Tallec et al. 2019). This explains why differences in zeta potential values are not observable at high salinity (>100 mmol $L^{-1}$ NaCl) (Alimi, Farner, and Tufenkji 2021; López-León et al. 2003).

**Absorbance spectroscopy** can assess changes in particle concentration. In theory, absorbance is only suited to the analysis of species whose size is smaller than the wavelength of light to avoid scattering of the light beam. Despite this, absorbance spectroscopy can be used for larger particles if a linear relationship exists between concentration and absorbance. This must be done with caution since changes in size produce changes in absorbance at a given wavelength, as shown in Figure 1.24 (full lines). To avoid this effect, absorbance can be measured with a sphere that integrates all of the light signal emitted from the sample to erase any changes in absorbance caused by the light scattering of large particles. Indeed, Figure 1.24 shows that particles' absorption spectra (dashed lines) are relatively parallel with an integration sphere.

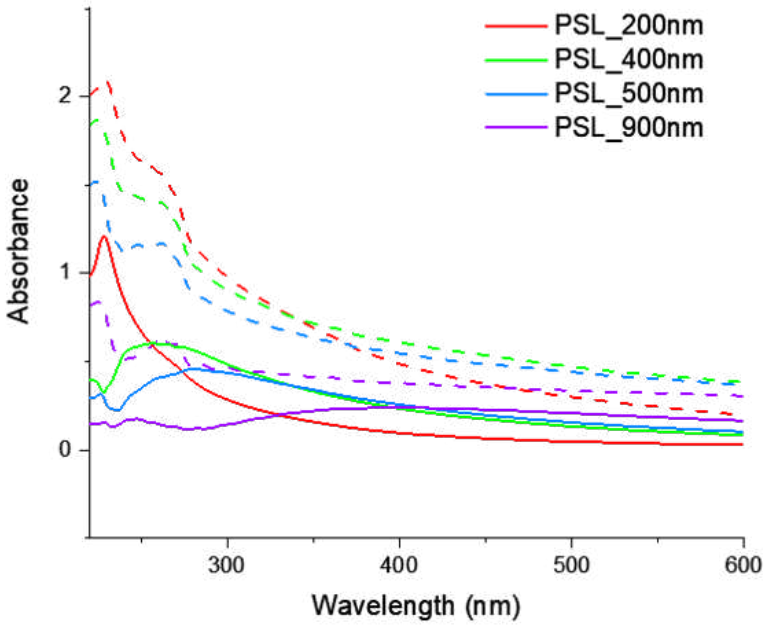


*Figure 1.24: Absorbance spectra of PSL-NF of different diameters. Full lines show the absorbance in direct measurement mode and dashed lines show the absorbance using the integrating sphere (Measurements were done with a UV-2600 UV-Visible Spectrophotometer, Shimadzu, Japan).*

Finally, scattering spectroscopy techniques such as small-angle neutron scattering (SANS) and Ultra SANS (USANS) can analyze particle interactions. Unlike microscopy, SANS allows for in situ measurements of size, shape, and aggregation of particles. The neutrons are non-destructive, and the continuous phase of the dispersion can be modified to reduce its signal and observe only the particles (i.e.: contrast matching) (A. F. Astner et al. 2020). The spectra obtained show the relationship between the intensity and angle of the neutron beam. After fitting a power law, zones of excess scattering are observed and fitted using form factors to obtain volume fractions and polydispersity of the particles or aggregates. For example, SANS was used to characterize proteins' conformation on *PSL-COOH(-)* (Kihara et al. 2019).

### 1.3.5 Interpretation in light of theoretical frameworks

Several studies have interpreted their results in light of the DLVO theory of colloidal stability (Alimi, Farner, and Tufenkji 2021; Mao et al. 2020; J. Wu et al. 2019; Yu, Shen, et al. 2019; Y. Liu et al. 2019). Most have observed that their results obey the DLVO theory, except in cases where steric repulsion occurs and was not modeled by the XDLVO (Yu, Shen, et al. 2019) or in cases where particle composition changed due to aging(Y.

Liu et al. 2019). Several studies have also used the theoretical framework of collision rates ($\beta$) and attachment efficiencies ($\alpha$). Methods to determine aggregation rate ($k_{agg}$) varied between studies. Some studies base it on a specific linear section of a kinetic study ((Mao et al. 2020; Yu, Shen, et al. 2019). Indeed, aggregation rate can first be a linear function of time and then reach a plateau. The linear section is sometimes determined visually or other times defined as the time at which the initial size increased by 25% (Yu, Shen, et al. 2019). Others do not specify how the two aggregation rates were measured, suggesting implicitly that it is calculated over the entire aggregation duration (Singh et al. 2019). These methods must be described to correctly compare studies.

## 1.4 Nanoplastics transport and retention in interfaces of the hydrosphere

As discussed in section 1.2 and described in Figure 1.3, nanoplastic aggregation in water is only one process that dictates nanoplastics' environmental fate. Other critical processes occur in **environmental interfaces**. Interfaces are zones where the structure or function of an environmental system changes abruptly over space or time. Interfaces can be thought of as *[...] a semipermeable membrane regulating the flow of energy and material between adjacent environmental patches. [...] Interfaces between adjacent ecological systems have a set of characteristics uniquely defined by space and time scales and by the strength of interactions between the adjacent systems.* (Naiman et al. 1988). Interfaces have been called interchangeably transition zone, ecotone, and boundary. From the point of view of physicochemists and hydrologists studying the flux of colloids, interfaces are zones that impact particle's transformations and motion due to the presence of physical and chemical gradients.

Interfaces' physicochemical gradients are controlled by the properties of the environmental systems at each extremity of the interface. Estuaries, with their salinity gradients are emblematic examples of interfaces (Griffiths et al. 2017). Different estuaries have different salinity gradients, depending on the salinity of the river and sea, as well as the speed at which these waters mix (which depends on the river flow rate and the sea's turbulence). Figure 1.25 illustrates some spatial physicochemical gradients that exist in environmental systems. For example, porous media (e.g.: soils, sediments and aquifers) contain velocity gradients (Figure 1.25a), but can also contain gradients of charge and hydrophobicity on the solid matrix, as well as gradients of dissolved gases and solutes in the liquid. Figure 1.25b shows that the interface between seawater and sea ice contains gradients in salinity. There are also temperature gradients and flow velocity gradients

(not represented)(Thomas and Dieckmann 2003). For both of these interfaces, gradients can also develop through time. For example, as the soil dries up, gradients in moisture occur, and as sea ice melts and refreezes, salinity gradients are modified.

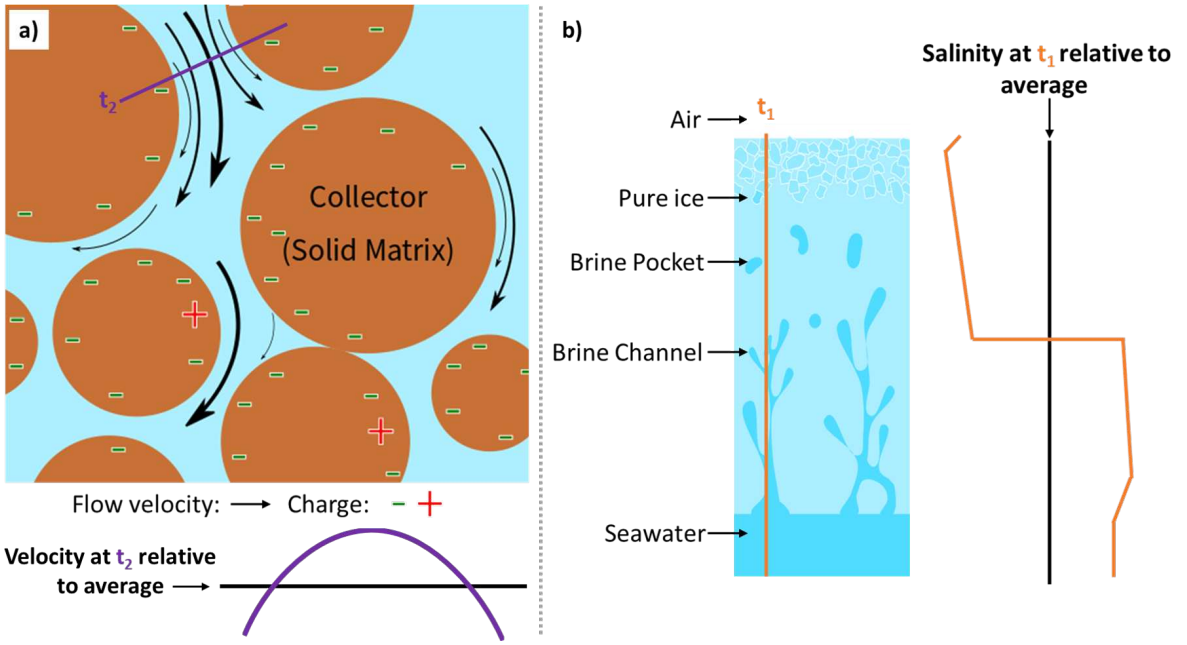


*Figure 1.25: Schematics of a) terrestrial solid/liquid interfaces, showing various charges and gradients in velocity and b) polar solid/liquid interface showing gradients in salinity (not to scale).*

Therefore, studying nanoplastic transport across interfaces provides the focused lens of physicochemical gradients to better constrain probable transport mechanisms and accumulation zones of nanoplastics in the environment.

### 1.4.1 Solid/Liquid interfaces of continental systems: porous media

The transport of particulate and colloidal contaminants in subsurface environments has been extensively studied to protect potable water from pathogens or colloidal contaminants (McDowell-Boyer, Hunt, and Sitar 1986). The transport of particles and their transformations along the way (e.g.: degradation to smaller molecular weights, sorption of NOM, etc.) determines which environmental system it will impact and the hazard it may pose. For example, depending on the strength of precipitation (e.g.: rain, snow, etc.) and geographical features (e.g.: soil type, slope, etc.) a portion of nanoplastics can be carried by surface run-off while the other percolates underground. The fraction that is transported by surface run-off quickly reaches streams and rivers. In contrast, the fraction that percolates vertically can accumulate in the unsaturated zone which is rich

in biological activity and the foundations of the terrestrial food web, or deeper, into the saturated zone, where it forms part of the groundwater stocks. This vertical transport is often conceptualized as transport in porous media (Elimelech 1998; McDowell-Boyer, Hunt, and Sitar 1986).

A rich body of knowledge, techniques, and theory has been developed concerning colloidal transport and deposition in porous media, with studies using different approaches, length-scales and degrees of complexity, as well as the development of several theoretical frameworks (Babakhani et al. 2017; Molnar et al. 2015). Two distinct approaches exist to study colloidal transport: the Lagrangian approach, which deals with individual particles, and the Eulerian approach, which deals with entire colloidal populations using advection and diffusion equations.

- At the particle scale, colloidal transport can be assessed by studying the forces acting between the colloid and a surface. This can be achieved using Quartz Crystal MicroBalance with dissipation monitoring (QCM-D)(McNew et al. 2017; Seymour et al. 2013).
- At a slightly larger scale (a few micrometers), transport has been modeled in controlled pores, with microfluidic systems (Baumann, Toops, and Niessner 2010; Venel et al. 2021). These methods can track particles down to sizes of approximately 200 nm using confocal microscopy.
- Zooming out from the pore scale, transport has been studied in columns with 3-dimensional network of pores composed of a variety of different media, ranging in complexity from glass beads (Elimelech and O'Melia 1990) to sand (Bradford, Torkzaban, and Walker 2007), soils (Quevedo and Tufenkji 2012), and rocks (Chinju et al. 2001). While they are more representative of environmental systems, the difficulty is to understand what occurs *in-situ*.
- Finally, colloidal transport has been tracked in the environment by collecting samples at appropriate spatiotemporal intervals (McDowell-Boyer, Hunt, and Sitar 1986).

For each of these approaches, different degrees of complexity exist (illustrated in Figure 1.26). For example, the surface type can be entirely controlled and homogenous (e.g.: glass beads with controlled shape and chemistry) or have controlled complexity (e.g.: addition of surface coatings, creating irregular but controlled pores in microfluidic systems). Complexity starts being less controlled and therefore less easy to model as soon as environmental media is used. The simplest environmental media is quartz sand, as its composition can be practically pure. Indeed, quartz sand, while mainly composed of silicon dioxide ($SiO_2$) can also contain other minerals (e.g.: $Al_2O_3$), as well as NOM if

it is not extensively washed). Despite this, even the most smooth and spherical natural quartz sand has irregular physical features at the scale of a colloid which are difficult to integrate in conceptual frameworks (Molnar et al. 2015; Sefrioui et al. 2013).


*Figure 1.26: Parameters that can be complexified (inner circles) and degrees of complexity (outer circles) for experiments studying terrestrial porous media.*

### 1.4.2 Solid/Liquid interfaces of polar systems: sea ice

As opposed to particle aggregation and deposition, the transport of particles into and out of sea ice has been largely understudied. This could be explained by difficulties accessing and sampling sea ice and by the fact that polar environments are often perceived as pristine due to their remoteness. The study of particle fluxes into and out of sea ice lacks a conceptual framework due to the inherent complexity of this system. Indeed, the frozen water, that acts as the solid part of this interface, is orders of magnitude more dynamic than the solid fraction of porous media. While terrestrial interfaces change over decadal to centennial time scales (e.g.: bedrock weathering and soil formation), sea ice is rapidly impacted by changing weather. Seawater can freeze within hours and even the structure of old (multi-annual) ice varies over months. The structure and porosity of sea ice result

from the environmental conditions in which sea ice has grown and aged (Eicken 2003).

Sea ice results from the freezing of seawater, either as land-fast ice (attached to continental surfaces) or pack ice (in open waters). Seawater freezes as soon as surface temperatures persist under the freezing point of seawater (-1.86 °C for seawater with 34 Practical Salinity Units). As seawater freezes it expulses impurities (electrolytes, dissolved gases, and particles) from its pure crystalline structure. Most of these dissolved species accumulate in localized areas of the sea ice, which leads to the formation of bubbles (when gas' solubility limits are exceeded) and brine pockets (as salts lower the freezing temperature of the liquid), as illustrated in Figure 1.27a. As sea ice grows, some brine pockets get expelled to the surface due to the pressure of expanding ice, and others coalesce and drain to the underlying seawater, forming brine channels (Figure 1.25b). These brine channels create a highly interconnected porosity (≈30%) in the transitional layer between the ice and the underlying liquid (Eicken 2003). Brine channels play an essential geochemical and biological role since they enable the transfer of dissolved and particulate species and organisms between seawater and ice. At micrometric scales, sea ice structure can be viewed as the relative ratio of pure crystalline ice, brine pockets, gas bubbles, and brines channels, the degree to which these three are interconnected, and the texture of the pure ice crystals.

Large-scale processes also shape sea ice structure. Winds structure sea ice by causing ice packs to deconsolidate or collide. The upper portion of sea ice is restructured more easily by melting and freezing than deeper portions that are more thermally insulated. Meltwater from the sea ice surface can seep into the sea ice. In the Arctic Ocean, sea ice receives significant amounts of snowfall which can cause sea ice to sink into seawater. Seawater then infiltrates into the sea ice due to the porosity of sea ice and due to the higher heat and salinity of seawater which can melt the ice. Finally, biological activity has a relatively minor role in restructuring sea ice. Microorganisms' secretions (Figure 1.27b) can modify water's freezing point and, therefore, the porosity of sea ice, but organisms larger than 1 mm have little to no role in re-structuring sea ice since their movement in sea ice is limited by brine channel width (Eicken 2003; Arrigo, Mock, and Lizotte 2009; Bluhm, Gradinger, and Schnack-Schiel 2009; Deming 2009). As ice ages, various processes can modify its structure, such as temperature cycles, precipitation, wind and ocean turbulence, biological activity, etc. Therefore, there are as many types of sea ice structures as there are combinations of environmental processes.

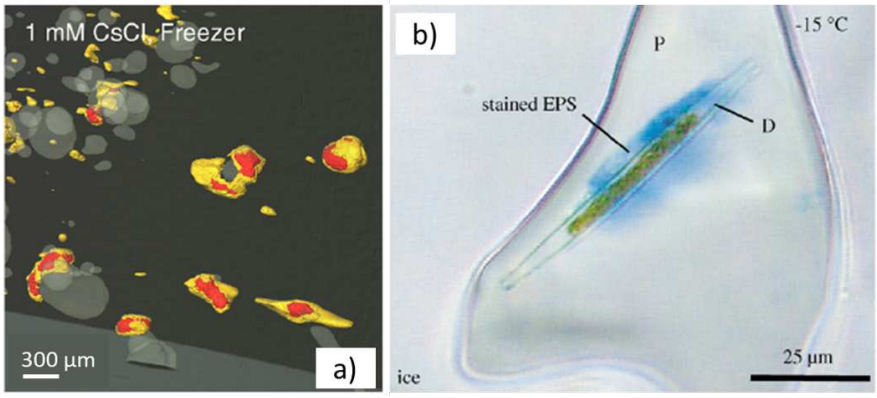


*Figure 1.27: Illustrations of ice porosity a) created by freezing CsCl and imaging ice by micro-computed tomography. Air bubbles in light gray, ice matrix in darker gray, low concentrations of CsCl in yellow and high concentrations in red. b) observed in Arctic sea ice and showing a diatom (D) and its EPS in a pore (P). (Reproduced from a) Crabeck et al. 2015, and b) Krembs et al. 2002, Creative Commons 4.0 License).*

The mobility of suspended particles (e.g.: sediments, microorganisms, or plastics) during sea ice growth is complex. Particles are enriched in sea ice relative to seawater by processes such as entrainment by ice during the early stages of freezing in turbulent conditions and entrapment during the growth of sea ice in calmer waters (Eicken 2003). However, these processes are highly dependent on the nature of the particle. For example, microorganisms are most abundant at the surface and in the transitional layer due to the importance of liquid and space for their survival (Arrigo, Mock, and Lizotte 2009; Deming 2009), while sediments are suspended by turbulences, which explains their location in frazil ice (Ito et al. 2019). In summary, the processes of particle entrapment by sea ice cannot be generalized to predict how nanoplastics may become trapped. Nanoplastics' entrapment during sea ice growth is particularly important to study because i) nanoplastics are expected to be abundant in the Arctic (Andrés Cózar et al. 2017; Rowlands, T. Galloway, and Manno 2021; van Sebille, England, and Froyland 2012) and ii) due to climate change, most sea ice is expected to form annually not surviving its first winter (Perovich et al. 2020). Once particles are in the ice structure, they may become trapped by processes similar to those that occur in terrestrial porous media (e.g.: retention in zones of low water flow, physical entrapment in constriction, etc.) as well as other specific processes, such as capillary forces as brine channels solidify or drain. Finally, particles in sea ice may aggregate due to i) the mechanical stress of ice growth which pushes particles together (Chou et al. 2014), ii) the high salinity, and iii) the presence of NOM with agglomerating potentials, such as EPS (Dumont et al. 2009; Janssens et al. 2016). Once nanoplastics are agglomerated, they may be too large to be flushed out of the ice porosity.

To understand the processes by which particles become included in sea ice, there is a need for experiments with controlled experimental conditions and a systematic assessment of the parameters which may promote or inhibit particle entrapment in ice. Particle inclusion in a freezing front and particle aggregation caused by freezing has been studied from a physical and engineering perspective for a wide range of applications (e.g.: freeze-resistance of paints suspensions (Suzuki et al. 2011), improving the taste of ice cream (Aichinger et al. 2017), dewatering sludge (John, Häkkinen, and Louhi-Kultanen 2020), and producing materials with controlled properties (Sylvain Deville 2013). Particle engulfment at a freezing front that advances at a steady-state has been conceptualized as a balance of attractive interfacial forces and repulsive viscous forces acting on the particle. While the complexity of natural systems (e.g.: presence of salts, particles, and macromolecules) makes modeling particle capture in sea ice difficult, conceptualizations such as these are essential to develop in order to have a more systematic understanding of processes that may inform environmental sampling, as summarized in Figure 1.4.

# References


Aichinger, Pierre-Anton, Christophe Schmitt, Deniz Z. Gunes, Martin E. Leser, Laurent Sagalowicz, and Martin Michel (Mar. 2017). "Phase Separation in Food Material Design Inspired by Nature". en. In: *Current Opinion in Colloid & Interface Science* 28, pp. 56–62. ISSN: 13590294. DOI: 10.1016/j.cocis.2017.03.002.

Alimi, Olubukola S., Jeffrey M. Farner, and Nathalie Tufenkji (Feb. 2021). "Exposure of Nanoplastics to Freeze-Thaw Leads to Aggregation and Reduced Transport in Model Groundwater Environments". en. In: *Water Research* 189, p. 116533. ISSN: 00431354. DOI: 10.1016/j.watres.2020.116533.

Alimi, Olubukola S., Jeffrey Farner Budarz, Laura M. Hernandez, and Nathalie Tufenkji (Feb. 2018). "Microplastics and Nanoplastics in Aquatic Environments: Aggregation, Deposition, and Enhanced Contaminant Transport". en. In: *Environmental Science & Technology* 52.4, pp. 1704–1724. ISSN: 0013-936X, 1520-5851. DOI: 10.1021/acs.est.7b05559.

Allan, Jacqueline, Birgit Sokull-Kluettgen, and Anil Patri (2020). *Global Summit on Regulatory Science 2019 Nanotechnology and Nanoplastics*. eng. Publications Office of the European Union. ISBN: 978-92-76-18435-5.

Allen, Steve, Deonie Allen, Vernon R. Phoenix, Gaël Le Roux, Pilar Durántez Jiménez, Anaëlle Simonneau, Stéphane Binet, and Didier Galop (Apr. 2019). "Atmospheric Transport and Deposition of Microplastics in a Remote Mountain Catchment". en. In: *Nature Geoscience*. ISSN: 1752-0894, 1752-0908. DOI: 10.1038/s41561-019-0335-5.

Andrady, Anthony L. (Aug. 2011). "Microplastics in the Marine Environment". en. In: *Marine Pollution Bulletin* 62.8, pp. 1596–1605. ISSN: 0025326X. DOI: 10.1016/j.marpolbul.2011.05.030.

Andrady, Anthony L. and Mike A. Neal (July 2009). "Applications and Societal Benefits of Plastics". en. In: *Philosophical Transactions of the Royal Society B: Biological Sciences* 364.1526, pp. 1977–1984. ISSN: 0962-8436, 1471-2970. DOI: 10.1098/rstb.2008.0304.

Arrigo, Kevin R., Thomas Mock, and Michael P. Lizotte (2009). "Primary Producers and Sea Ice". In: *Sea Ice*. John Wiley & Sons, Ltd. Chap. 8, pp. 283–325. ISBN: 978-1-4443-1714-5. DOI: 10.1002/9781444317145.ch8. eprint: https://onlinelibrary.wiley.com/doi/pdf/10.1002/9781444317145.ch8.

Astner, A.F., D.G. Hayes, H. O'Neill, B.R. Evans, S.V. Pingali, V.S. Urban, and T.M. Young (Oct. 2019). "Mechanical Formation of Micro- and Nano-Plastic Materials for Environmental Studies in Agricultural Ecosystems". en. In: *Science of The Total Environment* 685, pp. 1097–1106. ISSN: 00489697. DOI: 10.1016/j.scitotenv.2019.06.241.

Astner, Anton F., Douglas G. Hayes, Sai Venkatesh Pingali, Hugh M. ONeill, Kenneth C. Littrell, Barbara R. Evans, and Volker S. Urban (July 2020). "Effects of Soil Particles and Convective Transport on Dispersion and Aggregation of Nanoplastics via Small-Angle Neutron Scattering (SANS) and Ultra SANS (USANS)". en. In: *PLOS ONE* 15.7. Ed. by Pratheep K. Annamalai, e0235893. ISSN: 1932-6203. DOI: 10.1371/journal.pone.0235893.

Baalousha, M. and J. R. Lead (June 2012). "Rationalizing Nanomaterial Sizes Measured by Atomic Force Microscopy, Flow Field-Flow Fractionation, and Dynamic Light Scattering: Sample Preparation, Polydispersity, and Particle Structure". en. In: *Environmental Science & Technology* 46.11, pp. 6134–6142. ISSN: 0013-936X, 1520-5851. DOI: 10.1021/es301167x.

Baalousha, Mohammed (Apr. 2017). "Effect of Nanomaterial and Media Physicochemical Properties on Nanomaterial Aggregation Kinetics". en. In: *NanoImpact* 6, pp. 55–68. ISSN: 24520748. DOI: 10.1016/j.impact.2016.10.005.

Babakhani, Peyman, Jonathan Bridge, Ruey-an Doong, and Tanapon Phenrat (Aug. 2017). "Continuum-Based Models and Concepts for the Transport of Nanoparticles in Saturated Porous Media: A State-of-the-Science Review". en. In: *Advances in Colloid and Interface Science* 246, pp. 75–104. ISSN: 00018686. DOI: 10.1016/j.cis.2017.06.002.

Bank, Michael S. and Sophia V. Hansson (June 2019). "The Plastic Cycle: A Novel and Holistic Paradigm for the Anthropocene". en. In: *Environmental Science & Technology*, acs.est.9b02942. ISSN: 0013-936X, 1520-5851. DOI: 10.1021/acs.est.9b02942.

Barnard, James G., Matthew N. Rhyner, and John F. Carpenter (Jan. 2012). "Critical Evaluation and Guidance for Using the Coulter Method for Counting Subvisible Particles in Protein Solutions". en. In: *Journal of Pharmaceutical Sciences* 101.1, pp. 140–153. ISSN: 00223549. DOI: 10.1002/jps.22732.

Baumann, Thomas, Laura Toops, and Reinhard Niessner (Feb. 2010). "Colloid Dispersion on the Pore Scale". en. In: *Water Research* 44.4, pp. 1246–1254. ISSN: 00431354. DOI: 10.1016/j.watres.2009.11.035.

Benner, Ronald (Jan. 2002). "Chapter 3 - Chemical Composition and Reactivity". In: *Biogeochemistry of Marine Dissolved Organic Matter*. Ed. by Dennis A. Hansell and Craig A. Carlson. San Diego: Academic Press, pp. 59–90. ISBN: 978-0-12-323841-2. DOI: 10.1016/B978-012323841-2/50005-1.

Bergami, E., A. Krupinski Emerenciano, M. González-Aravena, C. A. Cárdenas, P. Hernández, J. R. M. C. Silva, and I. Corsi (Apr. 2019). "Polystyrene Nanoparticles Affect the Innate Immune System of the Antarctic Sea Urchin Sterechinus Neumayeri". en. In: *Polar Biology* 42.4, pp. 743–757. ISSN: 0722-4060, 1432-2056. DOI: 10.1007/s00300-019-02468-6.

Bergmann, Melanie, Sophia Mützel, Sebastian Primpke, Mine B. Tekman, Jürg Trachsel, and Gunnar Gerdts (Aug. 2019). "White and Wonderful? Microplastics Prevail in Snow from the Alps to the Arctic". en. In: *Science Advances* 5.8, eaax1157. ISSN: 2375-2548. DOI: 10.1126/sciadv.aax1157.

Besseling, Ellen, Joris T.K. Quik, Muzhi Sun, and Albert A. Koelmans (Jan. 2017). "Fate of Nano- and Microplastic in Freshwater Systems: A Modeling Study". en. In: *Environmental Pollution* 220, pp. 540–548. ISSN: 02697491. DOI: 10.1016/j.envpol.2016.10.001.

Bhattacharjee, Subir, Jeffrey Y. Chen, and Menachem Elimelech (May 2000). "DLVO Interaction Energy between Spheroidal Particles and a Flat Surface". en. In: *Colloids and Surfaces A: Physicochemical and Engineering Aspects* 165.1-3, pp. 143–156. ISSN: 09277757. DOI: 10.1016/S0927-7757(99)00448-3.

Bhattacharjee, Subir and Menachem Elimelech (Sept. 1997). "Surface Element Integration: A Novel Technique for Evaluation of DLVO Interaction between a Particle and a Flat Plate". en. In: *Journal of Colloid and Interface Science* 193.2, pp. 273–285. ISSN: 00219797. DOI: 10.1006/jcis.1997.5076.

Bhattacharjee, Subir, Chun-Han Ko, and Menachem Elimelech (June 1998). "DLVO Interaction between Rough Surfaces". en. In: *Langmuir* 14.12, pp. 3365–3375. ISSN: 0743-7463, 1520-5827. DOI: 10.1021/la971360b.

Bluhm, Bodil A., Rolf R. Gradinger, and Sigrid B. Schnack-Schiel (2009). "Sea Ice Meio- and Macrofauna". In: *Sea Ice*. John Wiley & Sons, Ltd. Chap. 10, pp. 357–393. ISBN: 978-1-4443-1714-5. DOI: 10.1002/9781444317145.ch10. eprint: https://onlinelibrary.wiley.com/doi/pdf/10.1002/9781444317145.ch10.

Bradford, Scott A., Hyunjung Kim, Chongyang Shen, Salini Sasidharan, and Jianying Shang (Sept. 2017). "Contributions of Nanoscale Roughness to Anomalous Colloid Retention and Stability Behavior". en. In: *Langmuir* 33.38, pp. 10094–10105. ISSN: 0743-7463, 1520-5827. DOI: 10.1021/acs.langmuir.7b02445.

Bradford, Scott A. and Saeed Torkzaban (Mar. 2013). "Colloid Interaction Energies for Physically and Chemically Heterogeneous Porous Media". en. In: *Langmuir* 29.11, pp. 3668–3676. ISSN: 0743-7463, 1520-5827. DOI: 10.1021/la400229f.

Bradford, Scott A., Saeed Torkzaban, and Sharon L. Walker (July 2007). "Coupling of Physical and Chemical Mechanisms of Colloid Straining in Saturated Porous Media". en. In: *Water Research* 41.13, pp. 3012–3024. ISSN: 00431354. DOI: 10.1016/j.watres.2007.03.030.

Brown, Paul L. and Christian Ekberg (2016). *Hydrolysis of Metal Ions*. Wiley-VCH Verlag GmbH & Co. KGaA. ISBN: 978-3-527-65621-9.

Buffle, Jacques, Kevin J. Wilkinson, Serge Stoll, Montserrat Filella, and Jingwu Zhang (Oct. 1998). "A Generalized Description of Aquatic Colloidal Interactions: The Three-Colloidal Component Approach". en. In: *Environmental Science & Technology* 32.19, pp. 2887–2899. ISSN: 0013-936X, 1520-5851. DOI: 10.1021/es980217h.

Burdige, David J. (Jan. 2002). "Chapter 13 - Sediment Pore Waters". In: *Biogeochemistry of Marine Dissolved Organic Matter*. Ed. by Dennis A. Hansell and Craig A. Carlson. San Diego: Academic Press, pp. 611–663. ISBN: 978-0-12-323841-2. DOI: 10.1016/B978-012323841-2/50015-4.

Bystrzejewska-Piotrowska, Grazyna, Jerzy Golimowski, and Pawel L. Urban (Sept. 2009). "Nanoparticles: Their Potential Toxicity, Waste and Environmental Management". en. In: *Waste Management* 29.9, pp. 2587–2595. ISSN: 0956053X. DOI: 10.1016/j.wasman.2009.04.001.

Cai, Li, Lingling Hu, Huahong Shi, Junwei Ye, Yunfei Zhang, and Hyunjung Kim (Apr. 2018). "Effects of Inorganic Ions and Natural Organic Matter on the Aggregation of Nanoplastics". en. In: *Chemosphere* 197, pp. 142–151. ISSN: 00456535. DOI: 10.1016/j.chemosphere.2018.01.052.

Canesi, Laura, Caterina Ciacci, Rita Fabbri, Teresa Balbi, Annalisa Salis, Gianluca Damonte, Katia Cortese, Valentina Caratto, Marco P. Monopoli, Kenneth Dawson, Elisa Bergami, and Ilaria Corsi (Oct. 2016). "Interactions of Cationic Polystyrene Nanoparticles with Marine Bivalve Hemocytes in a Physiological Environment: Role of Soluble Hemolymph Proteins". en. In: *Environmental Research* 150, pp. 73–81. ISSN: 00139351. DOI: 10.1016/j.envres.2016.05.045.

Catrouillet, Charlotte, Benjamin Mazeaud, Bruno Grassl, Florent Blancho, and Julien Gigault (2021 (Submitted)). "Speciation of Metals in Solution: A New Paradigm for the Nanoplastics Aggregation Evaluation". In: *Journal of the American Chemical Society*.

Chamas, Ali, Hyunjin Moon, Jiajia Zheng, Yang Qiu, Tarnuma Tabassum, Jun Hee Jang, Mahdi Abu-Omar, Susannah L. Scott, and Sangwon Suh (Feb. 2020). "Degradation Rates of Plastics in the Environment". en. In: *ACS Sustainable Chemistry & Engineering*, acssuschemeng.9b06635. ISSN: 2168-0485, 2168-0485. DOI: 10.1021/acssuschemeng.9b06635.

Chen, Chi-Shuo, Clarence Le, Meng-Hsuen Chiu, and Wei-Chun Chin (Sept. 2018). "The Impact of Nanoplastics on Marine Dissolved Organic Matter Assembly". en. In: *Science of The Total Environment* 634, pp. 316–320. ISSN: 00489697. DOI: 10.1016/j.scitotenv.2018.03.269.

Chen, Ziying, Junhong Liu, Chengyu Chen, and Zhujian Huang (Mar. 2020). "Sedimentation of Nanoplastics from Water with Ca/Al Dual Flocculants: Characterization, Interface Reaction, Effects of pH and Ion Ratios". en. In: *Chemosphere*, p. 126450. ISSN: 00456535. DOI: 10.1016/j.chemosphere.2020.126450.

Chinju, Hirofumi, Yoshio Kuno, Shinya Nagasaki, and Satoru Tanaka (June 2001). "Deposition Behavior of Polystyrene Latex Particles on Solid Surfaces during Migration through an Artificial Fracture in a Granite

Rock Sample". en. In: *Journal of Nuclear Science and Technology* 38.6, pp. 439–443. ISSN: 0022-3131, 1881-1248. DOI: 10.1080/18811248.2001.9715051.

Chou, Kan-Sen, Hsuan-Liang Liu, Li-Hsing Kao, Chi-Ming Yang, and Shu-Hao Huang (Apr. 2014). "A Quick and Simple Method to Test Silica Colloids' Ability to Resist Aggregation". en. In: *Colloids and Surfaces A: Physicochemical and Engineering Aspects* 448, pp. 115–118. ISSN: 09277757. DOI: 10.1016/j.colsurfa.2014.02.020.

Clavier, Arnaud, Antonia Praetorius, and Serge Stoll (Feb. 2019). "Determination of Nanoparticle Heteroaggregation Attachment Efficiencies and Rates in Presence of Natural Organic Matter Monomers. Monte Carlo Modelling". en. In: *Science of The Total Environment* 650, pp. 530–540. ISSN: 00489697. DOI: 10.1016/j.scitotenv.2018.09.017.

Cózar, A., F. Echevarria, J. I. Gonzalez-Gordillo, X. Irigoien, B. Ubeda, S. Hernandez-Leon, A. T. Palma, S. Navarro, J. Garcia-de-Lomas, A. Ruiz, M. L. Fernandez-de-Puelles, and C. M. Duarte (July 2014). "Plastic Debris in the Open Ocean". en. In: *Proceedings of the National Academy of Sciences* 111.28, pp. 10239–10244. ISSN: 0027-8424, 1091-6490. DOI: 10.1073/pnas.1314705111.

Cózar, Andrés, Elisa Martí, Carlos M. Duarte, Juan García-de-Lomas, Erik van Sebille, Thomas J. Ballatore, Victor M. Eguíluz, J. Ignacio González-Gordillo, Maria L. Pedrotti, Fidel Echevarría, Romain Troublè, and Xabier Irigoien (Apr. 2017). "The Arctic Ocean as a Dead End for Floating Plastics in the North Atlantic Branch of the Thermohaline Circulation". In: *Science Advances* 3.4, e1600582. DOI: 10.1126/sciadv.1600582.

Crabeck, O, R J Galley, B Delille, and B G T Else (2015). "Imaging Air Volume Fraction in Sea Ice Using Non-Destructive X-Ray Tomography". en. In: *Discussion Paper*, p. 49.

Crandon, Lauren E., Kylie M. Boenisch, Bryan J. Harper, and Stacey L. Harper (June 2020). "Adaptive Methodology to Determine Hydrophobicity of Nanomaterials in Situ". en. In: *PLOS ONE* 15.6. Ed. by Amitava Mukherjee, e0233844. ISSN: 1932-6203. DOI: 10.1371/journal.pone.0233844.

da Costa, João Pinto, Patrícia S.M. Santos, Armando C. Duarte, and Teresa Rocha-Santos (Oct. 2016). "(Nano)Plastics in the Environment Sources, Fates and Effects". en. In: *Science of The Total Environment* 566-567, pp. 15–26. ISSN: 00489697. DOI: 10.1016/j.scitotenv.2016.05.041.

Dale, Amy L., Elizabeth A. Casman, Gregory V. Lowry, Jamie R. Lead, Enrica Viparelli, and Mohammed Baalousha (Mar. 2015). "Modeling Nanomaterial Environmental Fate in Aquatic Systems". en. In: *Environmental Science & Technology* 49.5, pp. 2587–2593. ISSN: 0013-936X, 1520-5851. DOI: 10.1021/es505076w.

Dawson, Amanda L., So Kawaguchi, Catherine K. King, Kathy A. Townsend, Robert King, Wilhelmina M. Huston, and Susan M. Bengtson Nash (Dec. 2018). "Turning Microplastics into Nanoplastics through Digestive Fragmentation by Antarctic Krill". en. In: *Nature Communications* 9.1. ISSN: 2041-1723. DOI: 10.1038/s41467-018-03465-9.

Della Torre, C., E. Bergami, A. Salvati, C. Faleri, P. Cirino, K. A. Dawson, and I. Corsi (Oct. 2014). "Accumulation and Embryotoxicity of Polystyrene Nanoparticles at Early Stage of Development of Sea Urchin Embryos *Paracentrotus Lividus*". en. In: *Environmental Science & Technology* 48.20, pp. 12302–12311. ISSN: 0013-936X, 1520-5851. DOI: 10.1021/es502569w.

Deming, Jody W. (2009). "Sea Ice Bacteria and Viruses". In: *Sea Ice*. John Wiley & Sons, Ltd. Chap. 7, pp. 247–282. ISBN: 978-1-4443-1714-5. DOI: 10.1002/9781444317145.ch7. eprint: https://onlinelibrary.wiley.com/doi/pdf/10.1002/9781444317145.ch7.

Derjaguin, B and L Landau (May 1993). "Theory of the Stability of Strongly Charged Lyophobic Sols and of the Adhesion of Strongly Charged Particles in Solutions of Electrolytes". en. In: *Progress in Surface Science* 43.1-4, pp. 30–59. ISSN: 00796816. DOI: 10.1016/0079-6816(93)90013-L.

Deville, Sylvain (Sept. 2013). "Ice-Templating, Freeze Casting: Beyond Materials Processing". en. In: *Journal of Materials Research* 28.17, pp. 2202–2219. ISSN: 0884-2914, 2044-5326. DOI: 10.1557/jmr.2013.105.

Dong, Zhiqiang, Wen Zhang, Yuping Qiu, Zhenglong Yang, Junliang Wang, and Yidi Zhang (Jan. 2019). "Cotransport of Nanoplastics (NPs) with Fullerene (C60) in Saturated Sand: Effect of NPs/C60 Ratio and Seawater Salinity". en. In: *Water Research* 148, pp. 469–478. ISSN: 00431354. DOI: 10.1016/j.watres.2018.10.071.

Dumont, I., V. Schoemann, D. Lannuzel, L. Chou, J.-L. Tison, and S. Becquevort (May 2009). "Distribution and Characterization of Dissolved and Particulate Organic Matter in Antarctic Pack Ice". en. In: *Polar Biology* 32.5, pp. 733–750. ISSN: 0722-4060, 1432-2056. DOI: 10.1007/s00300-008-0577-y.

Dwivedi, Amarendra Dhar, Shashi Prabha Dubey, Mika Sillanpää, Young-Nam Kwon, Changha Lee, and Rajender S. Varma (Mar. 2015). "Fate of Engineered Nanoparticles: Implications in the Environment". en. In: *Coordination Chemistry Reviews* 287, pp. 64–78. ISSN: 00108545. DOI: 10.1016/j.ccr.2014.12.014.

Efimova, Irina, Margarita Bagaeva, Andrei Bagaev, Alexander Kileso, and Irina P. Chubarenko (Sept. 2018). "Secondary Microplastics Generation in the Sea Swash Zone With Coarse Bottom Sediments: Laboratory Experiments". en. In: *Frontiers in Marine Science* 5, p. 313. ISSN: 2296-7745. DOI: 10.3389/fmars.2018.00313.

Eicken, Hajo (May 2003). "From the Microscopic, to the Macroscopic, to the Regional Scale: Growth, Microstructure and Properties of Sea Ice". en. In: *Sea Ice*. Ed. by David N. Thomas and Gerhard S. Dieckmann. Oxford, UK: Blackwell Science Ltd, pp. 22–81. ISBN:

978-0-470-75716-1 978-0-632-05808-2. DOI: 10.1002/9780470757161.ch2.

Einstein, A. (Jan. 1905). "Über Die von Der Molekularkinetischen Theorie Der Wärme Geforderte Bewegung von in Ruhenden Flüssigkeiten Suspendierten Teilchen". In: *Annalen der Physik* 322.8, pp. 549–560. DOI: 10.1002/andp.19053220806.

Elhacham, Emily, Liad Ben-Uri, Jonathan Grozovski, Yinon M. Bar-On, and Ron Milo (Dec. 2020). "Global Human-Made Mass Exceeds All Living Biomass". en. In: *Nature* 588.7838, pp. 442–444. ISSN: 0028-0836, 1476-4687. DOI: 10.1038/s41586-020-3010-5.

Elimelech, Menachem, ed. (1998). *Particle Deposition and Aggregation: Measurement, Modelling and Simulation*. en. Colloid and Surface Engineering Series. Oxford: Butterworth-Heinemann. ISBN: 978-0-7506-7024-1.

Elimelech, Menachem and Charles R. O'Melia (June 1990). "Effect of Particle Size on Collision Efficiency in the Deposition of Brownian Particles with Electrostatic Energy Barriers". en. In: *Langmuir* 6.6, pp. 1153–1163. ISSN: 0743-7463, 1520-5827. DOI: 10.1021/la00096a023.

Eriksen, Marcus, Sherri Mason, Stiv Wilson, Carolyn Box, Ann Zellers, William Edwards, Hannah Farley, and Stephen Amato (Dec. 2013). "Microplastic Pollution in the Surface Waters of the Laurentian Great Lakes". en. In: *Marine Pollution Bulletin* 77.1-2, pp. 177–182. ISSN: 0025326X. DOI: 10.1016/j.marpolbul.2013.10.007.

Fan, Wei, Xuehui Jiang, Ying Lu, Mingxin Huo, Shanshan Lin, and Zhi Geng (Sept. 2015). "Effects of Surfactants on Graphene Oxide Nanoparticles Transport in Saturated Porous Media". en. In: *Journal of Environmental Sciences* 35, pp. 12–19. ISSN: 10010742. DOI: 10.1016/j.jes.2015.02.007.

Filella, Montserrat (Jan. 2007). "Colloidal Properties of Submicron Particles in Natural Waters". en. In: *Environmental Colloids and Particles*. Ed. by Kevin J. Wilkinson and Jamie R. Lead. Chichester, UK: John Wiley & Sons, Ltd, pp. 17–93. ISBN: 978-0-470-02453-9 978-0-470-02432-4 978-0-470-02433-1. DOI: 10.1002/9780470024539.ch2.

Flemming, Hans-Curt and Jost Wingender (Sept. 2010). "The Biofilm Matrix". en. In: *Nature Reviews Microbiology* 8.9, pp. 623–633. ISSN: 1740-1526, 1740-1534. DOI: 10.1038/nrmicro2415.

Fritz, Gerhard, Volker Schädler, Norbert Willenbacher, and Norman J. Wagner (Aug. 2002). "Electrosteric Stabilization of Colloidal Dispersions". en. In: *Langmuir* 18.16, pp. 6381–6390. ISSN: 0743-7463, 1520-5827. DOI: 10.1021/la015734j.

Fu, Wanyi (2018). "Measurement of the Surface Hydrophobicity of Engineered Nanoparticles Using an Atomic Force Microscope". en. In: p. 10.

Galgani, Francois, Aleke Stoefen-o Brien, Judith Weis, Christos Ioakeimidis, Qamar Schuyler, Iryna Makarenko, Huw Griffiths, Joan Bondareff, Dick Vethaak, Alan Deidun, Paula Sobral, Konstantinos Topouzelis, Penny Vlahos, Fernanda Lana, Martin Hassellov, Olivia Gerigny, Bera Arsonina, Archis Ambulkar, Maurizio Azzaro, and Maria João Bebianno (Dec. 2021). "Are Litter, Plastic and Microplastic Quantities Increasing in the Ocean?" en. In: *Microplastics and Nanoplastics* 1.1, p. 2. ISSN: 2662-4966. DOI: 10.1186/s43591-020-00002-8.

Galgani, Luisa and Steven A. Loiselle (Sept. 2020). "Plastic Pollution Impacts on Marine Carbon Biogeochemistry". en. In: *Environmental Pollution*, p. 115598. ISSN: 02697491. DOI: 10.1016/j.envpol.2020.115598.

Geitner, Nicholas K., Niall J. O'Brien, Amalia A. Turner, Enda J. Cummins, and Mark R. Wiesner (Nov. 2017). "Measuring Nanoparticle Attachment Efficiency in Complex Systems". en. In: *Environmental Science & Technology* 51.22, pp. 13288–13294. ISSN: 0013-936X, 1520-5851. DOI: 10.1021/acs.est.7b04612.

GESAMP (1991). *Reducing Environmental Impacts of Coastal Aquaculture*. Tech. rep. 47, p. 35.

— (2015). *Sources, Fate and Effects of Microplastics in the Marine Environment: A Global Assessment*. English. Ed. by PJ Kershaw. GESAMP Reports & Studies Series 90. GESAMP (Group of Experts on the Scientific Aspects of Marine Environmental Protection). ISBN: 1020-4873.

— (2016). "Sources, Fate and Effects of Microplastics in the Marine Environment: Part Two of a Global Assessment". In: 93, p. 220. ISSN: 1020-4873.

Gewert, Berit, Merle M. Plassmann, and Matthew MacLeod (2015). "Pathways for Degradation of Plastic Polymers Floating in the Marine Environment". en. In: *Environmental Science: Processes & Impacts* 17.9, pp. 1513–1521. ISSN: 2050-7887, 2050-7895. DOI: 10.1039/C5EM00207A.

Geyer, Roland, Jenna R. Jambeck, and Kara Lavender Law (July 2017). "Production, Use, and Fate of All Plastics Ever Made". en. In: *Science Advances* 3.7, e1700782. ISSN: 2375-2548. DOI: 10.1126/sciadv.1700782.

Gigault, Julien, Hind El Hadri, Brian Nguyen, Bruno Grassl, Laura Rowenczyk, Nathalie Tufenkji, Siyuan Feng, and Mark Wiesner (May 2021). "Nanoplastics Are Neither Microplastics nor Engineered Nanoparticles". In: *Nature Nanotechnology* 16.5, pp. 501–507. ISSN: 1748-3395. DOI: 10.1038/s41565-021-00886-4.

Gigault, Julien, Hind El Hadri, Stéphanie Reynaud, Elise Deniau, and Bruno Grassl (Nov. 2017). "Asymmetrical Flow Field Flow Fractionation Methods to Characterize Submicron Particles: Application to Carbon-Based Aggregates and Nanoplastics". en. In: *Analytical and Bioanalytical Chemistry* 409.29, pp. 6761–6769. ISSN: 1618-2642, 1618-2650. DOI: 10.1007/s00216-017-0629-7.

Gigault, Julien, Alexandra ter Halle, Magalie Baudrimont, Pierre-Yves Pascal, Fabienne Gauffre, Thuy-Linh Phi, Hind El Hadri, Bruno Grassl, and Stéphanie Reynaud (Apr. 2018). "Current Opinion: What Is a Nanoplas-

tic?" en. In: *Environmental Pollution* 235, pp. 1030–1034. ISSN: 02697491. DOI: 10.1016/j.envpol.2018.01.024.

Gigault, Julien, Boris Pedrono, Benoît Maxit, and Alexandra Ter Halle (Apr. 2016). "Marine Plastic Litter: The Unanalyzed Nano-Fraction". en. In: *Environmental Science: Nano* 3.2, pp. 346–350. ISSN: 2051-8161. DOI: 10.1039/C6EN00008H.

González-Fernández, Carmen, Jordan Toullec, Christophe Lambert, Nelly Le Goïc, Marta Seoane, Brivaela Moriceau, Arnaud Huvet, Mathieu Berchel, Dorothée Vincent, Lucie Courcot, Philippe Soudant, and Ika Paul-Pont (July 2019). "Do Transparent Exopolymeric Particles (TEP) Affect the Toxicity of Nanoplastics on Chaetoceros Neogracile?" en. In: *Environmental Pollution* 250, pp. 873–882. ISSN: 02697491. DOI: 10.1016/j.envpol.2019.04.093.

Goodwin, James William (2004). *Colloids and Interfaces with Surfactants and Polymers: An Introduction*. Wiley. ISBN: 0-470-84143-5.

Grasso, D., K. Subramaniam, M. Butkus, K. Strevett, and J. Bergendahl (Mar. 2002). "A Review of Non-DLVO Interactions in Environmental Colloidal Systems". en. In: *Reviews in Environmental Science and Bio/Technology* 1.1, pp. 17–38. ISSN: 1569-1705, 1572-9826. DOI: 10.1023/A:1015146710500.

Gregory, John (Sept. 1981). "Approximate Expressions for Retarded van Der Waals Interaction". en. In: *Journal of Colloid and Interface Science* 83.1, pp. 138–145. ISSN: 00219797. DOI: 10.1016/0021-9797(81)90018-7.

Griffiths, Jennifer R., Martina Kadin, Francisco J. A. Nascimento, Tobias Tamelander, Anna Törnroos, Stefano Bonaglia, Erik Bonsdorff, Volker Brüchert, Anna Gårdmark, Marie Järnström, Jonne Kotta, Martin Lindegren, Marie C. Nordström, Alf Norkko, Jens Olsson, Benjamin Weigel, Ramunas ydelis, Thorsten Blenckner, Susa Niiranen, and Monika Winder (June 2017). "The Importance of Benthic-Pelagic Coupling for Marine Ecosystem Functioning in a Changing World". en. In: *Global Change Biology* 23.6, pp. 2179–2196. ISSN: 13541013. DOI: 10.1111/gcb.13642.

Hackley, Vincent A. and Marc A. Anderson (Jan. 1989). "Effects of Short-Range Forces on the Long-Range Structure of Hydrous Iron Oxide Aggregates". en. In: *Langmuir* 5.1, pp. 191–198. ISSN: 0743-7463, 1520-5827. DOI: 10.1021/la00085a036.

Hahladakis, John N., Costas A. Velis, Roland Weber, Eleni Iacovidou, and Phil Purnell (Feb. 2018). "An Overview of Chemical Additives Present in Plastics: Migration, Release, Fate and Environmental Impact during Their Use, Disposal and Recycling". en. In: *Journal of Hazardous Materials* 344, pp. 179–199. ISSN: 03043894. DOI: 10.1016/j.jhazmat.2017.10.014.

Happel, John (June 1958). "Viscous Flow in Multiparticle Systems: Slow Motion of Fluids Relative to Beds of Spherical Particles". en. In: *AIChE Journal* 4.2, pp. 197–201. ISSN: 0001-1541, 1547-5905. DOI: 10.1002/aic.690040214.

Harrison, Jesse P., Carl Boardman, Kenneth O'Callaghan, Anne-Marie Delort, and Jim Song (May 2018). "Biodegradability Standards for Carrier Bags and Plastic Films in Aquatic Environments: A Critical Review". en. In: *Royal Society Open Science* 5.5, p. 171792. ISSN: 2054-5703. DOI: 10.1098/rsos.171792.

Hartmann, Nanna B., Thorsten Hüffer, Richard C. Thompson, Martin Hassellöv, Anja Verschoor, Anders E. Daugaard, Sinja Rist, Therese Karlsson, Nicole Brennholt, Matthew Cole, Maria P. Herrling, Maren C. Hess, Natalia P. Ivleva, Amy L. Lusher, and Martin Wagner (Feb. 2019). "Are We Speaking the Same Language? Recommendations for a Definition and Categorization Framework for Plastic Debris". en. In: *Environmental Science & Technology* 53.3, pp. 1039–1047. ISSN: 0013-936X, 1520-5851. DOI: 10.1021/acs.est.8b05297.

Hassan, Puthusserickal A., Suman Rana, and Gunjan Verma (Jan. 2015). "Making Sense of Brownian Motion: Colloid Characterization by Dynamic Light Scattering". en. In: *Langmuir* 31.1, pp. 3–12. ISSN: 0743-7463, 1520-5827. DOI: 10.1021/la501789z.

Haynes, William H., David R. Lide, and Thomas J. Bruno (2015). *CRC Handbook of Chemistry and Physics, 96th Edition*. CRC Press. ISBN: 978-1-4822-6097-7.

Hendren, Christine Ogilvie, Gregory V. Lowry, Jason M. Unrine, and Mark R. Wiesner (Dec. 2015). "A Functional Assay-Based Strategy for Nanomaterial Risk Forecasting". en. In: *Science of The Total Environment* 536, pp. 1029–1037. ISSN: 00489697. DOI: 10.1016/j.scitotenv.2015.06.100.

Hiemenz, Paul C. and Raj. Rajagopalan (1997). *Principles of Colloid and Surface Chemistry*. English. New York; Basel; Hong Kong: Dekker. ISBN: 0-8247-9397-8 978-0-8247-9397-5.

Hoek, Eric M.V. and Gaurav K. Agarwal (June 2006). "Extended DLVO Interactions between Spherical Particles and Rough Surfaces". en. In: *Journal of Colloid and Interface Science* 298.1, pp. 50–58. ISSN: 00219797. DOI: 10.1016/j.jcis.2005.12.031.

Hogg, R., T. W. Healy, and D. W. Fuerstenau (1966). "Mutual Coagulation of Colloidal Dispersions". en. In: *Transactions of the Faraday Society* 62, p. 1638. ISSN: 0014-7672. DOI: 10.1039/tf9666201638.

Horton, Alice A., Alexander Walton, David J. Spurgeon, Elma Lahive, and Claus Svendsen (May 2017). "Microplastics in Freshwater and Terrestrial Environments: Evaluating the Current Understanding to Identify the Knowledge Gaps and Future Research Priorities". en. In: *Science of The Total Environment* 586, pp. 127–141. ISSN: 00489697. DOI: 10.1016/j.scitotenv.2017.01.190.

Hotze, Ernest M., Tanapon Phenrat, and Gregory V. Lowry (2010). "Nanoparticle Aggregation: Challenges to Understanding Transport and Reactivity in the Environ-

ment". en. In: *Journal of Environment Quality* 39.6, p. 1909. ISSN: 1537-2537. DOI: 10.2134/jeq2009.0462.

Huang, Xiaofei, Subir Bhattacharjee, and Eric M. V. Hoek (Feb. 2010). "Is Surface Roughness a "Scapegoat" or a Primary Factor When Defining Particle-Substrate Interactions?" en. In: *Langmuir* 26.4, pp. 2528–2537. ISSN: 0743-7463, 1520-5827. DOI: 10.1021/la9028113.

Israelachvili, Jacob N. (2015). *Intermolecular and Surface Forces*. English.

Ito, Masato, Kay I. Ohshima, Yasushi Fukamachi, Daisuke Hirano, Andrew R. Mahoney, Joshua Jones, Toru Takatsuka, and Hajo Eicken (Dec. 2019). "Favorable Conditions for Suspension Freezing in an Arctic Coastal Polynya". en. In: *Journal of Geophysical Research: Oceans* 124.12, pp. 8701–8719. ISSN: 2169-9275, 2169-9291. DOI: 10.1029/2019JC015536.

IUPAC (1997). "Colloidally Stable". In: *Compendium of Chemical Terminology (the "Gold Book"). Second Edition. Compiled by A. D. McNaught and A. Wilkinson.* Blackwell Scientific Publications. ISBN: 0-9678550-9-8.

Jambeck, J. R., R. Geyer, C. Wilcox, T. R. Siegler, M. Perryman, A. Andrady, R. Narayan, and K. L. Law (Feb. 2015). "Plastic Waste Inputs from Land into the Ocean". en. In: *Science* 347.6223, pp. 768–771. ISSN: 0036-8075, 1095-9203. DOI: 10.1126/science.1260352.

Janssens, Julie, Klaus M. Meiners, Jean-Louis Tison, Gerhard Dieckmann, Bruno Delille, and Delphine Lannuzel (Aug. 2016). "Incorporation of Iron and Organic Matter into Young Antarctic Sea Ice during Its Initial Growth Stages". en. In: *Elem Sci Anth* 4.0, p. 000123. ISSN: 2325-1026. DOI: 10.12952/journal.elementa.000123.

John, Miia, Antti Häkkinen, and Marjatta Louhi-Kultanen (Feb. 2020). "Purification Efficiency of Natural Freeze Crystallization for Urban Wastewaters". en. In: *Cold Regions Science and Technology* 170, p. 102953. ISSN: 0165232X. DOI: 10.1016/j.coldregions.2019.102953.

Johnson, Clifford P., Xiaoyan Li, and Bruce E. Logan (Jan. 1996). "Settling Velocities of Fractal Aggregates". en. In: *Environmental Science & Technology* 30.6, pp. 1911–1918. ISSN: 0013-936X, 1520-5851. DOI: 10.1021/es950604g.

Julienne, Fanon, Nicolas Delorme, and Fabienne Lagarde (Dec. 2019). "From Macroplastics to Microplastics: Role of Water in the Fragmentation of Polyethylene". en. In: *Chemosphere* 236, p. 124409. ISSN: 00456535. DOI: 10.1016/j.chemosphere.2019.124409.

Kihara, Shinji, Nadine J. van der Heijden, Chris K. Seal, Jitendra P. Mata, Andrew E. Whitten, Ingo Köper, and Duncan J. McGillivray (Apr. 2019). "Soft and Hard Interactions between Polystyrene Nanoplastics and Human Serum Albumin Protein Corona". en. In: *Bioconjugate Chemistry* 30.4, pp. 1067–1076. ISSN: 1043-1802, 1520-4812. DOI: 10.1021/acs.bioconjchem.9b00015.

Klein, Sascha, Eckhard Worch, and Thomas P. Knepper (May 2015). "Occurrence and Spatial Distribution of Microplastics in River Shore Sediments of the Rhine-Main Area in Germany". en. In: *Environmental Science & Technology* 49.10, pp. 6070–6076. ISSN: 0013-936X, 1520-5851. DOI: 10.1021/acs.est.5b00492.

Koelmans, Albert A, Merel Kooi, Kara Lavender Law, and Erik van Sebille (Nov. 2017a). "All Is Not Lost: Deriving a Top-down Mass Budget of Plastic at Sea". In: *Environmental Research Letters* 12.11, p. 114028. ISSN: 1748-9326. DOI: 10.1088/1748-9326/aa9500.

Koelmans, Albert A., Ellen Besseling, Edwin Foekema, Merel Kooi, Svenja Mintenig, Bernadette C. Ossendorp, Paula E. Redondo-Hasselerharm, Anja Verschoor, Annemarie P. van Wezel, and Marten Scheffer (Oct. 2017b). "Risks of Plastic Debris: Unravelling Fact, Opinion, Perception, and Belief". en. In: *Environmental Science & Technology* 51.20, pp. 11513–11519. ISSN: 0013-936X, 1520-5851. DOI: 10.1021/acs.est.7b02219.

Kooi, Merel, Egbert H. van Nes, Marten Scheffer, and Albert A. Koelmans (July 2017). "Ups and Downs in the Ocean: Effects of Biofouling on Vertical Transport of Microplastics". en. In: *Environmental Science & Technology* 51.14, pp. 7963–7971. ISSN: 0013-936X, 1520-5851. DOI: 10.1021/acs.est.6b04702.

Kooi, Merel, Sebastian Primpke, Svenja M. Mintenig, Claudia Lorenz, Gunnar Gerdts, and Albert A. Koelmans (July 2021). "Characterizing the Multidimensionality of Microplastics across Environmental Compartments". en. In: *Water Research*, p. 117429. ISSN: 00431354. DOI: 10.1016/j.watres.2021.117429.

Krembs, C, H Eicken, K Junge, and J.W Deming (Dec. 2002). "High Concentrations of Exopolymeric Substances in Arctic Winter Sea Ice: Implications for the Polar Ocean Carbon Cycle and Cryoprotection of Diatoms". In: *Deep Sea Research Part I: Oceanographic Research Papers* 49.12, pp. 2163–2181. ISSN: 0967-0637. DOI: 10.1016/S0967-0637(02)00122-X.

Lambert, Scott and Martin Wagner (Feb. 2016). "Characterisation of Nanoplastics during the Degradation of Polystyrene". en. In: *Chemosphere* 145, pp. 265–268. ISSN: 00456535. DOI: 10.1016/j.chemosphere.2015.11.078.

Lebordais, Marc, Zélie Venel, Julien Gigault, Valerie S. Langlois, and Magalie Baudrimont (Apr. 2021). "Molecular Impacts of Dietary Exposure to Nanoplastics Combined or Not with Arsenic in the Caribbean Mangrove Oysters (Isognomon Alatus)." en. In: *Nanomaterials (Basel, Switzerland)* 11.5. ISSN: 2079-4991. DOI: 10.3390/nano11051151.

Lehner, Roman, Christoph Weder, Alke Petri-Fink, and Barbara Rothen-Rutishauser (Jan. 2019). "Emergence of Nanoplastic in the Environment and Possible Impact on Human Health". en. In: *Environmental Science & Technology*. ISSN: 0013-936X, 1520-5851. DOI: 10.1021/acs.est.8b05512.

Lenz, Robin, Kristina Enders, and Torkel Gissel Nielsen (July 2016). "Microplastic Exposure Studies Should Be Environmentally Realistic". en. In: *Proceedings of the*

*National Academy of Sciences* 113.29, E4121–E4122. ISSN: 0027-8424, 1091-6490. DOI: 10.1073/pnas.1606615113.

Lewis, Simon L. and Mark A. Maslin (Mar. 2015). "Defining the Anthropocene". en. In: *Nature* 519.7542, pp. 171–180. ISSN: 0028-0836, 1476-4687. DOI: 10.1038/nature14258.

Li, Lianzhen, Yongming Luo, Ruijie Li, Qian Zhou, Willie J. G. M. Peijnenburg, Na Yin, Jie Yang, Chen Tu, and Yunchao Zhang (Nov. 2020). "Effective Uptake of Submicrometre Plastics by Crop Plants via a Crack-Entry Mode". In: *Nature Sustainability* 3.11, pp. 929–937. ISSN: 2398-9629. DOI: 10.1038/s41893-020-0567-9.

Li, Yang, Xinjie Wang, Wanyi Fu, Xinghui Xia, Changqing Liu, Jiacheng Min, Wen Zhang, and John Charles Crittenden (Sept. 2019). "Interactions between Nano/Micro Plastics and Suspended Sediment in Water: Implications on Aggregation and Settling". en. In: *Water Research* 161, pp. 486–495. ISSN: 00431354. DOI: 10.1016/j.watres.2019.06.018.

Lin, Shihong and Mark R. Wiesner (Dec. 2012a). "Deposition of Aggregated Nanoparticles  A Theoretical and Experimental Study on the Effect of Aggregation State on the Affinity between Nanoparticles and a Collector Surface". en. In: *Environmental Science & Technology* 46.24, pp. 13270–13277. ISSN: 0013-936X, 1520-5851. DOI: 10.1021/es3041225.

— (July 2012b). "Paradox of Stability of Nanoparticles at Very Low Ionic Strength". en. In: *Langmuir* 28.30, pp. 11032–11041. ISSN: 0743-7463, 1520-5827. DOI: 10.1021/la3016589.

Lithner, Delilah, Åke Larsson, and Göran Dave (Aug. 2011). "Environmental and Health Hazard Ranking and Assessment of Plastic Polymers Based on Chemical Composition". en. In: *Science of The Total Environment* 409.18, pp. 3309–3324. ISSN: 00489697. DOI: 10.1016/j.scitotenv.2011.04.038.

Liu, Yanjun, Yiben Hu, Chen Yang, Chengyu Chen, Weilin Huang, and Zhi Dang (Oct. 2019). "Aggregation Kinetics of UV Irradiated Nanoplastics in Aquatic Environments". en. In: *Water Research* 163, p. 114870. ISSN: 00431354. DOI: 10.1016/j.watres.2019.114870.

López-León, Teresa, Ana B. Jódar-Reyes, Delfi Bastos-González, and Juan L. Ortega-Vinuesa (June 2003). "Hofmeister Effects in the Stability and Electrophoretic Mobility of Polystyrene Latex Particles". en. In: *The Journal of Physical Chemistry B* 107.24, pp. 5696–5708. ISSN: 1520-6106, 1520-5207. DOI: 10.1021/jp0216981.

Lusher, Amy L., Valentina Tirelli, Ian O'Connor, and Rick Officer (Oct. 2015). "Microplastics in Arctic Polar Waters: The First Reported Values of Particles in Surface and Sub-Surface Samples". In: *Scientific Reports* 5.1, p. 14947. ISSN: 2045-2322. DOI: 10.1038/srep14947.

Magrì, Davide, Paola Sánchez-Moreno, Gianvito Caputo, Francesca Gatto, Marina Veronesi, Giuseppe Bardi, Tiziano Catelani, Daniela Guarnieri, Athanassia Athanassiou, Pier Paolo Pompa, and Despina Fragouli (Aug. 2018). "Laser Ablation as a Versatile Tool To Mimic Polyethylene Terephthalate Nanoplastic Pollutants: Characterization and Toxicology Assessment". en. In: *ACS Nano* 12.8, pp. 7690–7700. ISSN: 1936-0851, 1936-086X. DOI: 10.1021/acsnano.8b01331.

Manfra, L., A. Rotini, E. Bergami, G. Grassi, C. Faleri, and I. Corsi (Nov. 2017). "Comparative Ecotoxicity of Polystyrene Nanoparticles in Natural Seawater and Reconstituted Seawater Using the Rotifer Brachionus Plicatilis". en. In: *Ecotoxicology and Environmental Safety* 145, pp. 557–563. ISSN: 01476513. DOI: 10.1016/j.ecoenv.2017.07.068.

Mao, Yufeng, Hong Li, Xiaoliu Huangfu, Yao Liu, and Qiang He (Mar. 2020). "Nanoplastics Display Strong Stability in Aqueous Environments: Insights from Aggregation Behaviour and Theoretical Calculations". en. In: *Environmental Pollution* 258, p. 113760. ISSN: 02697491. DOI: 10.1016/j.envpol.2019.113760.

Mattsson, K., L.-A. Hansson, and T. Cedervall (2015). "Nano-Plastics in the Aquatic Environment". en. In: *Environmental Science: Processes & Impacts* 17.10, pp. 1712–1721. ISSN: 2050-7887, 2050-7895. DOI: 10.1039/C5EM00227C.

Mattsson, Karin, Frida Björkroth, Therese Karlsson, and Martin Hassellöv (Jan. 2021). "Nanofragmentation of Expanded Polystyrene Under Simulated Environmental Weathering (Thermooxidative Degradation and Hydrodynamic Turbulence)". en. In: *Frontiers in Marine Science* 7, p. 578178. ISSN: 2296-7745. DOI: 10.3389/fmars.2020.578178.

McDowell-Boyer, Laura M., James R. Hunt, and Nicholas Sitar (Dec. 1986). "Particle Transport through Porous Media". en. In: *Water Resources Research* 22.13, pp. 1901–1921. ISSN: 00431397. DOI: 10.1029/WR022i013p01901.

McNew, Coy P., Negin Kananizadeh, Yusong Li, and Eugene J. LeBoeuf (Feb. 2017). "The Attachment of Colloidal Particles to Environmentally Relevant Surfaces and the Effect of Particle Shape". en. In: *Chemosphere* 168, pp. 65–79. ISSN: 00456535. DOI: 10.1016/j.chemosphere.2016.10.039.

Messaud, Fathi A., Ron D. Sanderson, J. Ray Runyon, Tino Otte, Harald Pasch, and S. Kim Ratanathanawongs Williams (Apr. 2009). "An Overview on Field-Flow Fractionation Techniques and Their Applications in the Separation and Characterization of Polymers". en. In: *Progress in Polymer Science* 34.4, pp. 351–368. ISSN: 00796700. DOI: 10.1016/j.progpolymsci.2008.11.001.

Min, Kyungjun, Joseph D. Cuiffi, and Robert T. Mathers (Dec. 2020). "Ranking Environmental Degradation Trends of Plastic Marine Debris Based on Physical Properties and Molecular Structure". en. In: *Nature Communications* 11.1, p. 727. ISSN: 2041-1723. DOI: 10.1038/s41467-020-14538-z.

Mintenig, S. M., P. S. Bäuerlein, A. A. Koelmans, S. C. Dekker, and A. P. van Wezel (2018). "Closing the Gap between Small and Smaller: Towards a Framework to Analyse Nano- and Microplastics in Aqueous Environmental Samples". en. In: *Environmental Science: Nano* 5.7, pp. 1640–1649. ISSN: 2051-8153, 2051-8161. DOI: 10.1039/C8EN00186C.

Mitrano, Denise M., Peter Wick, and Bernd Nowack (Apr. 2021). "Placing Nanoplastics in the Context of Global Plastic Pollution". en. In: *Nature Nanotechnology*. ISSN: 1748-3387, 1748-3395. DOI: 10.1038/s41565-021-00888-2.

Mitrano, Denise M. and Wendel Wohlleben (Dec. 2020). "Microplastic Regulation Should Be More Precise to Incentivize Both Innovation and Environmental Safety". en. In: *Nature Communications* 11.1, p. 5324. ISSN: 2041-1723. DOI: 10.1038/s41467-020-19069-1.

Molnar, Ian L., William P. Johnson, Jason I. Gerhard, Clinton S. Willson, and Denis M. O'Carroll (Sept. 2015). "Predicting Colloid Transport through Saturated Porous Media: A Critical Review". en. In: *Water Resources Research* 51.9, pp. 6804–6845. ISSN: 00431397. DOI: 10.1002/2015WR017318.

Naiman, Robert J., Henri Décamps, John Pastor, and Carol A. Johnston (1988). "The Potential Importance of Boundaries of Fluvial Ecosystems". In: *Journal of the North American Benthological Society* 7.4, pp. 289–306. DOI: 10.2307/1467295. eprint: https://doi.org/10.2307/1467295.

Napper, D.H (Feb. 1977). "Steric Stabilization". In: *Journal of Colloid and Interface Science* 58.2, pp. 390–407. ISSN: 0021-9797. DOI: 10.1016/0021-9797(77)90150-3.

Ninham, Barry W. (2006). "The Present State of Molecular Forces". In: *Smart Colloidal Materials*. Ed. by Walter Richtering. Berlin, Heidelberg: Springer Berlin Heidelberg, pp. 65–73. ISBN: 978-3-540-32702-8.

Okshevsky, Mira, Eva Gautier, Jeffrey M. Farner, Lars Schreiber, and Nathalie Tufenkji (Apr. 2020). "Biofilm Formation by Marine Bacteria Is Impacted by Concentration and Surface Functionalization of Polystyrene Nanoparticles in a Species-specific Manner". en. In: *Environmental Microbiology Reports* 12.2, pp. 203–213. ISSN: 1758-2229, 1758-2229. DOI: 10.1111/1758-2229.12824.

Oriekhova, Olena and Serge Stoll (2018). "Heteroaggregation of Nanoplastic Particles in the Presence of Inorganic Colloids and Natural Organic Matter". en. In: *Environmental Science: Nano* 5.3, pp. 792–799. ISSN: 2051-8153, 2051-8161. DOI: 10.1039/C7EN01119A.

Peijnenburg, Willie J. G. M., Mohammed Baalousha, Jingwen Chen, Qasim Chaudry, Frank Von der kammer, Thomas A. J. Kuhlbusch, Jamie Lead, Carmen Nickel, Joris T. K. Quik, Mareile Renker, Zhuang Wang, and Albert A. Koelmans (Oct. 2015). "A Review of the Properties and Processes Determining the Fate of Engineered Nanomaterials in the Aquatic Environment". en. In: *Critical Reviews in Environmental Science and Technology* 45.19, pp. 2084–2134. ISSN: 1064-3389, 1547-6537. DOI: 10.1080/10643389.2015.1010430.

Peng, Guyu, Richard Bellerby, Feng Zhang, Xuerong Sun, and Daoji Li (Jan. 2020). "The Ocean's Ultimate Trashcan: Hadal Trenches as Major Depositories for Plastic Pollution". en. In: *Water Research* 168, p. 115121. ISSN: 00431354. DOI: 10.1016/j.watres.2019.115121.

Perovich, Donald, W. Meier, M. Tschudi, S. Hendricks, A. A. Petty, D. Divine, S. Farrell, S. Gerland, C. Haas, L. Kaleschke, O. Pavlova, R. Ricker, X. Tian-Kunze, M. Webster, and K. Wood (2020). "Arctic Report Card 2020: Sea Ice". In: Arctic Report Card. Ed. by United States. National Oceanic and Atmospheric Administration. Office of Oceanic and Atmospheric Research. Pacific Marine Environmental Laboratory (U.S.), Thayer School of Engineering, National Snow and Ice Data Center (U.S.), University of Colorado (Boulder campus), Helmholtz Centre for Polar and Marine Research Alfred-Wegener-Institut für Polar- und Meeresforschung / Alfred Wegener Institute, Goddard Space Flight Center, Norsk polarinstitutt / Norwegian Polar Institute, and University of Alaska Fairbanks. Geophysical Institute. DOI: 10.25923/n170-9h57.

Petosa, Adamo R., Deb P. Jaisi, Ivan R. Quevedo, Menachem Elimelech, and Nathalie Tufenkji (Sept. 2010). "Aggregation and Deposition of Engineered Nanomaterials in Aquatic Environments: Role of Physicochemical Interactions". en. In: *Environmental Science & Technology* 44.17, pp. 6532–6549. ISSN: 0013-936X, 1520-5851. DOI: 10.1021/es100598h.

Pikuda, Oluwadamilola, Elvis Genbo Xu, Dimitrios Berk, and Nathalie Tufenkji (Jan. 2019). "Toxicity Assessments of Micro- and Nanoplastics Can Be Confounded by Preservatives in Commercial Formulations". en. In: *Environmental Science & Technology Letters* 6.1, pp. 21–25. ISSN: 2328-8930, 2328-8930. DOI: 10.1021/acs.estlett.8b00614.

Poulain, Marie, Matthieu J. Mercier, Laurent Brach, Marion Martignac, Corinne Routaboul, Emile Perez, Marie Christine Desjean, and Alexandra ter Halle (Feb. 2019). "Small Microplastics As a Main Contributor to Plastic Mass Balance in the North Atlantic Subtropical Gyre". en. In: *Environmental Science & Technology* 53.3, pp. 1157–1164. ISSN: 0013-936X, 1520-5851. DOI: 10.1021/acs.est.8b05458.

Praetorius, Antonia, Nathalie Tufenkji, Kai-Uwe Goss, Martin Scheringer, Frank von der Kammer, and Menachem Elimelech (2014). "The Road to Nowhere: Equilibrium Partition Coefficients for Nanoparticles". en. In: *Environ. Sci.: Nano* 1.4, pp. 317–323. ISSN: 2051-8153, 2051-8161. DOI: 10.1039/C4EN00043A.

Prata, Joana C., João P. da Costa, Isabel Lopes, Anthony L. Andrady, Armando C. Duarte, and Teresa Rocha-Santos (Feb. 2021). "A One Health Perspective of the Impacts of Microplastics on Animal, Human and Envi-

ronmental Health". en. In: *Science of The Total Environment*, p. 146094. ISSN: 00489697. DOI: 10.1016/j.scitotenv.2021.146094.

Primpke, Sebastian, Silke H. Christiansen, Win Cowger, Hannah De Frond, Ashok Deshpande, Marten Fischer, Erika B. Holland, Michaela Meyns, Bridget A. O'Donnell, Barbara E. Ossmann, Marco Pittroff, George Sarau, Barbara M. Scholz-Böttcher, and Kara J. Wiggin (Sept. 2020). "Critical Assessment of Analytical Methods for the Harmonized and Cost-Efficient Analysis of Microplastics". en. In: *Applied Spectroscopy* 74.9, pp. 1012–1047. ISSN: 0003-7028, 1943-3530. DOI: 10.1177/0003702820921465.

Primpke, Sebastian, Richard K. Cross, Svenja M. Mintenig, Marta Simon, Alvise Vianello, Gunnar Gerdts, and Jes Vollertsen (Sept. 2020). "Toward the Systematic Identification of Microplastics in the Environment: Evaluation of a New Independent Software Tool (siMPle) for Spectroscopic Analysis". en. In: *Applied Spectroscopy* 74.9, pp. 1127–1138. ISSN: 0003-7028, 1943-3530. DOI: 10.1177/0003702820917760.

Provencher, J.F., J. Ammendolia, C.M. Rochman, and M.L. Mallory (Sept. 2019). "Assessing Plastic Debris in Aquatic Food Webs: What We Know and Don't Know about Uptake and Trophic Transfer". en. In: *Environmental Reviews* 27.3, pp. 304–317. ISSN: 1181-8700, 1208-6053. DOI: 10.1139/er-2018-0079.

Quevedo, Ivan R. and Nathalie Tufenkji (Apr. 2012). "Mobility of Functionalized Quantum Dots and a Model Polystyrene Nanoparticle in Saturated Quartz Sand and Loamy Sand". en. In: *Environmental Science & Technology* 46.8, pp. 4449–4457. ISSN: 0013-936X, 1520-5851. DOI: 10.1021/es2045458.

Quik, J.T.K., I. Velzeboer, M. Wouterse, A.A. Koelmans, and D. van de Meent (Jan. 2014). "Heteroaggregation and Sedimentation Rates for Nanomaterials in Natural Waters". en. In: *Water Research* 48, pp. 269–279. ISSN: 00431354. DOI: 10.1016/j.watres.2013.09.036.

Ramirez, Lina, Stephan Ramseier Gentile, Stéphane Zimmermann, and Serge Stoll (Apr. 2019). "Behavior of TiO2 and CeO2 Nanoparticles and Polystyrene Nanoplastics in Bottled Mineral, Drinking and Lake Geneva Waters. Impact of Water Hardness and Natural Organic Matter on Nanoparticle Surface Properties and Aggregation". en. In: *Water* 11.4, p. 721. ISSN: 2073-4441. DOI: 10.3390/w11040721.

Rochman, Chelsea M., Cole Brookson, Jacqueline Bikker, Natasha Djuric, Arielle Earn, Kennedy Bucci, Samantha Athey, Aimee Huntington, Hayley McIlwraith, Keenan Munno, Hannah De Frond, Anna Kolomijeca, Lisa Erdle, Jelena Grbic, Malak Bayoumi, Stephanie B. Borrelle, Tina Wu, Samantha Santoro, Larissa M. Werbowski, Xia Zhu, Rachel K. Giles, Bonnie M. Hamilton, Clara Thaysen, Ashima Kaura, Natasha Klasios, Lauren Ead, Joel Kim, Cassandra Sherlock, Annissa Ho, and Charlotte Hung (Apr. 2019). "Rethinking Microplastics as a Diverse Contaminant Suite". en. In: *Environmental Toxicology and Chemistry* 38.4, pp. 703–711. ISSN: 0730-7268, 1552-8618. DOI: 10.1002/etc.4371.

Rowlands, Emily, Tamara Galloway, and Clara Manno (Feb. 2021). "A Polar Outlook: Potential Interactions of Micro- and Nano-Plastic with Other Anthropogenic Stressors". en. In: *Science of The Total Environment* 754, p. 142379. ISSN: 00489697. DOI: 10.1016/j.scitotenv.2020.142379.

Saavedra, Juan, Serge Stoll, and Vera I. Slaveykova (Sept. 2019). "Influence of Nanoplastic Surface Charge on Eco-Corona Formation, Aggregation and Toxicity to Freshwater Zooplankton". en. In: *Environmental Pollution* 252, pp. 715–722. ISSN: 02697491. DOI: 10.1016/j.envpol.2019.05.135.

Saleh, Navid B., A. R. M. Nabiul Afrooz, Nirupam Aich, and Jaime Plazas-Tuttle (2016). "Aggregation Kinetics and Fractal Dimensions of Nanomaterials in Environmental Systems". In: *Engineered Nanoparticles and the Environment: Biophysicochemical Processes and Toxicity*. John Wiley & Sons, Ltd. Chap. 8, pp. 139–159. ISBN: 978-1-119-27585-5. DOI: 10.1002/9781119275855.ch8. eprint: https://onlinelibrary.wiley.com/doi/pdf/10.1002/9781119275855.ch8.

Sanderman, Jonathan, Jeffrey A. Baldock, and Ronald Amundson (June 2008). "Dissolved Organic Carbon Chemistry and Dynamics in Contrasting Forest and Grassland Soils". In: *Biogeochemistry* 89.2, pp. 181–198. ISSN: 1573-515X. DOI: 10.1007/s10533-008-9211-x.

SAPEA, Science Advice for Policy by European Academies (2019). *A Scientific Perspective on Microplastics in Nature and Society*. en. Berlin: SAPEA. ISBN: 978-3-9820301-0-4.

Sauvé, Sébastien and Mélanie Desrosiers (Dec. 2014). "A Review of What Is an Emerging Contaminant". en. In: *Chemistry Central Journal* 8.1, p. 15. ISSN: 1752-153X. DOI: 10.1186/1752-153X-8-15.

Scarlett, B. (1992). "25 Years of Particle Size Conferences". en. In: *Special Publication*. Ed. by N G Stanley-Wood and R W Lines. Vol. 0. Cambridge: Royal Society of Chemistry, pp. 1–12. ISBN: 978-0-85186-487-7. DOI: 10.1039/9781847551627-00001.

Scheurer, Michael and Moritz Bigalke (Mar. 2018). "Microplastics in Swiss Floodplain Soils". en. In: *Environmental Science & Technology* 52.6, pp. 3591–3598. ISSN: 0013-936X, 1520-5851. DOI: 10.1021/acs.est.7b06003.

Schwarz, A.E., T.N. Ligthart, E. Boukris, and T. van Harmelen (June 2019). "Sources, Transport, and Accumulation of Different Types of Plastic Litter in Aquatic Environments: A Review Study". en. In: *Marine Pollution Bulletin* 143, pp. 92–100. ISSN: 0025326X. DOI: 10.1016/j.marpolbul.2019.04.029.

Sefrioui, Nisrine, Azita Ahmadi, Aziz Omari, and Henri Bertin (June 2013). "Numerical Simulation of Retention and Release of Colloids in Porous Media at the

Pore Scale". en. In: *Colloids and Surfaces A: Physicochemical and Engineering Aspects* 427, pp. 33–40. ISSN: 09277757. DOI: 10.1016/j.colsurfa.2013.03.005.

Sendra, Marta, Eleonora Staffieri, María Pilar Yeste, Ignacio Moreno-Garrido, José Manuel Gatica, Ilaria Corsi, and Julián Blasco (June 2019). "Are the Primary Characteristics of Polystyrene Nanoplastics Responsible for Toxicity and Ad/Absorption in the Marine Diatom Phaeodactylum Tricornutum?" en. In: *Environmental Pollution* 249, pp. 610–619. ISSN: 02697491. DOI: 10.1016/j.envpol.2019.03.047.

Seoane, Marta, Carmen González-Fernández, Philippe Soudant, Arnaud Huvet, Marta Esperanza, Ángeles Cid, and Ika Paul-Pont (Aug. 2019). "Polystyrene Microbeads Modulate the Energy Metabolism of the Marine Diatom Chaetoceros Neogracile". en. In: *Environmental Pollution* 251, pp. 363–371. ISSN: 02697491. DOI: 10.1016/j.envpol.2019.04.142.

Seymour, Megan B., Gexin Chen, Chunming Su, and Yusong Li (July 2013). "Transport and Retention of Colloids in Porous Media: Does Shape Really Matter?" en. In: *Environmental Science & Technology*, p. 130722083052008. ISSN: 0013-936X, 1520-5851. DOI: 10.1021/es4016124.

Shiu, Ruei-Feng, Carlos I. Vazquez, Yi-Yen Tsai, Gabriela V. Torres, Chi-Shuo Chen, Peter H. Santschi, Antonietta Quigg, and Wei-Chun Chin (Mar. 2020). "Nano-Plastics Induce Aquatic Particulate Organic Matter (Microgels) Formation". en. In: *Science of The Total Environment* 706, p. 135681. ISSN: 00489697. DOI: 10.1016/j.scitotenv.2019.135681.

Silva, M.S.S., Miguel Oliveira, Pedro Valente, Etelvina Figueira, Manuel Martins, and Adília Pires (Mar. 2020). "Behavior and Biochemical Responses of the Polychaeta Hediste Diversicolor to Polystyrene Nanoplastics". en. In: *Science of The Total Environment* 707, p. 134434. ISSN: 00489697. DOI: 10.1016/j.scitotenv.2019.134434.

Singh, Nisha, Ekta Tiwari, Nitin Khandelwal, and Gopala Krishna Darbha (2019). "Understanding the Stability of Nanoplastics in Aqueous Environments: Effect of Ionic Strength, Temperature, Dissolved Organic Matter, Clay, and Heavy Metals". en. In: *Environmental Science: Nano* 6.10, pp. 2968–2976. ISSN: 2051-8153, 2051-8161. DOI: 10.1039/C9EN00557A.

Song, Young Kyoung, Sang Hee Hong, Soeun Eo, Gi Myung Han, and Won Joon Shim (Sept. 2020). "Rapid Production of Micro- and Nanoplastics by Fragmentation of Expanded Polystyrene Exposed to Sunlight". en. In: *Environmental Science & Technology* 54.18, pp. 11191–11200. ISSN: 0013-936X, 1520-5851. DOI: 10.1021/acs.est.0c02288.

Song, Zefeng, Xinyao Yang, Fangmin Chen, Fangyuan Zhao, Ying Zhao, Lili Ruan, Yinggang Wang, and Yuesuo Yang (June 2019). "Fate and Transport of Nanoplastics in Complex Natural Aquifer Media: Effect of Particle Size and Surface Functionalization". en. In: *Science of The Total Environment* 669, pp. 120–128. ISSN: 00489697. DOI: 10.1016/j.scitotenv.2019.03.102.

Stetefeld, Jörg, Sean A. McKenna, and Trushar R. Patel (Dec. 2016). "Dynamic Light Scattering: A Practical Guide and Applications in Biomedical Sciences". en. In: *Biophysical Reviews* 8.4, pp. 409–427. ISSN: 1867-2450, 1867-2469. DOI: 10.1007/s12551-016-0218-6.

Stokes, G. G. (Jan. 1851). "On the Effect of the Internal Friction of Fluids on the Motion of Pendulums". In: *Transactions of the Cambridge Philosophical Society* 9, p. 8.

Stumm, Werner and James J. Morgan (1996). *Aquatic Chemistry : Chemical Equilibria and Rates in Natural Waters*. English. New York: Wiley. ISBN: 0-471-51184-6 978-0-471-51184-7 0-471-51185-4 978-0-471-51185-4.

Summers, Stephen, Theodore Henry, and Tony Gutierrez (May 2018). "Agglomeration of Nano- and Microplastic Particles in Seawater by Autochthonous and de Novo-Produced Sources of Exopolymeric Substances". en. In: *Marine Pollution Bulletin* 130, pp. 258–267. ISSN: 0025326X. DOI: 10.1016/j.marpolbul.2018.03.039.

Sutherland, William (1905). "LXXV. A Dynamical Theory of Diffusion for Non-Electrolytes and the Molecular Mass of Albumin". In: *The London, Edinburgh, and Dublin Philosophical Magazine and Journal of Science* 9.54, pp. 781–785. DOI: 10.1080/14786440509463331. eprint: https://doi.org/10.1080/14786440509463331.

Suzuki, Hisatomo, Masanobu Murou, Hiromi Kitano, Kohji Ohno, and Yoshiyuki Saruwatari (May 2011). "Silica Particles Coated with Zwitterionic Polymer Brush: Formation of Colloidal Crystals and Anti-Biofouling Properties in Aqueous Medium". en. In: *Colloids and Surfaces B: Biointerfaces* 84.1, pp. 111–116. ISSN: 09277765. DOI: 10.1016/j.colsurfb.2010.12.023.

Tallec, Kevin, Océane Blard, Carmen González-Fernández, Guillaume Brotons, Mathieu Berchel, Philippe Soudant, Arnaud Huvet, and Ika Paul-Pont (June 2019). "Surface Functionalization Determines Behavior of Nanoplastic Solutions in Model Aquatic Environments". en. In: *Chemosphere* 225, pp. 639–646. ISSN: 00456535. DOI: 10.1016/j.chemosphere.2019.03.077.

Ter Halle, Alexandra, Laurent Jeanneau, Marion Martignac, Emilie Jardé, Boris Pedrono, Laurent Brach, and Julien Gigault (Dec. 2017). "Nanoplastic in the North Atlantic Subtropical Gyre". en. In: *Environmental Science & Technology* 51.23, pp. 13689–13697. ISSN: 0013-936X, 1520-5851. DOI: 10.1021/acs.est.7b03667.

ter Halle, Alexandra, Lucie Ladirat, Xavier Gendre, Dominique Goudouneche, Claire Pusineri, Corinne Routaboul, Christophe Tenailleau, Benjamin Duployer, and Emile Perez (June 2016). "Understanding the Fragmentation Pattern of Marine Plastic Debris". en. In: *Environmental Science & Technology* 50.11, pp. 5668–

5675. ISSN: 0013-936X, 1520-5851. DOI: 10.1021/acs.est.6b00594.

Thomas, David N. and Gerhard Dieckmann (2003). *Sea Ice: An Introduction to Its Physics, Chemistry, Biology, and Geology*. en. Oxford, UK ; Malden, MA, USA: Blackwell Science. ISBN: 978-0-632-05808-2.

Thompson, R. C. (May 2004). "Lost at Sea: Where Is All the Plastic?" en. In: *Science* 304.5672, pp. 838–838. ISSN: 0036-8075, 1095-9203. DOI: 10.1126/science.1094559.

Tufenkji, Nathalie and Menachem Elimelech (Jan. 2004). "Correlation Equation for Predicting Single-Collector Efficiency in Physicochemical Filtration in Saturated Porous Media". en. In: *Environmental Science & Technology* 38.2, pp. 529–536. ISSN: 0013-936X, 1520-5851. DOI: 10.1021/es034049r.

Valsesia, Andrea, Cloé Desmet, Isaac Ojea-Jiménez, Arianna Oddo, Robin Capomaccio, François Rossi, and Pascal Colpo (Dec. 2018). "Direct Quantification of Nanoparticle Surface Hydrophobicity". en. In: *Communications Chemistry* 1.1, p. 53. ISSN: 2399-3669. DOI: 10.1038/s42004-018-0054-7.

van Oss, C.J. (Oct. 1993). "AcidBase Interfacial Interactions in Aqueous Media". en. In: *Colloids and Surfaces A: Physicochemical and Engineering Aspects* 78, pp. 1–49. ISSN: 09277757. DOI: 10.1016/0927-7757(93)80308-2.

van Sebille, Erik, Matthew H England, and Gary Froyland (Dec. 2012). "Origin, Dynamics and Evolution of Ocean Garbage Patches from Observed Surface Drifters". en. In: *Environmental Research Letters* 7.4, p. 044040. ISSN: 1748-9326. DOI: 10.1088/1748-9326/7/4/044040.

van Sebille, Erik, Chris Wilcox, Laurent Lebreton, Nikolai Maximenko, Britta Denise Hardesty, Jan A van Franeker, Marcus Eriksen, David Siegel, Francois Galgani, and Kara Lavender Law (Dec. 2015). "A Global Inventory of Small Floating Plastic Debris". In: *Environmental Research Letters* 10.12, p. 124006. ISSN: 1748-9326. DOI: 10.1088/1748-9326/10/12/124006.

Venel, Zélie, Hervé Tabuteau, Alice Pradel, Pierre-Yves Pascal, Bruno Grassl, Hind El Hadri, Magalie Baudrimont, and Julien Gigault (Feb. 2021). "Environmental Fate Modeling of Nanoplastics in a Salinity Gradient Using a Lab-on-a-Chip: Where Does the Nanoscale Fraction of Plastic Debris Accumulate?" en. In: *Environmental Science & Technology*, acs.est.0c07545. ISSN: 0013-936X, 1520-5851. DOI: 10.1021/acs.est.0c07545.

Verwey, E. J. W., J. Th. G. Overbeek, and K. Van Nes (1948). *Theory of the Stability of Lyophobic Colloids : The Interaction of Sol Particles Having an Electric Double Layer*. English. Amsterdam [etc]: Elsevier.

Vold, Marjorie J (Oct. 1954). "Van Der Waals' Attraction between Anisometric Particles". en. In: *Journal of Colloid Science* 9.5, pp. 451–459. ISSN: 00958522. DOI: 10.1016/0095-8522(54)90032-X.

Wagner, Martin and Scott Lambert, eds. (2018). *Freshwater Microplastics: Emerging Environmental Contaminants?* en. Vol. 58. The Handbook of Environmental Chemistry. Cham: Springer International Publishing. ISBN: 978-3-319-61614-8 978-3-319-61615-5. DOI: 10.1007/978-3-319-61615-5.

Wang, Hongtao, Adeyemi S. Adeleye, Yuxiong Huang, Fengting Li, and Arturo A. Keller (Dec. 2015). "Heteroaggregation of Nanoparticles with Biocolloids and Geocolloids". en. In: *Advances in Colloid and Interface Science* 226, pp. 24–36. ISSN: 00018686. DOI: 10.1016/j.cis.2015.07.002.

Waters, C. N., J. Zalasiewicz, C. Summerhayes, A. D. Barnosky, C. Poirier, A. Ga uszka, A. Cearreta, M. Edgeworth, E. C. Ellis, M. Ellis, C. Jeandel, R. Leinfelder, J. R. McNeill, D. d. Richter, W. Steffen, J. Syvitski, D. Vidas, M. Wagreich, M. Williams, A. Zhisheng, J. Grinevald, E. Odada, N. Oreskes, and A. P. Wolfe (Jan. 2016). "The Anthropocene Is Functionally and Stratigraphically Distinct from the Holocene". en. In: *Science* 351.6269, aad2622–aad2622. ISSN: 0036-8075, 1095-9203. DOI: 10.1126/science.aad2622.

Weiss, Lisa, Wolfgang Ludwig, Serge Heussner, Miquel Canals, Jean-François Ghiglione, Claude Estournel, Mel Constant, and Philippe Kerhervé (2021). "The Missing Ocean Plastic Sink: Gone with the Rivers". In: *Science* 373.6550, pp. 107–111. DOI: 10.1126/science.abe0290.

Wheeler, Korin E., Andrew J. Chetwynd, Kira M. Fahy, Brian S. Hong, Jose A. Tochihuitl, Lilah A. Foster, and Iseult Lynch (June 2021). "Environmental Dimensions of the Protein Corona". en. In: *Nature Nanotechnology* 16.6, pp. 617–629. ISSN: 1748-3387, 1748-3395. DOI: 10.1038/s41565-021-00924-1.

Wik, Anna and Göran Dave (2009). "Occurrence and Effects of Tire Wear Particles in the Environment  A Critical Review and an Initial Risk Assessment". In: *Environmental Pollution* 157.1, pp. 1–11. ISSN: 0269-7491. DOI: 10.1016/j.envpol.2008.09.028.

Wood, Jeffery A. and Lars Rehmann (Apr. 2014). "Geometric Effects on Non-DLVO Forces: Relevance for Nanosystems". en. In: *Langmuir* 30.16, pp. 4623–4632. ISSN: 0743-7463, 1520-5827. DOI: 10.1021/la500664c.

Wu, Jiayi, Ruifen Jiang, Wei Lin, and Gangfeng Ouyang (Feb. 2019). "Effect of Salinity and Humic Acid on the Aggregation and Toxicity of Polystyrene Nanoplastics with Different Functional Groups and Charges". en. In: *Environmental Pollution* 245, pp. 836–843. ISSN: 02697491. DOI: 10.1016/j.envpol.2018.11.055.

Wu, Lei, Bin Gao, Yuan Tian, Rafael Muñoz-Carpena, and Kirk J. Zigler (Mar. 2013). "DLVO Interactions of Carbon Nanotubes with Isotropic Planar Surfaces". en. In: *Langmuir* 29.12, pp. 3976–3988. ISSN: 0743-7463, 1520-5827. DOI: 10.1021/la3048328.

Wu, W., R.F. Giese, and C.J. van Oss (Aug. 1999). "Stability versus Flocculation of Particle Suspensions in WaterCorrelation with the Extended DLVO Approach for Aqueous Systems, Compared with Classical DLVO Theory". en. In: *Colloids and Surfaces B: Biointerfaces*

14.1-4, pp. 47–55. ISSN: 09277765. DOI: 10.1016/S0927-7765(99)00023-5.

Xiao, Yao, Kay T. Ho, Robert M. Burgess, and Michaela Cashman (Feb. 2017). "Aggregation, Sedimentation, Dissolution, and Bioavailability of Quantum Dots in Estuarine Systems". en. In: *Environmental Science & Technology* 51.3, pp. 1357–1363. ISSN: 0013-936X, 1520-5851. DOI: 10.1021/acs.est.6b04475.

Xing, Baoshan, Chad D. Vecitis, and N. Senesi, eds. (2016). *Engineered Nanoparticles and the Environment: Biophysicochemical Processes and Toxicity*. en. Wiley-IUPAC Series in Biophysico-Chemical Processes in Environmental Systems. Hoboken, New Jersey: Wiley. ISBN: 978-1-119-27582-4 978-1-119-27584-8.

Xu, R. (2006). *Particle Characterization: Light Scattering Methods*. Springer Netherlands. ISBN: 978-0-306-47124-7.

Yu, Sujuan, Jingfu Liu, Yongguang Yin, and Mohai Shen (Jan. 2018). "Interactions between Engineered Nanoparticles and Dissolved Organic Matter: A Review on Mechanisms and Environmental Effects". en. In: *Journal of Environmental Sciences* 63, pp. 198–217. ISSN: 10010742. DOI: 10.1016/j.jes.2017.06.021.

Yu, Sujuan, Mohai Shen, Shasha Li, Yueju Fu, Dan Zhang, Huayi Liu, and Jingfu Liu (Dec. 2019). "Aggregation Kinetics of Different Surface-Modified Polystyrene Nanoparticles in Monovalent and Divalent Electrolytes". en. In: *Environmental Pollution* 255, p. 113302. ISSN: 02697491. DOI: 10.1016/j.envpol.2019.113302.

Zettler, Erik R., Tracy J. Mincer, and Linda A. Amaral-Zettler (July 2013). "Life in the "Plastisphere": Microbial Communities on Plastic Marine Debris". en. In: *Environmental Science & Technology* 47.13, pp. 7137–7146. ISSN: 0013-936X, 1520-5851. DOI: 10.1021/es401288x.

Zhang, Fan, Zhuang Wang, Se Wang, Hao Fang, and Degao Wang (Aug. 2019). "Aquatic Behavior and Toxicity of Polystyrene Nanoplastic Particles with Different Functional Groups: Complex Roles of pH, Dissolved Organic Carbon and Divalent Cations". en. In: *Chemosphere* 228, pp. 195–203. ISSN: 00456535. DOI: 10.1016/j.chemosphere.2019.04.115.

Zhang, Qi, Qian Qu, Tao Lu, Mingjing Ke, Youchao Zhu, Meng Zhang, Zhenyan Zhang, Benben Du, Xiangliang Pan, Liwei Sun, and Haifeng Qian (Dec. 2018). "The Combined Toxicity Effect of Nanoplastics and Glyphosate on Microcystis Aeruginosa Growth". en. In: *Environmental Pollution* 243, pp. 1106–1112. ISSN: 02697491. DOI: 10.1016/j.envpol.2018.09.073.

Zhu, Lixin, Shiye Zhao, Thais B. Bittar, Aron Stubbins, and Daoji Li (Aug. 2019). "Photochemical Dissolution of Buoyant Microplastics to Dissolved Organic Carbon: Rates and Microbial Impacts". en. In: *Journal of Hazardous Materials*, p. 121065. ISSN: 03043894. DOI: 10.1016/j.jhazmat.2019.121065.

Zimmermann, Sören, James L. Mead, and Fabian T. von Kleist-Retzow (Nov. 2020). "Probing Friction and Adhesion of Individual Nanoplastic Particles". en. In: *The Journal of Physical Chemistry C* 124.44, pp. 24145–24155. ISSN: 1932-7447, 1932-7455. DOI: 10.1021/acs.jpcc.0c05826.

Zubris, Kimberly Ann V. and Brian K. Richards (Nov. 2005). "Synthetic Fibers as an Indicator of Land Application of Sludge". en. In: *Environmental Pollution* 138.2, pp. 201–211. ISSN: 02697491. DOI: 10.1016/j.envpol.2005.04.013.

**Acronyms:** ASW = artificial seawater; AGW = Artificial groundwater; BSA = bovine serum albumin ; CD = circular dichroism; DLS = dynamic light scattering; $d_H$ = hydrodynamic diameter; dzH = z-average hydrodyanmic diameter; EDL = electronic double layer; EPS = extracellular polymeric substances ; DMEM = Dulbecco's modified Eagle's medium; DOM = dissolved organic matter; FA = fulvic acid; FBS = fetal bovine serum; F-T=Freeze-Thaw; HS = hemolymph serum; HSA = human serum albumin; IS = ionic strength; NF = Non-functionalized; NOM = natural organic matter; NSW = natural seawater; NLW = natural lake water; NRW = natural river water; PEI = polyethylenimine; PDI = polydispersity index; POM = particulate organic matter; PS = polystyrene; PSL = polystyrene latex; PSU = practical salinity units; SA = sodium alginate ; SANS = small angle neutron scattering; SLS = static light scattering; SS = suspended sediments; SRFA = suwannee river fulvic acid; SRHA = suwannee river humic acid ; TEM = transmission electron microscopy; TEP = transparent exopolymeric particles (TEP); TR-DLS = time-resolved dynamic light scattering; USANS=ultra small-angle neutron scattering SEM = scanning electron microscopy; ZP = Zeta-potential

| **Nanoplastic Model Studied** | **Solution chemistry** | **Indicators of Stability** | **Behavior and Stability, and Mechanisms** | **Reference** |
|---|---|---|---|---|
| • Composition Surface functionalization-Size (nm) Shape (if present) (Charge)<br>• Presence of surfactants<br>• Concentration | • Ion type<br>  ○ Concentration<br>  ○ pH<br>• Organic matter<br>  ○ Type<br>  ○ Concentration<br>  ○ Filtered | • Instantaneous measurements of $d_{zH}$, PDI and zeta potential at time (t)<br>• Time-resolved measurements $d_{zH}$ and duration | | |
| • PSL COOH-28 sphere (-)<br>• Not surfactant-free<br>• 2 mg $L^{-1}$ | • NaCl<br>  ○ 3 to 100 mmol $L^{-1}$<br>  ○ pH = 6<br>• SRHA<br>  ○ 5 mg $L^{-1}$ | • Determination of $d_{zH}$, intensity-based $d_H$ and number-based $d_H$. PDI, ZP and TEM images | • F-T cycles caused strong aggregation, with or without NOM and irrespective of ionic strength. Aggregates are stable up to 5 days after F-T. No significant impact of F-T on ZP<br>• ZP slightly more negative in the presence of NOM than without NOM (except at 100 mmol $L^{-1}$).<br>• At 10°C for 24 hours, no significant aggregation and ZP unchanged up to 100 mmol $L^{-1}$ NaCl.<br>• F-T significantly reduces mobility in soils, but SRHA increases mobility in porous media. | (Alimi et al., 2021) |
| • PBAT 366 (bimodal distribution) nonpsherical (-)<br>• Surfactant free<br>• 1% w/w (10 000mg $L^{-1}$) | • D2O and H2O<br>• Vermicullite 0.5% w/w (50 000 mg $L^{-1}$)<br>• 9.54 | • USANS and SANS : Allows the in-situ detection of NP size shape and agglomeration | • NPs of larger size self-associate and also aggregate with vermiculite.<br>• NPs of smaller size remain dispersed<br>• Ex situ stirring during 24 hours at 400 rpm improved the dispersion of the NPs by disrupting the formation of agglomerates | (Astner et al., 2020) |
| • PSL COOH-40 sphere (-)<br>• PSL NH2-50 sphere (+)<br>• Not surfactant-free<br>• Concentration not mentioned | • DI water<br>• NSW from King George Island (South Shetland Islands)<br>  ○ Filtered at 0.22 µm<br>  ○ Salinity 34 ‰<br>  ○ pH = 7.89 | • Measurements of $d_{zH}$, zeta potential, PDI at t= 0 and 24h | • Particles remained well dispersed in DI water at 0oC<br>• In NSW, initial stability is followed by aggregation after 24 h.<br>• Freezing dispersions resulted in very high aggregation rate in DI water and NSW | (Bergami et al., 2019) |

| | | | | |
|---|---|---|---|---|
| • PSL-100 sphere (-)<br>• Not surfactant-free<br>• 10mg $L^{-1}$ and 50 mg $L^{-1}$ | • NaCl<br>  ○ 1 to 100 mmol $L^{-1}$<br>• $CaCl_2$<br>  ○ 0.1 to 15 mmol $L^{-1}$<br>• $FeCl_3$<br>  ○ 0.01 to 1 mmol $L^{-1}$<br>  ○ Unadjusted pH<br>• SRFA and SRHA<br>  ○ 10 mgC $L^{-1}$<br>  ○ Filtered at 0.22 µm | • Time-resolved measurement of $d_{zH}$ lasting 10 minutes<br>• Measurement of zeta potential | • Particles are generally stable in NaCl. Slight aggregation observed at low particle concentration in 50 and 100 mmol $L^{-1}$ NaCl.<br>• Stability in CaCl2 attributed to the absence of COOH on particles.<br>• Stability of particles in FeCl3 attributed to full charge reversal.<br>• Aggregation with SRHA and SRFA in FeCL3 due to heterogenous surface charge and cation bridging. | (Cai et al., 2018) |
| • PSL NH2-50 sphere (+)<br>• Not surfactant-free<br>• 1, 5 and 50 mg $L^{-1}$ | • ASW<br>• Hemolymph serum (HS) sterilized (contains proteins)<br>  ○ ~ 2g $L^{-1}$<br>  ○ pH 7.3<br>  ○ Filtered at 0.22 µm | • Measurement of $d_{zH,}$ PDI and zeta potential at t=0, 1 and 2 hours | • In ASW aggregates > 200 nm are immediately formed<br>• In HS, after 2 hours aggregate size < 200nm. This is attributed to differences in pH and presence of protein which form a hard corona around nanoplastics | (Canesi et al., 2016) |
| • PSL NF-25 sphere (-)<br>• PSL COOH-25 sphere (-)<br>• PSL NH2-25 sphere (+)<br>• PMMAL-25 sphere (-)<br>• PMMAL COOH-25 sphere (-)<br>•<br>• Not surfactant free<br>• 0.01 mg $L^{-1}$ and 0.1 mg $L^{-1}$ | • NSW from Puget Sound<br>  ○ Filtered at 0.22 µm and treated with biocide<br>  ○ 2.75 mgC $L^{-1}$<br>• NSW from Gulf of Mexico<br>  ○ Filtered at 0.22 µm and treated with biocide | • Measurements of $d_{zH}$ over 24 hours<br>• Measurements of zeta potential | • All particles accelerated the self-assembly of DOM into POM.<br>• Zeta potential measurements and kinetics of aggregation after incubation at different temperatures, show that this is attributed to hydrophobic interactions between nanoplastic and OM. | (Chen et al., 2018) |
| • PSL NF-100 nm sphere (-)<br>• Not surfactant-free<br>• 10 mg $L^{-1}$ | • DI water<br>• NLW<br>• Ca:Al ratios (mol:mol) of 1:0, 1:1, 2:1, 3:1, 4:1, and 0:1<br>  ○ pH 3, 4, 5, 6, 7, 8, 9 and 10 studied at Ca:Al of 2:1 | • After a stirring and settling period, the supernatant absorbance and zeta potential were measured. | • Particles do not settle well in the presence of Ca ion alone. In the presence of Al, flocs gathered at the surface layer. For all other Ca/Al ratios, close to 90% PSNP settling was observed<br>• At low pH, the negative surface charge of NPs became more neutral due to high proton concentration and the positive charges of Ca and Al ions.<br>• In moderately alkaline water, Ca and Al formed crystals that captured PSL<br>• At pH 10, PSNPs adsorbed onto Ca/Al crystals<br>• Removal by crystal precipitation performs better than removal by compression of the electronic double layer. | (Chen et al., 2020) |

| | | | | |
|---|---|---|---|---|
| • PSL COOH-40nm sphere (-)<br>• PSL NH2-50nm sphere (-)<br>• Not surfactant-free<br>• 50 mg $L^{-1}$ | • NSW from the Tuscany Archipelago, filtered at 0.45 µm<br>  ○ 38g $L^{-1}$ salinity<br>  ○ pH 8.3 | • Measurement of $d_{zH}$, PDI and zeta potential at t=0, 6, 24 and 48 hours | • PS-NH2 is more stable than PS-COOH. Their zeta potential in NSW, is +13 and +7 mV, respectively<br>• Stability is attributed to interplay between electronic layer screening due to salinity and adsorption of proteins and naturally occurring organic matter | (Della Torre et al., 2014) |
| • PSL COOH-200nm sphere (-)<br>• Not surfactant-free<br>• 1.5, 5 and 15 mg $L^{-1}$ | • ASW<br>  ○ 0, 3.5 and 35 PSU | • Time-resolved measurement of $d_{zH}$ lasting 40 minutes<br>• Measurement of zeta potential | • PSL COOH-200nm sphere (-) are stable up to 35 PSU<br>• Zeta potential varies from -37.72 mV in 0 PSU to -20.29 mV in 35 PSU<br>• Stability in ASW attributed to electrostatic repulsion | (Dong et al., 2019) |
| • PSL NH2-50 nm sphere (+)<br>• Not surfactant-free<br>• Concentration not mentioned | • DI water<br>• NSW<br>  ○ Filtered at 0.20 µm<br>• Supernatant of algal culture from the exponential and stationary growth phases<br>  ○ Filtered at 0.20 µm | • Measurement of $d_{zH}$, PDI and zeta potential at t=0 | • In NSW aggregation was negligible<br>• In the spent media of algal culture aggregation was moderate: more pronounced in stationary algal growth phase than in the exponential growth phase.<br>• This aggregation is attributed to increase in transparent exopolymeric particles (TEP) and screening of the electronic double layer. | (González-Fernández et al., 2019) |
| • PSL COOH-20 nm sphere (-)<br>• PSL COOH-135 nm sphere (-)<br>• Not surfactant-free<br>• 1 to 3mg $L^{-1}$ | • Buffer solution composed of NaCl, KCl, $Na_2HPO_4$, $KH_2PO_4$ and citric acid<br>  ○ pH 7.4 and 5<br>• HSA proteins<br>  ○ 3, 9, 15 mg $L^{-1}$<br>  ○ Unfiltered | • Measurement of $d_{zH}$, and zeta potential at t=1h<br>• Circular Dichrosm (CD) spectroscopy<br>• Small-angle Neutron Scattering (SANS) measurements | • At pH 7.4, PSL COOH-20 nm sphere (-) aggregated after addition of HSA. The incorporation of HSA onto the surface, lasts 30 minutes.<br>• At pH 5, PSL COOH-20 nm sphere (-) aggregated more strongly with HSA, due to HSA's close to neutral zeta potential.<br>• Larger particles formed a softer corona than small particles, due to the decreased PS−HSA attraction.<br>• Fractal formation occurred when interaction between PS and HSA was strong. | (Kihara et al., 2019) |
| • PSL SO3-100nm sphere (-)<br>• Not surfactant-free<br>• 10 mg $L^{-1}$ | • Di water, with pH 2 to 12.<br>• NaCl<br>  ○ 50, 200, 500 mmol $L^{-1}$<br>• Suspended sediments (SS) obtained Pearl River (top 10 cm)<br>  ○ Diameters from 100 to 500 µm.<br>  ○ 100 mg $L^{-1}$<br>  ○ Diameters < 10 µm<br>  ○ 500 mg $L^{-1}$<br>• HA<br>  ○ 10, 20, or 50 mg $L^{-1}$<br>  ○ Unfiltered | • Suspension were mixed, sonicated and then left undisturbed for settling.<br>• Measurement of $d_{zH}$, and zeta potential at t=0<br>• The settling kinetics was determined by measuring concentration changes by absorbance and fluorescence. | • The adsorption of particles on large SS results in the formation of heteroaggregates, which can settle rapidly in the water column<br>• NaCl and SS increased settling rate of PSNPs, while HA decreased the settling rate.<br>• The effect of NaCl and HA was the same for small and large SS.<br>• HA increased stability of particles by increasing electronegativity and providing steric hindrance. | (Li et al., 2019) |

| | | | | |
|---|---|---|---|---|
| • PSL NF-50nm sphere (-)<br>• PSL NF-100nm sphere (-)<br>• PSL COH and COOH-50nm aged (-) *photochemically-aged with UVA for up to 24 h*<br>• Not surfactant-free<br>• 10 mg $L^{-1}$ | • Monovalent electrolytes<br>  ○ NaCl, KCl<br>  ○ 0.02 to 2 M<br>• Divalent electrolytes<br>  ○ $CaCl_2$, $BaCl_2$, $MgCl_2$<br>  ○ 2 to 200 mmol $L^{-1}$<br>  ○ Filtered at 0.22 µm<br>  ○ pH = 6<br>• DOM increased with UV irradiation from 4.88 to 44.01 mg $L^{-1}$ over 24h | • Measurement of $d_{zH}$, and zeta potential<br>• Time-resolved measurement of $d_{zH}$ lasting 20 to 100 min | • Aged PS NPs were smaller, more hydrophilic (contact angle measurement) and more negatively charged.<br>• In the presence of NaCl, UVA-aged PSNP had enhanced stability due to a reduced Hamaker constants, the formation of O-functional groups which enhanced EDL repulsion, steric hindrance arising from released organic matter.<br>• In CaCl2 solutions, the stability of UV-irradiated particles decreased since $Ca^{2+}$ bridged with O-containing functional groups. | (Liu et al., 2019) |
| • PET CO & COOH-30nm Ablated (-) *heterogenous shape, produced by laser ablation*<br>• Surfactant-free<br>• 300 mg $L^{-1}$ | • NaCl<br>  ○ 2 to 2000 mmol $L^{-1}$<br>  ○ pH not adjusted<br>• Dulbecco's modified Eagle's medium (DMEM)<br>• Fetal bovine serum (FBS)<br>  ○ 10% | • In NaCl, aggregation kinetics by measuring absorbance over time. (λ = 570 nm)<br>• Time-resolved measurement of $d_{zH}$ lasting 72h | • Same initial $d_{zH}$ at pH 4 to 9<br>• In NaCl, CCC = 700 mmol $L^{-1}$<br>• FBS stabilized particles in NaCl concentrations up to 4 mmol $L^{-1}$ by forming a corona<br>• Particles were aggregated in DMEM but stabilized with 10% FBS in DMEM<br>• Stabilization by FBS attributed to the formation of a protein corona. | Magrì et al., 2018 |
| • PSL COOH-40 sphere (-)<br>• PSL NH2-50 sphere (+)<br>• Not surfactant-free<br>• 50 mg $L^{-1}$ | • DI water<br>• ASW<br>• NSW collected from the Tuscan Archipelago, NW Tyrrhenian Sea<br>  ○ Filtered at 0.45 µm<br>  ○ salinity 38‰<br>  ○ total organic carbon 13 mg $L^{-1}$<br>  ○ water hardness 1940 mg $L^{-1}$<br>  ○ oxygen 6.6 mg $L^{-1}$ | • Measurement of $d_{zH}$, PDI and zeta potential at t=0 | • Both particles aggregated in ASW and NSW.<br>• Anionic NPs formed microscale aggregates<br>• Cationic NPs formed nano-scale aggregates<br>• Electrostatic repulsion played a dominant role in stability. | Manfra et al., 2017 |

| | | | | |
|---|---|---|---|---|
| • PSL NF-100nm sphere (-)<br>• PSL NF-100nm aged (-) *photochemically-aged with UVC +H2O2 for up to 120 hours*<br><br>• Not surfactant-free<br>• 10 mg L-1 | • Monovalent electrolytes<br>  ○ NaCl, KCl<br>  ○ 50 to 800 mmol $L^{-1}$<br>  ○ pH 3.5, 5.5, 7.5 and 9.5 (NaCl)<br>  ○ pH 7.5<br>• Divalent electrolytes<br>  ○ $MgCl_2$, $CaCl_2$, $BaCl_2$,<br>  ○ 1 to 100 mmol $L^{-1}$<br>  ○ pH 7.5<br>• Plurivalent electrolytes<br>  ○ AlCl3 and FeCl3<br>  ○ 0.1 to 10 mmol $L^{-1}$<br>  ○ pH 7.5<br>• EPS produced by Chlorella pyrenoidosa<br>  ○ Filtered at 0.45 µm<br>  ○ 25 mg $L^{-1}$ | • Time-resolved measurement of $d_{zH}$ lasting 30 min<br>• Measurement of zeta potentials | • Multivalent ions are more efficient at screening the particles' electronic charge.<br>• Increase in CCC due to aging is attributed to particle's increased hydrophilicity.<br>• Lower aggregation rate in NaCl and in the presence of EPS, due to steric repulsion. | (Mao et al., 2020) |
| • PSL COOH-20 sphere (-)<br>• PSL NH2-20 sphere (+)<br><br>• Surfactant-free<br>• 200 mg L-1 | • ASW<br>  ○ 40 g $L^{-1}$<br>• Marine Broth | • Measurements of $d_{zH}$, PDI and zeta potential at t=0 | • Both particles were significantly aggregated in both ASW and marine broth.<br>• Aggregation was higher in ASW than in marine broth, especially for PS-COOH. This was attributed to the stabilizing effect of NOM contained in marine broth.<br>• In marine broth, both particles had a similar zeta potential, suggesting that constituents of the broth adsorb onto the particle surfaces (corona). | (Okshevsky et al., 2020) |
| • PSL NH2-20 sphere (+)<br><br>• Not surfactant-free<br>• 40 and 50mg $L^{-1}$ | • NRW from the Rhône River<br>  ○ Filtered at 0.45 µm<br>  ○ DOC – 0.72<br>  ○ Conductivity = 302 µS $cm^{-1}$<br>  ○ pH = 7.9<br>• $Fe_2O_3$ (particulate iron)<br>  ○ 5 mg $L^{-1}$<br>  pH = 8<br>• Alginate<br>  ○ 0.25 mg $L^{-1}$ to 5 mg $L^{-1}$<br>  ○ pH = 8 | • Measurements of $d_{zH}$ and zeta potential at t=15 minutes | • Aggregation in NRW is intermediate between hetero-aggregation with Fe2O3 only and in the Fe2O3/alginate mixture.<br>• The concentration ratio between Fe2O3, alginate and nanoplastics controls the rate of hetero-aggregation<br>• When PSL NH2-20 (+) are added to river water, isoelectric point is reached at a concentration of 5 mg $L^{-1}$ PSL and sufficient charge inversion to lead to stabilization is reached at concentration of 20 mg $L^{-1}$<br>• When PSL NH2-20(+) are added to Fe2O3 and/or alginate and NRW, the aggregation rate increases linearly with concentration. Then, after charge reversal, aggregation rate decreases exponentially with concentration. | (Oriekhova and Stoll, 2018) |

| | | | | |
|---|---|---|---|---|
| • PSL NH2-90 sphere (+)<br>• Surfactant-free surface<br>• 10 mg $L^{-1}$ | • DI water<br>  ○ pH from 3 to 11<br>• Mineral water 1 (MW1)<br>  ○ pH : 7.0<br>  ○ IS : 2.66 meq $L^{-1}$<br>  ○ DOC = 0.28 mgC $L^{-1}$<br>• MW2<br>  ○ pH: 7.2<br>  ○ IS: 9.70 meq $L^{-1}$<br>  ○ DOC = 0.03 mgC $L^{-1}$<br>• MW3<br>  ○ pH: 7.4<br>  ○ IS: 56.3 meq $L^{-1}$<br>  ○ DOC = 0.25 mgC $L^{-1}$<br>• Lake Geneva water<br>  ○ Filtered at 0.22 µm.<br>  ○ pH: 8.1<br>  ○ IS: 4.97 meq $L^{-1}$<br>  ○ DOC= 1.12 mgC $L^{-1}$<br>• Drinking water<br>  ○ pH: 8.2<br>  ○ IS: 5.04 meq $L^{-1}$<br>  ○ DOC = 0.40 mgC $L^{-1}$ | • Measurements of $d_{zH}$ and zeta potential at t=10 min<br>• Time-resolved measurements of $d_{zH}$, lasting 135 minutes (with continuous stirring at 100rpm) | • In DI water, PSL NH2-90 sphere (+) become unstable at pH = 9<br>• Particles are stable in MW1 and MW2. Particles aggregate in MW3 due low concentrations of NOM and higher IS, which both reduce zeta potential < 20 mV.<br>• Aggregation in drinking water and NLW due to near-neutral charge.<br>• Charge reversal is observed in NLW due to the adsorption of NOM.<br>• Aggregation of PSL NH2-90 sphere (+) attributed to the interplay between, screening of electronic double layer and adsorption of NOM.<br>• Water hardness is not an important parameter impacting PSL NH2-90 sphere (+) | (Ramirez et al., 2019) |
| • PSL COOH-200 sphere (-)<br>• PSL NH2-200 sphere (+)<br>• Surfactant-free<br>• 50 mg $L^{-1}$ | • DI water<br>• Bioassay media:<br>  ○ DAPHTOXKIT F-magna<br>  ○ acute ROTOXKIT F<br>  ○ THAMNOTOXKIT F<br>  ○ pH ~ 8.<br>• SRHA and Alginate<br>  ○ 1 to 5 mg $L^{-1}$<br>  ○ Not filtered | • Measurements of $d_{zH}$ and zeta potential at t=0 | • In DI water PSL COOH-200 sphere (-) is stable from pH 4 to 11 and PSL NH2-200 sphere (+) is stable from pH 3 to 9.<br>• In the bioassay mediums, electrostatic repulsion was diminished causing some aggregation.<br>• Surface complexation of anions caused PSL NH2-200 sphere (+) charge reversal.<br>• Both alginate and SRHA reversed the surface charge of PSL NH2-200 sphere (+) and reduced their aggregation<br>• NOM had no significant influence on PSL COOH-200 sphere (-)<br>• While SRHA did not impact $d_{zH}$, alginate increased particle $d_{zH}$. | (Saavedra et al., 2019) |

| | | | | |
|---|---|---|---|---|
| • PSL NF-50 sphere (-)<br>• PSL NF-100 sphere (-)<br>• Not surfactant-free<br>• 1 or 26 mg $L^{-1}$ | • DI water<br>• ASW | • Measurements of $d_{zH}$ and zeta potential at t=0, 10, 60 and 180 min<br>• Measurements of size by SLS at t=0, 1, 3, 24 and 72 h | • All particles stable in DI water<br>• Aggregation in ASW was attributed to reduced electrostatic repulsion.<br>• Due to high PDI, agglomeration was also evaluated by laser diffraction<br>• Observed deagglomeration of PS NPs after 3 hours by DLS and SLS in ASW<br>• SEM images showed that the agglomerates become more spherical over 72 hours | (Sendra et al., 2019) |
| • PSL NH2-500 sphere (-)<br>• Not surfactant-free<br>• 2.5 mg $L^{-1}$ | • DI water<br>• NSW<br>  ○ Filtered at 0.2 µm<br>• Microalgae medium (NSW + 1mL $L^{-1}$ Conway medium)<br>  ○ Filtered at 0.2 µm<br>  ○ pH 7.5 to 7.9 | • Measurements of $d_{zH}$, PDI and zeta potential at 0, 10, 60 and 180 min | • Significant aggregation in both NSW and microalgae medium.<br>• The high IS eliminates EDL repulsion between particles.<br>• NOM likely interacts with the particle surface groups, which promotes aggregation | Seoane et al., 2019 |
| • PSL NF-25 sphere (-)<br>• Not surfactant-free<br>• 10 µg $L^{-1}$ | • NLW from Lake Yosemite<br>  ○ pH = 7.57<br>  ○ Filtered at 0.22 µm<br>  ○ $Ca^{2+}$ 0.62 mmol $L^{-1}$<br>  ○ $Mg^{2+}$ 0.25 mmol $L^{-1}$<br>• NRW from Hartley Slough River<br>  ○ pH= 6.92<br>  ○ Filtered at 0.22 µm<br>  ○ $Ca^{2+}$ 0.21 mmol $L^{-1}$<br>  ○ $Mg^{2+}$ 0.065 mmol $L^{-1}$<br>  ○ DOC = 1.28 mg $L^{-1}$<br>• ASW | • Description of microgel formation by $d_{zH}$ measurements at t= 0h up to 10 days and by flow cytometry at t= 10 days | • Nanoplastic particles promoted POM formation in lake and river water and accelerated the transition from dissolved to particulate organic matter.<br>• This is attributed to the hydrophobic interactions between plastics and DOM | (Shiu et al., 2020) |
| • PSL NF-100 sphere (-)<br>• Emulsified with SDS<br>• 0.005, 0.05, 0.5, 5, 50 mg $L^{-1}$ | • Di water<br>• ASW | • Measurements of $d_{zH}$ of PSL NF-100 sphere (-) collected from top medium and bottom part of exposure media after 1, 24 and 72 h. | • PS NPs in seawater aggregate and sediment.<br>• At lower particle concentration lower aggregation is expected due to lower probability of particles collisions | (Silva et al., 2020) |

| | | | | |
|---|---|---|---|---|
| • PSL NF-240 spherical (-)<br>• Surfactants removed by dialysis<br>• 10mg $L^{-1}$ | • Monovalent electrolyte<br>• NaCl<br>  ○ pH=6<br>  ○ 10 mmol L-1 to 250 mmol $L^{-1}$<br>• Divalent electrolyte<br>• CaCl2 HgCl2, ZnCl2, CdCl2<br>  ○ pH=6<br>  ○ 1 mmol L-1 to 50 mmol $L^{-1}$<br>• HA<br>  ○ pH =6<br>  ○ Filtered at 0.45 µm<br>  ○ 5 mg $L^{-1}$<br>• Bentonite clay suspension<br>  ○ pH = 6<br>  ○ 50 and 100 mg $L^{-1}$<br>  ○ 138 ± 6 nm<br>• NRW Hooghly River<br>  ○ pH 8.4<br>  ○ TOC = 1.90 mg $L^{-1}$<br>  ○ TDS = 255 mg $L^{-1}$<br>  ○ Filtered at 0.22 µm<br>• NGW from Kolkata Campus (<br>  ○ pH = 7.3<br>  ○ TOC = 3.33 mg $L^{-1}$<br>  ○ TDS = 538 mg $L^{-1}$<br>  ○ Filtered at 0.22 µm<br>• NSW from Digha, India<br>  ○ pH = 8.3<br>  ○ TOC = 4.89 mg $L^{-1}$<br>  ○ TDS = 36 000 mg $L^{-1}$<br>  ○ Filtered at 0.22 µm | • Time-resolved measurement of $d_{zH}$ lasting 10 minutes<br>• Measurements of zeta potential as a function of pH | • CCC detemined in different conditions<br>• Divalent cations have a greater influence on stability than monovalent cations, at all temperatures.<br>• Increase in temperature decreases stability.<br>• DOM stabilizes particles by steric repulsion and electrostatic repulsion in NaCl.<br>• DOM destabilizes particles in CaCl2. This was attributed to due to cationic bridging<br>• Clay colloids heteroaggregate with NPs.<br>• Heavy metal salts such as ZnCl2 and CdCl2 behave similarly to CaCl2. However, redox speciation of HgCl2 into Hg(0) does not cause PSNP aggregation.<br>• PSNPs were least stable in NSW, followed by NRW and NGW due to different salt and organic matter concentrations. | (Singh et al., 2019) |

| | | | | |
|---|---|---|---|---|
| • PSL COOH-200 nm (-)<br>• PSL COOH-50 nm (-)<br>• PSL NH2-50 nm (+)<br><br>• Not surfactant-free<br>• 10 mg $L^{-1}$ | • NGW<br>  ○ pH 7.11<br>  ○ Conductivity 878 µS $cm^{-1}$<br>  ○ 0.01 to 0.03 mmol $L^{-1}$ Fe<br>  ○ Unfiltered : > 50 mgC.$L^{-1}$<br>  ○ Filtered at 1.00 µm : > 25 mgC.$L^{-1}$<br>  ○ Filtered at 0.45 µm : > 25 mgC.$L^{-1}$<br>• AGW<br>  ○ identical $Ca^{2+}$ concentration and pH as NGW | • Measurements of $d_{zH}$ and zeta potential, at t= 0, 1, 2, and 3 h | • Surface functional groups affect the affinity of NOM and $Ca^{2+}$ to nanoplastics.<br>• DOM increased particle stability and suspended POM decreased stability of both particles<br>• DOM adsorbed onto PSL NH2-50 nm (+)<br>• POM did not adsorb onto PSL NH2-50 nm (+)<br>• PS COOH adsorbed both $Ca^{2+}$, DOM and POM | (Song et al., 2019) |
| • PSL NF-50 sphere (-)<br>• PSL NF-100 sphere (-)<br>• PSL NF-500 sphere (-)<br>• PSL NF-1000 sphere (-)<br><br>• Not surfactant-free (presence of Tween 20)<br>• 5 mg $L^{-1}$ | • NSW from the Faroe-Shetland Channel<br>• NSW from the Leven docks on the Firth of Forth estuary<br>• EPS isolated from Halomonas sp. TGOS-10<br>  ○ Filtered at 0.22 µm<br>  ○ 1500 mg $L^{-1}$ | • 24h incubation with NSW or NSW + EPS, then aggregates of plastic and NOM retained on filter analysed by microscopy and flow cytometry.<br>• After 7 days of incubation, agglomerates > 5µm recovered and their settling rate studied in sand-filtered NSW. | • Total number of aggregates formed was not affected by particle size.<br>• Larger aggregated were formed with PSL NF-50 nm sphere (-) due to higher particle concentration and higher probability of collision.<br>• Low (<1 mg $L^{-1}$) EPS concentration has a dispersant effect. Then (> 1 mg $L^{-1}$) EPS has a flocculant effect (higher numbers of agglomerates).<br>• Size of agglomerates were constantly around ~4 µm (attributed to shear stress caused by the mixing of the bottles).<br>• All sedimentation rates were equal, due to same size of agglomerates | (Summers et al., 2018) |
| • PSL NF-50 sphere (-)<br>• PSL COOH-50 sphere (-)<br>• PSL NH2-50 sphere (+)<br><br>• Not surfactant-free<br>• 100 mg $L^{-1}$ | • DI water<br>  ○ pH 6.6 ± 0.2<br>• ASW<br>  ○ pH 8.1 ± 0.1<br>  ○ 63.25, 326.5, 489.75 and 653 mmol L-1<br>• NSW from the Bay of Brest<br>  ○ Filtered at 2 µm<br>  ○ pH 8.2 ± 0.1<br>• HA<br>  ○ Filtered at 0.22 µm<br>  ○ 1, 10 and 30 mg $L^{-1}$ | • Measurements of $d_{zH}$, PDI and zeta potential, at t= 0 24 and 48h for ASW and DI water; at t=0 for NSW | • In DI water, all particles were stable.<br>• In ASW and NSW, PSL NH2-50 nm sphere (+) remain stable while PSL NF-50 nm sphere (-) and PSL COOH-50 nm sphere (-) aggregated in ASW (up to t=48h) and NSW (t=0). Aggregation was attributed to EDL screening<br>• HA did not significantly increase stability of nanoplastic particles. | (Tallec et al., 2019) |
| • PSL -100 sphere (-)<br>• PSL COOH-100 sphere (-)<br>• PSL NH2-100 sphere (-)<br>• PSL NH2-100 sphere (+)<br>• Not surfactant-free<br>• 300 mg $L^{-1}$ | • NaCl<br>  ○ 0, 5, 10, 20, 30 and 35 g.$L^{-1}$<br>  ○ pH 4, 7 and 9<br>• FA<br>  ○ Unfiltered<br>  ○ 0, 5, 10, 25, and 50 mg $L^{-1}$ | • Sonication for 15minute followed by shaker for 24h at 200 rpm<br>• Measurements of $d_{zH}$ and zeta potential, at t= 0 and 24h | • No effect of pH on stablility<br>• NaCl accelerated the aggregation of all particles<br>• FA mainly stabilized the three negatively charged NPs.<br>• Low FA concentrations caused PSL NH2-100 nm sphere (+) aggregation. The joint effect mainly depended on their concentration ratio. | (Wu et al., 2019) |

| | | | | |
|---|---|---|---|---|
| • PSL NF-100 sphere (-)<br>• PSL COOH-100 sphere (-)<br>• PSL NH2-100 sphere (+) (grafted PEI)<br><br>• Not surfactant-free<br>• 10 mg L-1<br><br>• PS -60 nm Ablated (-) *polydisperse particles formed by laser ablation of polystyrene films*<br>• Surfactant-free<br>• 1 mg $L^{-1}$ | • NaCl<br>  ○ 200 to 1000 mmol $L^{-1}$<br>• CaCl2<br>  ○ 5 to 150 mmol $L^{-1}$<br>  ○ pH 7.4<br>• SRHA<br>  ○ Filtered at 0.22 µm<br>  ○ 1, 2, 5, 10 mg $L^{-1}$ | • Time-resolved measurement of $d_{zH}$ lasting 10 to 90 minutes<br><br>• For PS Ablated-60 nm (-), 4 individual $d_{zH}$ measurements, corresponding to an average over 3 minute after 30 minutes. | • CCCs determined for all three spherical nanoplastic models.<br>• Negatively charged PSLs were stabilized by electrostatic repulsion in NaCl and CaCl2 solutions.<br>• SRHA provided steric hindrance and suppressed aggregation in NaCl<br>• In CaCl2 low concentrations of SRHA (<5mgC $L^{-1}$) enhanced stability since there was insufficient free SRHA to create bridges between particles. At high concentrations (>5mgC $L^{-1}$) SRHA decreased stability, due to bridging.<br>• PSL NH2-100 nm sphere (+) were destabilized in NaCl, by low SRHA concentrations (displacement of grafted PEI). Higher SRHA concentrations increased stability by neutralizing or reversing positive surface charges<br>• No bridging between SRHA and PSL NH2-100 nm sphere (+) by $Ca^{2+}$<br>• For PS Ablated-60 nm (-) aggregation occurred at lower ionic strength than for all PSLs.<br>• SRHA decreased aggregation in NaCl and in low concentrations of CaCl2.<br>• Cation bridging was observed for PS Ablated-60 nm (-) at high concentrations of divalent electrolytes and SRHA. | (Yu et al., 2019) |
| • PSL NH2-200 sphere (+)<br><br>• Not surfactant-free<br>• 5, 10 and 20 mg $L^{-1}$ | • DI water<br>  ○ pH not adjusted<br>• BG1 Algae growth medium<br>  ○ pH 7.12<br>• Glyphosate<br>  ○ 5 mg $L^{-1}$ | • Measurements of $d_{zH}$ and zeta potential at t = 0 | • In BG1 algal medium, a decrease in size was observed in the presence of glyphosate.<br>• Stabilization of negatively charged PS NH2-200 nm sphere (+) by glyphosate is attributed to the adsorption of glyphosate to the surface and subsequent increase in hydrophilicity. | (Zhang et al., 2018) |
| • PSL NF-100 sphere (-)<br>• PSL COOH-100 sphere (-)<br>• PSL NH2-100 sphere (-)<br><br>• Not surfactant-free<br>• 10 mg $L^{-1}$ | • $CaCl_2$ and $MgSO_4$ (mol:mol of 4:1)<br>  ○ 2.5 and 10 mmol $L^{-1}$ divalent cations<br>  ○ pH 6, 7.8 and 9<br>• FA<br>  ○ Filtered at 0.22 µm<br>  ○ 0.5 and 5 mg $L^{-1}$ | • Particles were allowed to settle in a climate chamber.<br>• Measurements of $d_{zH}$ and zeta potential of dispersions at t=1h, 12h, 1, 2, 3, 7, 14 and 21 days | • 0.5 mg $L^{-1}$ NOM has no effect on zeta potential or size. 5mg $L^{-1}$ NOM decreased absolute value of zeta potential and had negligible effects on the size.<br>• Divalent cations decreased absolute value of zeta potential and increased size.<br>• Together, DOC and divalent cations enhanced the extent of aggregation of all particles due to cation bridging. With both DOC and divalent cations, there is no significant difference in the zeta-potential of different particles. | (Zhang et al., 2019) |

The previous Chapter has revealed that a shortcoming of current studies on nanoplastic aggregation is that the nanoplastic models are often not representative of environmental nanoplastics. Indeed, latex spheres are often used as nanoplastic models. These have spherical shapes and smooth surfaces either composed of pristine polymer or polymer grafted with chemical groups that do not always naturally occur. Furthermore, these particles are often dispersed with surfactants and other additives. As explained, the degradation of plastic debris in the environment is expected to produce particles with irregular morphologies and devoid of any surfactants. Therefore, there is a critical knowledge gap concerning the stability of environmentally relevant nanoplastic models.

The following Chapter aims to start filling this knowledge gap by comparing the stability of two nanoplastic models with different degrees of environmental relevance: a carboxylated latex sphere and a novel nanoplastic model produced from fragmenting polystyrene pellets. Due to its nonspherical, irregular shape, polydisperse size distribution, and moderate surface charge, this fragmental nanoplastic is more environmentally relevant than latex spheres. The stability is assessed in simplified solution chemistry, where only electrostatic screening occurs. Then, the process by which NOM stabilizes nanoplastics is assessed using two complementary optical methods (DLS and A4F-SLS). These findings contribute to our assessment of nanoplastics' transport in porous media (Chapter 4) and their mobility in polar surface waters (Chapter 5).

This Chapter was published as a research article in the journal *Environmental Science and Technology Water* in March 2021. **Cite as:** Pradel, A., Ferreres, S., Veclin, C., El Hadri, H., Gautier, M., Grassl, B., Gigault, J., 2021. Stabilization of Fragmental Polystyrene Nanoplastic by Natural Organic Matter: Insight into Mechanisms. *ACS EST Water*. doi: https://doi.org/10.1021/acsestwater.0c00283

# Chapter 2

# Stabilization of fragmental polystyrene nanoplastic by natural organic matter: Insight into mechanisms

Alice Pradel[a], Séléna Ferreres[a], Cloé Veclin[b], Hind el Hadri[b], Maud Gautier[a], Bruno Grassl[b], Julien Gigault[a,c]

[a]Univ Rennes, CNRS, Géosciences Rennes - UMR 6118, 35000 Rennes, France

[b]CNRS/Univ Pau & Pays Adour/E2S UPPA, Institut des sciences analytiques et de physicochimie pour l'environnement et les matériaux, UMR 5254, 64000 Pau, France

[c]TAKUVIK, CNRS/Université Laval, UM I3376, G1V 0A6 Québec, Canada

**Abstract:** The increasing amount of plastic debris in the environment and its disintegration into submicrometric particles is a cause for concern. Due to the colloidal nature of nanoplastics, their environmental fate should be investigated separately from that of microplastics. Abiotic factors greatly influence nanoplastics' stability. This will affect its residence time in the hydrosphere. So, we investigated the behavior of two different nanoplastic models (with different sizes and shapes) regarding ionic strength, pH, and varying concentrations of two natural organic matters: humic acid and sodium alginate. The results demonstrate that both natural organic matters enhanced the aqueous stability of nanoplastics over time at high ionic strengths. Depending on the organic matter's nature, different stabilizing mechanisms were revealed using dynamic light scattering and asymmetrical flow field flow fractionation coupled to static light scattering. Humic acid provides electrostatic repulsion between particles, and some larger humic acid molecules provide a steric hindrance. Sodium alginate sorbs onto and bridges separate particles and small aggregates of nanoplastics. The covered particles are stabilized by steric hindrance. The results highlight the importance of considering natural organic matters' properties when assessing nanoplastics behavior in the environment.

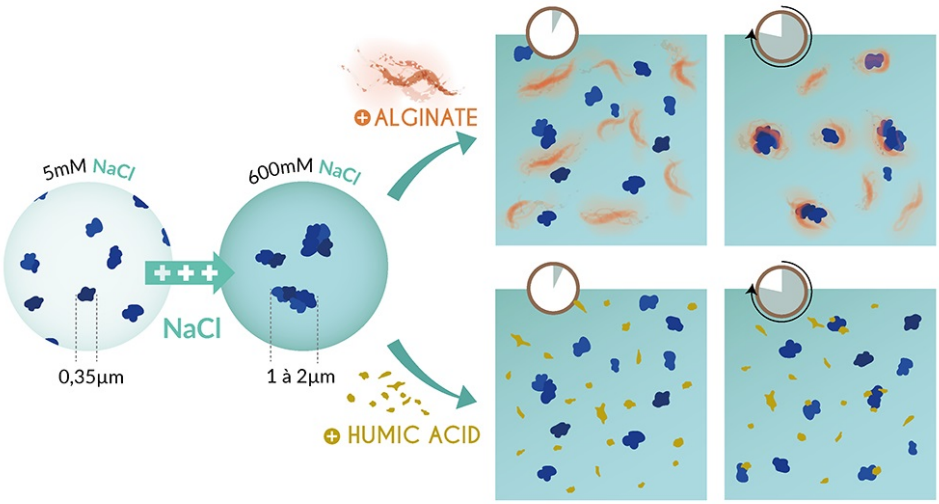


**Keywords:** Plastic debris, Environmental fate, Aggregation, Ionic strength, Morphology

**Synopsis:** Mechanisms of nanoplastic stabilization will depend on the composition of the natural organic matter.

## 2.1 Introduction

As the use of plastic-based materials increases, plastic waste in the environment increases proportionally(Geyer, Jenna R. Jambeck, and Kara Lavender Law 2017; J. R. Jambeck et al. 2015). These last five years, it was demonstrated that plastic debris could persist as nanoplastic ($< 1\mu$m) before eventual mineralization of the polymer (Gigault, Pedrono, et al. 2016; Lambert and M. Wagner 2016; Lixin Zhu et al. 2019). Environmental sampling of plastic debris at the ocean surface, coupled to numerical modeling, suggests that a substantial part of all the plastic debris is composed of nanoplastics (Albert A Koelmans et al. 2017a; Ter Halle et al. 2017; van Sebille, Wilcox, et al. 2015). Since nanoplastics are an emerging contaminant, their environmental fate should be better described. While airborne transport of microplastics is increasingly coming under scrutiny (Allen et al. 2019; Evangeliou et al. 2020), water remains the environmental compartment where most plastic debris is found (GESAMP 2016; Horton et al. 2017) and where oxidative and hydrolytic conditions are favorable to plastic degradation (Chamas et al. 2020; Gewert, Plassmann, and MacLeod 2015; Julienne, Delorme, and Lagarde 2019; Min, Cuiffi, and Mathers 2020). As such, it is crucial to understand the behavior of nanoplastics in aqueous systems.

To describe a colloidal material's environmental fate in aqueous systems, successive and complementary approaches consist of modeling simple environmental systems in the lab, using these results to establish numerical simulations, and, finally, confronting these simulations with the analysis of environmental samples (Buffle et al. 1998). Based on this approach, experimental systems describing nanoplastics' fate have emerged (Alimi, Farner, and Tufenkji 2021), especially concerning porous media(Z. Dong, Ling Zhu, et al. 2019; A. S. Keller, Jimenez-Martinez, and Mitrano 2019; Jin Liu, T. Zhang, et al. 2019) and water (Y. Li et al. 2019; Oriekhova and Stoll 2018). Nanoplastics' stability in water is generally determined by measuring changes in their size and sedimentation rates. Using this approach, the stability of nanoplastics has been assessed in natural waters (Bergami et al. 2019; Z. Chen et al. 2020; Della Torre et al. 2014; González-Fernández et al. 2019; Manfra et al. 2017; Oriekhova and Stoll 2018; Ramirez et al. 2019; Seoane et al. 2019; Singh et al. 2019; Z. Song et al. 2019; Tallec et al. 2019), in deionized water with various ionic compositions, ionic strengths, and pHs(Cai et al. 2018; Z. Chen et al. 2020; Z. Dong, W. Zhang, et al. 2019; Y. Li et al. 2019; Jin Liu, T. Zhang, et al. 2019; Magrì et al. 2018; Mao et al. 2020; Singh et al. 2019; J. Wu et al. 2019; Yu, Shen, et al. 2019; F. Zhang et al. 2019), in the presence of NOM and suspended sediments (Cai et al. 2018; González-Fernández et al. 2019; Y. Li et al. 2019; Magrì et al. 2018; Oriekhova and Stoll 2018; Saavedra, Stoll, and Slaveykova 2019; Singh et al. 2019;

Tallec et al. 2019; J. Wu et al. 2019; Yu, Shen, et al. 2019; F. Zhang et al. 2019) and in the presence of extracellular polymeric substances (EPS)(Mao et al. 2020; Summers, Henry, and Gutierrez 2018). Most studies have used polystyrene (PS) latex spheres, which are perfectly smooth, spherical, and monodisperse in size. Recently, the stability of more environmentally relevant models, such as aged polystyrene (PS) latex spheres, laser-ablated PS, or fragmental PET, has been studied (S. Dong et al. 2020; Y. Liu et al. 2019; Mao et al. 2020; Yu, Shen, et al. 2019).

While these studies allow the emergence of global trends concerning nanoplastic stability, they also have inconsistent conclusions. For example, nanoplastic models have been observed to be both stable and unstable in artificial seawater (Okshevsky et al. 2020; Tallec et al. 2019), and in the presence of iron (Cai et al. 2018; Oriekhova and Stoll 2018). Such discrepancies can be explained first by the physical and chemical properties of the nanoplastics models used (size, shape, surface functionalization, composition, purity, etc.), which are known to strongly affect the behavior of colloidal materials. Additionally, nanoplastics are strongly sensitive to the media's properties (type, concentration, and speciation of electrolytes, nature of the organic matter, pH). Indeed, according to the relative concentration of spherical PS nanoplastic models, NOM, and cations, opposite behaviors have been observed (Oriekhova and Stoll 2018; Yu, Shen, et al. 2019).

In light of these observations, the stability of two nanoplastic models was studied. The first model is a monodisperse polystyrene latex (PSL) sphere. The second model is produced from the mechanically degraded primary microplastic (PS pellets) and, as such, is more environmentally relevant due to its irregular, asymmetrical shape and polydisperse size. NPs' aqueous stability was assessed at different ionic strengths (5 to 770 mmol $L^{-1}$ NaCl) and in the presence of varying concentrations (0.005 to 140 mg $L^{-1}$) of two NOMs which have different properties: humic acid (HA) and sodium alginate (SA). HA has a relatively compact structure and amphiphilic properties, whereas SA has a more linear structure with hydrophilic properties. HA represents terrestrial organic matter, whereas SA represents marine organic matter and is a significant component of EPS produced by microbial communities (Flemming and Wingender 2010; Stumm and Morgan 1996). It was demonstrated that both NOMs stabilize the environmentally relevant NP model at high ionic strength. However, due to their different physicochemical properties, the NOMs have different stabilizing mechanisms. These were characterized by asymmetrical flow field flow fractionation coupled to static light scattering (A4F-SLS) and confirmed by dynamic dynamic light scattering (DLS). The present work discusses these mechanisms and their possible implication for the fate of nanoplastics in both terrestrial and marine environments.

## 2.2 Experimental section

### 2.2.1 Sample Preparation

All aqueous solutions and dispersions were prepared with analytical grade deionized (DI) water (Millipore, 18.2 MΩ). A stock solution of NaCl (solid, LabKem ExtraPure) at 1.80 mol $L^{-1}$ was prepared. The pH of all solutions was fixed at pH of 5, 6.5, or 8 using NaOH (Fisher Scientific, Analytical Grade) and HCl (70%, Sigma Aldrich, ACS Grade). All solutions and dispersions were stored at 4 °C in the dark before use. Two nanoplastic (NPs) models were used in this study and are described in Table 2.1 and illustrated in Figure 2.1. Carboxylated polystyrene latex spheres of 200 nm (*PSL COOH*) are purchased from Polysciences© (Polybead®Carboxylate Orange Dyed Microspheres 0.20 $\mu$m, Warrington USA). A stock dispersion at a concentration of 100 mg $L^{-1}$ was prepared. A NP model with irregular and polymorphic shapes (*NPT-P*) was produced by the mechanical abrasion of industrial-grade polystyrene (PS) pellets (Total, Paris, France) as described by El Hadri et al. 2020. The pellets are composed of primary (*-P*) PS, which contains no additives and has not been aged. Due to the less stable nature of the *NPT-P* compared to *PSL COOH*, the experiments presented here used different batches of *NPT-P* to avoid a bias brought about by the aging of the stock dispersion. Each batch was produced using PS from the same degradation round. Before each experiment, the size of the nanoplastic dispersions was verified with DLS measurements. Concentration of the stock *NPT-P* solution was measured with a Total Carbon Analyzer (Shimadzu TOC-V CSH) and varied between 22 and 35 mg $L^{-1}$. According to the molecular composition of PS, 1 mg $L^{-1}$ of organic carbon was converted to 1.08 mg $L^{-1}$ *NPT-P*.

*Table 2.1: Characteristics of the two nanoplastic (NP) models. The polydispersity index (PDI) is defined as the variance of the Gaussian-fitted size distribution. The aspect ratio is defined as the ratio of the length of the major axi and minor axi as determined by TEM images (Figures 2.1 and 2.2)*

| *Nanoplastic model* | z-average diameter (nm) | Polydispersity Index (PDI) | Aspect ratio* | Zeta potential in 5 mmol $L^{-1}$ NaCl (mV) | | |
|---|---|---|---|---|---|---|
| | | | | pH 5 | pH 6.5 | pH 8 |
| *PSL COOH* | 197 ± 2 | 0.03 ± 0.01 | 1.02 ± 0.05 | -37.69 ± 1.91 | -38.65 ± 2.23 | -42.80 ± 2.98 |
| *NPT-P* | 339 ± 7 | 0.18 ± 0.03 | 1.70 ± 0.57 | -31.67 ± 1.01 | -33.54 ± 2.72 | -35.14 ± 2.13 |

**Figure 2.2 illustrates the aspect ratio of NPT-P particles*

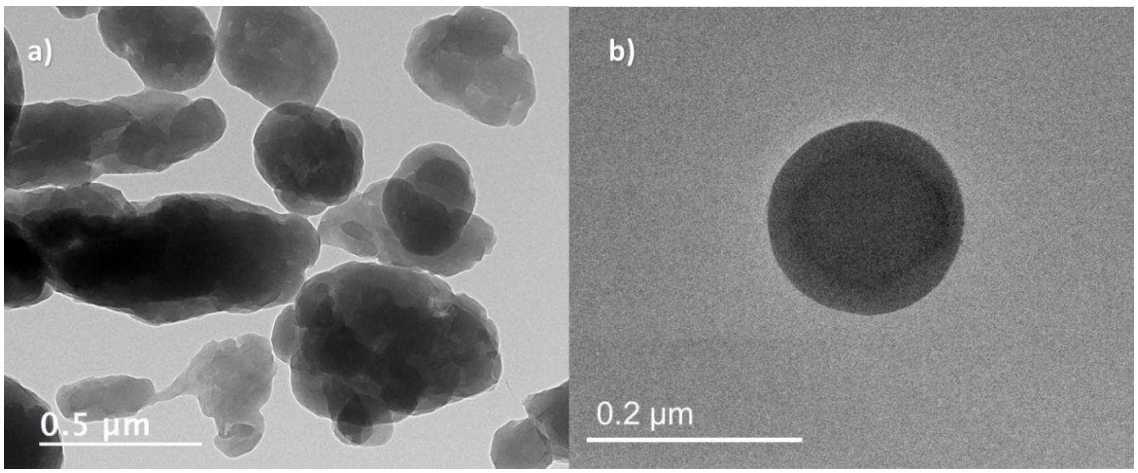


*Figure 2.1: Transmission Electron Microscopy Images of a) NPT-P and b) PSL COOH*

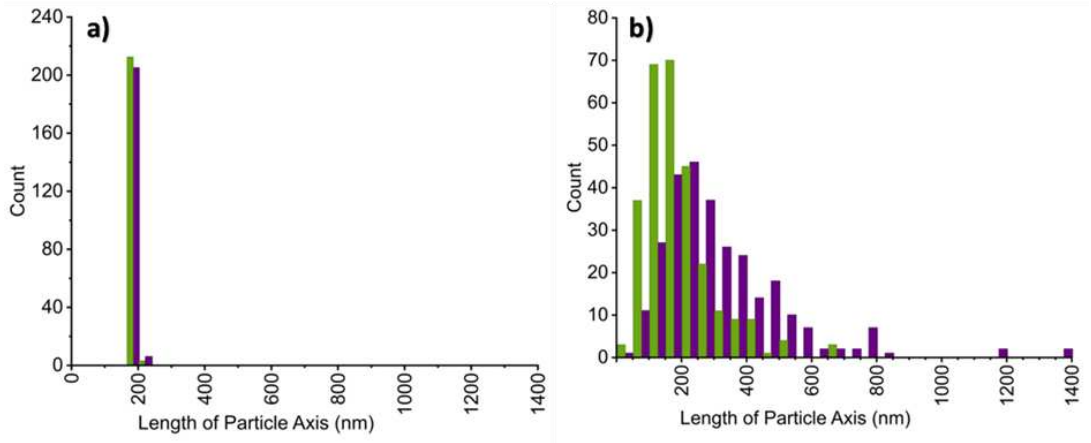


*Figure 2.2: Histogram of short axis (green) and long axis (purple), as determined by TEM images of a) PSL COOH and b) NPT-P nanoplastic models in linear distribution (PSL COOH: n = 212 and NPT-P: n = 283)*

TEM images were obtained by a Jeol JEM 2100 HR (200kV) with an $LaB_6$ filament. The camera was a Gatan Orius SC 200 D. A 4 '$\mu$L drop was deposited on a full carbon grid and allowed to air dry. Data was analyzed with ImageJ software and the NanoDefine plugin, using the watershed fitting mode (Verleysen et al. 2019). The length of the major axi and minor axi were the longest and shortest lengths of the minimum bounding rectangle. Based on these images and assuming the *NPT-P* particles is either a sphere or an ellipsoid, the specific surface area was determined to be 30.2 $\pm$ 16.4 and 34.2 $\pm$ 18.9 $m^2g^{-1}$, respectively. The specific surface area was determined to be 29.6 $\pm$ 0.6 $m^2g^{-1}$ for *PSL COOH*. The *NPT-P* minor and major axi followed a log-normal distribution, as determined with the orthogonal distance regression method. Equation 2.1 was used to fit the data, with $\mu$ the average of distribution and $\sigma$ the standard deviation of distribution.

$$y = \frac{A}{\sigma x \sqrt{2\pi}} \cdot \exp \frac{-\ln (x/\mu)^2}{2\sigma^2} \tag{2.1}$$

The following parameters were determined, for the *NPT-P* major axis:

- $\mu = 395.70 \pm 30.65$
- $\sigma = 380.52 \pm 48.34$
- $A = 20734.02 \pm 6774.76$
- $R^2(COD) = 0.99994$

and for the *NPT-P* minor axis :

- $\mu = 213.54 \pm 3.93$
- $\sigma = 461.88 \pm 13.53$
- $A = 9986.26 \pm 260.98$
- $R^2(COD) = 0.98101$

Sodium alginate (SA) was prepared by introducing 60 mg of SA powder (solid, Acros Organics) into 0.1 L DI water and mixing at 350 rpm in a square bottle overnight. The humic acid (HA) used in this work was Leonardite purchased from the International Humic Substance Society (IHSS). The stock solution of HA was prepared by adding 50 mg of Leonardite powder to 0.1 L of DI water. To solubilize the stock solution, pH was adjusted to 11 (with NaOH at 0.1 mol $L^{-1}$) under continual agitation with a magnetic stirrer. Then, the solution was mixed at 350 rpm for 24h. pH was then fixed to either 5, 6.5, or 8 using 0.1 mol $L^{-1}$ HCl. The concentrations of the NOM stock solutions were determined with a Total Carbon Analyzer (Shimadzu TOC-V CSH). According to the NOM's molecular composition, 1 mg $L^{-1}$ of organic carbon was converted to 1.6 mg $L^{-1}$ HA and 2.8 mg $L^{-1}$ SA.

### 2.2.2 Size characterization

Hydrodynamic diameters ($d_H$) were determined by dynamic light scattering (DLS) probe (Vasco-Flex, Cordouan Technologies, Pessac, France). The measured $d_H$ of an agglomerating suspension is the average of the $d_H$ of the individual particles and aggregates, weighted by their scattered light intensities (Holthoff et al. 1996). The backscattered light is collected at a geometric angle of 170° with respect to the incident beam direction. For time-resolved DLS, each correlation function was accumulated for 60 seconds and were spaced 30 seconds apart. DLS measurements of stock solutions are composed of an

average of six measurements of 60 seconds. The z-average hydrodynamic diameter ($d_{zH}$) was determined by fitting a normal distribution to the raw data using the cumulant algorithm. To analyze the different populations in size present in a dispersion, the Sparse Bayesian learning (SBL) algorithm was used. The distribution of the NPs' gyration radii was measured by static light scattering (DAWN HELEOS 18 Angles, Wyatt Technology) with prior size fractionation using an asymmetrical flow field flow fractionation (A4F, Eclipse 3+, Wyatt Technology, Dernbach, Germany) and a UV-vis absorbance detector (1200 series, Agilent Technologies, France) as a concentration detector at 254 nm.

A global method of A4F separation was used. It was previously optimized by Gigault, El Hadri, Reynaud, et al. 2017 and is briefly described here. The mobile phase flow was generated by a 1200 series high-performance liquid chromatography (HPLC) pump (Agilent Technologies, Les Ulis, France). The Asymmetrical Flow Field Flow Fractionation (A4F) system was an Eclipse 3+ (Wyatt Technology, Dernbach, Germany). Injections were performed with an Agilent Technologies 1200 series autosampler. At the outlet, the detectors were a 1200 series UVvis absorbance detector (Agilent Technologies, Les Ulis, France) and a DAWN HELEOS multi-angle laser, static light scattering (SLS) detector (Wyatt Technology). For UV-Vis detection, the selected wavelength was 254 nm. The A4F channel height was established using a spacer (Mylar film) of 250 $\mu$m. The dimensions of the spacer were 26.5 cm length and narrowing width from 2.1 to 0.6 cm. The accumulation wall was composed of Polyethersulfone (PES) 10 kDa membranes (Wyatt Technology). The A4F method was based on the general (fast) method O described by Gigault, El Hadri, Reynaud, et al. 2017. The elution flow rate was fixed at 0.5 mL $min^{-1}$. The injection flow rate was fixed at 0.2 mL $min^{-1}$. The focus-flow during the relaxation was 0.5 mL $min^{-1}$ and the cross-flow rate during elution ($V_c$), was a function of time (t) $V_c = 2\exp^{0.27t}$. The mobile phase was composed of 0.5 mmol $L^{-1}$ NaNO3 (>99% purity Reagent Plus, Sigma Aldrich), which was filtered on polyethersulfone (PES) filters (0.1 $\mu$m, Pall®), purchased from VWR (Fontenay-sous-Bois, France). The injection volume was 100 $\mu$L. First, the effects of the duration of the focus period and the ionic strength of the injected dispersion, on the quality of detection were studied. Subsequently, a focus time of 5 minutes and an ionic strength of 600 mmol $L^{-1}$ was selected. The injected dispersion was prepared in the same way as for the aggregation kinetic study, described below. Data from a minimum of 14 out of 18 SLS detectors were collected and processed using Astra software, version 6 (Wyatt Technology). The radius of gyration ($R_g$) was determined using the Berry formalism using SLS signal at different angles.

### 2.2.3 Kinetics of Colloidal Aggregation

The kinetics of nanoplastic aggregation were determined by measuring the z-average hydrodynamic diameters ($d_{zH}$) of the dispersions over one hour. A total volume of 3 mL was prepared by adding NaCl and DI water to the vial, followed by NOM (when it was studied), and vigorously mixing the solution. Finally, the nanoplastic dispersion was added to the vial, marking the beginning of the kinetic study. All kinetic studies were performed in triplicate. The aggregation rate (k) was determined from the slope of the one hour-long kinetic study, according to equation 2.2:

$$\left(\frac{\partial d_{zH}(t)}{\partial t}\right)_{t\to 0} \propto kN_0 \tag{2.2}$$

where $d_{zH}(t)$ is the hydrodynamic diameter of aggregates as a function of time t and $N_0$ is the initial number-based particle concentration. Statistical analyses were operated using one-way ANOVA. Pairwise comparisons of aggregation rates were made using Tukey's method.

At low ionic strengths, electrostatic repulsion between particles is high due to a thick electrical double layer (EDL): the colloidal dispersion is said to be in the reaction-limited aggregation (RLA) regime. As ionic strength increases, electrostatic repulsion decreases, and the aggregation rate increases. At an ionic strength corresponding to the critical coagulation concentration (CCC), the interparticle energy barrier is eliminated, aggregation rate is maximal ($k_{fast}$), and the diffusion-limited aggregation (DLA) regime is reached. The attachment efficiency $\alpha$ describes aggregation kinetics by normalizing aggregation rates under RLA regime (k) by the DLA regime ($k_{fast}$):

$$\alpha = \frac{k}{k_{fast}} = \frac{\left(\frac{\partial d_{zH}(t)}{\partial t}\right)_{t\to 0}}{\left(\frac{\partial d_{zH}(t)}{\partial t}\right)_{t\to 0,fast}} \tag{2.3}$$

### 2.2.4 Derjaguin Landau Verwey Overbeek (XDLVO) theory of colloidal stability

The total interaction energy as a function of the distance separating the particles, $G^{tot}(h)$, is calculated as the sum of the Lifshitz-van der Waals attraction, $G^{LW}(h)$, the electrical double layer (EDL) repulsion, $G^{el}(h)$, and the Lewis acid-base energy of interaction

$G^{AB}$(h). The surface interaction energy was calculated at an ionic strength of 5 mmol $L^{-1}$. Particle diameters and zeta-potential are presented in Table 2.1. The Lifshitz-van der Waals component, $G^{LW}$(h), was calculated using the expression of the retarded van der Waals interactions between two identical approaching spheres proposed by Gregory 1981:

$$G^{LW} = -\frac{H r_{p1} r_{p2}}{6\left(r_{p1} + r_{p2}\right) h} \cdot \left[1 - \frac{bh}{\lambda} ln\left(1 + \frac{\lambda}{bh}\right)\right] \tag{2.4}$$

where H is the Hamaker constant of polystyrene particles interacting through water, equal to 1.23 $10^{-20}$ J; $r_{p1}$ and $r_{p2}$ are the radii of particles 1 and 2, respectively; b is an empirically defined constant, b = 5.32; and $\lambda$ is the characteristic wavelength of the interaction with a value of 100 nm (Elimelech 1998).

The electrical double layer repulsion $G^{el}$(h) was calculated using the expression proposed by Hogg, Healy, and Fuerstenau 1966:

$$G^{el} = \pi\epsilon \frac{r_{p1} r_{p2}}{r_{p1} + r_{p2}} \left[2\zeta_{p1}\zeta_{p2} ln\left(\frac{1 + \exp^{(-\kappa h)}}{1 - \exp^{(-\kappa h)}}\right) + \left(\zeta_{p1}^2 \zeta_{p2}^2\right) \cdot \ln\left(1 - exp^{\left(-2\kappa h\right)}\right)\right] \tag{2.5}$$

where $\epsilon$ is the permittivity of the medium, equal to 6.95 $10^{-10}$ $C^2$ $J^{-1}$ $m^{-1}$, $\zeta_{p1}$, and $\zeta_{p2}$ are the surface potentials of particles 1 and 2 (mV), respectively, approximated by the zeta potential; and $\kappa$ is the inverse of the EDL thickness (Debye-Hückel length reciprocal length), determined by the following equation:

$$\kappa = \left(\frac{e^2}{\epsilon k_B T} \sum_{i=1}^{n} z_i^2 n_i\right)^{1/2} \tag{2.6}$$

where e is the charge of the electron; $k_B$ the Boltzmann constant, T the temperature, $z_i$ the valency of the ions i, and $n_i$ the number of ions i per unit volume.

The Lewis acid-base energy of interaction $G^{AB}$(h) of our system is the expression proposed by van Oss 1993:

$$G^{AB} = 2\pi \frac{r_{p1} r_{p2}}{r_{p1} + r_{p2}} \lambda_{AB} \Delta G^{AB}_{h=h_0} \exp\left(\frac{h_0 - h}{\lambda_{AB}}\right) \tag{2.7}$$

where $\lambda_{AB}$ is the correlation length, chosen as 1.65 nm, according to Valsesia et al. 2018, and $h_0$ is the minimum distance of separation between the particle and the surface, taken

as 0.158 nm. The acid-base potential $\Delta G^{AB}_{h=h_0}$ is expressed as:

$$\Delta G^{AB}_{h=h_0} = -2\left(\gamma^{AB}_{p1} + \gamma^{AB}_{p2} - 2\sqrt{\gamma^{AB}_{p1}\gamma^{AB}_{p2}}\right) \tag{2.8}$$

With $\gamma^{AB}_{p1}$ and $\gamma^{AB}_{p2}$ the polar component of the surface free energy for particles 1 and 2, respectively. $\gamma^{AB}_{p}$was directly quantified using the method by Valsesia et al. 2018 and found to be equal to 33.91 and 31.82 mJ.m$^{-2}$ for *PSL COOH* and *NPT-P*, respectively.

## 2.3 Results and Discussion

### 2.3.1 Colloidal stability of nanoplastic models

Figure 2.3 shows that both particles are stable at low ionic strengths (5 mmol $L^{-1}$). However, as ionic strength increases, the particles show differences in stability: *PSL COOH* is stable at high ionic strength (600 mmol $L^{-1}$), while *NPT-P* aggregates, with $d_{zH}$ increasing from 359 to 623 nm in one hour. While the aggregation kinetics presented in Figure 2.3 took place at a pH of 6.5, the trends in stability were the same at pH 5 and 8, representing the pH range of natural waters (Figure 2.4).

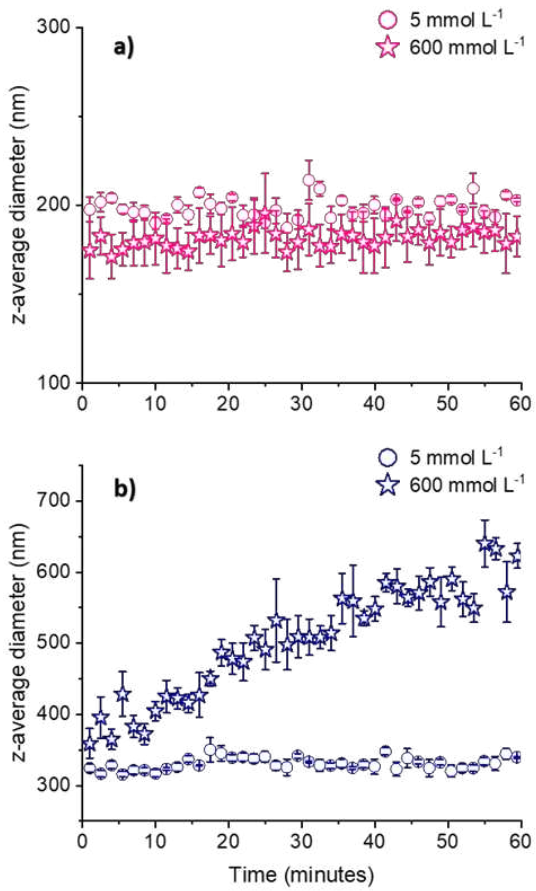


*Figure 2.3: Aggregation kinetics of 4 mg $L^{-1}$ a) PSL COOH and b) NPT-P in either 5 mmol $L^{-1}$ or 600 mmol $L^{-1}$ NaCl at pH 6.5 (Error bar = standard deviation)*

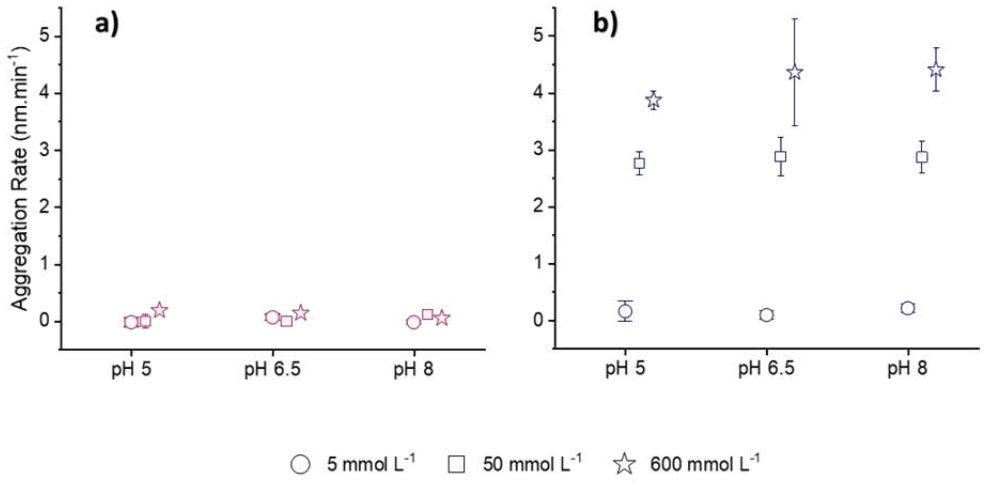


*Figure 2.4: Aggregation rate of a) PSL COOH and b) NPT-P models, as a function of NaCl concentration and pH (Error bars = standard deviation)*

Based on these kinetics of aggregation, the *NPT-P*'s critical coagulation concentration (CCC) in NaCl was determined to be 59 and 67 mmol $L^{-1}$ NaCl at pH 6.5 and 8, respectively (Figure 2.5). These values are lower than the CCC of 260 mmol $L^{-1}$ (NaCl, unadjusted pH) previously determined by El Hadri et al. 2020 and show no significant increase in stability with pH. This suggests that the *NPT-P* studied here has lower surface oxidation than those studied by El Hadri et al. 2020, as confirmed by a lower zeta (-33 vs. -44 mV). For *NPT-P*, the concentration of -COOH on the surface is lower, inhomogeneous, and uncontrolled. The mechanical degradation method used to produce *NPT-P* cannot control the -COOH functionalization of their surface, which induces possible variability on the CCC. The CCC value of *PSL COOH* was not assessed since these particles were stable up to 1 mmol $L^{-1}$ NaCl, which is above environmentally relevant concentrations. The CCC of *NPT-P* was lower than that of PSL models, as illustrated in Table 2.2. The reasons behind differences in stability between our PSL and *NPT-P* models are discussed below.

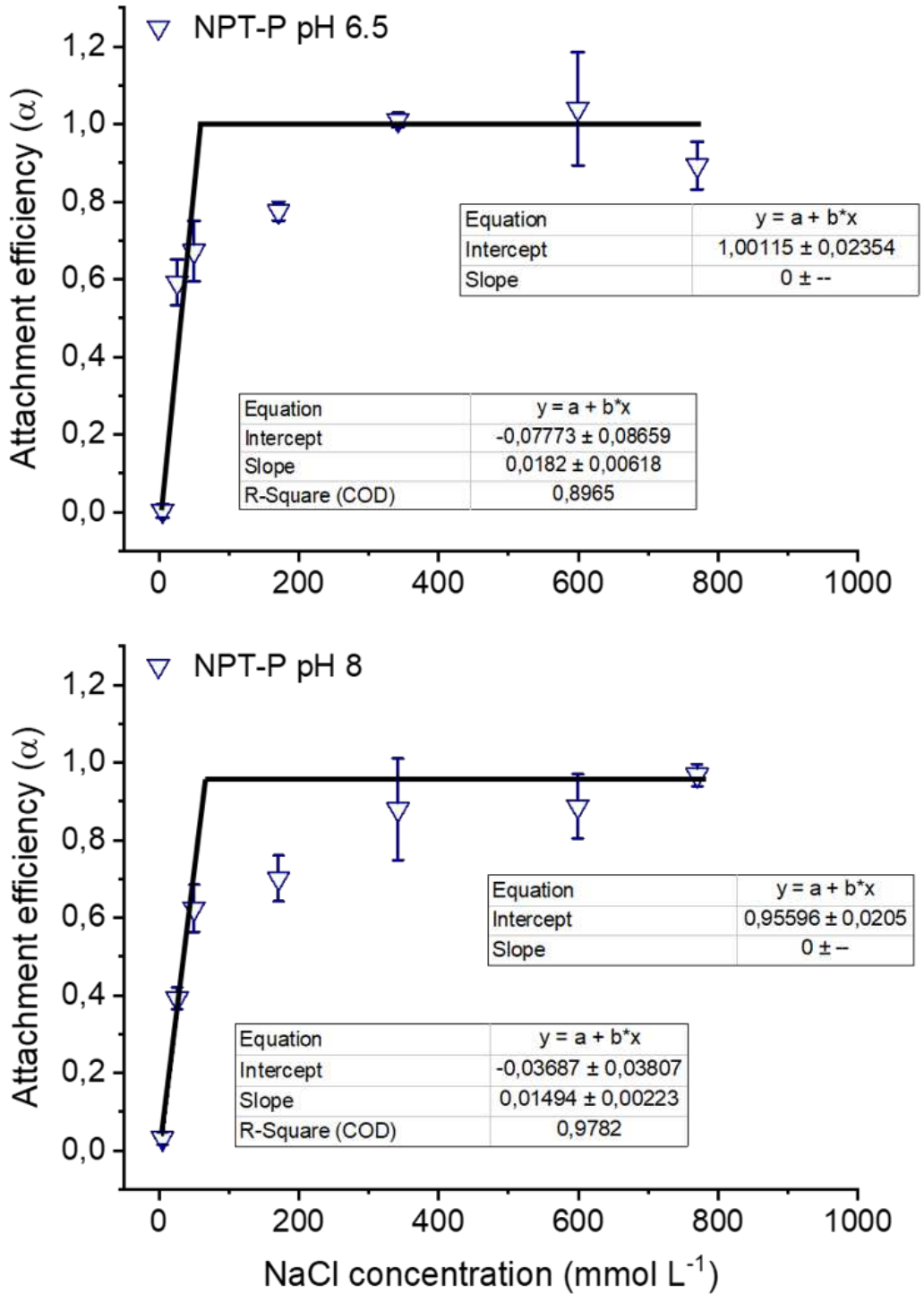


*Figure 2.5: Determination of the Critical Coagulation Concentration (CCC) of NPT-P particles in NaCl at pH 6.5 and pH 8*

Differences in stability between PSL particles and environmentally relevant nanoplastic models are commonly observed. Indeed, Yu, Shen, et al. 2019 determined that non-

functionalized and carboxylated PSL spheres have a CCC of 310 and 308 mmol $L^{-1}$ NaCl, respectively. Mao et al. 2020 found an even greater CCC of 591 mmol $L^{-1}$ NaCl for non-functionalized PSL spheres. The aging of these particles by UV-irradiation strongly oxidized their surface. This caused stronger electrostatic repulsion, and consequently, the CCC increased up to 1108 mmol $L^{-1}$. Singh et al. 2019 found a lower CCC of 140 mmol $L^{-1}$ NaCl for non-functionalized PSL and attributed this difference to the removal of surfactants. The CCC calculated for *NPT-P* was coherent with observations made on other non-spherical, non-emulsified and surfactant-free, nanoplastic models. For example, NPs produced by laser ablation of PS show strong aggregation in 300 mmol $L^{-1}$ NaCl (Yu, Shen, et al. 2019). NPs produced from mechanical fragmentation polyethylene glycol terephthalate (PET-G) had a CCC of 54 mmol $L^{-1}$ NaCl at pH 6, and 110 mmol $L^{-1}$ NaCl at pH 10 (S. Dong et al. 2020). These recent observations confirm that particles' surface functionalization and morphology, as well as the presence of surfactants play key roles in the kinetics of aggregation.

*Table 2.2: Summary of different critical coagulation concentrations (CCC) of NaCl for various NP models*

| NPs models studied<br>Nomenclature : Composition<br>Type of particle *Surface functionalization** <br>Nominal size (Charge) | CCC (mmol $L^{-1}$) | Reference |
|---|---|---|
| PS Latex sphere *NF* 100nm (-) | 310 in NaCl at pH 7.4 | Yu, Shen, et al. 2019 |
| PS Latex sphere *COOH* 100nm (-) | 308 in NaCl at pH 7.4 | |
| PS Laser ablation 60 nm (-) | Not determined. Strong aggregation in 300 mmol $L^{-1}$ NaCl pH 7.4 | |
| PS Latex sphere *NF* 100 nm (-) | 591 in NaCl pH 7.5 | Mao et al. 2020 |
| PS Latex sphere aged by UV-irradiation during 60 hours *NF* 100 nm (-) ** | 957 in NaCl pH 7.5 | |
| PS Latex sphere aged by UV-irradiation during 120 hours *NF* 100 nm (-) ** | 1108 in NaCl pH 7.5 | |
| PS Latex sphere *NF* 240(-) | 140 in NaCl pH 6 | Singh et al. 2019 |
| PET-G Mechanical degradation 500 nm (-) | 54 in NaCl pH 6 | S. Dong et al. 2020 |
| PS Mechanical degradation 350 nm (-) | 110 in NaCl pH 10<br>260 in NaCl pH unadjusted | El Hadri et al. 2020 |
| PS Mechanical degradation 350 nm (-) | 59 in NaCl pH 6.5 | *NPT-P* studied here |

**NF = Non-functionalized, COOH = carboxylated .*

***Initial particles were non-functionalized. Aging produced an increasing amount of carbonyl functional groups on the surface.*

To characterize the effect of the particles' properties (size, surface potential, etc.) on their stability, the level of repulsion (energy barrier) between particles can be modeled

by the extended Derjaguin Landau Verwey Overbeek (XDLVO) theory. According to the XDLVO theory, the interaction energies between *NPT-P* and *PSL COOH* are not significantly different (Table 2.3 and Figure 2.6). This demonstrates that size, surface charge, and hydrophobicity (Table 2.1), which are used to calculate interaction energy profiles, do not explain differences in stability. Instead, it suggests that *NPT-P*'s morphologies and polydispersity (Table 2.1 and Figure 2.1), as well as the lack of surfactants in the dispersion, are responsible for the aggregation rates observed. Indeed, particle morphology will affect their attachment efficiency. *NPT-P* has an aspect ratio of 1.70 ± 0.57 and asperities on their surface, whereas *PSL COOH* has an aspect ratio of 1.02 ± 0.05 and a smooth surface. At close approach, particles with elongated shapes (high aspect ratios) have larger van der Waals attraction when their major axii face each other (Vold 1954). While this has been difficult to demonstrate experimentally (Mohammed Baalousha 2017), a few aggregation experiments support this theory (S. Dong et al. 2020; Zhou and A. A. Keller 2010). Also, the collision of irregular and rough particles is likely to occur between particle protrusions and edges (W. Wu, Giese, and van Oss 1999).

*Table 2.3: Energy barrier between particles according to DLVO and XDLVO theories, scaled to* $k_B T$

| Particle 1 | *PSL COOH* | *NPT-P* | | |
|---|---|---|---|---|
| Particle 2 | *PSL COOH* | *NPT-P* | small (50 nm) *NPT-P* asperity* | large (100 nm) *NPT-P* asperity* |
| DLVO theory | 70 | 76 | 21 | 38 |
| XDLVO theory | 28 | 24 | 7 | 12 |

**Assuming the NPT-P particles are ellipsoids, the smallest radius of curvature, defined as the square of the short axis divided by the long axis, is on average 64 nm.*

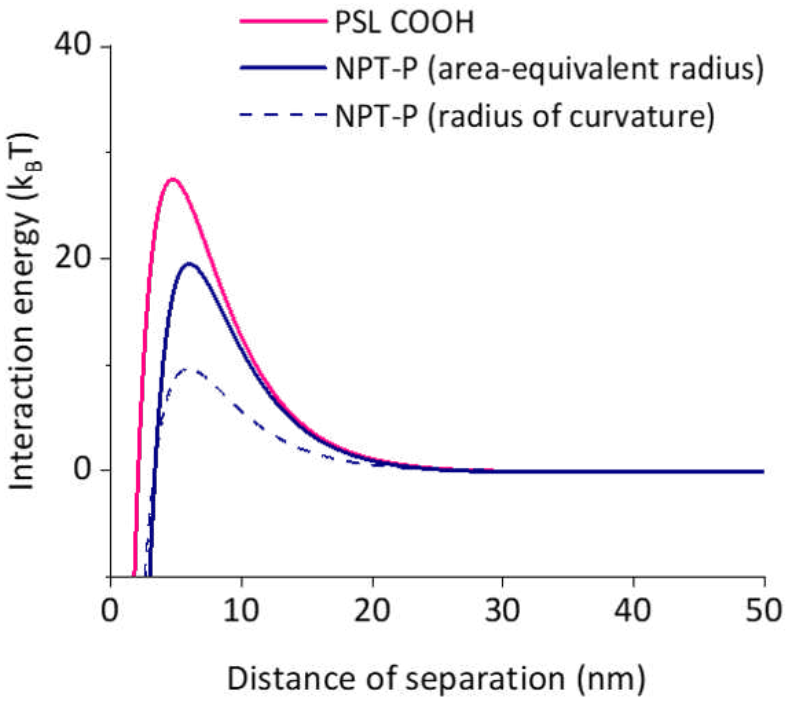


*Figure 2.6: Interaction energy, scaled to $k_B T$, between different nanoplastic models, according to XDLVO theory*

For this reason, it is more accurate to model the interaction energy between *NPT-P* and asperities, using the smallest radius of curvature as the asperity radius (Lan et al. 2018). This significantly reduces the level of repulsion (Figure 2.6) since the final volume of interaction is reduced and repulsive forces (electrostatic and acid-base) decay more quickly with distance than attractive forces (Lifshitz-van der Waals) (DelRio et al. 2005; Huang, Bhattacharjee, and E. M. V. Hoek 2010). Secondly, particle collision rate during perikinetic aggregation (i.e., induced by collisions driven by the Brownian motion) is always more significant for dispersions containing different particle sizes (Petosa et al. 2010). Finally, *NPT-P* particles are free of surfactants, which have a stabilizing effect (Goodwin 2004; Petosa et al. 2010). Since the more environmentally relevant nanoplastic model, *NPT-P*, is not stable at high ionic strengths, the stabilizing effect of natural organic matters (NOMs) was studied.

### 2.3.2 Stabilization of *NPT-P* by natural organic matters

Two different NOMs were chosen to represent the wide variety of physicochemical properties of NOM. The interaction of the *NPT-P* with the natural organic matter was described by characterizing the size of *NPT-P* with NOM at high ionic strength. Asymmetrical flow field-flow fractionation coupled to static light scattering (A4F-SLS) was used to characterize the assembly of *NPT-P* with NOM as this technique can discriminate different size populations and changes in polydispersity. Figure 2.7 illustrates the fractograms obtained for *NPT-P* in the presence of HA (Figure 2.7a) and SA (Figure 2.7b).

*NPT-P* and HA alone have similar times of elution and variation of their radii of gyration ($R_g$) over time. For *NPT-P* with HA, the peak's elution time range is identical, suggesting that *NPT-P* and HA stay dispersed and retain their initial sizes. However, the maximum of the peak increases from 26 to 28 minutes, with the corresponding $R_g$ increasing from 100 nm up to 270 nm. This shift suggests that a specific size fraction of HA is associated with *NPT-P* and formed larger hetero-aggregates. Concerning the mixture of *NPT-P* with SA (Figure 2.7b), no fractograms were obtained for SA in these fractionation conditions due to its low scattering properties at this concentration (57 mg $L^{-1}$). In the presence of SA, two peaks are observed: one eluted around 23 minutes and another around 26 minutes. The first peak corresponds to a $R_g > 400$ nm, while the second corresponds to a smaller $R_g$, around 250 nm. In A4F, the normal elution mode occurs when the relative diffusion between the different populations through the channel's height allows their separation according to the parabolic profile of the main velocity flow. However, an earlier peak with a high $R_g$ is indicative of steric elution mode (Messaud et al. 2009). In this mode, the particles become too large to be separated based on diffusion coefficient and are instead eluted by dragging forces. This first peak, in steric mode, corresponds to SA bridging separate *NPT-P* particles and sorbing onto small aggregates of *NPT-P*. The second peak overlaps with that of *NPT-P* alone and can be explained by the association of SA with single *NPT-P* or smaller aggregates.

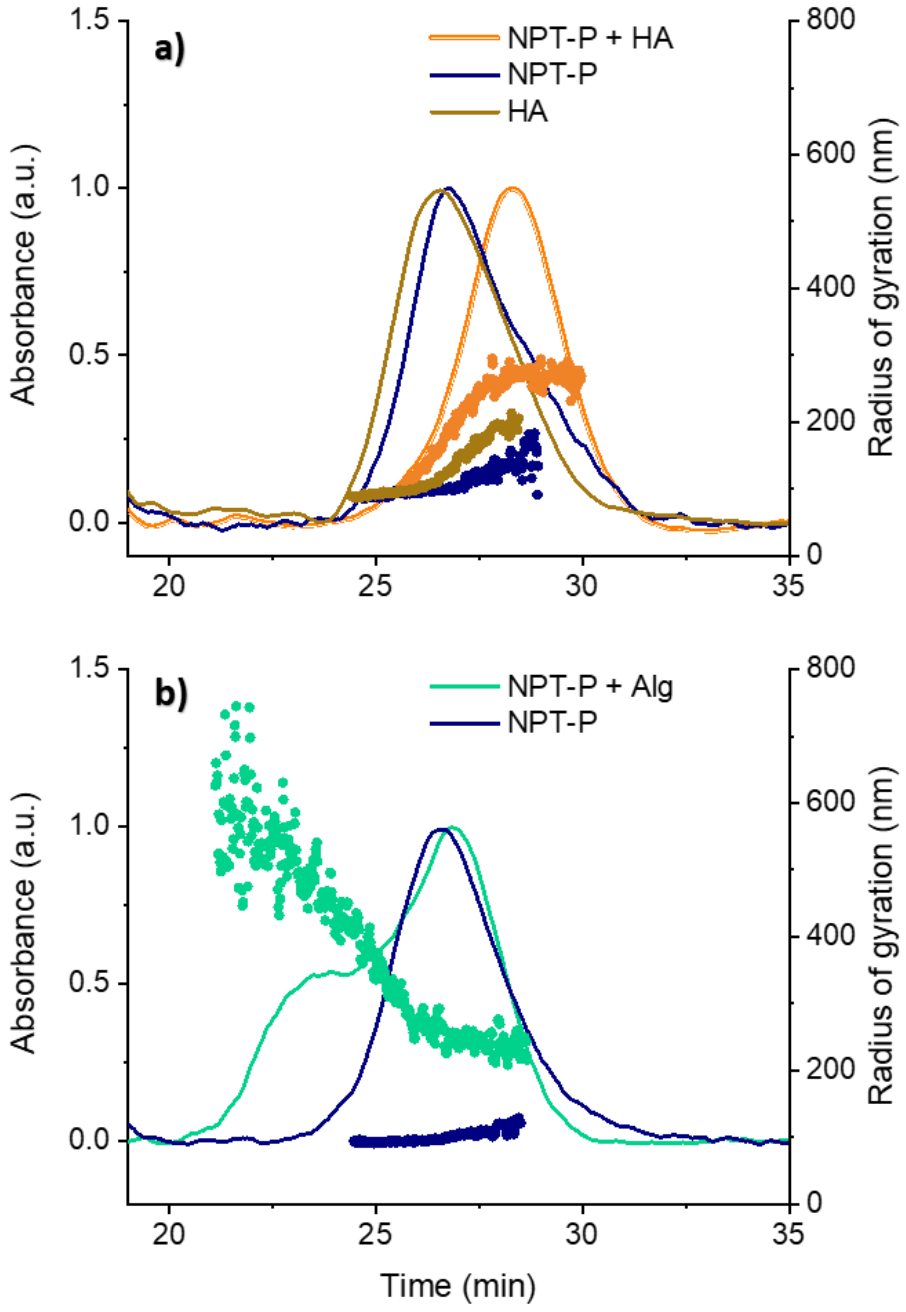


*Figure 2.7: Fractograms showing absorbance (line) and radius of gyration ($R_g$) (points) of a) NPT-P in 5 mmol $L^{-1}$ NaCl, NPT-P with 30 mg $L^{-1}$ HA in 600 mmol $L^{-1}$ NaCl, and 30 mg $L^{-1}$ HA in 600 mmol $L^{-1}$ NaCl at pH 6.5 and b) NPT-P in 5 mmol $L^{-1}$ NaCl and NPT-P with 57 mg $L^{-1}$ SA in 600 mmol $L^{-1}$ NaCl at pH 8, as a function of retention time*

To validate the variations in size populations and distributions, Figure 2.8 shows the size distributions of *NPT-P* with HA and with SA at high ionic strength based on the Sparse Bayesian Learning (SBL) algorithm. This algorithm allows investigating

differences in size population within the limits of the DLS resolution. With HA, the *NPT-P* size distribution is large but still covering the size range of the initial *NPT-P*. However, HA induces a shift towards a higher $d_H$ of 530 nm compared to the initial $d_H$ of 320 nm for *NPT-P* alone. This shift may be due to the non-covalent adsorption of larger HA molecules onto the *NPT-P* surface. In the presence of SA, the size distribution is less polydisperse but with a maximum $d_H$ around 820 nm. This larger size population can be explained by the physical association of SA with several (n> 2) *NPT-P* particles. The A4F-SLS fractograms and DLS size distributions (Figures 2.7 and 2.8) suggest that HA and SA have different stabilization mechanisms. On the one hand, the HA molecules that are free in solution stabilize *NPT-P* by providing electrostatic repulsion. Some low molecular weight HA molecules are also adsorbing onto the *NPT-P* surface and providing steric repulsion. The co-occurrence of these two mechanisms is supported by the fact that leonardite humic acid is one of the more large and polydisperse humic acids (Beckett, Jue, and Giddings 1987). Indeed, electrostatic repulsion is attributed to the smaller size fraction of humic and fulvic acids (J. Wu et al. 2019; F. Zhang et al. 2019), while surface adsorption of the larger size fraction of HAs may occur via $\pi$-$\pi$ interactions (with the aromatic structures of HA) and result in steric hindrance (Y. Li et al. 2019; Singh et al. 2019; Yu, Shen, et al. 2019; Yu, Jingfu Liu, et al. 2018).

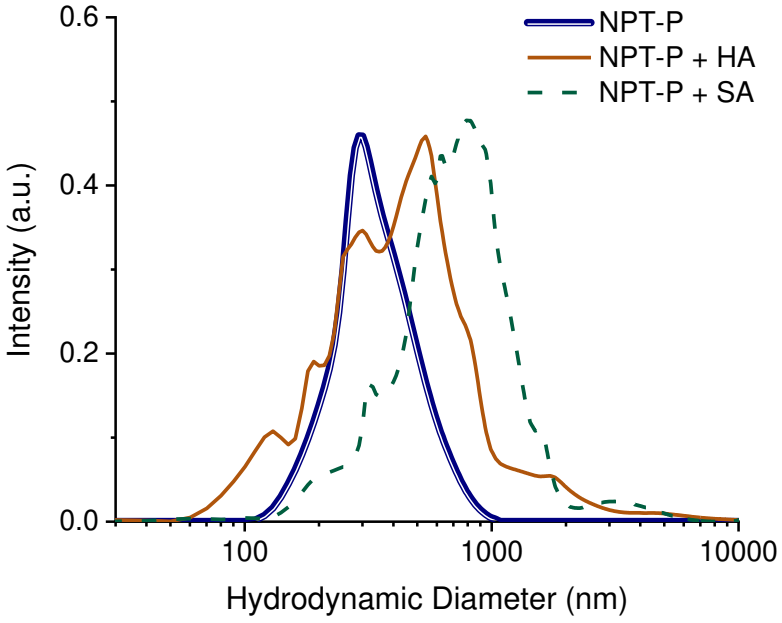


*Figure 2.8: Average of intensity-based size distributions according to SBL algorithm of NPT-P with 30 mg $L^{-1}$ HA at pH 6.5 or 57 mg $L^{-1}$ SA at pH 8, in 600 mmol $L^{-1}$ NaCl measured between 45 and 60 minutes ($n \geq 18$).*

Saavedra, Stoll, and Slaveykova 2019 noted that both HA and SA stabilized negatively charged particles. Due to HA's compact structure, adsorption of HA onto colloids did not increase their size. However, SA's high molecular weight (282 kDa, Figure 2.9) and semi-rigid chains can lead to the formation of larger aggregates (Buffle et al. 1998). Indeed, SA chains stabilize *NPT-P* particles by wrapping around single particles and small aggregates and bridging separate particles. These hetero-aggregates are then prevented from further aggregating by steric hindrance. Since SA is highly hydrophilic, its adsorption onto nanoplastics can be attributed to hydrogen bonds and van der Waals interactions (C.-S. Chen et al. 2018; Flemming and Wingender 2010; L. He, Rong, et al. 2020; Summers, Henry, and Gutierrez 2018). Indeed, Bhattacharya et al. 2010 demonstrated a significant affinity between negatively charged carboxylated PSL and negatively charged algae. This affinity has been attributed to hydrogen bonds forming between the cellulosic component of algae and the PSL. Finally, using TEM, it appears that *NPT-P* is embedded in SA, while HA does not seem to have such a strong affinity with the *NPT-P* surface (Figure 2.10).

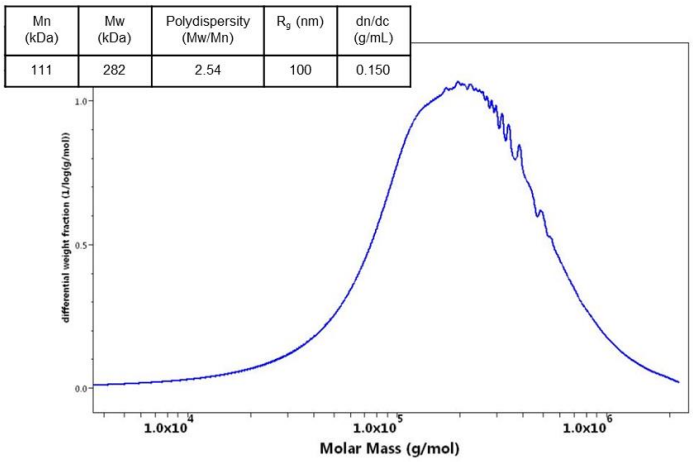


*Figure 2.9: Molar mass distribution of SA, as determined by SEC coupled to SLS and RI*

The source and extraction method of SA are not standardized, which results in variations in molar mass (Masuelli and Illanes 2014). So, the weight-averaged molar mass of this macromolecule was measured by SEC coupled to SLS and refractive index (RI) measurement. On-line purified mobile phase (0.1 mmol $L^{-1}$ $NaNO_3$) was delivered with an 1200 series HPLC pump (Agilent Technologies) at a flow rate of 5 mL $min^{-1}$ to a chromatographic pre-column SB-807G, followed by four columns, SB-805HQ, SB-807HQ, SB-802HQ and SB-803HQ (Shodex, Munich, Germany). 500 mg $L^{-1}$ SA in 600 mmol $L^{-1}$ NaCl was injected. At the outlet, SA was characterized by the DAWN HELEOS SLS detector and RI was measured by an Optilab T-rEX (Wyatt Technology).

Images a, c and e, show *NPT-P* at a lower magnification, to illustrate the matrix of NOM (c and e) or lack thereof. Images b, d, and f were taken at a higher magnification to observe the interface between NOM and *NPT-P*. The particles appear to be embedded in SA (e and f). In image e, the lighter halo around the particle is probably caused by the displacement of the particle. Figures c and d show that while *NPT-P* is also embedded in HA (c), at closer magnification, they seem less closely associated (d).

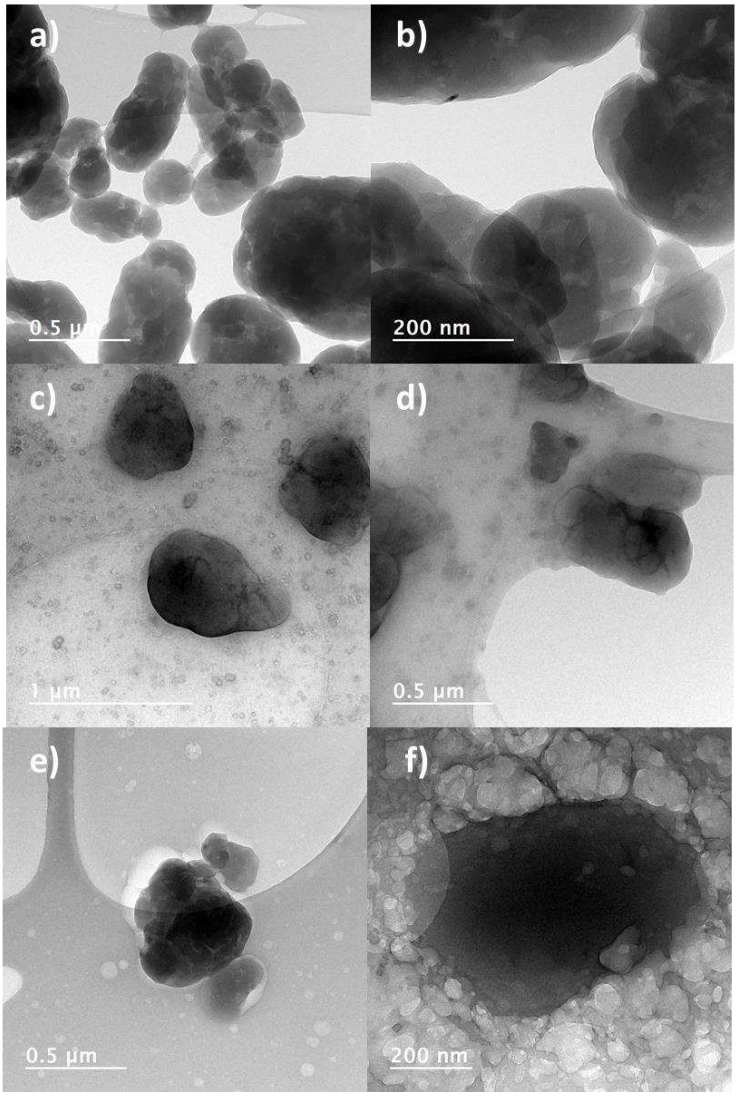


*Figure 2.10: Transmission Electron Microscopy Images of a) b) NPT-P without organic matter c) d) NPT-P with humic acid (HA) and e) f) NPT-P with sodium alginate (SA)*

### 2.3.3 Colloidal stability of *NPT-P* according to the nature and concentrations of NOM

These two mechanisms of stabilization will have distinct impacts on nanoplastics' colloidal stability in aqueous media. Figure 2.11 illustrates the size variation of *NPT-P* in 600 mmol $L^{-1}$ NaCl with either HA or SA. At 600 mmol $L^{-1}$ NaCl, the size of *NPT-P* increases in the absence of NOM (Figure 2.3). Figure 2.11 shows that HA can stabilize *NPT-P* immediately, while SA stabilizes *NPT-P* within 10 minutes. The final sizes obtained (i.e.: 300 nm for HA and 560 nm for SA) corroborate that different interactions occur between *NPT-P* and the two NOMs. In the presence of HA, the $d_{zH}$ of *NPT-P* remains constant around 300 nm. HA is highly polydisperse with a colloidal fraction centered around 230 nm. So, for kinetics of *NPT-P* with HA, the $d_{zH}$ presented in Figure 2.11 is a combination of both the $d_{zH}$ of *NPT-P* (339 nm) and the $d_{zH}$ of HA (230 nm). Despite this significant contribution of HA to the DLS signal, DLS will rapidly detect if aggregation occurs since scattering is highly sensitive to increases in size (R. Xu 2006). In the presence of SA, the size of *NPT-P* increases within the first 10 minutes and stabilizes around 560 nm. Without NOM, such an increase in size takes more than 30 minutes (Figure 2.3).

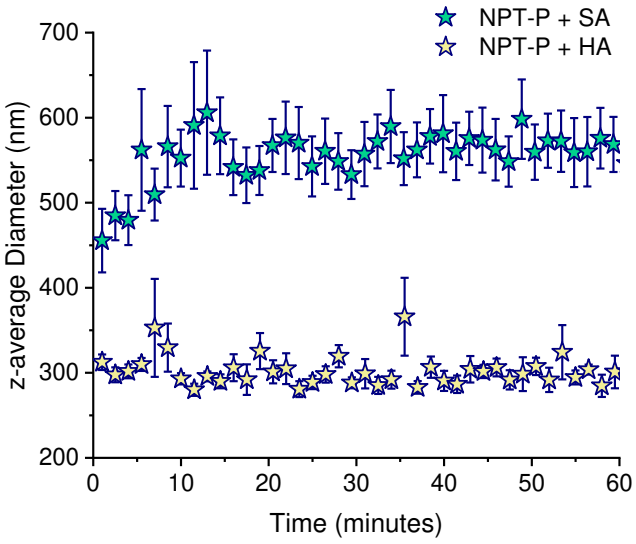


*Figure 2.11: Aggregation kinetics of 4.0 mg $L^{-1}$ NPT-P, in 600 mmol $L^{-1}$ NaCl, with 57 mg $L^{-1}$ sodium alginate (SA) at pH 8 and 30 mg $L^{-1}$ humic acid (HA) at pH 6.5 (Error bar = standard deviation)*

Contrary to HA, 57 mg $L^{-1}$ SA does not contribute to the DLS signal. Therefore this increase in size followed by a stabilization is explained by a rapid hetero-association between *NPT-P* (particles and/or aggregates) and SA. Instead of keeping all particles

separate as HA does, the SA biopolymer wraps separate or slightly aggregated plastic nanoparticles. Alginate molecules have been observed to form a layer with an approximate thickness of 20 nm around positively charged PSLs (Oriekhova and Stoll 2018). Also, when studying the aggregation of NPs with the dissolved ($< 0.22$ $\mu$m) fraction of organic matter that is naturally present in seawater, C.-S. Chen et al. 2018 obtained similar kinetics of hetero-aggregation, with a rapid increase in size followed by a plateau around micrometric sizes.

The relative quantity of particles and aggregates present in the dispersions over time was estimated based on the hydrodynamic diameter ($d_{zH}$), the intensity of scattered light ($I_\Theta$), and a spherical form factor ($P_\Theta$) with the following method:

The relative particle concentration ($n/n_0$) was determined according to the relation that links the intensity of scattered light and the particle size. This relationship is only valid assuming that all particles are spherical (Wyatt 1993). The intensity of scattered light, at a give scattering angle and particle concentration $I_{(,c)}$, is given by the following equation:

$$I_{\Theta,c} = KcM_W P_{(\Theta)} \tag{2.9}$$

with $\Theta$, the angle at which light is scattered, which is equal to 170 degrees and c the concentration in g $L^{-1}$, K the instrument constant, $M_W$ the molar mass in g $mol^{-1}$ and $P_\Theta$ the form factor. For a sphere, the form factor $P_\Theta$ is given by:

$$P_{(\Theta)} = \left[\frac{3}{u^3}\Big(sin(u) - ucos(u)\Big)\right]^2 \tag{2.10}$$

For a sphere, u is defined as:

$$u = qr_p \tag{2.11}$$

with $r_p$ the sphere's radius and q the wave vector, defined as:

$$q = \frac{4\pi}{\lambda} sin\left(\frac{\Theta}{2}\right) \tag{2.12}$$

with $\lambda$ the wavelength of scattered light, which is 658 nm. So we have:

$$u = \frac{2\pi d_{zH} sin\left(\frac{\Theta}{2}\right)}{\lambda} \tag{2.13}$$

For a sphere the $M_W$ is proportional to the sphere volume:

$$M_W \propto \left(\frac{d_{zH}}{2}\right)^3 \tag{2.14}$$

So, equation 2.9 can be written as:

$$I_{\Theta,c} \propto Kc\left(\frac{d_{zH}}{2}\right)^3 \left[\frac{3}{u^3}\Big(sin(u) - ucos(u)\Big)\right]^2 \tag{2.15}$$

Since, c is proportional to the particle concentration n and K and $\Theta$ are held constant, so:

$$n \propto \frac{I_{\Theta,c}}{\left(\frac{d_{zH}}{2}\right)^3 \left[\frac{3}{u^3}\Big(sin(u) - ucos(u)\Big)\right]^2} \tag{2.16}$$

Equation 2.16 can be simplified to:

$$n \propto \frac{I_{\Theta,c}}{\left(\frac{9}{q^6 r_p^6}\right)\Big(sin(u) - ucos(u)\Big)^2} \tag{2.17}$$

At high ionic strength, results show that the relative concentration of *NPT-P* plummets without NOM (Figure 2.12)). The relative *NPT-P* particle concentration does not decrease in the presence of HA, indicating colloidal stabilization induced by electrostatic repulsion. On the contrary, with SA, the relative *NPT-P* particle concentration decreases significantly and then stabilizes. Such behavior can be explained by the hetero-association of SA with *NPT-P* leading to a final state where all the *NPT-P* are associated with SA. Consequently, the rate of collision is reduced because of (i) the low rate of diffusion of large aggregates, (ii) the reduced number of separate particles and aggregates, and (iii) the effective repulsion between SA-coated surfaces.

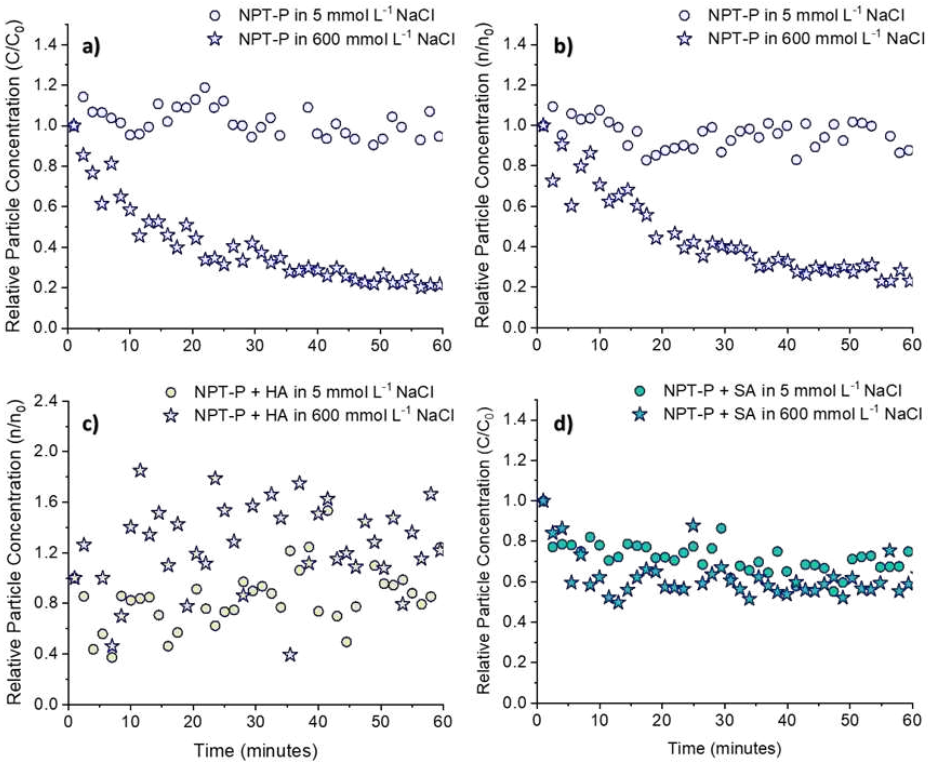


*Figure 2.12: Relative particle concentration of NPT-P at 5 and 600 mmol $L^{-1}$ NaCl at a) pH 6.5, b) pH 8, c) with 30 mg $L^{-1}$ humic acid (HA) at pH 6.5 and d) with 50 mg $L^{-1}$ sodium alginate (SA) at pH 8*

To validate this hypothesis, Figure 2.13 illustrates the different kinetics of association according to NaCl and NOM concentration. Due to the nature of the kinetics of aggregation of *NPT-P* in the presence of SA, two different slopes were compared: $k_{0-10}$, which represents the fast rate of aggregation from 0 to 10 minutes, and $k_{10-60}$ representing the plateau, observed from 10 to 60 minutes. Figure 2.13a shows that *NPT-P* and SA's association is always faster than the homo-aggregation of *NPT-P* for the whole range of the ionic strength investigated (5 to 770 mmol $L^{-1}$, pH 8). So, the aggregation kinetics are initially accelerated by SA, which sorbs onto and bridges *NPT-P* particles. Figure 2.13b shows no significant increase in the rate of the initial, fast aggregation rate ($k_{10-60}$) as a function of SA concentration. This suggests that small SA concentrations are sufficient to cover and stabilize *NPT-P*. The SA that remains free in the solution (non-adsorbed) may have a stabilizing effect by increasing the solution's electrostatic repulsion. This agrees with Summers et al. (2018), who observed that a low concentration ($\leq$ 1 mg $L^{-1}$) of EPS in a nanoplastic dispersion could play a dispersant effect (Summers, Henry, and Gutierrez 2018).

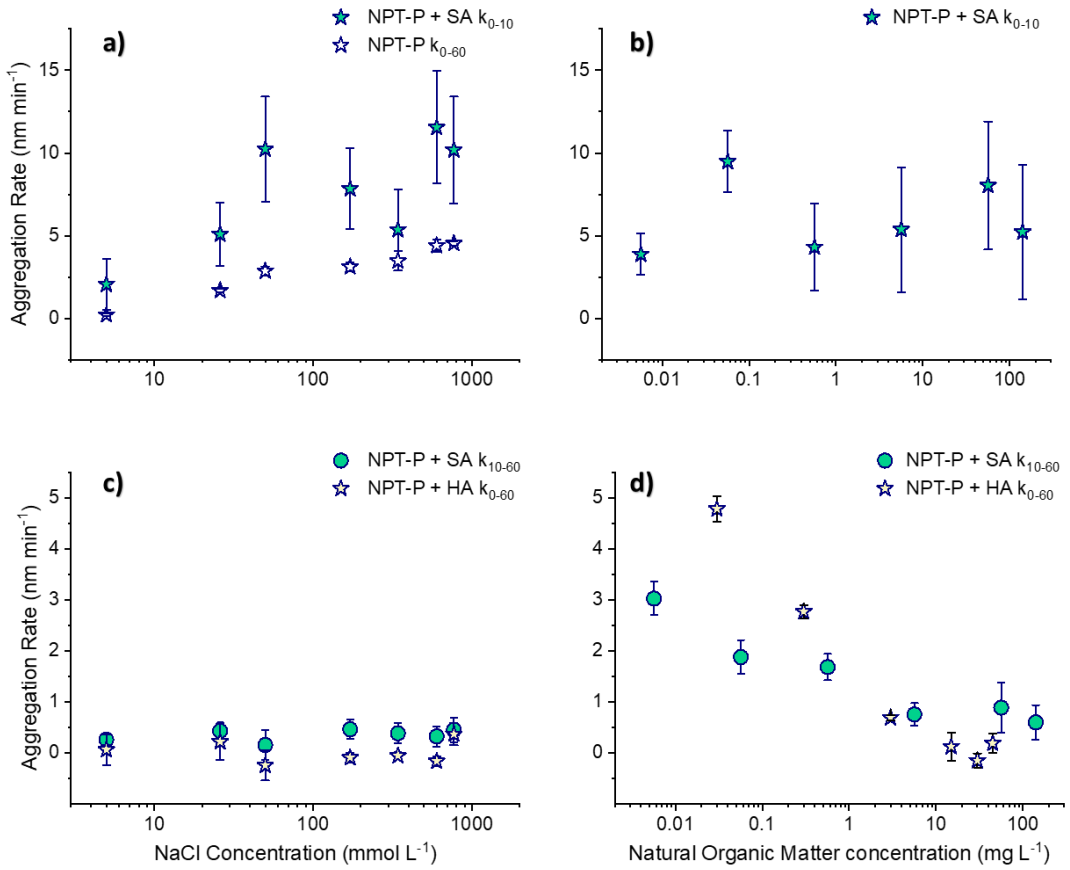


*Figure 2.13: a) Aggregation rate of NPT-P and fast aggregation rate ($k_{0-10}$) of NPT-P with 57 mg $L^{-1}$ SA, at pH 8 as a function of NaCl concentration b) fast aggregation rate ($k_{0-10}$) of NPT-P with varying concentrations of SA at 600 mmol $L^{-1}$ NaCl and pH 8. Aggregation rates of NPT-P with c) 57 mg $L^{-1}$ SA ($k_{10-60}$) at pH 8 and with 30 mg $L^{-1}$ HA ($k_{0-60}$) at pH 6.5 as a function of NaCl and d) in 600 mmol $L^{-1}$ NaCl, with varying concentrations of HA at pH 6.5 and different concentrations of SA at pH 8.*

Figure 2.13c presents the aggregation rate of *NPT-P* with NOM as a function of ionic strength during the stable section of aggregation's kinetics. In the presence of NOM, all aggregation rates were lower than without NOM, except at 5 mmol $L^{-1}$ NaCl, where there was no significant difference (Figure 2.13c and Figure 2.4). In the presence of HA, *NPT-P*'s aggregation rate is not significantly different from 0 nm $min^{-1}$ except at 26 and 770 mmol $L^{-1}$ ($p < 0.05$). At 770 mmol $L^{-1}$, the aggregation rate increases, suggesting that HA is losing its stabilizing effect due to a strong electrostatic screening by this high ionic strength. In the presence of SA, the aggregation rate hovers around 0.4 nm $min^{-1}$, especially at higher ionic strengths. This suggests that HA may have a stronger stabilizing effect than SA. The NOM concentration in Figure 2.13c was the minimum concentration required best stabilize the nanoplastic models at 600 mmol $L^{-1}$ NaCl (cf: Figure 2.13d). Figure 2.13d shows that at high ionic strength HA rapidly reduces *NPT-*

*P*'s attachment efficiency. This is supported by the observations made by Singh et al. 2019, indicating that low concentrations of HA increased the CCC of negatively charged PSL spheres almost 4-fold. However, even high SA concentrations do not reduce $k_{10-60}$ under 0.6 nm $min^{-1}$. This agrees with Summers, Henry, and Gutierrez 2018, who show that high alginate concentrations can have a flocculant effect.
Furthermore, Lodeiro et al. 2016 noted that SA only slightly increased the stability of silver nanoparticles. Saleh, Pfefferle, and Elimelech 2010 also noted that HA was more effective than SA at stabilizing carbon nanotubes in NaCl. The slightly more effective stabilizing capacity of HA compared to SA can be attributed to the fact that SA sorbs onto particles while HA causes repulsion between them. Indeed, the first mechanism is more likely to form flocs that are large enough to be affected by gravity.

### 2.3.4 Environmental Implications of NOM-NP interactions

The aggregation rates presented in Figure 2.13 were determined at pH 6.5 for HA and pH 8 for SA, as these pHs are representative of terrestrial and marine aquatic systems, respectively. Kinetic studies performed at pH 5, 6.5, and 8 for both NOMs show that the same stabilizing mechanisms operate in the pH range of natural waters (Figure 2.14). At a given ionic strength, aggregation rates did not significantly differ with pH ($p < 0.05$). This minimal pH-dependency is to be expected since (i) *NPT-P*'s stability is not pH-dependent, (ii) HA stabilizes these particles by electrostatic and steric repulsion, which only requires the NOM to be significantly negatively charged and unfolded, (iii) SA stabilizes *NPT-P* by sorption via hydrogen bonds and van der Waals attraction, which are operational in this range of pH.

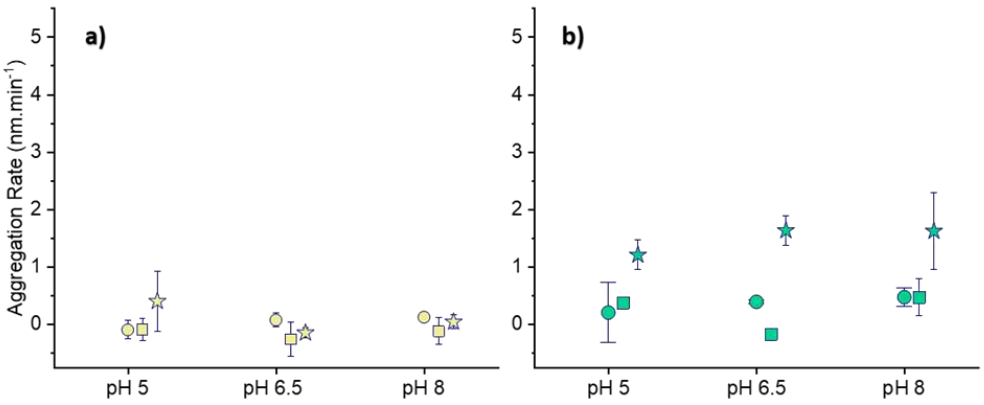


*Figure 2.14: Aggregation rate of NPT-P with a) 30 mg $L^{-1}$ humic acid b) 57 mg $L^{-1}$ sodium alginate, as a function of ionic strength and pH (Error bars = standard deviation)*

The different stabilizing mechanisms are summarized in Figure 2.15. These mechanisms have been shown to stabilize natural colloids (Buffle et al. 1998) as well as engineered nanomaterials (K. L. Chen, Mylon, and Elimelech 2006; Espinasse, Hotze, and Wiesner 2007; Hyung and J.-H. Kim n.d.; Loosli et al. 2015; Saleh, Pfefferle, and Elimelech 2010). When studying the stability of fullerene, Espinasse, Hotze, and Wiesner 2007 also noted the different mechanisms of stabilization of HA and SA. Fullerene were more water-soluble in the presence of HA. HA's combination of hydrophobic regions and ionizable functional groups allows the former to sorb to hydrophobic particles and the latter to increase the particle's hydrophilicity. The amount of HA sorption onto carbon nanotubes was proportional to the HA aromaticity (Hyung and J.-H. Kim n.d.). So, HA increases particles' stability by steric and charge stabilization. However, SA's large size promoted the aggregation of stable, polar fullerenes by bridging and encapsulating them (Espinasse, Hotze, and Wiesner 2007). Indeed, in NaCl, SA coats positively charged titanium dioxide and hematite nanoparticles which then confers electrostatic stability(K. L. Chen, Mylon, and Elimelech 2006; Loosli et al. 2015). SA also coats and stabilizes negatively charged, carbonaceous nanomaterials, such as single-walled carbon nanotubes (Saleh, Pfefferle, and Elimelech 2010).

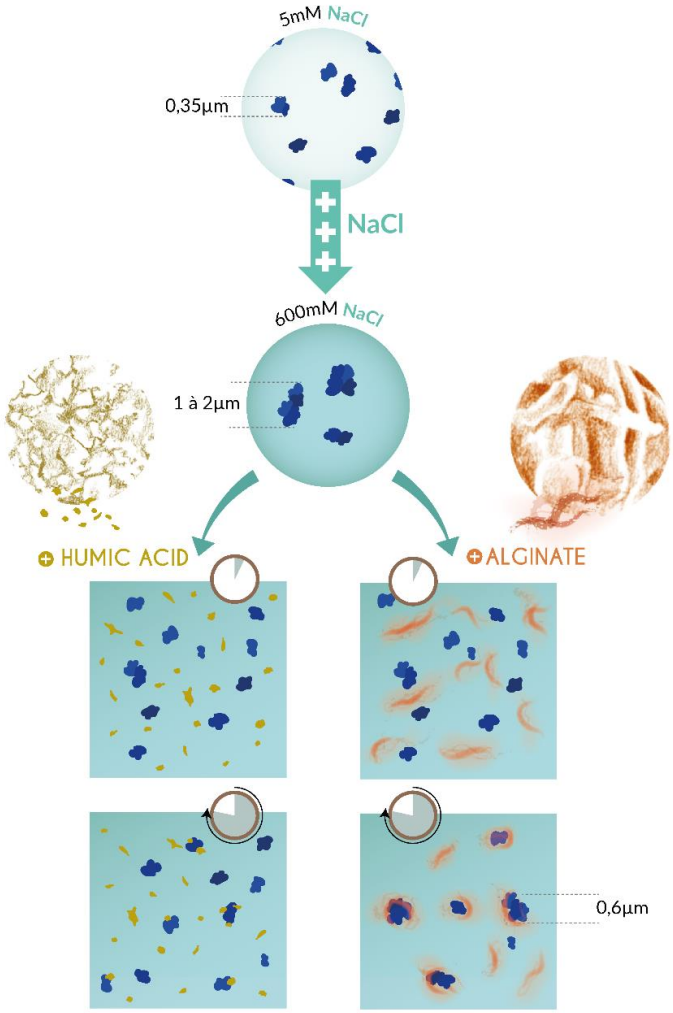


*Figure 2.15: Summary of the mechanisms of stabilization of NPT-P by humic acid (HA) and sodium alginate (SA) in NaCl*

In aqueous media, we might expect that SA will stabilize NPs and increase their dispersal. At the same time, it will induce retention when it is attached to a solid interface (i.e., soils, sediments, etc.)(Espinasse, Hotze, and Wiesner 2007; L. He, Rong, et al. 2020). Furthermore, Cunha et al. 2020 showed that nanoplastics and microplastics' presence enhanced the production of EPS carbohydrates by freshwater *Cyanothece sp.*, suggesting a feedback-loop may occur. The presence of NOM will impact nanoplastics environmental fate and affect the potential for co-transport of contaminants (Jin Liu, Ma, et al. 2018; Velzeboer, Kwadijk, and A. A. Koelmans 2014). For example, compared to a matrix containing only a nanoplastic model and hydrophobic organic compounds (HOCs), the addition of HA to the matrix increased Daphnia magna's rate of uptake of the HOCs by ingestion (W. Lin et al. 2020).

## 2.4 Conclusion

This study investigated the mechanisms of stabilization of nanoplastics by natural organic matter (NOM) according to the media's ionic strength. The interaction of the nanoplastics with NOMs was determined by characterizing the size distributions and shapes using asymmetrical flow field-flow fractionation coupled to static light scattering (A4F-SLS) and confirmed by dynamic light scattering (DLS). According to their origin, the different NOM models, i.e., sodium alginate (SA) for marine environments and humic acid (HA) for terrestrial ones, present different stabilization mechanisms. HA stabilizes the nanoplastic dispersion by electrostatic repulsion between particles, while larger molecules may sorb onto nanoplastics and provide a steric hindrance. However, SA adsorbs onto the nanoplastics' surface and bridges particles to form small aggregates that remain stable by steric hindrance against the increase in ionic strength. This study highlights the need to consider NOM's physicochemical properties when assessing nanoplastics behavior in the aqueous environment.

# References


Alimi, Olubukola S., Jeffrey M. Farner, and Nathalie Tufenkji (Feb. 2021). "Exposure of Nanoplastics to Freeze-Thaw Leads to Aggregation and Reduced Transport in Model Groundwater Environments". en. In: *Water Research* 189, p. 116533. ISSN: 00431354. DOI: 10.1016/j.watres.2020.116533.

Allen, Steve, Deonie Allen, Vernon R. Phoenix, Gaël Le Roux, Pilar Durántez Jiménez, Anaëlle Simonneau, Stéphane Binet, and Didier Galop (Apr. 2019). "Atmospheric Transport and Deposition of Microplastics in a Remote Mountain Catchment". en. In: *Nature Geoscience*. ISSN: 1752-0894, 1752-0908. DOI: 10.1038/s41561-019-0335-5.

Baalousha, Mohammed (Apr. 2017). "Effect of Nanomaterial and Media Physicochemical Properties on Nanomaterial Aggregation Kinetics". en. In: *NanoImpact* 6, pp. 55–68. ISSN: 24520748. DOI: 10.1016/j.impact.2016.10.005.

Beckett, Ronald., Zhang. Jue, and J. Calvin. Giddings (Mar. 1987). "Determination of Molecular Weight Distributions of Fulvic and Humic Acids Using Flow Field-Flow Fractionation". en. In: *Environmental Science & Technology* 21.3, pp. 289–295. ISSN: 0013-936X, 1520-5851. DOI: 10.1021/es00157a010.

Bergami, E., A. Krupinski Emerenciano, M. González-Aravena, C. A. Cárdenas, P. Hernández, J. R. M. C. Silva, and I. Corsi (Apr. 2019). "Polystyrene Nanoparticles Affect the Innate Immune System of the Antarctic Sea Urchin Sterechinus Neumayeri". en. In: *Polar Biology* 42.4, pp. 743–757. ISSN: 0722-4060, 1432-2056. DOI: 10.1007/s00300-019-02468-6.

Bhattacharya, Priyanka, Sijie Lin, James P. Turner, and Pu Chun Ke (Oct. 2010). "Physical Adsorption of Charged Plastic Nanoparticles Affects Algal Photosynthesis". en. In: *The Journal of Physical Chemistry C* 114.39, pp. 16556–16561. ISSN: 1932-7447, 1932-7455. DOI: 10.1021/jp1054759.

Buffle, Jacques, Kevin J. Wilkinson, Serge Stoll, Montserrat Filella, and Jingwu Zhang (Oct. 1998). "A Generalized Description of Aquatic Colloidal Interactions: The Three-Colloidal Component Approach". en. In: *Environmental Science & Technology* 32.19, pp. 2887–2899. ISSN: 0013-936X, 1520-5851. DOI: 10.1021/es980217h.

Cai, Li, Lingling Hu, Huahong Shi, Junwei Ye, Yunfei Zhang, and Hyunjung Kim (Apr. 2018). "Effects of Inorganic Ions and Natural Organic Matter on the Aggregation of Nanoplastics". en. In: *Chemosphere* 197, pp. 142–151. ISSN: 00456535. DOI: 10.1016/j.chemosphere.2018.01.052.

Chamas, Ali, Hyunjin Moon, Jiajia Zheng, Yang Qiu, Tarnuma Tabassum, Jun Hee Jang, Mahdi Abu-Omar, Susannah L. Scott, and Sangwon Suh (Feb. 2020). "Degradation Rates of Plastics in the Environment". en. In: *ACS Sustainable Chemistry & Engineering*, acssuschemeng.9b06635. ISSN: 2168-0485, 2168-0485. DOI: 10.1021/acssuschemeng.9b06635.

Chen, Chi-Shuo, Clarence Le, Meng-Hsuen Chiu, and Wei-Chun Chin (Sept. 2018). "The Impact of Nanoplastics on Marine Dissolved Organic Matter Assembly". en. In: *Science of The Total Environment* 634, pp. 316–320. ISSN: 00489697. DOI: 10.1016/j.scitotenv.2018.03.269.

Chen, Kai Loon, Steven E. Mylon, and Menachem Elimelech (Mar. 2006). "Aggregation Kinetics of Alginate-Coated Hematite Nanoparticles in Monovalent and Divalent Electrolytes". en. In: *Environmental Science & Technology* 40.5, pp. 1516–1523. ISSN: 0013-936X, 1520-5851. DOI: 10.1021/es0518068.

Chen, Ziying, Junhong Liu, Chengyu Chen, and Zhujian Huang (Mar. 2020). "Sedimentation of Nanoplastics from Water with Ca/Al Dual Flocculants: Characterization, Interface Reaction, Effects of pH and Ion Ratios". en. In: *Chemosphere*, p. 126450. ISSN: 00456535. DOI: 10.1016/j.chemosphere.2020.126450.

Cunha, César, Laura Silva, Jorge Paulo, Marisa Faria, Natacha Nogueira, and Nereida Cordeiro (2020). "Microalgal-Based Biopolymer for Nano- and Microplastic Removal: A Possible Biosolution for Wastewater Treatment". In: *Environmental Pollution* 263, p. 114385. ISSN: 0269-7491. DOI: 10.1016/j.envpol.2020.114385.

Della Torre, C., E. Bergami, A. Salvati, C. Faleri, P. Cirino, K. A. Dawson, and I. Corsi (Oct. 2014). "Accumulation and Embryotoxicity of Polystyrene Nanoparticles at Early Stage of Development of Sea Urchin Embryos *Paracentrotus Lividus*". en. In: *Environmental Science & Technology* 48.20, pp. 12302–12311. ISSN: 0013-936X, 1520-5851. DOI: 10.1021/es502569w.

DelRio, Frank W., Maarten P. de Boer, James A. Knapp, E. David Reedy, Peggy J. Clews, and Martin L. Dunn (Aug. 2005). "The Role of van Der Waals Forces in Adhesion of Micromachined Surfaces". en. In: *Nature Materials* 4.8, pp. 629–634. ISSN: 1476-1122, 1476-4660. DOI: 10.1038/nmat1431.

Dong, Shunan, Wangwei Cai, Jihong Xia, Liting Sheng, Weimu Wang, and Hui Liu (Oct. 2020). "Aggregation Kinetics of Fragmental PET Nanoplastics in Aqueous Environment: Complex Roles of Electrolytes, pH and Humic Acid". In: *Environmental Pollution*, p. 115828. ISSN: 0269-7491. DOI: 10.1016/j.envpol.2020.115828.

Dong, Zhiqiang, Wen Zhang, Yuping Qiu, Zhenglong Yang, Junliang Wang, and Yidi Zhang (Jan. 2019). "Cotransport of Nanoplastics (NPs) with Fullerene (C60) in Saturated Sand: Effect of NPs/C60 Ratio and Seawater Salinity". en. In: *Water Research* 148, pp. 469–478. ISSN: 00431354. DOI: 10.1016/j.watres.2018.10.071.

Dong, Zhiqiang, Ling Zhu, Wen Zhang, Rui Huang, Xiang-Wei Lv, Xinyu Jing, Zhenglong Yang, Junliang Wang, and Yuping Qiu (Dec. 2019). "Role of Surface Functionalities of Nanoplastics on Their Transport in Seawater-

Saturated Sea Sand". en. In: *Environmental Pollution* 255, p. 113177. ISSN: 02697491. DOI: 10.1016/j.envpol.2019.113177.

El Hadri, Hind, Julien Gigault, Benoit Maxit, Bruno Grassl, and Stéphanie Reynaud (2020). "Nanoplastic from Mechanically Degraded Primary and Secondary Microplastics for Environmental Assessments". In: *NanoImpact*, p. 100206. ISSN: 2452-0748. DOI: 10.1016/j.impact.2019.100206.

Elimelech, Menachem, ed. (1998). *Particle Deposition and Aggregation: Measurement, Modelling and Simulation*. en. Colloid and Surface Engineering Series. Oxford: Butterworth-Heinemann. ISBN: 978-0-7506-7024-1.

Espinasse, Benjamin, Ernest M. Hotze, and Mark R. Wiesner (Nov. 2007). "Transport and Retention of Colloidal Aggregates of C $_{60}$ in Porous Media: Effects of Organic Macromolecules, Ionic Composition, and Preparation Method". en. In: *Environmental Science & Technology* 41.21, pp. 7396–7402. ISSN: 0013-936X, 1520-5851. DOI: 10.1021/es0708767.

Evangeliou, N., H. Grythe, Z. Klimont, C. Heyes, S. Eckhardt, S. Lopez-Aparicio, and A. Stohl (Dec. 2020). "Atmospheric Transport Is a Major Pathway of Microplastics to Remote Regions". en. In: *Nature Communications* 11.1, p. 3381. ISSN: 2041-1723. DOI: 10.1038/s41467-020-17201-9.

Flemming, Hans-Curt and Jost Wingender (Sept. 2010). "The Biofilm Matrix". en. In: *Nature Reviews Microbiology* 8.9, pp. 623–633. ISSN: 1740-1526, 1740-1534. DOI: 10.1038/nrmicro2415.

GESAMP (2016). "Sources, Fate and Effects of Microplastics in the Marine Environment: Part Two of a Global Assessment". In: 93, p. 220. ISSN: 1020-4873.

Gewert, Berit, Merle M. Plassmann, and Matthew MacLeod (2015). "Pathways for Degradation of Plastic Polymers Floating in the Marine Environment". en. In: *Environmental Science: Processes & Impacts* 17.9, pp. 1513–1521. ISSN: 2050-7887, 2050-7895. DOI: 10.1039/C5EM00207A.

Geyer, Roland, Jenna R. Jambeck, and Kara Lavender Law (July 2017). "Production, Use, and Fate of All Plastics Ever Made". en. In: *Science Advances* 3.7, e1700782. ISSN: 2375-2548. DOI: 10.1126/sciadv.1700782.

Gigault, Julien, Hind El Hadri, Stéphanie Reynaud, Elise Deniau, and Bruno Grassl (Nov. 2017). "Asymmetrical Flow Field Flow Fractionation Methods to Characterize Submicron Particles: Application to Carbon-Based Aggregates and Nanoplastics". en. In: *Analytical and Bioanalytical Chemistry* 409.29, pp. 6761–6769. ISSN: 1618-2642, 1618-2650. DOI: 10.1007/s00216-017-0629-7.

Gigault, Julien, Boris Pedrono, Benoît Maxit, and Alexandra Ter Halle (Apr. 2016). "Marine Plastic Litter: The Unanalyzed Nano-Fraction". en. In: *Environmental Science: Nano* 3.2, pp. 346–350. ISSN: 2051-8161. DOI: 10.1039/C6EN00008H.

González-Fernández, Carmen, Jordan Toullec, Christophe Lambert, Nelly Le Goïc, Marta Seoane, Brivaela Moriceau, Arnaud Huvet, Mathieu Berchel, Dorothée Vincent, Lucie Courcot, Philippe Soudant, and Ika Paul-Pont (July 2019). "Do Transparent Exopolymeric Particles (TEP) Affect the Toxicity of Nanoplastics on Chaetoceros Neogracile?" en. In: *Environmental Pollution* 250, pp. 873–882. ISSN: 02697491. DOI: 10.1016/j.envpol.2019.04.093.

Goodwin, James William (2004). *Colloids and Interfaces with Surfactants and Polymers: An Introduction*. Wiley. ISBN: 0-470-84143-5.

Gregory, John (Sept. 1981). "Approximate Expressions for Retarded van Der Waals Interaction". en. In: *Journal of Colloid and Interface Science* 83.1, pp. 138–145. ISSN: 00219797. DOI: 10.1016/0021-9797(81)90018-7.

He, Lei, Haifeng Rong, Dan Wu, Meng Li, Chengyi Wang, and Meiping Tong (Apr. 2020). "Influence of Biofilm on the Transport and Deposition Behaviors of Nano- and Micro-Plastic Particles in Quartz Sand". en. In: *Water Research*, p. 115808. ISSN: 00431354. DOI: 10.1016/j.watres.2020.115808.

Hogg, R., T. W. Healy, and D. W. Fuerstenau (1966). "Mutual Coagulation of Colloidal Dispersions". en. In: *Transactions of the Faraday Society* 62, p. 1638. ISSN: 0014-7672. DOI: 10.1039/tf9666201638.

Holthoff, Helmut, Stefan U. Egelhaaf, Michal Borkovec, Peter Schurtenberger, and Hans Sticher (Jan. 1996). "Coagulation Rate Measurements of Colloidal Particles by Simultaneous Static and Dynamic Light Scattering". en. In: *Langmuir* 12.23, pp. 5541–5549. ISSN: 0743-7463, 1520-5827. DOI: 10.1021/la960326e.

Horton, Alice A., Alexander Walton, David J. Spurgeon, Elma Lahive, and Claus Svendsen (May 2017). "Microplastics in Freshwater and Terrestrial Environments: Evaluating the Current Understanding to Identify the Knowledge Gaps and Future Research Priorities". en. In: *Science of The Total Environment* 586, pp. 127–141. ISSN: 00489697. DOI: 10.1016/j.scitotenv.2017.01.190.

Huang, Xiaofei, Subir Bhattacharjee, and Eric M. V. Hoek (Feb. 2010). "Is Surface Roughness a "Scapegoat" or a Primary Factor When Defining Particle-Substrate Interactions?" en. In: *Langmuir* 26.4, pp. 2528–2537. ISSN: 0743-7463, 1520-5827. DOI: 10.1021/la9028113.

Hyung, Hoon and Jae-Hong Kim (n.d.). "Natural Organic Matter (NOM) Adsorption to Multi-Walled Carbon Nanotubes: Effect of NOM Characteristics and Water Quality Parameters". en. In: *Environmental Science & Technology* (), p. 6. DOI: 10.1021/es702916h.

Jambeck, J. R., R. Geyer, C. Wilcox, T. R. Siegler, M. Perryman, A. Andrady, R. Narayan, and K. L. Law (Feb. 2015). "Plastic Waste Inputs from Land into the Ocean". en. In: *Science* 347.6223, pp. 768–771. ISSN: 0036-8075, 1095-9203. DOI: 10.1126/science.1260352.

Julienne, Fanon, Nicolas Delorme, and Fabienne Lagarde (Dec. 2019). "From Macroplastics to Microplastics: Role of Water in the Fragmentation of Polyethylene". en. In: *Chemosphere* 236, p. 124409. ISSN: 00456535. DOI: 10.1016/j.chemosphere.2019.124409.

Keller, Andreas S., Joaquin Jimenez-Martinez, and Denise M. Mitrano (Dec. 2019). "Transport of Nano- and Microplastic through Unsaturated Porous Media from Sewage Sludge Application". en. In: *Environmental Science & Technology*, acs.est.9b06483. ISSN: 0013-936X, 1520-5851. DOI: 10.1021/acs.est.9b06483.

Koelmans, Albert A, Merel Kooi, Kara Lavender Law, and Erik van Sebille (Nov. 2017a). "All Is Not Lost: Deriving a Top-down Mass Budget of Plastic at Sea". In: *Environmental Research Letters* 12.11, p. 114028. ISSN: 1748-9326. DOI: 10.1088/1748-9326/aa9500.

Lambert, Scott and Martin Wagner (Feb. 2016). "Characterisation of Nanoplastics during the Degradation of Polystyrene". en. In: *Chemosphere* 145, pp. 265–268. ISSN: 00456535. DOI: 10.1016/j.chemosphere.2015.11.078.

Lan, Yang, Alessio Caciagli, Giulia Guidetti, Ziyi Yu, Ji Liu, Villads E. Johansen, Marlous Kamp, Chris Abell, Silvia Vignolini, Oren A. Scherman, and Erika Eiser (Dec. 2018). "Unexpected Stability of Aqueous Dispersions of Raspberry-like Colloids". en. In: *Nature Communications* 9.1, p. 3614. ISSN: 2041-1723. DOI: 10.1038/s41467-018-05560-3.

Li, Yang, Xinjie Wang, Wanyi Fu, Xinghui Xia, Changqing Liu, Jiacheng Min, Wen Zhang, and John Charles Crittenden (Sept. 2019). "Interactions between Nano/Micro Plastics and Suspended Sediment in Water: Implications on Aggregation and Settling". en. In: *Water Research* 161, pp. 486–495. ISSN: 00431354. DOI: 10.1016/j.watres.2019.06.018.

Lin, Wei, Ruifen Jiang, Xiaoying Xiao, Jiayi Wu, Songbo Wei, Yan Liu, Derek C.G. Muir, and Gangfeng Ouyang (June 2020). "Joint Effect of Nanoplastics and Humic Acid on the Uptake of PAHs for Daphnia Magna: A Model Study". en. In: *Journal of Hazardous Materials* 391, p. 122195. ISSN: 03043894. DOI: 10.1016/j.jhazmat.2020.122195.

Liu, Jin, Yini Ma, Dongqiang Zhu, Tianjiao Xia, Yu Qi, Yao Yao, Xiaoran Guo, Rong Ji, and Wei Chen (Mar. 2018). "Polystyrene Nanoplastics-Enhanced Contaminant Transport: Role of Irreversible Adsorption in Glassy Polymeric Domain". en. In: *Environmental Science & Technology* 52.5, pp. 2677–2685. ISSN: 0013-936X, 1520-5851. DOI: 10.1021/acs.est.7b05211.

Liu, Jin, Tong Zhang, Lili Tian, Xinlei Liu, Zhichong Qi, Yini Ma, Rong Ji, and Wei Chen (Apr. 2019). "Aging Significantly Affects Mobility and Contaminant-Mobilizing Ability of Nanoplastics in Saturated Loamy Sand". en. In: *Environmental Science & Technology*, acs.est.9b00787. ISSN: 0013-936X, 1520-5851. DOI: 10.1021/acs.est.9b00787.

Liu, Yanjun, Yiben Hu, Chen Yang, Chengyu Chen, Weilin Huang, and Zhi Dang (Oct. 2019). "Aggregation Kinetics of UV Irradiated Nanoplastics in Aquatic Environments". en. In: *Water Research* 163, p. 114870. ISSN: 00431354. DOI: 10.1016/j.watres.2019.114870.

Lodeiro, Pablo, Eric P. Achterberg, Joaquín Pampín, Alice Affatati, and Mohammed S. El-Shahawi (Jan. 2016). "Silver Nanoparticles Coated with Natural Polysaccharides as Models to Study AgNP Aggregation Kinetics Using UV-Visible Spectrophotometry upon Discharge in Complex Environments". en. In: *Science of The Total Environment* 539, pp. 7–16. ISSN: 00489697. DOI: 10.1016/j.scitotenv.2015.08.115.

Loosli, Frédéric, Letícia Vitorazi, Jean-François Berret, and Serge Stoll (Sept. 2015). "Towards a Better Understanding on Agglomeration Mechanisms and Thermodynamic Properties of TiO2 Nanoparticles Interacting with Natural Organic Matter". en. In: *Water Research* 80, pp. 139–148. ISSN: 00431354. DOI: 10.1016/j.watres.2015.05.009.

Magrì, Davide, Paola Sánchez-Moreno, Gianvito Caputo, Francesca Gatto, Marina Veronesi, Giuseppe Bardi, Tiziano Catelani, Daniela Guarnieri, Athanassia Athanassiou, Pier Paolo Pompa, and Despina Fragouli (Aug. 2018). "Laser Ablation as a Versatile Tool To Mimic Polyethylene Terephthalate Nanoplastic Pollutants: Characterization and Toxicology Assessment". en. In: *ACS Nano* 12.8, pp. 7690–7700. ISSN: 1936-0851, 1936-086X. DOI: 10.1021/acsnano.8b01331.

Manfra, L., A. Rotini, E. Bergami, G. Grassi, C. Faleri, and I. Corsi (Nov. 2017). "Comparative Ecotoxicity of Polystyrene Nanoparticles in Natural Seawater and Reconstituted Seawater Using the Rotifer Brachionus Plicatilis". en. In: *Ecotoxicology and Environmental Safety* 145, pp. 557–563. ISSN: 01476513. DOI: 10.1016/j.ecoenv.2017.07.068.

Mao, Yufeng, Hong Li, Xiaoliu Huangfu, Yao Liu, and Qiang He (Mar. 2020). "Nanoplastics Display Strong Stability in Aqueous Environments: Insights from Aggregation Behaviour and Theoretical Calculations". en. In: *Environmental Pollution* 258, p. 113760. ISSN: 02697491. DOI: 10.1016/j.envpol.2019.113760.

Masuelli, Martin Alberto and Cristian Omar Illanes (2014). "Review of the Characterization of Sodium Alginate by Intrinsic Viscosity Measurements. Comparative Analysis between Conventional and Single Point Methods". en. In: *International Journal of BioMaterials Science and Engineering* 1.1, p. 11.

Messaud, Fathi A., Ron D. Sanderson, J. Ray Runyon, Tino Otte, Harald Pasch, and S. Kim Ratanathanawongs Williams (Apr. 2009). "An Overview on Field-Flow Fractionation Techniques and Their Applications in the Separation and Characterization of Polymers". en. In: *Progress in Polymer Science* 34.4, pp. 351–368. ISSN: 00796700. DOI: 10.1016/j.progpolymsci.2008.11.001.

Min, Kyungjun, Joseph D. Cuiffi, and Robert T. Mathers (Dec. 2020). "Ranking Environmental Degradation Trends of Plastic Marine Debris Based on Physical Properties and Molecular Structure". en. In: *Nature Communications* 11.1, p. 727. ISSN: 2041-1723. DOI: 10.1038/s41467-020-14538-z.

Okshevsky, Mira, Eva Gautier, Jeffrey M. Farner, Lars Schreiber, and Nathalie Tufenkji (Apr. 2020). "Biofilm Formation by Marine Bacteria Is Impacted by Concentration and Surface Functionalization of Polystyrene Nanoparticles in a Species-specific Manner". en. In: *Environmental Microbiology Reports* 12.2, pp. 203–213. ISSN: 1758-2229, 1758-2229. DOI: 10.1111/1758-2229.12824.

Oriekhova, Olena and Serge Stoll (2018). "Heteroaggregation of Nanoplastic Particles in the Presence of Inorganic Colloids and Natural Organic Matter". en. In: *Environmental Science: Nano* 5.3, pp. 792–799. ISSN: 2051-8153, 2051-8161. DOI: 10.1039/C7EN01119A.

Petosa, Adamo R., Deb P. Jaisi, Ivan R. Quevedo, Menachem Elimelech, and Nathalie Tufenkji (Sept. 2010). "Aggregation and Deposition of Engineered Nanomaterials in Aquatic Environments: Role of Physicochemical Interactions". en. In: *Environmental Science & Technology* 44.17, pp. 6532–6549. ISSN: 0013-936X, 1520-5851. DOI: 10.1021/es100598h.

Ramirez, Lina, Stephan Ramseier Gentile, Stéphane Zimmermann, and Serge Stoll (Apr. 2019). "Behavior of TiO2 and CeO2 Nanoparticles and Polystyrene Nanoplastics in Bottled Mineral, Drinking and Lake Geneva Waters. Impact of Water Hardness and Natural Organic Matter on Nanoparticle Surface Properties and Aggregation". en. In: *Water* 11.4, p. 721. ISSN: 2073-4441. DOI: 10.3390/w11040721.

Saavedra, Juan, Serge Stoll, and Vera I. Slaveykova (Sept. 2019). "Influence of Nanoplastic Surface Charge on Eco-Corona Formation, Aggregation and Toxicity to Freshwater Zooplankton". en. In: *Environmental Pollution* 252, pp. 715–722. ISSN: 02697491. DOI: 10.1016/j.envpol.2019.05.135.

Saleh, Navid B., Lisa D. Pfefferle, and Menachem Elimelech (Apr. 2010). "Influence of Biomacromolecules and Humic Acid on the Aggregation Kinetics of Single-Walled Carbon Nanotubes". en. In: *Environmental Science & Technology* 44.7, pp. 2412–2418. ISSN: 0013-936X, 1520-5851. DOI: 10.1021/es903059t.

Seoane, Marta, Carmen González-Fernández, Philippe Soudant, Arnaud Huvet, Marta Esperanza, Ángeles Cid, and Ika Paul-Pont (Aug. 2019). "Polystyrene Microbeads Modulate the Energy Metabolism of the Marine Diatom Chaetoceros Neogracile". en. In: *Environmental Pollution* 251, pp. 363–371. ISSN: 02697491. DOI: 10.1016/j.envpol.2019.04.142.

Singh, Nisha, Ekta Tiwari, Nitin Khandelwal, and Gopala Krishna Darbha (2019). "Understanding the Stability of Nanoplastics in Aqueous Environments: Effect of Ionic Strength, Temperature, Dissolved Organic Matter, Clay, and Heavy Metals". en. In: *Environmental Science: Nano* 6.10, pp. 2968–2976. ISSN: 2051-8153, 2051-8161. DOI: 10.1039/C9EN00557A.

Song, Zefeng, Xinyao Yang, Fangmin Chen, Fangyuan Zhao, Ying Zhao, Lili Ruan, Yinggang Wang, and Yuesuo Yang (June 2019). "Fate and Transport of Nanoplastics in Complex Natural Aquifer Media: Effect of Particle Size and Surface Functionalization". en. In: *Science of The Total Environment* 669, pp. 120–128. ISSN: 00489697. DOI: 10.1016/j.scitotenv.2019.03.102.

Stumm, Werner and James J. Morgan (1996). *Aquatic Chemistry : Chemical Equilibria and Rates in Natural Waters*. English. New York: Wiley. ISBN: 0-471-51184-6 978-0-471-51184-7 0-471-51185-4 978-0-471-51185-4.

Summers, Stephen, Theodore Henry, and Tony Gutierrez (May 2018). "Agglomeration of Nano- and Microplastic Particles in Seawater by Autochthonous and de Novo-Produced Sources of Exopolymeric Substances". en. In: *Marine Pollution Bulletin* 130, pp. 258–267. ISSN: 0025326X. DOI: 10.1016/j.marpolbul.2018.03.039.

Tallec, Kevin, Océane Blard, Carmen González-Fernández, Guillaume Brotons, Mathieu Berchel, Philippe Soudant, Arnaud Huvet, and Ika Paul-Pont (June 2019). "Surface Functionalization Determines Behavior of Nanoplastic Solutions in Model Aquatic Environments". en. In: *Chemosphere* 225, pp. 639–646. ISSN: 00456535. DOI: 10.1016/j.chemosphere.2019.03.077.

Ter Halle, Alexandra, Laurent Jeanneau, Marion Martignac, Emilie Jardé, Boris Pedrono, Laurent Brach, and Julien Gigault (Dec. 2017). "Nanoplastic in the North Atlantic Subtropical Gyre". en. In: *Environmental Science & Technology* 51.23, pp. 13689–13697. ISSN: 0013-936X, 1520-5851. DOI: 10.1021/acs.est.7b03667.

Valsesia, Andrea, Cloé Desmet, Isaac Ojea-Jiménez, Arianna Oddo, Robin Capomaccio, François Rossi, and Pascal Colpo (Dec. 2018). "Direct Quantification of Nanoparticle Surface Hydrophobicity". en. In: *Communications Chemistry* 1.1, p. 53. ISSN: 2399-3669. DOI: 10.1038/s42004-018-0054-7.

van Oss, C.J. (Oct. 1993). "AcidBase Interfacial Interactions in Aqueous Media". en. In: *Colloids and Surfaces A: Physicochemical and Engineering Aspects* 78, pp. 1–49. ISSN: 09277757. DOI: 10.1016/0927-7757(93)80308-2.

van Sebille, Erik, Chris Wilcox, Laurent Lebreton, Nikolai Maximenko, Britta Denise Hardesty, Jan A van Franeker, Marcus Eriksen, David Siegel, Francois Galgani, and Kara Lavender Law (Dec. 2015). "A Global Inventory of Small Floating Plastic Debris". In: *Environmental Research Letters* 10.12, p. 124006. ISSN: 1748-9326. DOI: 10.1088/1748-9326/10/12/124006.

Velzeboer, I., C. J. A. F. Kwadijk, and A. A. Koelmans (May 2014). "Strong Sorption of PCBs to Nanoplastics, Microplastics, Carbon Nanotubes, and Fullerenes". In: *En-*

*vironmental Science & Technology* 48.9, pp. 4869–4876. ISSN: 0013-936X. DOI: 10.1021/es405721v.

Verleysen, Eveline, Thorsten Wagner, Hans-Gerd Lipinski, Ralf Kägi, Robert Koeber, Ana Boix-Sanfeliu, Pieter-Jan De Temmerman, and Jan Mast (July 2019). "Evaluation of a TEM Based Approach for Size Measurement of Particulate (Nano)Materials". en. In: *Materials* 12.14, p. 2274. ISSN: 1996-1944. DOI: 10.3390/ma12142274.

Vold, Marjorie J (Oct. 1954). "Van Der Waals' Attraction between Anisometric Particles". en. In: *Journal of Colloid Science* 9.5, pp. 451–459. ISSN: 00958522. DOI: 10.1016/0095-8522(54)90032-X.

Wu, Jiayi, Ruifen Jiang, Wei Lin, and Gangfeng Ouyang (Feb. 2019). "Effect of Salinity and Humic Acid on the Aggregation and Toxicity of Polystyrene Nanoplastics with Different Functional Groups and Charges". en. In: *Environmental Pollution* 245, pp. 836–843. ISSN: 02697491. DOI: 10.1016/j.envpol.2018.11.055.

Wu, W., R.F. Giese, and C.J. van Oss (Aug. 1999). "Stability versus Flocculation of Particle Suspensions in WaterCorrelation with the Extended DLVO Approach for Aqueous Systems, Compared with Classical DLVO Theory". en. In: *Colloids and Surfaces B: Biointerfaces* 14.1-4, pp. 47–55. ISSN: 09277765. DOI: 10.1016/S0927-7765(99)00023-5.

Wyatt, Philip J. (Feb. 1993). "Light Scattering and the Absolute Characterization of Macromolecules". en. In: *Analytica Chimica Acta* 272.1, pp. 1–40. ISSN: 00032670. DOI: 10.1016/0003-2670(93)80373-S.

Xu, R. (2006). *Particle Characterization: Light Scattering Methods*. Springer Netherlands. ISBN: 978-0-306-47124-7.

Yu, Sujuan, Jingfu Liu, Yongguang Yin, and Mohai Shen (Jan. 2018). "Interactions between Engineered Nanoparticles and Dissolved Organic Matter: A Review on Mechanisms and Environmental Effects". en. In: *Journal of Environmental Sciences* 63, pp. 198–217. ISSN: 10010742. DOI: 10.1016/j.jes.2017.06.021.

Yu, Sujuan, Mohai Shen, Shasha Li, Yueju Fu, Dan Zhang, Huayi Liu, and Jingfu Liu (Dec. 2019). "Aggregation Kinetics of Different Surface-Modified Polystyrene Nanoparticles in Monovalent and Divalent Electrolytes". en. In: *Environmental Pollution* 255, p. 113302. ISSN: 02697491. DOI: 10.1016/j.envpol.2019.113302.

Zhang, Fan, Zhuang Wang, Se Wang, Hao Fang, and Degao Wang (Aug. 2019). "Aquatic Behavior and Toxicity of Polystyrene Nanoplastic Particles with Different Functional Groups: Complex Roles of pH, Dissolved Organic Carbon and Divalent Cations". en. In: *Chemosphere* 228, pp. 195–203. ISSN: 00456535. DOI: 10.1016/j.chemosphere.2019.04.115.

Zhou, Dongxu and Arturo A. Keller (May 2010). "Role of Morphology in the Aggregation Kinetics of ZnO Nanoparticles". en. In: *Water Research* 44.9, pp. 2948–2956. ISSN: 00431354. DOI: 10.1016/j.watres.2010.02.025.

Zhu, Lixin, Shiye Zhao, Thais B. Bittar, Aron Stubbins, and Daoji Li (Aug. 2019). "Photochemical Dissolution of Buoyant Microplastics to Dissolved Organic Carbon: Rates and Microbial Impacts". en. In: *Journal of Hazardous Materials*, p. 121065. ISSN: 03043894. DOI: 10.1016/j.jhazmat.2019.121065.

The two following Chapters study nanoplastic transport in porous media. These porous media are proxies for terrestrial interfaces, such as soils (interface between surface and underground environments), aquifers (interfaces between rocks and water), and sediments (interface between a sedimentary substrate and overlying/underlying water bodies such as rivers, lakes, oceans, and groundwater).

Chapter 3 was published as a research article in the journal *Chemosphere* in April 2020 and compares the deposition of three different nanoplastic models in a porous medium composed of sand. This article compares nanoplastic models with various physicochemical properties, and therefore, different degrees of environmental relevance. This allows elucidating which particle property is most likely to cause deposition in porous media. While this study demonstrates that specific particle properties cause increased deposition, it cannot establish the mechanism responsible for these differences in deposition.

Therefore, Chapter 4 investigates how fragmental nanoplastic models deposit by studying them in synthetic porous media with controlled and homogenous geometries, which removes the complexity of natural sand columns. Furthermore, these porous media are transparent, which allows for *in-situ* observation of deposits and provides insight into deposition mechanisms. Thanks to this experimental setup and the collaboration with scientists from the Rennes Institute of Physiques (IPR), we could better understand how size polydispersity and the presence of NOMs impact deposition of nanoplastics in porous media. This Chapter is an article that is currently in preparation.

**Cite chapter 3 as:** Pradel, A., El Hadri, H., Desmet, Cloé., Ponti, J., Reynaud, Sté., Grassl, B., Gigault, J., Deposition of environmentally relevant nanoplastic models in sand during transport experiments, *Chemosphere* (2020), doi:https://doi.org/10.1016/j.chemosphere.2020.126912.ext

# Chapter 3

# Deposition of environmentally relevant nanoplastic models in sand during transport experiments

Alice Pradel [a], Hind el Hadri[b], Cloé Desmet[c], Jessica Ponti[c], Stéphanie Reynaud[b], Bruno Grassl[b], Julien Gigault[a]

[a]Univ Rennes, CNRS, Géosciences Rennes - UMR 6118, 35000 Rennes, France

[b]CNRS/Univ Pau & Pays Adour/E2S UPPA, Institut des sciences analytiques et de physicochimie pour l'environnement et les matériaux, UMR 5254, 64000 Pau, France

[c]European Commission, Joint Research Centre (JRC), Via E. Fermi 2749, 21027 Ispra, VA, Italy

## Highlights:

- Nanoplastic models with environmentally relevant physicochemical properties were studied.
- Polymorphic (irregular and asymmetrical) particles are more likely to be trapped in porous media than spherical particles.
- Shape has a greater impact on the deposition rate than particle size or particle concentration.


## Abstract:

Nanoplastics (NPTs) are defined as colloids that originated from the unintentional degradation of plastic debris. To understand the possible risks caused by NPTs, it is crucial to determine how they are transported and where they may finally accumulate. Unfortunately, although most sources of plastic are land-based, risk assessments concerning NPTs in the terrestrial environmental system (soils, aquifers, freshwater sediments, etc.) have been largely lacking compared to studies concerning NPTs in the marine system. Furthermore, an important limitation of environmental fate studies is that the NPT models used are questionable in terms of their environmental representativeness. This study describes the fate of different NPT models in a porous media under unfavorable (repulsive) conditions, according to their physical and chemical properties: average hydrodynamic diameters (200 to 460 nm), composition (polystyrene with additives or primary polystyrene) and shape (spherical or polymorphic). NPTs that more closely mimic environmental NPTs present an inhomogeneous shape (i.e., deviating from a sphere) and are more deposited in a sand column by an order of magnitude. This deposition was attributed in part to physical retention, as confirmed by the straining that occurred for the larger size fractions. Additionally, different Derjaguin-Landau-Verwey-Overbeek (DLVO) models -the extended DLVO (XDLVO) and a DLVO modified by surface element integration (SEI) method- suggest that the environmentally relevant NPT models may alter its orientation to diminish repulsion from the sand surface and may find enough kinetic energy to deposit in the primary energetic minimum. These results point to the importance of choosing environmentally relevant NPT models.



**Keywords:** Nanoplastic; Size; Shape; Transport; Soil; Column

## 3.1 Introduction

It has been established that every environmental system contains plastic debris (Bank and S. V. Hansson 2019). The marine environment is the first system in which plastic pollution has been extensively studied, probably due to the highly visible accumulation that started in the 1970s (E. J. Carpenter and Smith 1972; A. Cózar et al. 2014; K. L. Law et al. 2010; Schwarz et al. 2019). Since then, the extent of this contamination has been more closely described. Plastic fragments or additives are found in remote areas as they can travel long distances (Jamieson et al. 2017; Peng et al. 2020).They have reached uninhabited forests after undergoing atmospheric transport (Allen et al. 2019) and have been incorporated into Artic sea ice after being transported by oceanic currents (Obbard et al. 2014). It is generally agreed upon that the terrestrial system is the major source of plastic waste (J. R. Jambeck et al. 2015). However, plastics in terrestrial and freshwater environments have received little attention (Horton et al. 2017; Rillig 2012; M. Wagner, Scherer, et al. 2014). Plastic accumulates in the terrestrial system due to common sources, such as faulty waste management systems, spreading of sewage sludge, use of plastic mulches and other plastic products in agriculture, and tire wear particles (Carr, Jin Liu, and Tesoro 2016; D. He et al. 2018; Scheurer and Bigalke 2018). This rapidly accumulating plastic in soils and sediments can be degraded by photo-oxidation, thermo-oxidation, abrasion and biodegradation, which causes the inevitable release of small plastic particles (Huerta Lwanga et al. 2017; Ng et al. 2018). In the terrestrial system (soils, aquifers, sediments, etc.), studies have generally focused on microplastics (1 $\mu$m to 5 mm) (Z. Dong, Ling Zhu, et al. 2019; Z. Dong, W. Zhang, et al. 2019; L. He, D. Wu, et al. 2018; Jin Liu, T. Zhang, et al. 2019; Tufenkji and Elimelech 2005), although it is clear that plastic fragmentation does not stop at the micrometer size (Gigault, Pedrono, et al. 2016; Lambert and M. Wagner 2016).

The fragmentation of macro- and microplastics to nanoplastics (<1 $\mu$m) adds complexity to the global plastic waste issue. Even if no clear definition of nanoplastics (NPTs) is proposed by policy-makers, a scientific consensus has been proposed to define NPTs as colloids that originate from the unintentional degradation of plastic (Gigault, Halle, et al. 2018; Hartmann et al. 2019). Compared to microplastics, NPTs acquire colloidal properties and become unaffected by gravity. At this scale, the fate of NPTs will be controlled by surface properties, shape and diffusion rather than by the bulk properties (Hiemenz and Rajagopalan 1997). The fact that the majority of plastic debris cannot be located by mass budgets at the ocean surface suggests that part of the missing fraction of plastic debris could be composed of fractions smaller than 300 $\mu$m in size (Albert A Koelmans et al. 2017a; van Sebille, Wilcox, et al. 2015). Since the nanoscale characteristics of plastic debris may pose potential risks, it is therefore crucial to determine where

this plastic originates from and where it accumulates (T. S. Galloway 2015; Albert A. Koelmans et al. 2017b; Lehner et al. 2019).

Due to limited data on the occurrence of NPTs, lab-scale models can aid in determining the transfer of NPTs from one environmental system to another. For the terrestrial system, a saturated sand column is generally used as a proxy for the study of colloid transfer in soils, sediments and aquifers (Geitner et al. 2017; Lecoanet, Bottero, and Wiesner 2004; Petosa et al. 2010; Redman, Walker, and Elimelech 2004; Syngouna and Chrysikopoulos 2013; Tufenkji and Elimelech 2004). Quevedo and Tufenkji compared the transport of spherical and size standardized polystyrene nanoparticles in quartz sand and loamy soil in the presence of monovalent or divalent salts (Quevedo and Tufenkji 2012). Recently, Hu et al. used quartz sand columns to investigate the cotransport of naphthalene with polystyrene nanoparticles (Hu et al. 2020). Another recent work demonstrated the influence of the soil type on the same nanoparticles (J. Wu et al. 2019). While these works highlight the importance and complexity of the transport mechanisms in soils, they only focused on NPT models that are not representative of the NPTs found in our environment (Ter Halle et al. 2017). Indeed, the composition, shape, size, and surface are known to play key roles in the transport of nanoparticles in the environment (Hotze, Phenrat, and Lowry 2010; Pelley and Tufenkji 2008; Salerno et al. 2006). Such parameters have only recently been investigated, with studies concerning UV-aged NPTs (Jin Liu, T. Zhang, et al. 2019) and polystyrene NPTs containing different surface functionalities (Z. Dong, Ling Zhu, et al. 2019).

Before investigating the influence of the soil properties, the objective of the present work is to investigate how the properties of NPTs affect their transport or accumulation in soils. Thus, different NPT models were used. All models were composed of polystyrene, since this is the only commercially available nanometer-sized plastic particle available. On the one hand, both commercial and noncommercial polystyrene latex spheres (PSL), *PSL COOH* and *PSL COOH-P*, respectively, are synthesized by a bottom-up process (Pessoni et al. 2019). This makes them highly spherical and monodisperse and it allows their surface to be modified by the addition of carboxylate functional groups (COOH), which are common on weathered plastics (Gewert, Plassmann, and MacLeod 2015). On the other hand, *NPT-P* are synthesized from a top-down method, which mimics the environmental mechanism of abrasion (El Hadri et al. 2020). They have polymorphic (asymmetrical and irregular) shapes, a polydisperse size distribution, and they may contain some oxidized functional groups. The transport of *NPT-P* models through a sand column shows that their irregular shape will increase their probability of accumulating in porous media. These results stress the importance of choosing NPT models that have environmentally relevant physicochemical properties.

## 3.2 Methods

### 3.2.1 Dispersions of nanoplastic models

Table 3.1 presents the different NPT models used in the study. Carboxylated polystyrene latex spheres of 200 nm (*PSL COOH 200*) were Polybead®Carboxylate Orange Dyed Microspheres 0.20 $\mu$m purchased from (Polysciences©Warrington USA). These particles contain additives for stabilizing purposes, whose composition and concentration are unknown. To study the effect of particle composition, additive-free particles composed of primary (*-P*) polystyrene were also used. Soap and metal-free carboxylated polystyrene spheres of 430 nm (*PSL COOH 430-P*) were produced by emulsion polymerization according to the method described by Pessoni et al. 2019. Finally, NPT models with polymorphic (asymmetrical and irregular) shapes and with an average hydrodynamic diameter of 350 nm or 460 nm (*NPT 350-P* and *NPT 460-P*, respectively) were formulated from mechanically crushed PS pellets, according to the method previously described El Hadri et al. 2020. All suspensions were composed of NaCl at a concentration of 5.0 $10^{-3}$ mol $L^{-1}$ with pH fixed at 6.5.

*Table 3.1: Summary of the physicochemical properties of the nanoplastic models studied*

| Model name | z-average diameter ($d_{z\,H}$) (nm) | Polydispersity Index (PDI) | Area Equivalent Diameter (nm) | Aspect Ratio | Asperity Frequency ($nm^{-1}$) and *Amplitude (nm)* | Zeta potential (mV) | Particle Concentration ($\#L^{-1}$) |
|---|---|---|---|---|---|---|---|
| *PSL COOH 200* | 200±13 | 0.04±0.03 | 193 ± 3 | 1.01±0.01 | 0 and *0* | -38.65±2.23 | 1.14 $10^{12}$ |
| *PSL COOH 430-P* | 430±28 | 0.07±0.01 | 430±19 | 1.01±0.01 | 0.013 and *12±2* | -29.07±1.81 | 1.14 $10^{11}$ |
| *NPT 350-P* | 350±10 | 0.11 | 244±133 | 1.67±0.56 | 0.013 and *11±6* | -33.54±2.72 | 2.12 $10^{11}$ |
| *NPT 460-P* | 460±25 | 0.19 | 329±223 | 1.68±0.58 | | | 9.34 $10^{10}$ |

### 3.2.2 Charge characterization

The zeta potential of the particles was assessed using a Wallis zetameter by Cordouan Technologies (Pessac, France). The particles were suspended in the same mobile phase as that used for the experimental conditions: NaCl at 5.0 $10^{-3}$ mol $L^{-1}$ and pH 6.5. The electrophoretic mobility of the colloidal particles was converted into a zeta potential by using Smoluchowski's formula. A zeta potential for sand of -50 mV was chosen according to Vinogradov, Jaafar, and Jackson 2010.

### 3.2.3 Size characterization

Hydrodynamic diameters ($d_H$) were determined by dynamic light scattering (DLS) using a Vasco-Flex particle size analyzer (Cordouan Technologies). The $d_H$ of the injected NPT models and the initial sand column signal, as well as 8 mL aliquots of the eluate, were characterized by DLS. Each DLS measurement corresponds to an average of six measurements of 60 seconds each. Each sample was assigned a z-average hydrodynamic diameter ($d_{zH}$) using the cumulant algorithm. Additionally, the Sparse Bayesian learning (SBL) algorithm provides a multimodal analysis to determine the presence of several $d_H$ (Figure 3.1). TEM images were obtained by a Jeol 2100 High Resolution Microscope (Figure 3.2). Data was analyzed with ImageJ software and the NanoDefine plugin to obtain the area equivalent diameters and the aspect ratios (length of major axis/length of minor axis), presented in Table 3.1 (Verleysen et al. 2019).

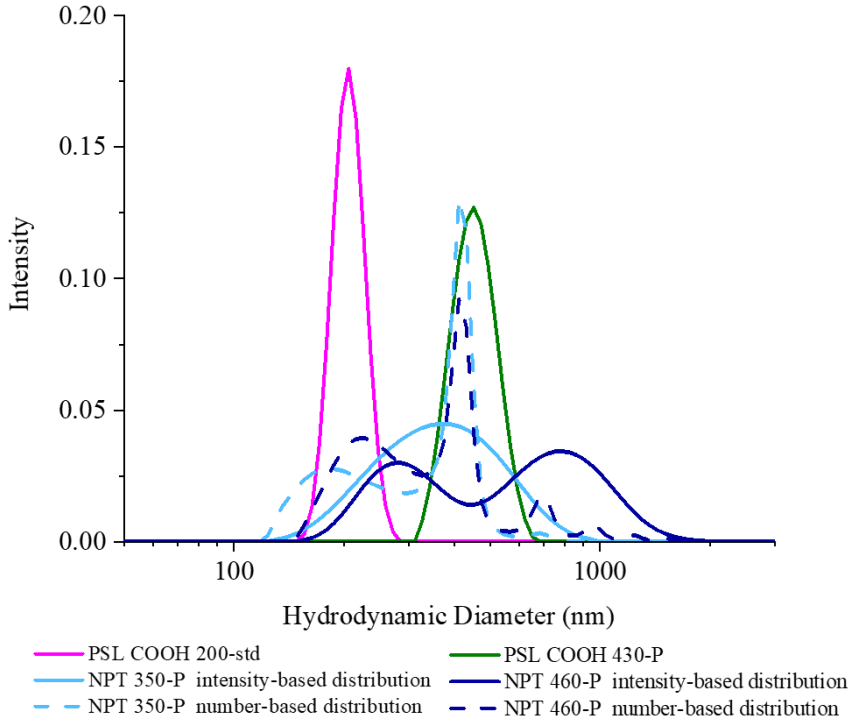


*Figure 3.1: Size distribution of the nanoplastic models, measured by Dynamic Light Scattering (DLS) and analyzed by the Cumulant and the Sparse Bayesian Learning (SBL) algorithms. Full lines illustrate intensity-based distributions (Cumulant) and dashed lines illustrate number-based distributions of polydisperse nanoplastic dispersions (SBL).*

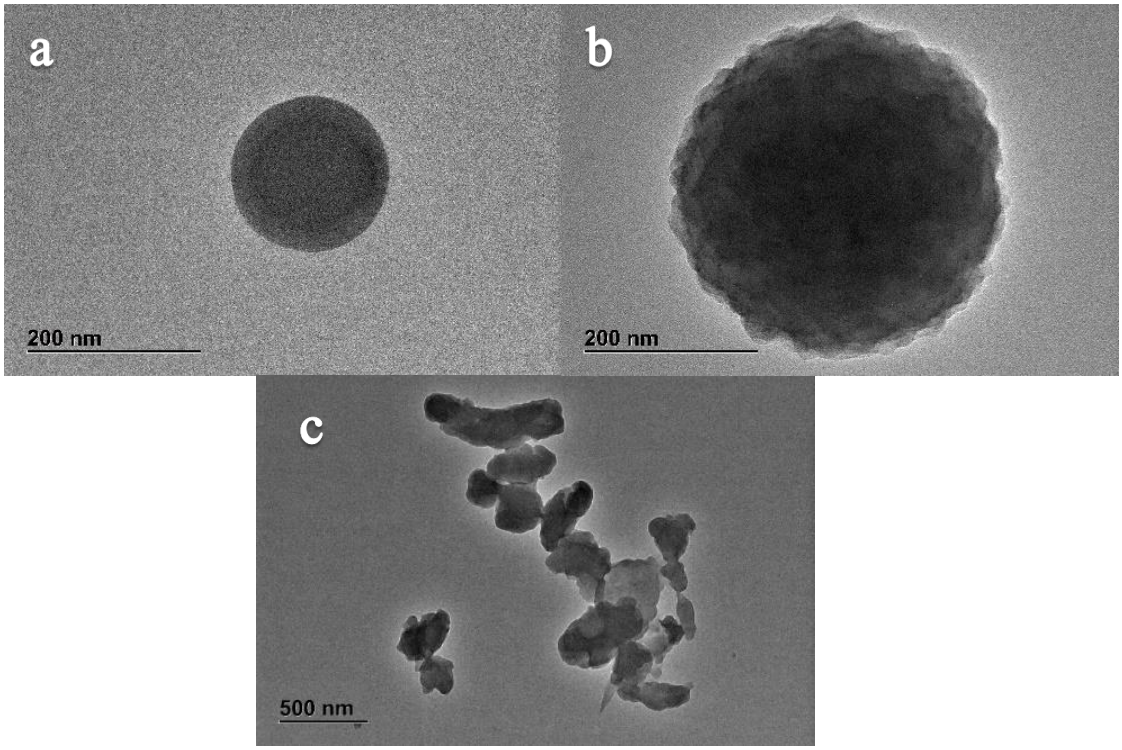


*Figure 3.2: Transmission Electron Microscopy (TEM) Images of a) PSL COOH 200, b) PSL COOH 430-P, and c) NPT-P*

The same *PSL COOH 200* and *PSL COOH 430-P* batches as the ones studied here were analyzed by TEM. The *NPT-P* batches that were analyzed by TEM were different from the ones used in the column experiments but had similar size distributions, with a $d_{zH}$ of 304 nm and a PDI of 0.23, corresponding to *NPT 350-P* and a $d_{zH}$ of 428nm and a PDI of 0.14, corresponding to *NPT 460-P*.

The Irregular Watershed analysis mode was used, as it can analyse irregular (non-ellipsoidal) shapes. The particle's roughness was visually determined by counting the amount of asperities (protrusions and depressions) on TEM images obtained at a magnification of 25000. The contour of the particle was delineated in by 60nm segments and all asperities that appeared to be on the same horizontal plane were counted and measured, to obtain asperity frequency and amplitude, respectively. Although user-dependent, this method illustrates the different degrees of roughness.

### 3.2.4 Transport in porous media

Transport and deposition were studied in a lab-scale sand-packed column using a liquid chromatography system (Äkta$^{TM}$ Pure by General Electric Healthcare). This porous media was composed of Fontainebleau sand (type NE34) with a median diameter ($d_{50}$) of 210 $\mu$ m and a uniformity index $d_{60}/d_{10}$ of 1.4. The sand was dry-packed into a

borosilicate column (XK 26, GE Healthcare, i.d. = 2.6 cm). The packed bed height varied from 11.2 to 12.7 cm. The porosity was 0.40 ± 0.01 on average. The eluent (mobile phase) was composed of NaCl at 5.0 $10^{-3}$ mol $L^{-1}$. The pH value was fixed at 6.5 using NaOH and HCl. The sand was washed with at least 14 pore volumes (PVs) of deionized water and 22 PVs of the eluent. The pore volume was determined by an injection of NaCl at 5.0 $10^{-3}$ mol $L^{-1}$. Complete tracer tests were performed with KBr. All reactants were analytical grade. The particles and tracers were injected during 6 PVs at a fixed rate of 1.57 $10^{-5}$ m $s^{-1}$, followed by at least six pore volumes of the plastic-free suspension at the same ionic strength and pH value. At the outlet, the concentration of the NPT models eluted from the porous media was continuously measured by the UV-Vis spectrophotometer paired to the chromatography system at a wavelength $\lambda$ = 226 nm, where polystyrene absorption is maximal. Breakthrough curves (BTC) were obtained by plotting the outflowing concentration of the NPT models normalized by the initial concentration as a function of pore volumes eluted. Duplicate experiments were performed for *PSL COOH 200* and *PSL COOH 430-P*. Due to the limited yield of *NPT-P* dispersions and to the variability in size distributions of different *NPT-P* batches, duplicates were not performed.

### 3.2.5 Theory

#### Colloid Filtration Theory (CFT)

Colloid filtration theory (CFT) is used to separate hydrodynamic processes from surface interactions that are occurring in the sand column. It is summarized by equation (3.1), which expresses the porous media's capacity to trap colloids. The single-collector removal efficiency ($\eta$) is the product of the single-collector contact efficiency ($\eta_0$) and the attachment efficiency of the particles ($\alpha$) (Petosa et al. 2010).

$$\eta = \eta_0 \cdot \alpha \tag{3.1}$$

The single-collector contact efficiency ($\eta_0$) is the capacity of colloids to be trapped by porous media due only to hydrodynamic mechanisms, without any favorable physicochemical conditions. It depends upon a number of factors, including the diameter of the colloids, the diameter of the sand grains in the porous media, the porosity of the sand column, and the flow rate. It was calculated according to the equation developed by Tufenkji and Elimelech 2004. The attachment efficiency ($\alpha$) is a function of the physicochemical properties of the colloid dispersion and of the sand grain surfaces, such as ionic strength, surface charge and the Hamaker constant of the system. The attachment efficiency ($\alpha$)

is obtained according to equation (3.2):

$$\alpha = -\frac{2d_{50}}{3(1-\epsilon)\eta_0 L} \cdot ln\left(\frac{C}{C_0}\right) \tag{3.2}$$

where $d_{50}$ is the median diameter of the sand grains, $\epsilon$ and L are the sand column porosity and length, respectively, and $(C/C_0)$ is the height of the breakthrough curve.

### DLVO theory of colloidal stability

Surface energetics between particles and an infinite flat plane were modeled by the Derjaguin-Landau-Verwey-Overbeek (DLVO) theory, such as the total energy of interaction $G^{tot}$ as the sum of the Lifshitz-van der Waals $G^{LW}$ attraction and the repulsion due to the electronic double layer $G^{el}$. DLVO theory can be expanded upon and modified to take into account the effect of hydrophobicity, roughness and particle shape, separately. First an extended version of the DLVO theory (XDLVO) was also modeled by adding the Lewis Acid-Base (hydrophopic) component $G^{AB}$ to the total energy of interaction. Secondly, the effect of particle shape and orientation was studied thanks to the surface element integration (SEI) method, since is what sets apart *PSL COOH 430-P* and both *NPT-P* particles.

The Lifshitz van der Waals component $G^{LW}$ of the free energy of interaction between a colloid and a surface is given by:

$$G^{LW} = -\frac{H}{6}\left[\frac{2d_p(h+d_p)}{h(h+d_p)} - \ln\frac{h+2d_p}{h}\right] \tag{3.3}$$

where H is the Hamaker constant for the polystyrene-silica-water system, h is the separation distance between the colloid and the sand, and $d_p$ is the radius of the colloid. A Hamaker constant of 1.45 $10^{-20}$ was calculated from Israelachvili 2015 for the interaction between quartz, water and polystyrene.

The electronic double layer component $G^{el}$ is given by:

$$G^{el} = \pi\epsilon d_p\left(\zeta_N^2 + \zeta_S^2\right)\left[\frac{2\zeta_N\zeta_S}{\zeta_N^2+\zeta_S^2}\cdot\ln\frac{1+\exp(-\kappa h)}{1-\exp(-\kappa h)} + \ln(1-\exp(-2\kappa h))\right] \tag{3.4}$$

where $\zeta_N$ and $\zeta_S$ are the surface charges of the plastic colloids and of the sand surface, respectively. The zeta potential was used instead of the surface potential. $\kappa$ is the inverse

of the double layer thickness, which is determined by the following equation:

$$\kappa = \left( \frac{e^2}{\epsilon k_B T} \sum_{i=1}^{n} z_i^2 n_i \right)^{1/2} \tag{3.5}$$

where e is the charge of the electron; $\epsilon$ is the permittivity of the medium, which is equal to 6.95 $10^{-10}$ $C^2.J^{-1}.m^{-1}$, $k_B$ the Boltzmann constant, T the temperature, $z_i$ the valency of the ions i, and $n_i$ the number of ions i per unit volume.

The Lewis Acid-Base energy of interaction $G^{AB}$ of our system is:

$$G^{AB} = \pi r d_p \lambda \Delta G^{AB} \exp\left( \frac{h_0 - h}{\lambda} \right) \tag{3.6}$$

where $\lambda$ is the correlation length, chosen as 1.65 nm, according to Valsesia et al. 2018, and $h_0$ is the minimum distance of separation between the particle and the surface, taken as 0.158 nm. The acid-base potential $\Delta G^{AB}$ is expressed as:

$$\Delta G^{AB} = -2 \left( \sqrt{\gamma_N^{AB}} - \sqrt{\gamma_W^{AB}} \right) \left( \sqrt{\gamma_S^{AB}} - \sqrt{\gamma_W^{AB}} \right) \tag{3.7}$$

with $\gamma^{AB}$ referring to the polar component of the surface free energy for W = water, S = sand surface and N = NPT model. $\gamma_W^{AB}$ is 51.00 mJ $m^{-2}$ and $\gamma_S^{AB}$ is 15.00 mJ $m^{-2}$ according to Barhoumi, Maaref, and Jaffrezic-Renault 2010. The polar component of the free energy was measured according the method of Valsesia et al. 2018 for each of the three types of NPT models. $\gamma_N^{AB}$ values of 33.91, 37.47 and 31.82 mJ $m^{-2}$ were obtained for *PSL COOH 200*, *PSL COOH 430-P* and *NPT-P*, respectively.

The DLVO theory was modified by the SEI method described by L. Wu et al. 2013 to understand the effect of *NPT-P*'s nonspherical shape and their different orientations, described by the angle $\phi$ that is formed between the major axis of the particle and the collector surface (Bhattacharjee, J. Y. Chen, and Elimelech 2000). The interaction energy between a plane surface (collector) and a curved object (particle) were calculated by integrating this energy over the exact surface geometry of the object. Our particles were considered to be rod-like. The semi-major axis (L) and semi-minor axis (a) were determined according to the aspect ratio and the $d_{zH}$ presented in Table 3.1.

## 3.3 Results and Discussion

Figure 3.3 illustrates the breakthrough curves (BTC) of the different NPT models after transport through a sand column at a constant flow rate. Reproducible results are obtained with this experimental setup, as shown by the error bars on the duplicate experiments of *PSL COOH 200* and *PSL COOH 430-P*. A KBr salt tracer shows only the effect of transport by advection and dispersion due to the absence of deposition ($C/C_0$ of unity). *PSL COOH 200* presents a BTC similar in shape to KBr with 92± 5 % recovered in column effluent. This result indicates transport through the column with negligible deposition onto the sand. However, 672± 1 % of *PSL COOH 430-P* are recovered in column effluent, which indicates some deposition occurred. Finally, both polymorphic PS models (*NPT-P*) are the most deposited, with only 28% of *NPT 350-P*, and 10% of *NPT 460-P* that are recovered in column effluent. These results indicate that an increase in particle size causes an increase in the deposition rate. Indeed, when comparing NPT models of similar shape, larger particles are less recovered in column effluent: *PSL COOH 430-P* vs *PSL COOH 200* and *NPT 460-P* vs *NPT 350-P*. The higher transport rate of *PSL COOH 200* compared to *PSL COOH 430-P* may also be due to the presence of surfactants used for commercial *PSL COOH 200*. Such molecules can enhance nanoparticle transport by decreasing adsorption in the secondary energetic minimum (see DLVO section below) (Tufenkji and Elimelech 2005). Finally, the absence of a tailing at the end of the BTCs shows that deposited particles did not detach from the porous media (Bradford, Yates, et al. 2002).

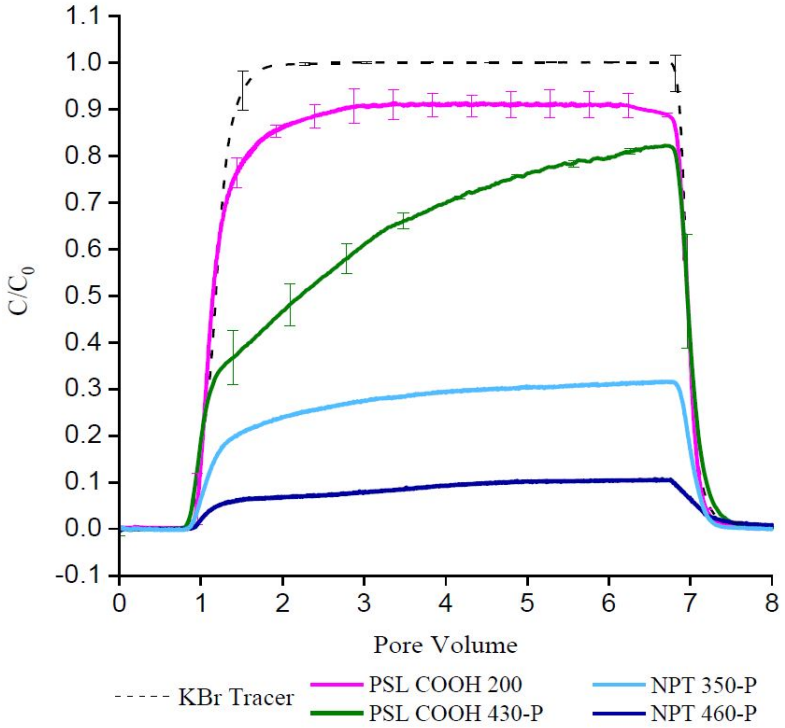


*Figure 3.3: Breakthrough curves of KCl tracer and nanoplastic models injected continuously for 6 pore volumes at an initial concentration ($C_0$) of 5.0 $10^{-3}$ g $L^{-1}$ in 5.0 $10^{-3}$ mol $L^{-1}$ NaCl and pH 6.5 (error bars = standard deviation, n = 2).*

Based on the BTCs, it appears that the particle shape strongly increases the deposition rate in the porous media under dynamic conditions. Surprisingly, *NPT 350-P* is significantly more deposited in porous media than *PSL COOH 430-P*, although they have a smaller initial hydrodynamic diameter and area equivalent diameter (Table 3.1). This confirms that the asymmetrical and irregular shape of the NPT model (*NPT-P*) significantly increases deposition in the porous media. It should be noted that these experiments were performed at equivalent mass concentrations instead of equivalent particle concentrations. This method was chosen to obtain a quality DLS signal at the outlet of the sand column since light scattering is proportional to the particle diameter. However, it creates a bias that favors elution of the smaller, more numerous particles (Table 3.1) (Bradford and Bettahar 2006). Despite this, *NPT 350-P*, which has a higher particle concentration, was more deposited than *PSL COOH 430-P*. This highlights the fact that an irregular asymmetrical shape has a greater impact on the deposition rate than that of size and particle concentration.

To investigate the retention mechanisms of these NPT models, both colloidal filtration theory (CFT) and various Derjaguin-Landau-Verwey-Overbeek (DLVO) theories were studied. According to the CFT, the single-collector contact efficiency ($\eta_0$) increases as sub-micrometric particle sizes decrease (Tufenkji and Elimelech 2004). Hence, smaller

particles should be more easily retained, which is not the case in the present study. This suggests that nanoplastic models used here have considerable differences in attachment efficiency ($\alpha$) and non-classical mechanisms of particle collision are operating. The attachment efficiency ($\alpha$) obtained by CFT, can be used to compare the affinity of particles with sand across different experimental conditions. Caution must be taken in interpreting $\alpha$ since the CFT is meant to study monodisperse and spherical particles and collectors. Since the sand grains are not monodisperse ($d_{60}/d_{10}$ of 1.4) and nanoplastic models have different degrees of polydispersity (see Table 3.1), an average $\alpha$ range, named $\bar{\alpha}$, and a range of $\alpha$ were presented in Table 3.2 with the corresponding heat-maps presented in Figure 3.4.

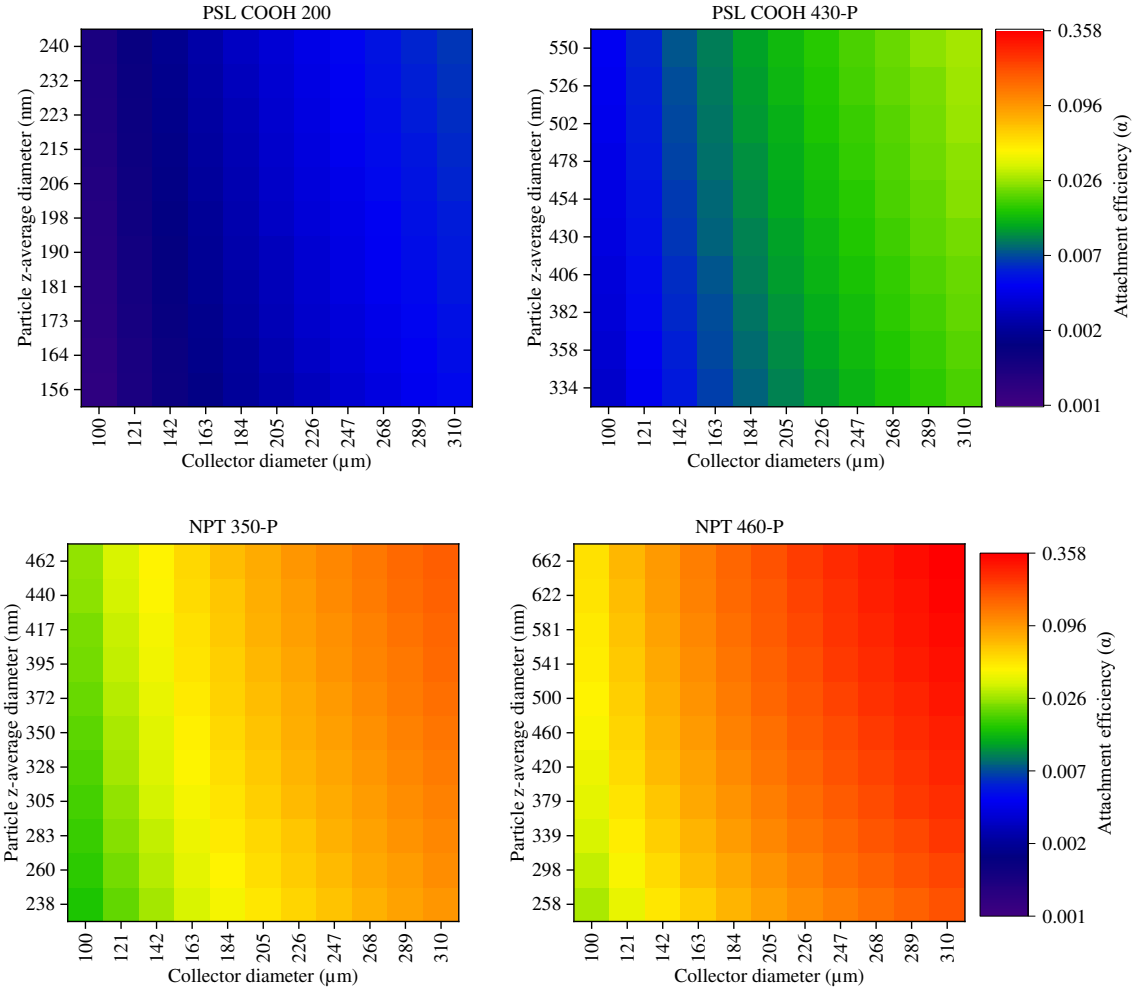


*Figure 3.4: Variation of attachment efficiencies ($\alpha$) over a range of particle and collector diameters that is equal to twice the standard deviation of the particle and collector size distributions. The scale is logarithmic.*

An $\bar{\alpha}$ of 0.0034 ± 0.0005 was obtained for *PSL COOH 200*, whereas *PSL COOH 430-P* had an $\bar{\alpha} = 0.012 \pm 0.0008$ (Table 3.2). These results are in agreement with other studies, such as Bradford, Yates, et al. 2002, who found that the attachment efficiency of 450 nm carboxylated PSL in $10^{-3}$ mol $L^{-1}$ KCl at pH 6.8 varied from $\alpha = 0.0037$ to $\alpha = 0.014$ according to the polydispersity and average grain size of the quartz sand. Tufenkji and Elimelech found $\alpha$ values of 0.0058 and 0.014 for 320 nm PSL COOH in 20 $10^{-3}$ mol $L^{-1}$ KCl at pH 8. For the polymorphic NPT models, the average attachment efficiency is one order of magnitude greater than that for the spherical models, with $\alpha = 0.069$ for *NPT 350-P* and 0.14 for *NPT 460-P*. This large increase in attachment efficiency is more likely to represent different hydrodynamic flow processes than a change in surface affinity. Indeed, the CFT theory is unsuitable to study the flow of nonspherical particles and largely overestimates $\alpha$ (and underestimates $\eta_0$) when the particle shape deviates from that of a sphere (Salerno et al. 2006).

*Table 3.2: Summary of the percent in column effluent and attachment efficiencies ($\alpha$) for the different nanoplastic models. The attachment efficiencies are based on average particle diameter ($d_p$) and collector diameters ($d_c$) and a range of $d_p$ and $d_c$ equal to the standard deviation ($\alpha$) of the size distributions. (Error bars = standard deviation of the duplicate experiments).*

| Nanoplastic | Percent in | Attachment Efficiency ($\alpha$) | | |
|---|---|---|---|---|
| Model | Column Effluent (%) | $d_p$ $\alpha$ and $d_c$ - $\alpha$ | Average $d_p$ and $d_c$ | $d_p + \alpha$ and $d_c + \alpha$ |
| *PSL COOH 200* | 92 ± 5 | $2.0\ 10^{-3} \pm 0.4\ 10^{-3}$ | $3.4\ 10^{-3} \pm 0.5\ 10^{-3}$ | $5.4\ 10^{-3} \pm 1.1\ 10^{-3}$ |
| *PSL COOH 430-P* | 67 ± 1 | $6.9\ 10^{-3} \pm 0.8\ 10^{-3}$ | $1.2\ 10^{-2} \pm 0.1\ 10^{-2}$ | $1.9\ 10^{-2} \pm 0.2\ 10^{-2}$ |
| *NPT 350-P* | 28 | $4.0\ 10^{-2}$ | $6.9\ 10^{-2}$ | $1.2\ 10^{-1}$ |
| *NPT 460-P* | 10 | $7.9\ 10^{-2}$ | $1.4\ 10^{-1}$ | $2.5\ 10^{-1}$ |

Since the attachment efficiencies ($\alpha$) obtained by the CFT theory should only reflect surface energetic interactions, they can be compared with the profiles of the interaction energy between the particles and the sand. Total surface energetic interactions ($G^{tot}$) are modeled according to DLVO theory by taking the sum of the Lifshitz-van der Waals attraction ($G^{LW}$) and the repulsion due to the electronic double layer ($G^{el}$). An extended version, the XDLVO theory, includes the Lewis acid-base (hydrophobic) interaction energy ($G^{AB}$). This component has been carefully quantified using the method described by Valsesia et al. 2018. It should be noted, however, that since DLVO and XDLVO theories assume that the particles are spherical, they cannot correctly determine the interaction energy of the asymmetrical and irregularly shaped *NPT-P*s (Hotze, Phenrat, and Lowry 2010). To overcome this limitation, a SEI-modified DLVO calculates $G^{LW}$ and $G^{el}$ between an elongated particle and the sand surface. This modified DLVO does not, however, incorporate the hydrophobic component of the interaction energy. It is important to note that in these experimental conditions, advection prevails over diffusion, with a Peclet

number varying from 112 to 240 for *PSL COOH 200* and *NPT 460-P*, respectively. In these conditions, particle deposition can occur if the adhesive forces are stronger than the hydrodynamic forces. Therefore, the objective is only to investigate whether the physical and chemical properties of the particles modeled by the different DLVO theories, are correlated to the attachment efficiencies in the sand column and hence a good predictor of adhesive forces. Surface energetic interactions should not be considered an absolute prediction of deposition behavior. If the energy of interaction predicts trends in transport, the most transported particles should have the highest energetic barrier to deposition($\Delta G^{tot}_{max}$) and lowest secondary energetic minimum ($\Delta G^{tot}_{min2}$), where reversible deposition can occur.

According to DLVO theory, all particles undergo significant repulsion from the sand grains, with ($\Delta G^{tot}_{max}$) equal to 175 $k_BT$ for *PSL COOH 200*, 235 $k_BT$ for *PSL COOH 430-P*, 244 $k_BT$ for *NPT 350-P*, and 321 $k_BT$ for *NPT 460-P* (Table 3.3 and full lines in Figure 3.5a). Based on the energy profiles, no colloid can overcome the energy barrier ($\Delta G^{tot}_{max}$) and irreversibly deposit in the primary minimum ($\Delta G^{tot}_{min1}$). The secondary energetic minimum ($\Delta G^{tot}_{min2}$) occurs between 20 and 60 nm from the sand surface. It varies from as low as -2.3 $k_BT$ for *NPT 460-P*, -2.2 $k_BT$ for *PSL COOH 430-P*, -1.6 $k_BT$ for *NPT 460-P* to -0.7 $k_BT$ for *PSL COOH 200* (Table 3.3 and full lines in Figure 3.5c). For the three larger particles, reversible retention in the secondary energetic minimum can occur since the depth is larger than 1.5 $k_BT$, which is the thermal energy of diffusion (Israelachvili 2015).

*Table 3.3: Summary of primary maximum $\Delta G^{tot}_{max}$ and secondary energetic minimum $\Delta G^{tot}_{min2}$ of interaction energies according to DLVO, SEI -modified DLVO and XDLVO theories, for the different nanoplastic models.*

| | DLVO Theory | | SEI-modified DLVO Theory | | | | XDLVO Theory | |
|---|---|---|---|---|---|---|---|---|
| Nanoplastic Model | $\Delta$ $G^{tot}_{max}$ ($k_BT$) | $\Delta$ $G^{tot}_{min2}$ ($k_BT$) | $\Delta$ $G^{tot}_{max}$ ($k_BT$) | $\Delta$ $G^{tot}_{min2}$ ($k_BT$) | $\Delta$ $G^{tot}_{max}$ ($k_BT$) | $\Delta$ $G^{tot}_{min2}$ ($k_BT$) | $\Delta$ $G^{tot}_{max}$ ($k_BT$) | $\Delta$ $G^{tot}_{min2}$ ($k_BT$) |
| *PSL COOH 200* | 175 | -0.7 | - | - | - | - | 51 | -0.7 |
| *PSL COOH 430-P* | 235 | -2.2 | - | - | - | - | 74 | -2 |
| *NPT 350-P* | 244 | -1.6 | $4.5\ 10^{10}$ | -0.4 | 45 | -1.5 | 64 | -1.6 |
| *NPT 460-P* | 321 | -2.3 | $5.9\ 10^{10}$ | -0.4 | 52 | -1.8 | 83 | -2.3 |

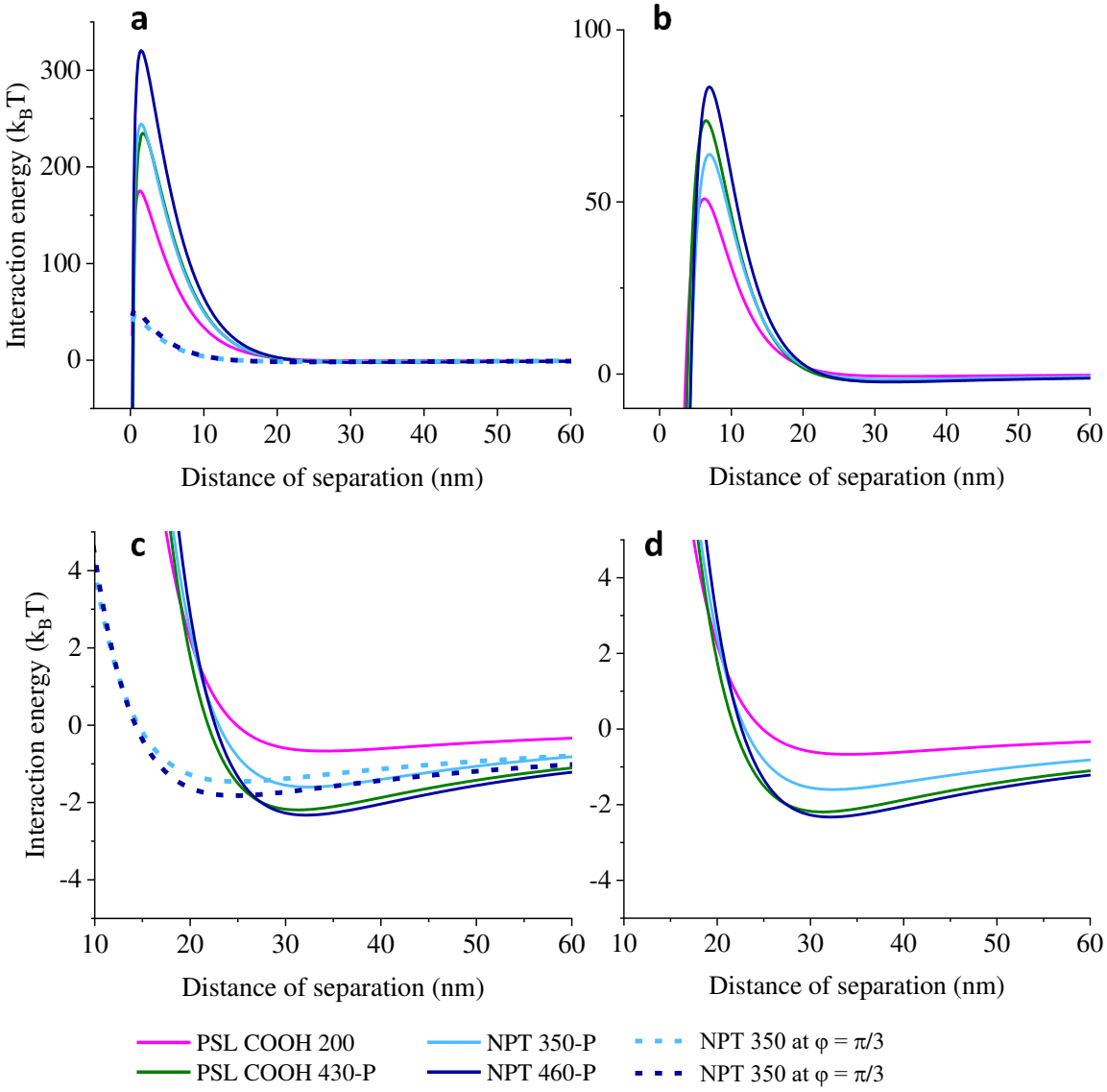


*Figure 3.5: Interaction energy, scaled to $kB_T$, between the nanoplastic models and the sand grain collector as a function of distance according to a) DLVO theory (full lines) and SEI-modified DLVO theory (dashed lines) and b) XDLVO theory. The identical data is replotted in c) and d) to highlight the secondary energetic minimum of panels a) and b) respectively.*

By accounting for the polar component of the interaction energy, the XDLVO theory predicts similar global trends but indicates a much lower repulsion of all particles from the sand surface (Figures 3.5b and 3.5d). The maximum heights of $\Delta G^{tot}_{max}$ for spherical particles *PSL COOH 200* and *PSL COOH 430-P* are equal to 51 $k_BT$ and 74 $k_BT$, respectively. For the asymmetrical and irregularly shaped particles, $\Delta G^{tot}_{max}$ is comparable: 64 $k_BT$ and 83 $k_BT$ for *NPT 460-P* and *NPT 460-P*, respectively (Table 3.3 and Fig-

ure 3.5b). Based on the height of the energy barriers, still no colloid deposition should occur in the primary minima. The depth of the secondary energetic minimum $\Delta G^{tot}_{min2}$ is unchanged compared to that determined by the DLVO theory (Table 3.3 and Figure 3.5d).

The dashed lines in Figures 3.5a and 3.5c show the minimal interaction energy between the sand surface and the NPT-P models, according to the SEI-modified DLVO theory. This occurs when they form an angle ($\phi$) of $\pi/3$ with the collector surface (Gomez-Flores et al. 2019). $\Delta G^{tot}_{max}$ is reduced to 45 $k_BT$ and 52 $k_BT$ for *NPT 460-P* and *NPT 460-P*, respectively (Table 3.3). The interaction energy is maximal at $\phi = 0$ (Table 3.3 and Figure 3.6). This is mostly due to the fact the particle surface is closer to the collector (Gomez-Flores et al. 2019). $\Delta G^{tot}_{min2}$ is only slightly less deep than predicted by DLVO and XDLVO theories (Table 3.3 and Figure 3.5c).

The high retention rate of the *NPT-P* particles can be in part attributed to the fact that they may find orientations where there is no energy barrier to irreversible deposition $\Delta G^{tot}_{min1}$ (Gomez-Flores et al. 2019). This can be expected to occur when both particle orientation and hydrophobicity are accounted for simultaneously. Furthermore, the magnitude of the total energies of interaction $\Delta G^{tot}$ of *PSL COOH 430-P*, *NPT 460-P* and *NPT 350-P* and the sand surfaces may be overestimated by the all DLVO models due to their surface roughness (Table 3.1 and Figure 3.2) (Bhattacharjee, Ko, and Elimelech 1998; E. M. Hoek and Agarwal 2006). *NPT-P* particles are characterized by a large range of orientation-dependent interaction energies (Table 3.3 and Figure 3.6), which will give them considerable torque. This added torque can provide the particles sufficient kinetic energy to overcome an energy barrier $\Delta G^{tot}_{max}$ that is significantly reduced at some orientations Figure 3.5a (Seymour et al. 2013).

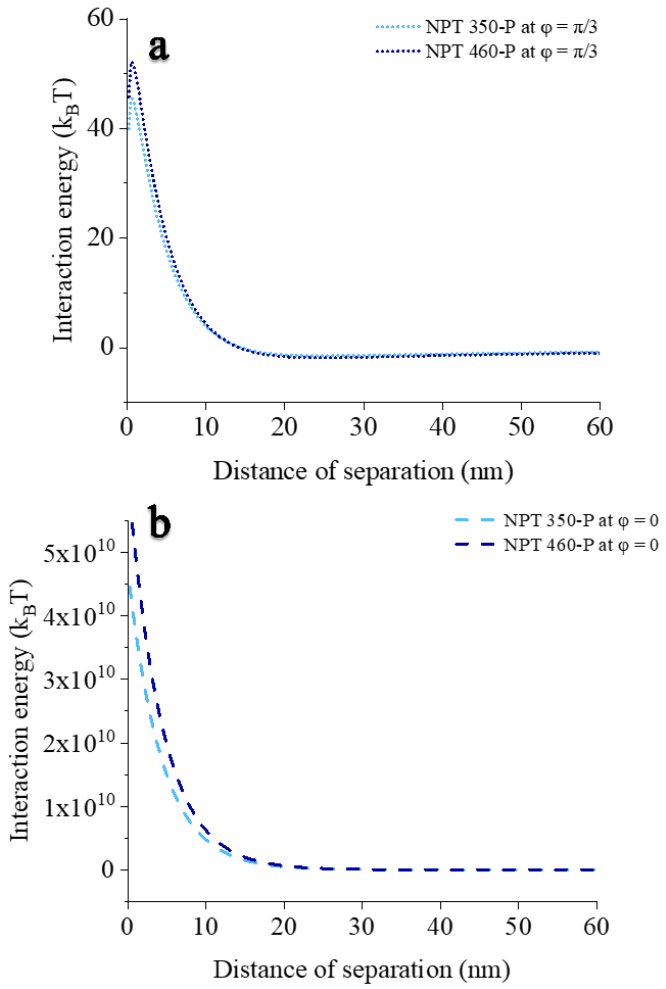


*Figure 3.6: Interaction energy, scaled to $k_B T$, between nanoplastic models and the sand grain collector, according to DLVO theory modified by the surface element integration method (SEI). Interaction energy when a) the particle's major axis forms an angle of $\pi/3$ with the collector surface and b) the particle's major axis forms an angle of 0 with the collector surface.*
For *NPT 350-P*, the particles' semi-major axis (L) and semi-minor axis (a) were L = 219 and a = 131 nm and for *NPT 460-P*: L= 288 nm and a= 172 nm.

However, the DLVO and XDLVO theories are inadequate to predict the deposition of plastic nanoparticles in porous media. On the one hand, the DLVO and XDLVO theories globally underestimate the amount of deposition that particles undergo. This is a well-known effect when studying the transport of particles in unfavorable (repulsive) conditions (Elimelech and O'Melia 1990). On the other hand, the height of the energy barrier is not proportional to the level of repulsion, nor is the depth of the secondary energetic minimum proportional to the level of deposition. For example, *PSL COOH*

*200* is the most transported particle, although it has the lowest energy barrier $\Delta G^{tot}_{max}$. This occurs because all interaction energies scale linearly with particle size (Elimelech and O'Melia 1990). In other words, larger particles should undergo more repulsion and be more transported, especially since all particles present comparable polar components of the surface free energy ($\gamma^{AB}$) and zeta potentials ($\zeta_N$). However, contrary to these DLVO and XDLVO predictions, *NPT 460-P*, which has a higher energy barrier, is more deposited than *NPT 460-P*. Although a high energy barrier is present, particles may be retained by 1) attachment onto chemical heterogeneities on the colloid and collector surfaces that act as favorable sites (Seymour et al. 2013; Tufenkji and Elimelech 2005) 2) reversible attachment in the secondary energetic minimum (Tufenkji and Elimelech 2005) and 3) straining (trapping of particles in pore throats that are too small to allow the passage of particles) (Bradford, Yates, et al. 2002; McDowell-Boyer, Hunt, and Sitar 1986). Furthermore, pore geometry creates a variety of speed profiles, such that particles may also be retained in zones with a lower flow velocity where the hydrodynamic forces are lowered (Elimelech and O'Melia 1990). Indeed, pore geometry plays a dominant role in colloid retention under conditions where a high energy barrier exists (Tong and W. P. Johnson 2006).

To determine the extent to which deposition can be attributed to chemical heterogeneity, batch adsorption experiments were conducted. Three conditions were studied : Sand with deionized water, nanoplastic dispersions alone (blank) and sand with nanoplastic dispersions. The following quantities were used : 20 $\pm$ 0.1 g of sand and 170.1 $\pm$ 0.1 g of the nanoplastic dispersions at concentration of 5 $10^{-3}$ mg $L^{-1}$ or deionized water. The sand underwent the same cleaning process as for the column experiments. Triplicates of each conditions were performed in square borosilicate bottles of 300 mL which were agitated at 250 rpm. At intervals of 10, 45, 153 and 186 minutes, agitation was stopped, the sand was left to settle for 1 minute and 1.5 mL of the supernatant was sampled. Concentrations were measured by UV absorbance (Akta Pur detector). Each measurement was done in triplicate. These experimental conditions optimized the sand to nanoparticle ratio in order to detect any small variation in particle in concentration, while maintaining a vigorous mixing of the sand and ensuring that the total volume sampled was less than 10% of the initial volume.

The results, presented in Figure 3.7, show that none of our plastic nanoparticles are significantly adsorbed onto the sand. While results from batch and column experiments can be difficult to compare when they are not normalized by $\bar{\alpha}$=1, our batch experiments do show that chemical heterogeneity is far from significative (Geitner et al. 2017; Treumann et al. 2014). This points to the importance of straining and adsorption in the secondary energetic minimum.

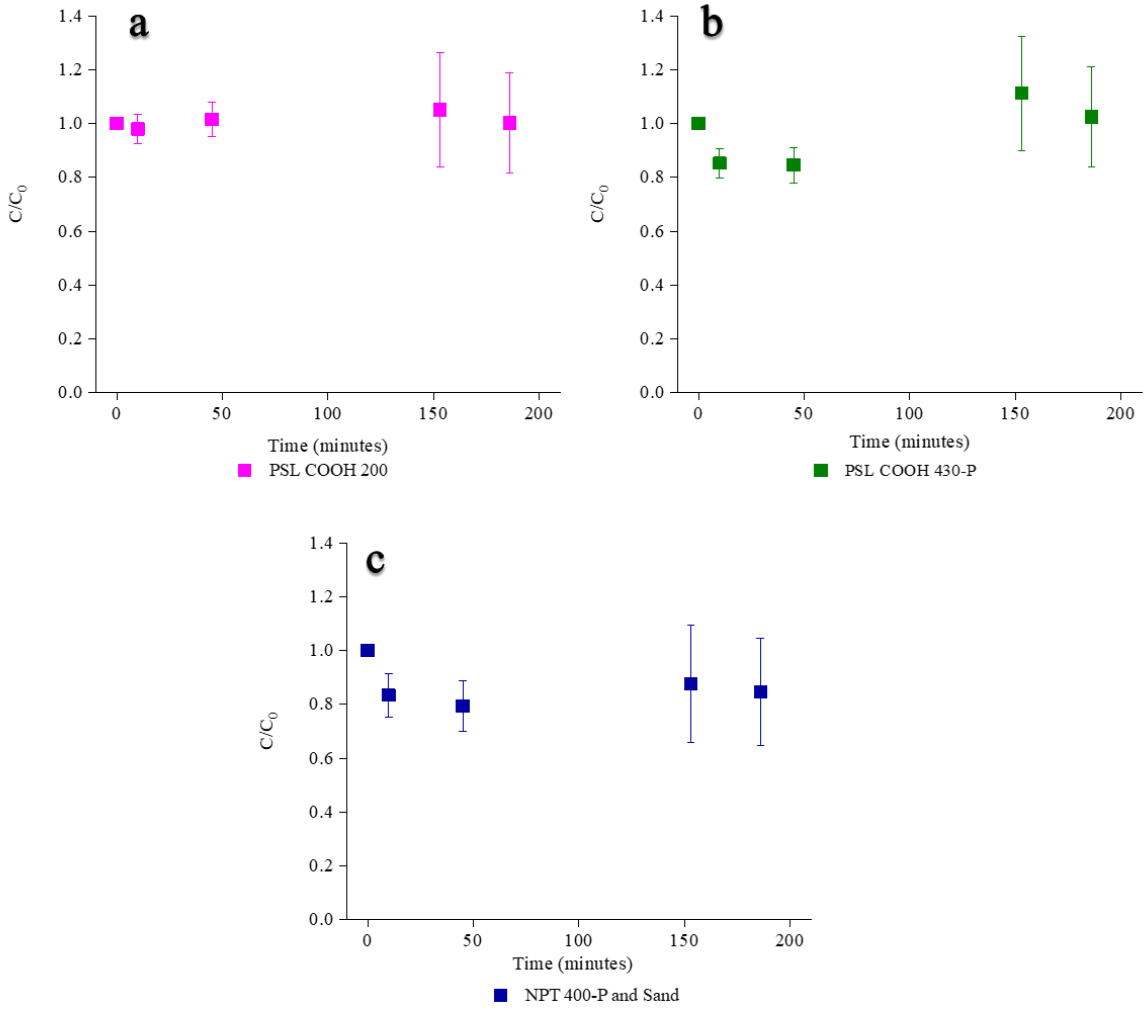


*Figure 3.7: Evolution of the relative concentration of dispersed a) PSL COOH 200, b) PSL COOH 430-P c) NPT-P nanoplastic models during batch adsorption experiments with Fontainebleau sand. (n = 3, error bars = 2 standard deviations)*

The evolution of the hydrodynamic diameters of the particles injected in and eluted from through the porous media can also indicate what processes occur in the column (Figure 3.8). The average size and polydispersity of eluted particles were constant during elution. The average hydrodynamic diameters ($d_{zH}$) of the smaller spheres, *PSL COOH 200*, do not change significantly (+4%). The larger spherical particles, *PSL COOH 430-P*, undergo a more pronounced decrease in $d_{zH}$ after flowing through the sand column (-11%). Both spherical particles' polydispersities do not vary significantly. For the asymmetrical NPT models, the decrease in $d_{zH}$ after elution is globally greater and even more pronounced for the larger particles (-45% for *NPT 460-P*) compared to that of the smaller particles (-20% for *NPT 350-P*). The smaller size fraction of irregularly shaped particles, approximately 200 nm in diameter, is most mobile in the sand column. Furthermore, the

polydispersity of the samples containing asymmetrical and irregular particles decreases. These changes in size point to a mechanism of physical retention of spherical particles larger than 380 nm and irregularly shaped particles larger than approximately 300 nm. This confirms that large particles are deposited by physical straining in the pores of the sand column, which is unaccounted for by the DLVO theories and underestimated by CFT (Bradford, Yates, et al. 2002). In similar experimental conditions, T. H. Weiss et al. 1995 noted a similar effect concerning the transport of 14 different bacterial strains. The bacterial cells recovered in the eluent were not only smaller but also rounder than the cells injected.

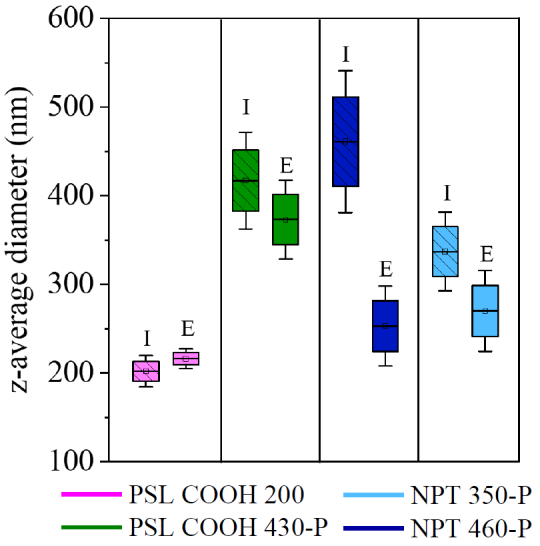


*Figure 3.8: z-average hydrodynamic diameters ($d_{zH}$) of the plastic nanoparticles before and after flowing through the sand column (n=6, error bars= standard deviation).*

The deposition rate increases as the particle size increases and as its shape deviates from that of a sphere. In other words, smaller and smoother particles are more easily transported. This can be partially attributed to straining. Straining is expected to start having an effect when the ratio of the particle radius to the median collector radius ($d_p/d_{50}$) exceeds 0.0017 (Bradford, Yates, et al. 2002). This is satisfied in the case of *PSL COOH 430-P* ($d_p/d_{50}$ = 0.002). Concerning *NPT-P*s, since most particles larger than approximately 200 nm are retained, straining occurs at a lower $d_p/d_{50}$ ratio (Figure 3.8). Straining of these particles is enhanced because the hydrodynamics of nonspherical particle flow in porous media are more complex than those of spherical particles. In highly repulsive conditions (thousands of $k_BT$), elongated particles are not more deposited than spherical particles since they can orient their major axis parallel to the flow (S. Xu, Liao, and Saiers 2008). However, in our conditions, where there is less repulsion (10s of $k_BT$)

nonspherical particles are increasingly deposited. This is attributed to larger collision frequencies with the porous media (Salerno et al. 2006). The CFT underestimates the single-collector contact efficiency ($\eta_0$) for spheroidal particles (Salerno et al. 2006). Finally, the *NPT-P* dispersions are highly polydisperse and as such will contain a higher fraction of large particles that are likely to be retained.

As mentioned above, reversible deposition in the secondary energetic minimum is possible for *PSL COOH 430-P* and both polymorphic particles *NPT 350-P* and *NPT 460-P*. The asymmetrical BTC shape of the *PSL COOH 430-P* is typical of either particle release from the secondary energetic minimum or blocking of the flowing particles by previously deposited particles (Bradford, Yates, et al. 2002; Bradford and Bettahar 2006; Redman, Walker, and Elimelech 2004; Tufenkji and Elimelech 2005). This was not observed for *NPT 350-P* and *NPT 460-P*, whose BTCs instead reach a plateau. It indicates either that the asymmetrical models are not detached and undergoing re-entrainment from the sand or that deposited particles do not block the incoming particles. Colloidal detachment and re-entrainment from the secondary energetic minimum mostly occur by rolling, which is easiest for spherical particles. Despite the fact that nonspherical particles have larger hydrodynamic torques than spherical particles, as particles deviate from an ideal spherical shape, they present a higher moment arm requiring more energy to induce rolling (Bergendahl and Domenico Grasso 2000; Seymour et al. 2013) The flat BTC may also indicate that deposited particles create more favorable sites for deposition by increasing the physical roughness of the porous media (Seymour et al. 2013). Finally, the shape of the *NPT-P*'s BTCs suggest that reversible deposition not be as dominant a mechanism as straining and deposition in the primary energetic minimum.

## 3.4 Conclusion

This study showed that the physicochemical properties of the NPT models significantly affect their propensity to be transported. The asymmetrical and irregular shape of the environmentally relevant NPT model has a strikingly positive impact on the deposition rate in the sand column compared to that impact of particle size, composition or concentration. The deposition of these models in the porous media may be attributed partially to physical retention, as witnessed by the straining of the larger size fractions. Their deposition is also attributed to an orientation-dependent level of repulsion $\Delta G^{tot}_{max}$ which allows the particles to take on the most thermodynamically preferable orientation, and possibly to overcome the energy barrier to irreversible deposition $\Delta G^{tot}_{max}$, given sufficient hydodynamic torque. These results point to the importance of choosing environmentally relevant NPT models. Their asymmetrical and irregular shape, which is characteristic of

the mechanical abrasion of plastic debris, increases their deposition rate in a sand column by an order of magnitude. It is clear that the relevance of environmental fate studies depends upon the quality of the proxies used (Albert A. Koelmans 2019). More particularly, the impact of the NPT composition (polymer type, additives and sorbed contaminants), average size and size distribution as well as NPT shape are crucial parameters to study (S. Wagner and Reemtsma 2019).

The importance of the physical and chemical properties of the NPT models has been demonstrated here. Further studies are needed on the one hand, to define single-collector contact efficiency ($\eta_0$) for nonspherical particles and to quantify the amount of deposition that can be attributed to straining, irreversible attachment (in $\Delta G^{tot}_{min}$) and reversible attachment (in $\Delta G^{tot}_{min2}$). On the other hand, more research is needed to implement these results by taking into account the environmental conditions of the porous media (ionic strength, natural organic matter, pH value, and soil composition). Such a complete approach is needed to fully assess the fate of NPTs in freshwater and terrestrial environments.

# References


Allen, Steve, Deonie Allen, Vernon R. Phoenix, Gaël Le Roux, Pilar Durántez Jiménez, Anaëlle Simonneau, Stéphane Binet, and Didier Galop (Apr. 2019). "Atmospheric Transport and Deposition of Microplastics in a Remote Mountain Catchment". en. In: *Nature Geoscience*. ISSN: 1752-0894, 1752-0908. DOI: 10.1038/s41561-019-0335-5.

Bank, Michael S. and Sophia V. Hansson (June 2019). "The Plastic Cycle: A Novel and Holistic Paradigm for the Anthropocene". en. In: *Environmental Science & Technology*, acs.est.9b02942. ISSN: 0013-936X, 1520-5851. DOI: 10.1021/acs.est.9b02942.

Barhoumi, H., A. Maaref, and N. Jaffrezic-Renault (May 2010). "Experimental Study of Thermodynamic Surface Characteristics and pH Sensitivity of Silicon Dioxide and Silicon Nitride". en. In: *Langmuir* 26.10, pp. 7165–7173. ISSN: 0743-7463, 1520-5827. DOI: 10.1021/la904251m.

Bergendahl, John and Domenico Grasso (May 2000). "Prediction of Colloid Detachment in a Model Porous Media: Hydrodynamics". en. In: *Chemical Engineering Science* 55.9, pp. 1523–1532. ISSN: 00092509. DOI: 10.1016/S0009-2509(99)00422-4.

Bhattacharjee, Subir, Jeffrey Y. Chen, and Menachem Elimelech (May 2000). "DLVO Interaction Energy between Spheroidal Particles and a Flat Surface". en. In: *Colloids and Surfaces A: Physicochemical and Engineering Aspects* 165.1-3, pp. 143–156. ISSN: 09277757. DOI: 10.1016/S0927-7757(99)00448-3.

Bhattacharjee, Subir, Chun-Han Ko, and Menachem Elimelech (June 1998). "DLVO Interaction between Rough Surfaces". en. In: *Langmuir* 14.12, pp. 3365–3375. ISSN: 0743-7463, 1520-5827. DOI: 10.1021/la971360b.

Bradford, Scott A. and Mehdi Bettahar (Jan. 2006). "Concentration Dependent Transport of Colloids in Saturated Porous Media". en. In: *Journal of Contaminant Hydrology* 82.1-2, pp. 99–117. ISSN: 01697722. DOI: 10.1016/j.jconhyd.2005.09.006.

Bradford, Scott A., Scott R. Yates, Mehdi Bettahar, and Jirka Simunek (Dec. 2002). "Physical Factors Affecting the Transport and Fate of Colloids in Saturated Porous Media: FACTORS AFFECTING THE FATE OF COLLOIDS". en. In: *Water Resources Research* 38.12, pp. 63-1-63–12. ISSN: 00431397. DOI: 10.1029/2002WR001340.

Carpenter, Edward J. and K. L. Smith (1972). "Plastics on the Sargasso Sea Surface". In: *Science* 175.4027, pp. 1240–1241. ISSN: 0036-8075. DOI: 10.1126/science.175.4027.1240.

Carr, Steve A., Jin Liu, and Arnold G. Tesoro (Mar. 2016). "Transport and Fate of Microplastic Particles in Wastewater Treatment Plants". en. In: *Water Research* 91, pp. 174–182. ISSN: 00431354. DOI: 10.1016/j.watres.2016.01.002.

Cózar, A., F. Echevarria, J. I. Gonzalez-Gordillo, X. Irigoien, B. Ubeda, S. Hernandez-Leon, A. T. Palma, S. Navarro, J. Garcia-de-Lomas, A. Ruiz, M. L. Fernandez-de-Puelles, and C. M. Duarte (July 2014). "Plastic Debris in the Open Ocean". en. In: *Proceedings of the National Academy of Sciences* 111.28, pp. 10239–10244. ISSN: 0027-8424, 1091-6490. DOI: 10.1073/pnas.1314705111.

Dong, Zhiqiang, Wen Zhang, Yuping Qiu, Zhenglong Yang, Junliang Wang, and Yidi Zhang (Jan. 2019). "Cotransport of Nanoplastics (NPs) with Fullerene (C60) in Saturated Sand: Effect of NPs/C60 Ratio and Seawater Salinity". en. In: *Water Research* 148, pp. 469–478. ISSN: 00431354. DOI: 10.1016/j.watres.2018.10.071.

Dong, Zhiqiang, Ling Zhu, Wen Zhang, Rui Huang, Xiang-Wei Lv, Xinyu Jing, Zhenglong Yang, Junliang Wang, and Yuping Qiu (Dec. 2019). "Role of Surface Functionalities of Nanoplastics on Their Transport in Seawater-Saturated Sea Sand". en. In: *Environmental Pollution* 255, p. 113177. ISSN: 02697491. DOI: 10.1016/j.envpol.2019.113177.

El Hadri, Hind, Julien Gigault, Benoit Maxit, Bruno Grassl, and Stéphanie Reynaud (2020). "Nanoplastic from Mechanically Degraded Primary and Secondary Microplastics for Environmental Assessments". In: *NanoImpact*, p. 100206. ISSN: 2452-0748. DOI: 10.1016/j.impact.2019.100206.

Elimelech, Menachem and Charles R. O'Melia (June 1990). "Effect of Particle Size on Collision Efficiency in the Deposition of Brownian Particles with Electrostatic Energy Barriers". en. In: *Langmuir* 6.6, pp. 1153–1163. ISSN: 0743-7463, 1520-5827. DOI: 10.1021/la00096a023.

Galloway, Tamara S. (2015). "Micro- and Nano-Plastics and Human Health". en. In: *Marine Anthropogenic Litter*. Ed. by Melanie Bergmann, Lars Gutow, and Michael Klages. Cham: Springer International Publishing, pp. 343–366. ISBN: 978-3-319-16509-7 978-3-319-16510-3. DOI: 10.1007/978-3-319-16510-3_13.

Geitner, Nicholas K., Niall J. O'Brien, Amalia A. Turner, Enda J. Cummins, and Mark R. Wiesner (Nov. 2017). "Measuring Nanoparticle Attachment Efficiency in Complex Systems". en. In: *Environmental Science & Technology* 51.22, pp. 13288–13294. ISSN: 0013-936X, 1520-5851. DOI: 10.1021/acs.est.7b04612.

Gewert, Berit, Merle M. Plassmann, and Matthew MacLeod (2015). "Pathways for Degradation of Plastic Polymers Floating in the Marine Environment". en. In: *Environmental Science: Processes & Impacts* 17.9, pp. 1513–1521. ISSN: 2050-7887, 2050-7895. DOI: 10.1039/C5EM00207A.

Gigault, Julien, Alexandra ter Halle, Magalie Baudrimont, Pierre-Yves Pascal, Fabienne Gauffre, Thuy-Linh Phi, Hind El Hadri, Bruno Grassl, and Stéphanie Reynaud (Apr. 2018). "Current Opinion: What Is a Nanoplastic?" en. In: *Environmental Pollution* 235, pp. 1030–1034. ISSN: 02697491. DOI: 10.1016/j.envpol.2018.01.024.

Gigault, Julien, Boris Pedrono, Benoît Maxit, and Alexandra Ter Halle (Apr. 2016). "Marine Plastic Litter: The Unanalyzed Nano-Fraction". en. In: *Environmental Science: Nano* 3.2, pp. 346–350. ISSN: 2051-8161. DOI: 10.1039/C6EN00008H.

Gomez-Flores, Allan, Scott A. Bradford, Lei Wu, and Hyunjung Kim (Nov. 2019). "Interaction Energies for Hollow and Solid Cylinders: Role of Aspect Ratio and Particle Orientation". en. In: *Colloids and Surfaces A: Physicochemical and Engineering Aspects* 580, p. 123781. ISSN: 09277757. DOI: 10.1016/j.colsurfa.2019.123781.

Hartmann, Nanna B., Thorsten Hüffer, Richard C. Thompson, Martin Hassellöv, Anja Verschoor, Anders E. Daugaard, Sinja Rist, Therese Karlsson, Nicole Brennholt, Matthew Cole, Maria P. Herrling, Maren C. Hess, Natalia P. Ivleva, Amy L. Lusher, and Martin Wagner (Feb. 2019). "Are We Speaking the Same Language? Recommendations for a Definition and Categorization Framework for Plastic Debris". en. In: *Environmental Science & Technology* 53.3, pp. 1039–1047. ISSN: 0013-936X, 1520-5851. DOI: 10.1021/acs.est.8b05297.

He, Defu, Yongming Luo, Shibo Lu, Mengting Liu, Yang Song, and Lili Lei (Dec. 2018). "Microplastics in Soils: Analytical Methods, Pollution Characteristics and Ecological Risks". en. In: *TrAC Trends in Analytical Chemistry* 109, pp. 163–172. ISSN: 01659936. DOI: 10.1016/j.trac.2018.10.006.

He, Lei, Dan Wu, Haifeng Rong, Meng Li, Meiping Tong, and Hyunjung Kim (Oct. 2018). "Influence of Nano- and Microplastic Particles on the Transport and Deposition Behaviors of Bacteria in Quartz Sand". en. In: *Environmental Science & Technology*, acs.est.8b01673. ISSN: 0013-936X, 1520-5851. DOI: 10.1021/acs.est.8b01673.

Hiemenz, Paul C. and Raj. Rajagopalan (1997). *Principles of Colloid and Surface Chemistry*. English. New York; Basel; Hong Kong: Dekker. ISBN: 0-8247-9397-8 978-0-8247-9397-5.

Hoek, Eric M.V. and Gaurav K. Agarwal (June 2006). "Extended DLVO Interactions between Spherical Particles and Rough Surfaces". en. In: *Journal of Colloid and Interface Science* 298.1, pp. 50–58. ISSN: 00219797. DOI: 10.1016/j.jcis.2005.12.031.

Horton, Alice A., Alexander Walton, David J. Spurgeon, Elma Lahive, and Claus Svendsen (May 2017). "Microplastics in Freshwater and Terrestrial Environments: Evaluating the Current Understanding to Identify the Knowledge Gaps and Future Research Priorities". en. In: *Science of The Total Environment* 586, pp. 127–141. ISSN: 00489697. DOI: 10.1016/j.scitotenv.2017.01.190.

Hotze, Ernest M., Tanapon Phenrat, and Gregory V. Lowry (2010). "Nanoparticle Aggregation: Challenges to Understanding Transport and Reactivity in the Environment". en. In: *Journal of Environment Quality* 39.6, p. 1909. ISSN: 1537-2537. DOI: 10.2134/jeq2009.0462.

Hu, Enzhu, Siyao Shang, Zhongtian Fu, Xin Zhao, Xiangli Nan, Yichun Du, and Xijuan Chen (Apr. 2020). "Co-transport of Naphthalene with Polystyrene Nanoplastics (PSNP) in Saturated Porous Media: Effects of PSNP/Naphthalene Ratio and Ionic Strength". en. In: *Chemosphere* 245, p. 125602. ISSN: 00456535. DOI: 10.1016/j.chemosphere.2019.125602.

Huerta Lwanga, Esperanza, Jorge Mendoza Vega, Victor Ku Quej, Jesus de los Angeles Chi, Lucero Sanchez del Cid, Cesar Chi, Griselda Escalona Segura, Henny Gertsen, Tamás Salánki, Martine van der Ploeg, Albert A. Koelmans, and Violette Geissen (Dec. 2017). "Field Evidence for Transfer of Plastic Debris along a Terrestrial Food Chain". en. In: *Scientific Reports* 7.1, p. 14071. ISSN: 2045-2322. DOI: 10.1038/s41598-017-14588-2.

Israelachvili, Jacob N. (2015). *Intermolecular and Surface Forces*. English.

Jambeck, J. R., R. Geyer, C. Wilcox, T. R. Siegler, M. Perryman, A. Andrady, R. Narayan, and K. L. Law (Feb. 2015). "Plastic Waste Inputs from Land into the Ocean". en. In: *Science* 347.6223, pp. 768–771. ISSN: 0036-8075, 1095-9203. DOI: 10.1126/science.1260352.

Jamieson, Alan J., Tamas Malkocs, Stuart B. Piertney, Toyonobu Fujii, and Zulin Zhang (Feb. 2017). "Bioaccumulation of Persistent Organic Pollutants in the Deepest Ocean Fauna". en. In: *Nature Ecology & Evolution* 1.3, p. 0051. ISSN: 2397-334X. DOI: 10.1038/s41559-016-0051.

Koelmans, Albert A, Merel Kooi, Kara Lavender Law, and Erik van Sebille (Nov. 2017a). "All Is Not Lost: Deriving a Top-down Mass Budget of Plastic at Sea". In: *Environmental Research Letters* 12.11, p. 114028. ISSN: 1748-9326. DOI: 10.1088/1748-9326/aa9500.

Koelmans, Albert A. (Apr. 2019). "Proxies for Nanoplastic". en. In: *Nature Nanotechnology* 14.4, pp. 307–308. ISSN: 1748-3387, 1748-3395. DOI: 10.1038/s41565-019-0416-z.

Koelmans, Albert A., Ellen Besseling, Edwin Foekema, Merel Kooi, Svenja Mintenig, Bernadette C. Ossendorp, Paula E. Redondo-Hasselerharm, Anja Verschoor, Annemarie P. van Wezel, and Marten Scheffer (Oct. 2017b). "Risks of Plastic Debris: Unravelling Fact, Opinion, Perception, and Belief". en. In: *Environmental Science & Technology* 51.20, pp. 11513–11519. ISSN: 0013-936X, 1520-5851. DOI: 10.1021/acs.est.7b02219.

Lambert, Scott and Martin Wagner (Feb. 2016). "Characterisation of Nanoplastics during the Degradation of Polystyrene". en. In: *Chemosphere* 145, pp. 265–268. ISSN: 00456535. DOI: 10.1016/j.chemosphere.2015.11.078.

Law, K. L., S. Moret-Ferguson, N. A. Maximenko, G. Proskurowski, E. E. Peacock, J. Hafner, and C. M. Reddy (Sept. 2010). "Plastic Accumulation in the North Atlantic Subtropical Gyre". en. In: *Science* 329.5996, pp. 1185–1188. ISSN: 0036-8075, 1095-9203. DOI: 10.1126/science.1192321.

Lecoanet, Hélène F., Jean-Yves Bottero, and Mark R. Wiesner (Oct. 2004). "Laboratory Assessment of the Mobility of Nanomaterials in Porous Media". en. In: *Environmental Science & Technology* 38.19, pp. 5164–5169. ISSN: 0013-936X, 1520-5851. DOI: 10.1021/es0352303.

Lehner, Roman, Christoph Weder, Alke Petri-Fink, and Barbara Rothen-Rutishauser (Jan. 2019). "Emergence of Nanoplastic in the Environment and Possible Impact on Human Health". en. In: *Environmental Science & Technology*. ISSN: 0013-936X, 1520-5851. DOI: 10.1021/acs.est.8b05512.

Liu, Jin, Tong Zhang, Lili Tian, Xinlei Liu, Zhichong Qi, Yini Ma, Rong Ji, and Wei Chen (Apr. 2019). "Aging Significantly Affects Mobility and Contaminant-Mobilizing Ability of Nanoplastics in Saturated Loamy Sand". en. In: *Environmental Science & Technology*, acs.est.9b00787. ISSN: 0013-936X, 1520-5851. DOI: 10.1021/acs.est.9b00787.

McDowell-Boyer, Laura M., James R. Hunt, and Nicholas Sitar (Dec. 1986). "Particle Transport through Porous Media". en. In: *Water Resources Research* 22.13, pp. 1901–1921. ISSN: 00431397. DOI: 10.1029/WR022i013p01901.

Ng, Ee-Ling, Esperanza Huerta Lwanga, Simon M. Eldridge, Priscilla Johnston, Hang-Wei Hu, Violette Geissen, and Deli Chen (June 2018). "An Overview of Microplastic and Nanoplastic Pollution in Agroecosystems". en. In: *Science of The Total Environment* 627, pp. 1377–1388. ISSN: 00489697. DOI: 10.1016/j.scitotenv.2018.01.341.

Obbard, Rachel W., Saeed Sadri, Ying Qi Wong, Alexandra A. Khitun, Ian Baker, and Richard C. Thompson (June 2014). "Global Warming Releases Microplastic Legacy Frozen in Arctic Sea Ice". en. In: *Earth's Future* 2.6, pp. 315–320. ISSN: 23284277. DOI: 10.1002/2014EF000240.

Pelley, Andrew J. and Nathalie Tufenkji (May 2008). "Effect of Particle Size and Natural Organic Matter on the Migration of Nano- and Microscale Latex Particles in Saturated Porous Media". en. In: *Journal of Colloid and Interface Science* 321.1, pp. 74–83. ISSN: 00219797. DOI: 10.1016/j.jcis.2008.01.046.

Peng, Guyu, Richard Bellerby, Feng Zhang, Xuerong Sun, and Daoji Li (Jan. 2020). "The Ocean's Ultimate Trashcan: Hadal Trenches as Major Depositories for Plastic Pollution". en. In: *Water Research* 168, p. 115121. ISSN: 00431354. DOI: 10.1016/j.watres.2019.115121.

Pessoni, Laurence, Cloé Veclin, Hind El Hadri, Cyril Cugnet, Mélanie Davranche, Anne-Catherine Pierson-Wickmann, Julien Gigault, Bruno Grassl, and Stéphanie Reynaud (2019). "Soap- and Metal-Free Polystyrene Latex Particles as a Nanoplastic Model". en. In: *Environmental Science: Nano* 6.7, pp. 2253–2258. ISSN: 2051-8153, 2051-8161. DOI: 10.1039/C9EN00384C.

Petosa, Adamo R., Deb P. Jaisi, Ivan R. Quevedo, Menachem Elimelech, and Nathalie Tufenkji (Sept. 2010). "Aggregation and Deposition of Engineered Nanomaterials in Aquatic Environments: Role of Physicochemical Interactions". en. In: *Environmental Science & Technology* 44.17, pp. 6532–6549. ISSN: 0013-936X, 1520-5851. DOI: 10.1021/es100598h.

Quevedo, Ivan R. and Nathalie Tufenkji (Apr. 2012). "Mobility of Functionalized Quantum Dots and a Model Polystyrene Nanoparticle in Saturated Quartz Sand and Loamy Sand". en. In: *Environmental Science & Technology* 46.8, pp. 4449–4457. ISSN: 0013-936X, 1520-5851. DOI: 10.1021/es2045458.

Redman, Jeremy A., Sharon L. Walker, and Menachem Elimelech (Mar. 2004). "Bacterial Adhesion and Transport in Porous Media: Role of the Secondary Energy Minimum". en. In: *Environmental Science & Technology* 38.6, pp. 1777–1785. ISSN: 0013-936X, 1520-5851. DOI: 10.1021/es0348871.

Rillig, Matthias C. (June 2012). "Microplastic in Terrestrial Ecosystems and the Soil?" en. In: *Environmental Science & Technology* 46.12, pp. 6453–6454. ISSN: 0013-936X, 1520-5851. DOI: 10.1021/es302011r.

Salerno, Michael B., Matt Flamm, Bruce E. Logan, and Darrell Velegol (Oct. 2006). "Transport of Rodlike Colloids through Packed Beds". en. In: *Environmental Science & Technology* 40.20, pp. 6336–6340. ISSN: 0013-936X, 1520-5851. DOI: 10.1021/es0614565.

Scheurer, Michael and Moritz Bigalke (Mar. 2018). "Microplastics in Swiss Floodplain Soils". en. In: *Environmental Science & Technology* 52.6, pp. 3591–3598. ISSN: 0013-936X, 1520-5851. DOI: 10.1021/acs.est.7b06003.

Schwarz, A.E., T.N. Ligthart, E. Boukris, and T. van Harmelen (June 2019). "Sources, Transport, and Accumulation of Different Types of Plastic Litter in Aquatic Environments: A Review Study". en. In: *Marine Pollution Bulletin* 143, pp. 92–100. ISSN: 0025326X. DOI: 10.1016/j.marpolbul.2019.04.029.

Seymour, Megan B., Gexin Chen, Chunming Su, and Yusong Li (July 2013). "Transport and Retention of Colloids in Porous Media: Does Shape Really Matter?" en. In: *Environmental Science & Technology*, p. 130722083052008. ISSN: 0013-936X, 1520-5851. DOI: 10.1021/es4016124.

Syngouna, Vasiliki I. and Constantinos V. Chrysikopoulos (Jan. 2013). "Cotransport of Clay Colloids and Viruses in Water Saturated Porous Media". en. In: *Colloids and Surfaces A: Physicochemical and Engineering Aspects* 416, pp. 56–65. ISSN: 09277757. DOI: 10.1016/j.colsurfa.2012.10.018.

Ter Halle, Alexandra, Laurent Jeanneau, Marion Martignac, Emilie Jardé, Boris Pedrono, Laurent Brach, and Julien Gigault (Dec. 2017). "Nanoplastic in the North Atlantic Subtropical Gyre". en. In: *Environmental Science & Technology* 51.23, pp. 13689–13697. ISSN: 0013-936X, 1520-5851. DOI: 10.1021/acs.est.7b03667.

Tong, Meiping and William P. Johnson (Dec. 2006). "Excess Colloid Retention in Porous Media as a Function of Colloid Size, Fluid Velocity, and Grain Angularity". en. In: *Environmental Science & Technology* 40.24, pp. 7725–7731. ISSN: 0013-936X, 1520-5851. DOI: 10.1021/es061201r.

Treumann, Svantje, Saeed Torkzaban, Scott A. Bradford, Rahul M. Visalakshan, and Declan Page (Aug. 2014). "An Explanation for Differences in the Process of Colloid Adsorption in Batch and Column Studies". en. In: *Journal of Contaminant Hydrology* 164, pp. 219–229. ISSN: 01697722. DOI: 10.1016/j.jconhyd.2014.06.007.

Tufenkji, Nathalie and Menachem Elimelech (Jan. 2004). "Correlation Equation for Predicting Single-Collector Efficiency in Physicochemical Filtration in Saturated Porous Media". en. In: *Environmental Science & Technology* 38.2, pp. 529–536. ISSN: 0013-936X, 1520-5851. DOI: 10.1021/es034049r.

— (Feb. 2005). "Breakdown of Colloid Filtration Theory: Role of the Secondary Energy Minimum and Surface Charge Heterogeneities". en. In: *Langmuir* 21.3, pp. 841–852. ISSN: 0743-7463, 1520-5827. DOI: 10.1021/la048102g.

Valsesia, Andrea, Cloé Desmet, Isaac Ojea-Jiménez, Arianna Oddo, Robin Capomaccio, François Rossi, and Pascal Colpo (Dec. 2018). "Direct Quantification of Nanoparticle Surface Hydrophobicity". en. In: *Communications Chemistry* 1.1, p. 53. ISSN: 2399-3669. DOI: 10.1038/s42004-018-0054-7.

van Sebille, Erik, Chris Wilcox, Laurent Lebreton, Nikolai Maximenko, Britta Denise Hardesty, Jan A van Franeker, Marcus Eriksen, David Siegel, Francois Galgani, and Kara Lavender Law (Dec. 2015). "A Global Inventory of Small Floating Plastic Debris". In: *Environmental Research Letters* 10.12, p. 124006. ISSN: 1748-9326. DOI: 10.1088/1748-9326/10/12/124006.

Verleysen, Eveline, Thorsten Wagner, Hans-Gerd Lipinski, Ralf Kägi, Robert Koeber, Ana Boix-Sanfeliu, Pieter-Jan De Temmerman, and Jan Mast (July 2019). "Evaluation of a TEM Based Approach for Size Measurement of Particulate (Nano)Materials". en. In: *Materials* 12.14, p. 2274. ISSN: 1996-1944. DOI: 10.3390/ma12142274.

Vinogradov, J., M. Z. Jaafar, and M. D. Jackson (Dec. 2010). "Measurement of Streaming Potential Coupling Coefficient in Sandstones Saturated with Natural and Artificial Brines at High Salinity". en. In: *Journal of Geophysical Research* 115.B12, B12204. ISSN: 0148-0227. DOI: 10.1029/2010JB007593.

Wagner, Martin, Christian Scherer, Diana Alvarez-Muñoz, Nicole Brennholt, Xavier Bourrain, Sebastian Buchinger, Elke Fries, Cécile Grosbois, Jörg Klasmeier, Teresa Marti, Sara Rodriguez-Mozaz, Ralph Urbatzka, A Dick Vethaak, Margrethe Winther-Nielsen, and Georg Reifferscheid (Dec. 2014). "Microplastics in Freshwater Ecosystems: What We Know and What We Need to Know". en. In: *Environmental Sciences Europe* 26.1. ISSN: 2190-4707, 2190-4715. DOI: 10.1186/s12302-014-0012-7.

Wagner, Stephan and Thorsten Reemtsma (Apr. 2019). "Things We Know and Don't Know about Nanoplastic in the Environment". en. In: *Nature Nanotechnology* 14.4, pp. 300–301. ISSN: 1748-3387, 1748-3395. DOI: 10.1038/s41565-019-0424-z.

Weiss, Thomas H., Aaron L. Mills, George M. Hornberger, and Janet S. Herman (July 1995). "Effect of Bacterial Cell Shape on Transport of Bacteria in Porous Media". In: *Environmental Science & Technology* 29.7, pp. 1737–1740. ISSN: 0013-936X. DOI: 10.1021/es00007a007.

Wu, Jiayi, Ruifen Jiang, Wei Lin, and Gangfeng Ouyang (Feb. 2019). "Effect of Salinity and Humic Acid on the Aggregation and Toxicity of Polystyrene Nanoplastics with Different Functional Groups and Charges". en. In: *Environmental Pollution* 245, pp. 836–843. ISSN: 02697491. DOI: 10.1016/j.envpol.2018.11.055.

Wu, Lei, Bin Gao, Yuan Tian, Rafael Muñoz-Carpena, and Kirk J. Zigler (Mar. 2013). "DLVO Interactions of Carbon Nanotubes with Isotropic Planar Surfaces". en. In: *Langmuir* 29.12, pp. 3976–3988. ISSN: 0743-7463, 1520-5827. DOI: 10.1021/la3048328.

Xu, Shangping, Qian Liao, and James E. Saiers (Feb. 2008). "Straining of Nonspherical Colloids in Saturated Porous Media". en. In: *Environmental Science & Technology* 42.3, pp. 771–778. ISSN: 0013-936X, 1520-5851. DOI: 10.1021/es071328w.

# Chapter 4

# Deposition of nanoplastics: The roles of size polydispersity and natural organic matter

Alice Pradel [ab], Nolwenn Delouche[c], Julien Gigault[b], Hervé Tabuteau[c]

[a]Univ Rennes, CNRS, Géosciences Rennes - UMR 6118, 35000 Rennes, France

[b] TAKUVIK, CNRS, Université Laval UMI 3376, Quebec, Canada

[c] Univ Rennes, CNRS, Institut de Physique de Rennes (IPR)-UMR 6251, F-35000 Rennes, France.

## 4.1 Introduction

While, environmental degradation of plastics is expected to produce particles with a continuous suite of properties such as shape, size, degree of aging, etc, the majority of model nanoplastics have limited environmental relevance since they are spherical and monodisperse in size. Choosing nanoplastic models with environmentally relevant properties is essential, since particles' properties will impact their transport and deposition behavior.

Spherical and nonspherical particles have different behaviors in fluid flow which leads to different deposition mechanisms. Indeed, while fluid drag causes both particles to rotate onto themselves, the forces acting on spherical particles will be isotropic due to their symmetry and therefore their trajectory will remain unchanged. However, rotation of nonspherical particles due to fluid drag will cause them to move off their initial path. They can take oscillatory or chaotic trajectories, which will increase their capacity to collide with the surfaces of porous media (Delouche, Schofield, and Tabuteau 2020).

Although macro-, micro- and nanoplastics are expected to co-occur in the same environmental systems since plastic degradation produces secondary particulate plastics with a continuous suite of sizes. Most studies have focused on the transport of monodisperse plastic particles. This is an important limitation since the polydispersity of particle dispersions will impact their deposition rate (Bradford and Leij 2018).

Furthermore, to increase the environmental relevance of studies concerned with nanoplastics' deposition in porous media, their transport must be assessed in the presence of natural organic matter (NOM) since NOM is ubiquitous in these environmental systems. Indeed, terrestrial porous media, contain humic and fulvic substances, from the degradation and aging of terrestrial organic matter. It is also common to find bacterial and algal extrapolymeric substances (EPS) in aqueous systems such as aquifers, wetlands, riparian zones, as well as in water treatment filters. Different types of NOM can have different effects on the transport of polystyrene latex (PSL) spheres in sand columns. On one hand, at low ionic strengths (1 to 10 mmol $L^{-1}$ KCl), humic acids (HA) decrease deposition of PSL spheres with sizes ranging from 50 to 1500 nm. This was attributed to the electrostatic and steric repulsions caused by HA (Pelley and Tufenkji 2008). On the other hand, at low to average ionic strengths (10 and 50 mmol L-1 NaCl), EPS increased deposition of PSL spheres with sizes ranging from 20 to 2000 nm. This was attributed to increased physical entrapment, since the EPS coating decreased the sizes of pores, and to PSL sphere's increased affinity for EPS' components (a protein, a polysaccharide and a HA), compared to a pure sand surface (L. He, Rong, et al. 2020) . However, the effect of EPS components, such as the polysaccharide sodium alginate (SA) on deposition of carbon-based nanoparticles is unclear. Indeed, Espinasse, Hotze, and Wiesner 2007

showed that the SA increased the attachment rate of C60-fullerene in porous media composed of glass beads. Whereas, K. L. Chen and Elimelech 2008 showed that SA decreased the attachment efficiency of PSL on silica surfaces using QCM-D experiments.

The previous study presented in Chapter 3 has compared the deposition of three different nanoplastic models in porous media composed of sand. In this study, fragmental nanoplastic models were produced using the method of El Hadri et al. 2020 and the dispersions were filtered at 40 $\mu$m. These fragmental nanoplastic models are more deposited than spherical nanoplastic models. Furthermore, fragmental nanoplastics with hydrodynamic radius larger than 300 nm were preferentially deposited (Pradel, Hadri, et al. 2020). To explain such observations, several hypotheses were emitted:

- The higher retention of fragmental particles compared to spherical particles is due to their higher collision frequency with the sand surfaces.
- Due to their nonspherical shape, fragmental particles have a higher torque that can give them sufficient kinetic energy to overcome the energy barrier.
- This nonspherical shape can also allow the particles to orient themselves in such a way to reduce electrostatic repulsion.
- Particles' rough surface may reduce electrostatic repulsion, which in turn increases the probability of deposition.
- The higher deposition of larger fragmental plastics was not due to differences in surface properties, since it was assumed that surface properties did not vary with size. It was suggested to be caused by physical retention larger particles by straining or size-dependent differences in hydrodynamic forces.

These hypotheses could not be correctly tested in the sand columns due to their complex geometries (e.g.: rough surfaces, variable pore sizes, zones of reduced flow rate, etc.). Also, this experimental set-up did not permit a quantification of the deposition profiles for fragmental nanoplastics since deposited particles could not be observed *in-situ* nor properly quantified *ex-situ*. Therefore, the objective of this study is to elucidate the mechanisms which cause deposition of fragmental nanoplastics in porous media. Transport experiments were performed in microfluidic channels with controlled geometries and particles' dimensions and morphology were thoroughly characterized by several complementary instruments: dynamic light scattering (DLS), transmission electron microscopy (TEM), and coulter counter for dimensions, as well as scanning electron microscopy (SEM) and atomic force microscopy (AFM) for morphology. The impact of particles' size polydispersity on deposition rates was assessed by filtering nanoplastic dispersions at 40 $\mu$m, 3 $\mu$m and 0.8 $\mu$m. The effect NOM was assessed by studying transport of

fragmental nanoplastics in the presence of SA and HA. Changes in concentration at the oulet of the microfluidic channels was measured by absorbance spectroscopy and changes in sizes were measured by DLS and Coulter Counter.

## 4.2 Materials and Methods

### 4.2.1 Materials

**Fragmental Nanoplastics and Natural Organic Matter**

All solutions and colloidal dispersions were prepared with deionized (DI) water (Millipore, 18.2 MΩ). A nanoplastic model (*NPT*) was produced with a top-down process which consists in mechanically fragmenting industrial-grade polystyrene pellets with the method described by El Hadri et al. 2020. This method made the particles additive-free, irregularly shaped and polydisperse in size (with a polydispersity index defined as the variance of the gaussian-fitted size distribution (PDI) $> 0.1$). As such they are more environmentally relevant than the spherical polystyrene latex particles produced from bottom-up methods. Due to the absence of surfactants in *NPT* dispersions, they are not stable over long time-periods. Therefore, new stock solutions were prepared weekly to avoid aggregation. Stock solutions had concentrations between 10 and 26 mg $L^{-1}$. To study the effect of size polydispersity, the *NPT* dispersions were filtered at three different size cut-offs: 40 $\mu$m, 3 $\mu$m and 0.8 $\mu$m and were called *NPT-F40*, *NPT-F3* and *NPT-F0.8*, respectively. Before filtering the nanoplastic dispersions, membrane filters (40 $\mu$m VWR Qualitative Cellulose Filter Paper 417 and 3 $\mu$m Pall Versapor® Acrylic Copolymer Membrane Disc Filters) were rinsed with 1 L of DI water and syringe filters (0.8 $\mu$m Pall Acrodisc® Syringe Filter with Hydrophilic polyethersulfone Supor® Membrane) were rinsed with with 50 mL of DI water. *NPT-F40* and *NPT-F3* concentrations were 8 mg $L^{-1}$. *NPT-F0.8* concentrations were only 4.5 mg $L^{-1}$ due to the important loss of particles when filtering. These concentrations are higher than those expected in the environment, but were necessary to remain within all instruments' detection limits.

The SA stock solution was prepared by adding solid SA (Acros Organics) in DI water and agitating at 400 rpm overnight (12 to 18 hours). Fresh SA solutions were prepared weekly, since this NOM is labile and subject to bacterial growth. The pH of the SA solution was not fixed and naturally varied around 7.5 to 8. The HA stock solution was prepared by dissolving Leonardite HA from the International Humic Substance Society (IHSS), using the method described in Pradel, Ferreres, et al. 2021. The pH of HA was fixed at 6.5. The SA stock solutions had concentrations between 504 and 1257 mg $L^{-1}$, and the HA stock solution had a concentration of 875 mg $L^{-1}$ as determined with a Total

Carbon Analyzer (TOC-V CSH, Shimadzu, Japan). These solutions were filtered at 0.2 $\mu$m using syringe filters (Pall Acrodisc® Syringe Filter with Hydrophilic polyethersulfone Supor® Membrane) and were then diluted to 50 mg $L^{-1}$ or 30 mg $L^{-1}$ for SA and HA, respectively. While *NPT* are dispersed in DI, SA and HA contain 5.75 mg $L^{-1}$ Na and 0.09 mg $L^{-1}$ NaCl, respectively.

**Microfluidic channels**

For the transport experiment, we used the soft lithography methodology to make microfluidic channels, as described by Delouche, Schofield, and Tabuteau 2020. All channel walls are made of polydimethylsiloxane (PDMS) for a uniform particle-surface interaction inside the pore. Two different channel geometries were used and are presented in Figure 4.1. The first channel contained 20 parallel single pores with a central constriction that is 30 $\mu$m wide and 30 $\mu$m high and a reservoir zone before and after this constriction that is 80 $\mu$m wide and 30 $\mu$m high (Figure 4.1a). The second system is a porous medium with pillars organized in a grid of 200 rows containing 50 pores. On each row, pillars are randomly spaced either 20 or 50 $\mu$m apart with a 50/50 ratio of each spacing. The channel height is 20 $\mu$m and the porosity 0.7 (Figure 4.1b).

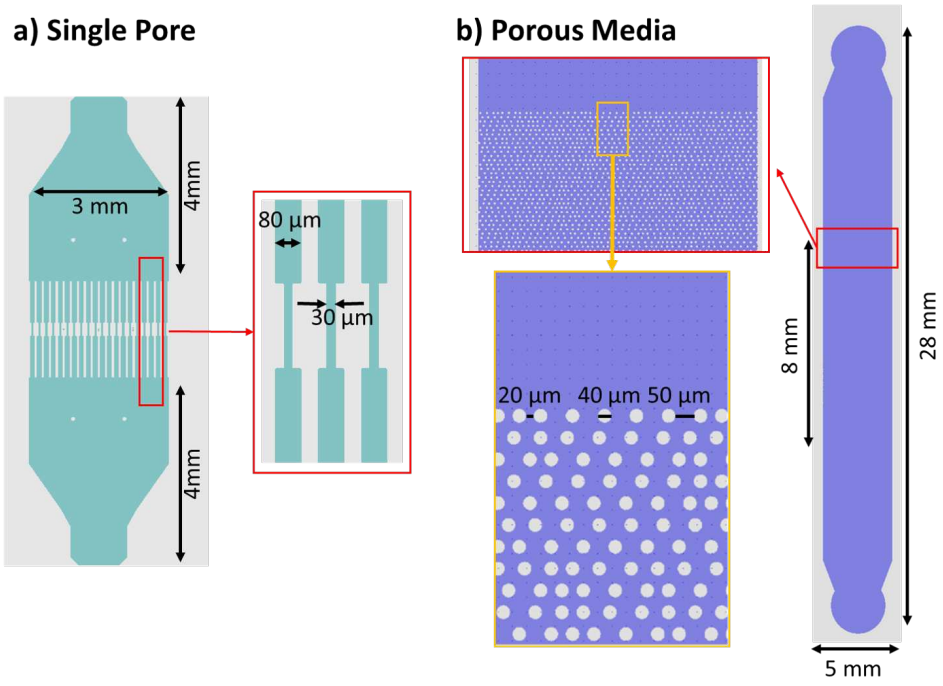


*Figure 4.1: Geometries of the two porous media used. The grey background corresponds to the solid PDMS material and the green and blue colors corresponds to void areas which are saturated with water*

### 4.2.2 Methods

**Transport experiments**

The nanoplastic dispersions are transported in the microfluidic channels at a constant pressure, and initial flow rates between 7 $\mu$L min$^{-1}$ and 50 $\mu$L min$^{-1}$, using a precise microfluidics pressure control system (Elveflow OB1 Mk2 or Fluidgent PSFC) At this pressure range, the Péclet number is superior to 1.24 105, thus particles' Brownian diffusion is negligible . The flow rate decreases as particles are progressively deposited. When deposited particles clog the channel, the flow rate becomes almost null, at which point the experiment is considered complete.

The type of *NPT* studied in each channel geometry and the analyses performed are summarized in Figure 4.2. In the single pores, only *NPT-F40* and *NPT-F3* were studied. In the porous media *NPT-F40*, *NPT-F3* and *NPT-F0.8* (filtered at 40, 30 and 0.8 $\mu$m, respectively) were studied, as well as *NPT-F40* with HA or SA. When studying transport of *NPT-F40* in the presence of NOM, the porous media was first saturated with the NOM of interest before injection of *NPT-F40* + NOM. For each experiment, deposits were observed by optical microscopy with a high-resolution camera (Hammamatsu Orca Flash 4.0 v2). Experiments conducted in the porous media had a sufficient outgoing volume ($\approx$4 to 5 mL) to measure the flow rate (by weighing the mass of dispersion eluted with a microbalance every 10 minutes), and to perform two other ex-situ analyses. First, we characterized the size distribution of dispersions before and after transport in the porous media by DLS and Coulter Counter (detailed below). When *NPT* dispersions caused a clogging, First, Middle and Final fractions correspond to the dispersion recovered when flow rate is superior to 25 $\mu$L min$^{-1}$, around 15 $\mu$L min$^{-1}$ and inferior to 10 $\mu$L min$^{-1}$, respectively. When *NPT* dispersions did not clog the porous media, the First, Middle and Final fractions were taken at the beginning, middle and end of the experiment. Second, we measured the changes in concentration by absorbance spectroscopy.

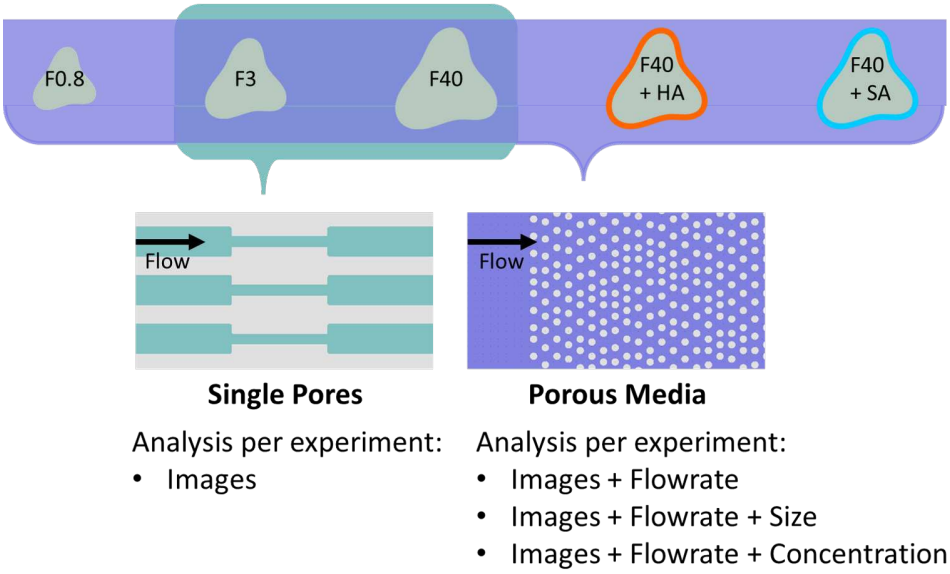


*Figure 4.2: Types of particles studied and analyses performed for experiments in single pores and in porous media*

**Size characterization**

The dimensions of *NPT* particles were characterized by three complementary methods: the ensemble method of dynamic light scattering (DLS) which measures and deconvolutes a scattering signal in order to obtain a size distribution of colloidal particles, as well as two methods which count individual particles: transmission electron microscopy (TEM) and the Coulter Counter (also called electrical sensing zone). Coulter Counter and DLS measurements were performed systematically, before and after transport experiments in porous media, to assess any changes in size. TEM analysis was performed once with a different batch of *NPT-F40* to compare size distribution obtained by DLS and Coulter Counter and TEM.

TEM images were captured with a Jeol JEM 2100 HR (200kV) with an LaB6 filament and a Gatan Orius SC 200 D camera. The method and analysis is thoroughly described in Pradel, Ferreres, et al. 2021. The number of particles within each size class was normalized by the total number of analyzed particles to obtain a PDF.

A DLS probe (Vasco-Flex, Cordouan Technologies, Pessac, France) determined particles' z-average hydrodynamic diameter ($d_{zH}$) and fitting a normal distribution to the raw data using the cumulant algorithm. This non-destructive measurement was composed of an average of six measurements lasting 60 s.

The Coulter Counter instrument was a Multisizer™ 4 (Beckman Coulter®, Inc. Brea CA, USA). This instrument measures the sphere-equivalent volume of particles passing through an aperture of 30 $\mu$m diameter. The principle of this analysis is that particles dispersed in a saline solution are pumped through an aperture. As they pass through

the aperture, they displace the saline solution and increase electrical resistivity, which is measured by two electrodes. The instrument was calibrated weekly with 3 $\mu$m NIST Traceable Latex Particle Size Standards (Beckman Coulter®, Inc. Brea CA, USA). Each calibration consisted of an average of 10 measurements of 30 000 particles with sizes comprised between 2.4 and 3.6 $\mu$m (based on the previous calibration).

All measurements were performed in an electrolytic solution composed of 9.914 g $L^{-1}$ NaCl with 4.743 $10^{-3}$ g $L^{-1}$ the surfactant Triton X-100 (Amresco, Proteomics grade), which corresponds to $1/30^{th}$ of its critical micellar concentration (CMC). This concentration of surfactant inhibited *NPT* aggregation, as illustrated in Figure 4.3, while not increasing significantly the background noise. Figure 4.3 shows that the $d_{zH}$ of 10 mg $L^{-1}$ *NPT-F40* increased by less than 10% per hour. However, *NPT* characterized after transport experiments, were diluted by the electrolytic solution and had a maximum concentration of 0.9 mg $L^{-1}$. Therefore, less aggregation is expected since particle collision is proportional to particle concentration. Aggregation could not be assessed by DLS at these low *NPT* concentrations since a minimum of $\approx$ 3 mg $L^{-1}$ *NPT-F40* is required to be within DLS' detection limits.

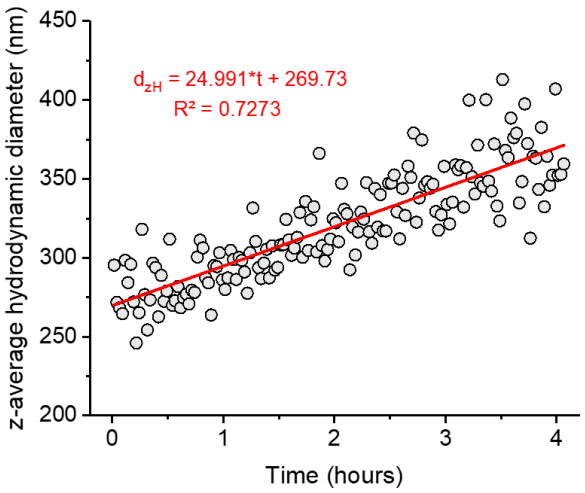


*Figure 4.3: Evolution of z-average hydrodynamic diameter ($d_{zH}$) as a function of time for 10 mg $L^{-1}$ NPT-F40 dispersed in 9.914 g $L^{-1}$ NaCl and 4.743 $10^{-3}$ g $L^{-1}$ the surfactant Triton X-100*

To avoid dilution of the solution when *NPT* particles were added, solutions with 20% higher concentrations of NaCl and Triton X-100 were prepared and diluted according to the total mass of *NPT* added. Coulter Counter measurements were performed in a cuvette without agitation and were composed of 20 measurements of 0.5 mL separated by unblocking the aperture and flushing the tube, to avoid any buildup of particles. The entire measurement (10 mL) lasted on average one hour. The analysis showed no devia-

tions or anomalies in the number of particles counted or aspect of the size distributions during the 20 measurements. The Coulter Counter with an aperture of 30 $\mu$m measures sizes between 0.60 and 2.00 $\mu$m. Due to the higher signal to noise ratio (SNR) close to the lower size detection limit, only the particles situated between 0.65 and 2.00 $\mu$m were analyzed. To compare particle size distributions of different samples, all data was normalized by the total number of particles to obtain a probability distribution function (PDF).

**Morphology**

Particles' morphology was characterized by scanning electron microscopy (SEM) and atomic force microscopy (AFM). Like TEM analysis, these analyses were only performed for a separate batch of *NPT-F40* (not analyzed here).

SEM analysis were performed with a JSM JEOL 7100F (JEOL, Ltd. Tokyo, Japan). A stock solution of 11 mg $L^{-1}$ *NPT* was diluted by to 5.5 mg $L^{-1}$ with ethanol (Purity 96%, Carlo Erba, Val de Reuil, France), and deposited on a metal surface and dried for a minimum of two hours. The use of ethanol allowed the particles to remain dispersed on the surface during drying.

*NPT*'s surface morphology was assessed by AFM with a Bruker Multimode 8-HR (Bruker, Billerica, Massachusetts, USA). 50 $\mu$L of solution was deposited on a cleaved mica surface and allowed to air dry for a minimum of 2 hours. Particles were analyzed by PeakForce Quantitative Nanomechanics (QNM) with a Bruker Sharp Microlever probe ($MSNL^{-1}$ 0) composed of silicon nitride. The probes E et F that were used had nominal values of spring constant 0.1 and 0.6 N $m^{-1}$ and frequencies ranging of 38 and 125 kHz, respectively.

**Concentration**

To assess the concentration of particles flowing out of the porous media, the outlet tubing was coupled to the absorbance detector of an Akta Prime Plus chromatography instrument (GE Healthcare, Illinois, USA). A constant tubing length of 60 cm was used and absorbance was measured at a wavelength of 254 nm. To compare *NPT* concentrations, the concentration of particles eluted (C) was normalized by the initial concentrations ($C_0$).

## 4.3 Results and Discussion

**Morphology of fragmental polystyrene dispersion**

The fragmental polystyrene dispersions (*NPT*) have heterogeneous dimensions and shapes. Therefore, their morphology was characterized by Scanning Electron Microscopy (SEM), Transmission Electron Microscopy (TEM) and Atomic Force Microscopy (AFM),

Figures 4.4, 4.5 and 4.6, respectively. SEM images show that *NPT-F40* particles have shapes that vary from spheroidal (orange arrow in Figure 4.4a), rod-like (purple arrow) to flakey (blue arrow). Some particles' surfaces are rough, suggesting that pieces of the particle were shed off (red arrows in Figure 4.4b). Similar observations can be made from by TEM images (Figure 4.5). Indeed, some spheroidal particles have homogenous densities (blue arrows Figure 4.5a), while other particles have zones with different densities. Zones of lower density suggest the loss of pieces from the surface (red arrows in Figure 4.5b). This diversity of shapes can be explained by the brittle nature of polystyrene and the process of mechanical abrasion by planetary ball milling. The rotation of the milling process can produce spheroidal particles and shed layers off of the particles' surfaces, producing rough surface morphologies.

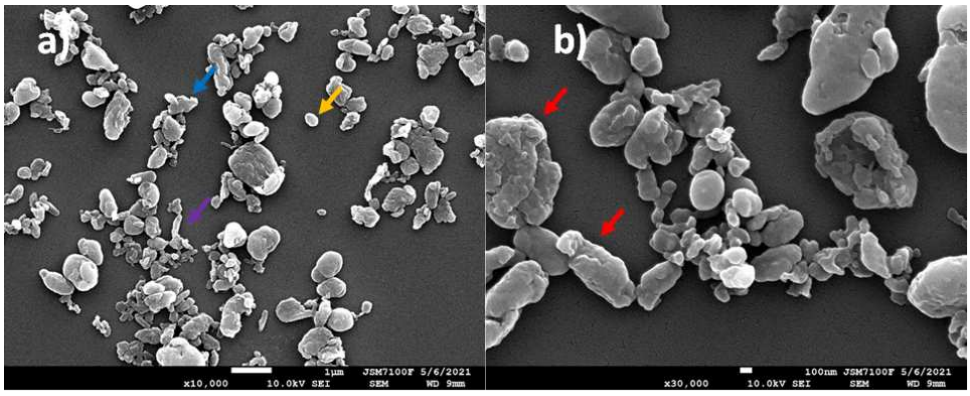


*Figure 4.4: Scanning Electron Microscopy (SEM) images of NPT-F40 at a) 1 µm and b) 100 nm magnification*

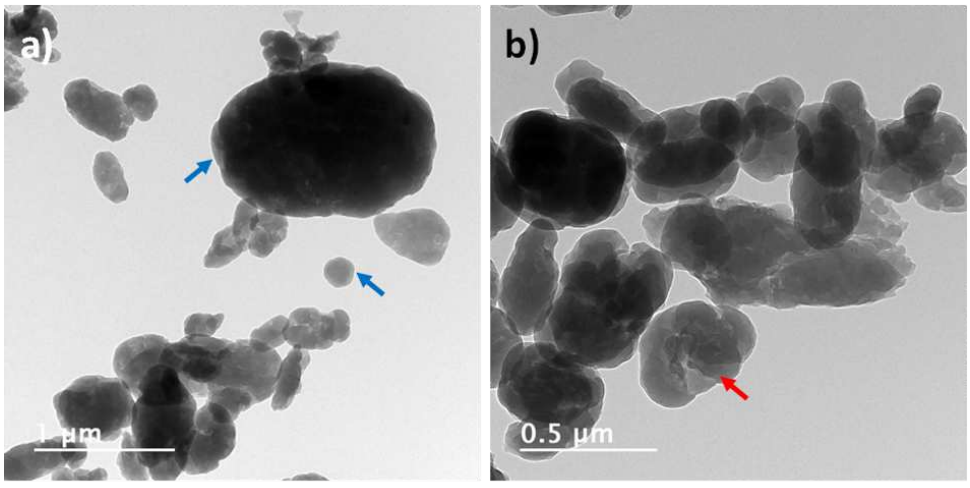


*Figure 4.5: Transmission Electron Microscopy images of NPT-F40 at a) 1 µm and b) 500 nm magnification*

While SEM and TEM provide a view of particles from above, AFM illustrates parti-

cles' topography, thereby allowing a three-dimensional representation of particles (Figure 4.6). As for SEM and TEM images, AFM images confirm the presence of both spheroidal, elongated and flaky particles. On one hand, Figure 4.6a shows the topography of flaky particles. These are approximately 1 $\mu$m wide and between 50 to 80 nm high (Figure 4.6b). On the other hand, Figure 4.6c and 4.6d show spheroidal particles that are more or less elongated. Finally, Figures 4.6e and 4.6d illustrate the heights and peak force error, respectively, of an enlarged section of Figure 4.6c. The peak force error, corresponds to the derivative of topography and illustrates the particle morphology as if viewing it from the side. These images show that the spheroidal particles have a rough surface, as viewed in SEM images (Figure 4.4). These surface irregularities are approximately 10s of nanometers high, which is similar to the thickness of *NPT-F40* flakes and therefore, suggests that flaky particles are shed from the larger spheroidal particles.

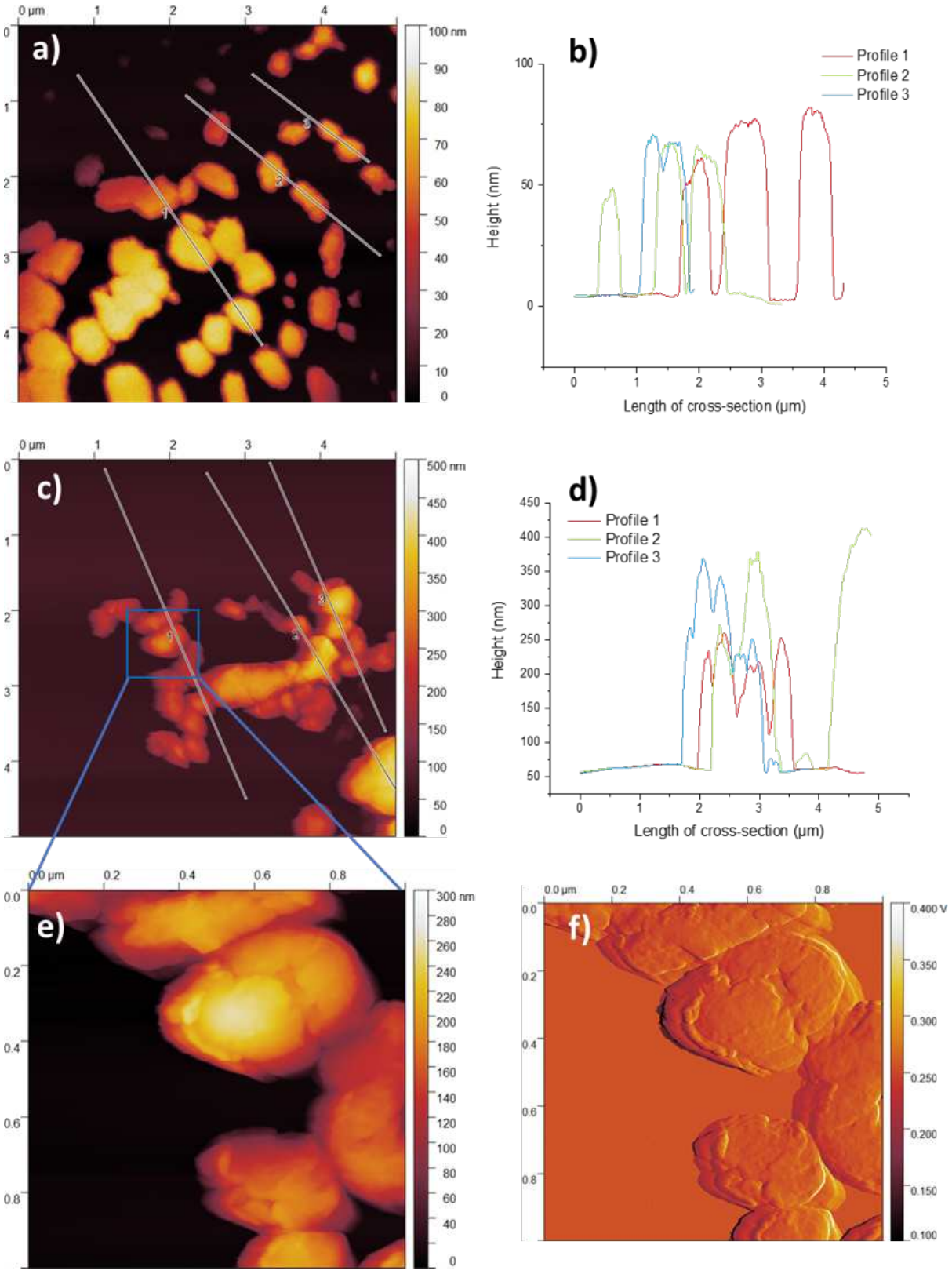


*Figure 4.6: Atomic Force Microscopy (AFM) images of NPT-F40 showing a) a map of heights of flaky particles and b) the corresponding height profile of transects of image a; and c) a map of heights of spheroidal particles, as well as d) the corresponding height profiles of transects of image c; and e) an enlarged section of image c, and f) a the corresponding map of peak force error.*

**Dimensions of fragmental polystyrene dispersion**

Particle dimensions can be extracted from SEM, TEM and AFM images and topographies. However, this is quite time-consuming. For example, 283 particles were characterized from approximately half a day of TEM analysis. Therefore, to accurately characterize particle dimensions, complementary techniques are required. Figure 4.7a compares *NPT-F40*'s area equivalent diameter, determined by TEM and z-average hydrodynamic diameter ($d_{zH}$) obtained by DLS. This reveals that the average size determined by DLS is larger than that determined by TEM. This is due to the fact that light scattering methods overestimate the amount of large particles since the intensity of scattered light is a power function of particle size (M. Baalousha and Lead 2012). It would also be worthwhile to compare dimensions obtained from SEM and AFM. It is also noteworthy that the size distribution is continuous in the case of DLS measurement, but not in the case of TEM analysis. This is due to the fact that the DLS fits a Gaussian size distribution to the signal, whereas the histogram of sizes obtained from TEM are composed of discrete measurements of 283 particles.

Both TEM and DLS suggest that a few micrometric particles are present in the nanoplastic dispersion. This is to be expected, since the dispersion of NTP-F40 has only been filtered at 40 $\mu$m. The Coulter Counter instrument is adapted to measure particles larger than 650 nm (red line in Figure 4.7a), and therefore to analyse the tail-end of the *NPT-F40* size distribution. Figure 4.7b presents the PDF of particles that have volume equivalent diameters larger than 650 nm for the 4 different batches of *NPT-F40* studied here, as determined by Coulter Counter. The probability distribution function (PDF) is significantly smoother than the PDF obtained from TEM images since the Coulter Counter measured 6 $10^5$ to 6 $10^6$ particles. The PDF of different *NPT-F40* batches almost overlap. Most of the particles have sub-micrometric diameters and as sizes decrease there is a sharp increase in the number of particles.

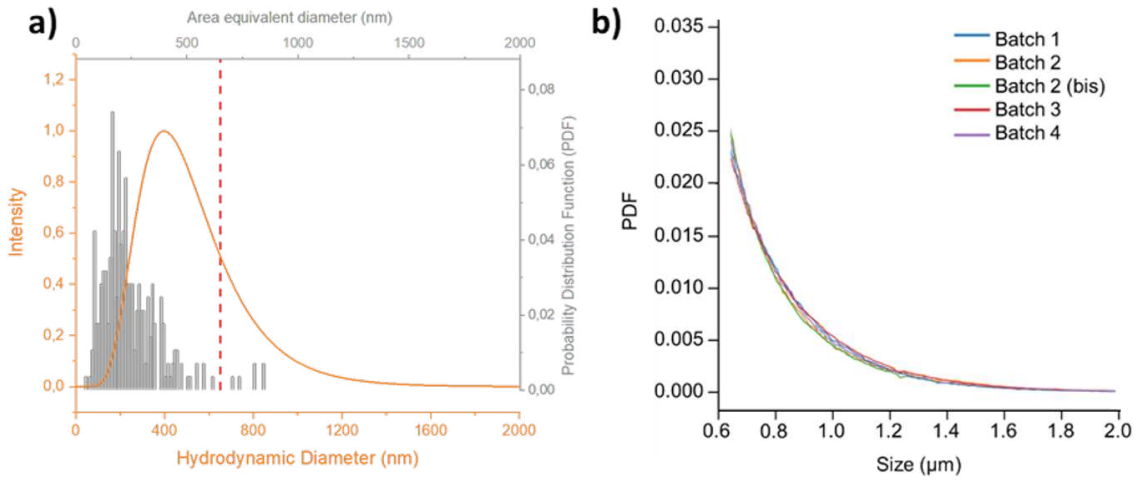


*Figure 4.7: NPT-F40 dimensions, as determined by a) DLS and TEM and b) Coulter Counter. a) The intensity-based size-distribution of the 3$^{rd}$ batch of NPT-F40 studied here is illustrated in orange. The area equivalent diameter of NPT-F40 from another batch which has a similar $d_{z_H}$ and PDI, was calculated from TEM images and is illustrated in gray (n = 283 particles). The vertical red line at 650 nm corresponds to the lower size threshold of the Coulter Counter. b) Coulter Counter size distribution for the 4 different batchs of NPT-F40 studied here.*

**Transport in single pores**

The size polydispersity of *NPT-F40* dispersions (PDI > 0.1) is expected to impact their transport and deposition dynamics. Indeed, during transport of in sand columns, the larger size fractions *NPT-F40* were preferentially retained (Pradel, Hadri, et al. 2020). To start analyzing the effect of size polydispersity on deposition, the dynamics of deposition of *NPT-F40* and *NPT-F3* were compared as they were transported in single pores. Figure 4.8 shows the time required to entirely clog single pores (30 $\mu$m high by 30 $\mu$m wide) as a function of the pressure applied to the microfluidic channel. It reveals that for both *NPT-F40* and *NPT-F3*, clogging occurs more rapidly as pressure increases. This is due to the fact since flow rate is proportional to the pressure applied, more particles are transported at higher pressures since. Therefore, at high pressures there is a higher probability that particles deposit and clog the channel within a certain amount of time. At pressures above approximately 50 mbar, the deposited particles are eroded and re-entrained by the water flow. Starting at approximately 100 mbar, erosion and re-entrainment of particles is so high that clogging never occurs (data not shown).

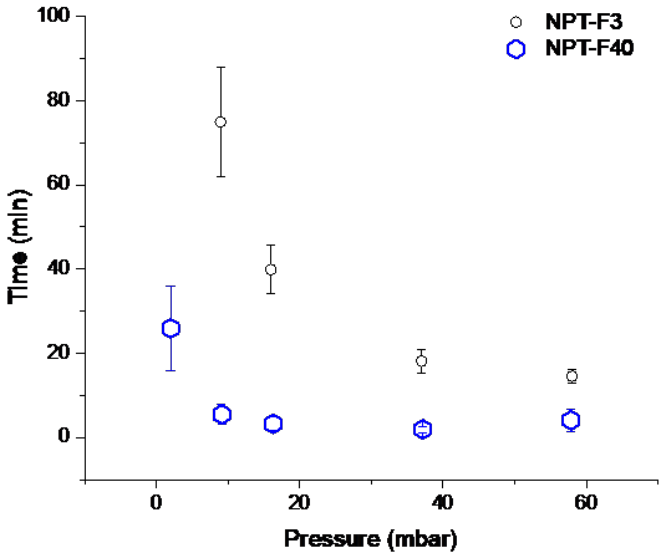


*Figure 4.8: Evolution of the time required to fully clog a single pore as a function of pressure, for NPT-F40 and NPT-F3*

Interestingly, *NPT-F40* systematically clog the single pores more rapidly than *NPT-F3*, at a given pressure (Figure 4.8). Therefore, filtering out the large particles decreases the rate at which particles are deposited. The clogging dynamics observed in single pores supports this hypothesis (Figure 4.9). Indeed, at 8 minutes particles large enough to be detected by optical microscopy ($> 1$ $\mu$m) are deposited on the walls of the single pore constrictions. Practically all particles that are subsequently deposited are captured by these first deposits. This suggests that the deposition of micrometric particles trigger clogging of single pores by forming deposits onto which other particles accumulate. Indeed, when flowing through constrictions, the presence of only a few percent (0.5 to 2%) aggregates (i.e.: non-spherical particles) in a dispersion of spherical PSL spheres of 1.8 $\mu$m was sufficient to cause the formation of deposits, and eventually clogging, in pressure-controlled transport experiments (Delouche, Schofield, and Tabuteau 2020). With advection, the rotation of nonspherical particles causes them to take an oscillatory or chaotic pathway, which increases their probability of colliding with the surface of the single pore. Furthermore, the deposition of particles in the pore channel increases contact zones for incoming particles which is suspected to increase deposition rate.

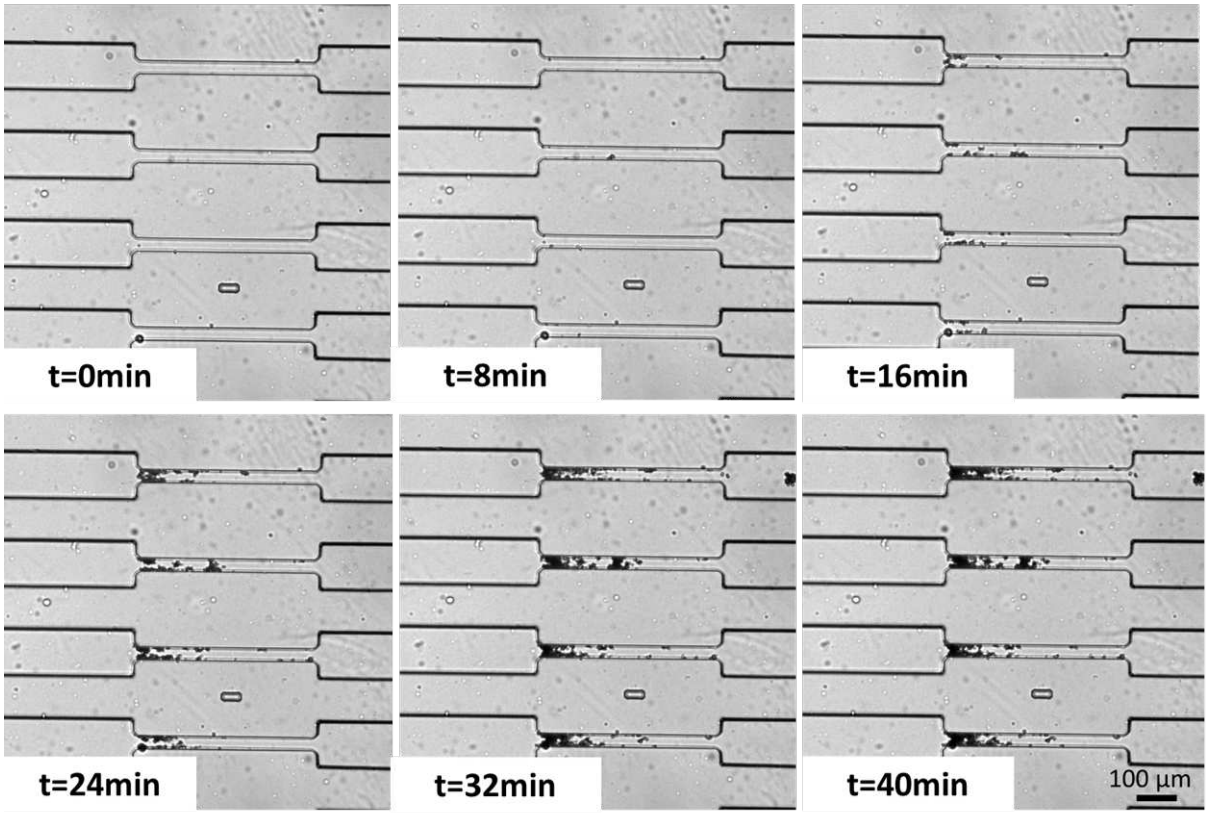


*Figure 4.9: : Images showing 4 single pores in a channel and the deposition of NPT-F3 over time .*

Since sub-micrometric particles are not visible by optical microscopy, it is not possible to quantify to what extent they are also deposited in the single pores. Therefore, if larger *NPT* particles are preferentially deposited, this can be observed as a loss of the larger *NPT* after transport experiments. The single pore channel geometry did not allow the recovery of sufficient volume of *NPT* dispersions to analyse changes in size (only approximately 10s of $\mu$L). So, the porous media were designed to favor particle deposition while delaying clogging, thanks to the randomized arrangements of pillars and to the larger total volume. Therefore, depending on *NPT* dispersion characteristics approximately 0.5 to 5 mL were recovered at the outlet of the porous media, which allowed the characterization of their concentrations (by absorbance spectroscopy) and changes in size (by DLS and Coulter Counter.)

**Transport in porous media : Effect of size polydispersity**

As for the single pore experiments, transport of different *NPT* dispersions in porous media were performed with a fixed pressure. Therefore, a decrease in flow rate was recorded as the porous media became clogged. *NPT* dispersions recovered from the porous media at different time intervals were called First, Middle and Final fractions.

The relative concentration ($C/C_0$) of *NPT-F40*, *NPT-F3*, *NPT-F0.8* dispersions

eluted from the porous media is shown in Figure 4.10 (for the same batch of *NPT*). *NPT* dispersion containing micrometric particles (*NPT-F40* and *NPT-F3*) clog the porous media, while without micrometric particles (*NPT-F0.8*) no clogging occurs. No *NPT-F0.8* deposition is observed by optical microscopy. Furthermore, with *NPT-F0.8* the flow rate remains constant and its concentration is relatively constant, decreasing from 1.10 to 1.06 over 220 minutes (3.6 hours), suggesting that no *NPT-F0.8* are deposited. *NPT* dispersions that contain more micrometric particles (*NPT-F40*) clog the porous media faster than those containing less micrometric particles (*NPT-F3*). This can be observed by the more rapid decrease in concentration and flow rate for *NPT-F40* compared to *NPT-F3*. Indeed, *NPT-F40*'s relative concentration decreased from 0.98 to 0.82 in 110 minutes (1.8 hours), while *NPT-F3*'s relative concentration decreased from 1.03 to 0.82 in 285 minutes (4.8 hours) (Figure 4.10 and Table 4.1).

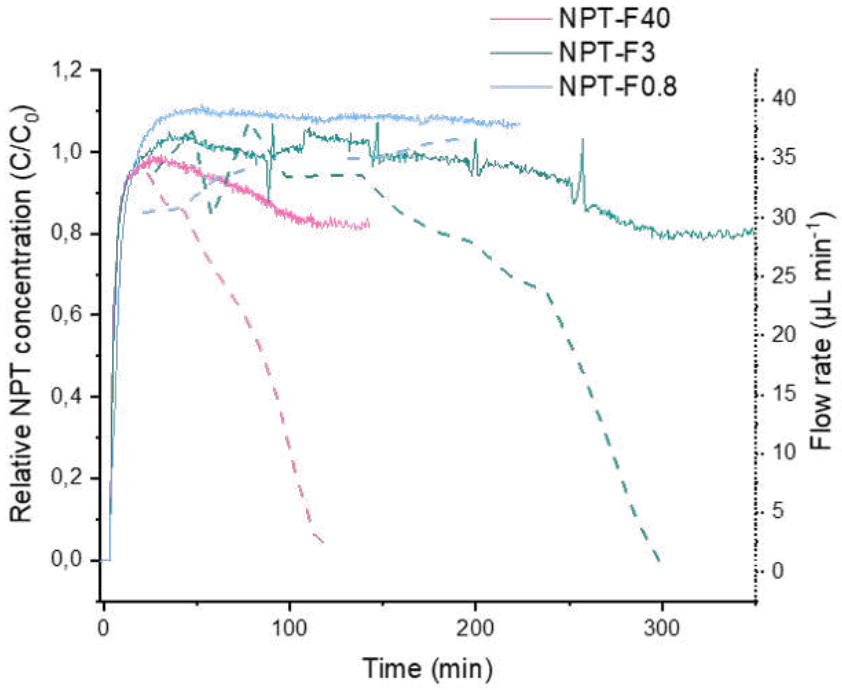


*Figure 4.10: Evolution of relative particle concentration (full lines, left axis) and flow rate (dashed lines, right axis) over time for 8 mg $L^{-1}$ NPT-F40, NPT-F3 and NPT-F0.8 (Batch 3)*

*Table 4.1: Time (min) required for flow rate to become inferior to 5 $\mu L\ min^{-1}$ for different batches of NPT filtered at 40, 3 or 0.8 $\mu m$. Each number corresponds to a separate experiment.*

| | *NPT-F40* | *NPT-F3* | *NPT-F0.8* |
|---|---|---|---|
| Batch 1 | 65 | | |
| | 80 | | |
| | 83 | | |
| Batch 2 | 40 | 145 | |
| | 30 | 120 | |
| | 35 | | |
| | 40 | | |
| | 42 | | |
| Batch 3 | 110 | 285 | >196 |
| | 86 | 500 | >530 |
| | 90 | | |
| Batch 4 | 50 | 190 | |
| | 57 | 135 | |
| | | 150 | |

As the porous media progressively became more fouled by deposited particles there was a significant loss of *NPT-F40* particles with sizes between 800 and 1500 nm as observed by comparing the first, middle and final fractions analyzed by Coulter Counter (Figure 4.11a). This indicates that these larger particles are preferentially deposited. Interestingly, the first fraction recovered already has a loss of particles in this size range. No particles were deposited in the tubing or in the reservoir zone before and after the porous media, therefore, this is indicative of a rapid deposition of large particles. The analysis of z-average size distributions by DLS show a slight but not significative decrease in size between the reference dispersion and the final fractions (Figure 4.11b). DLS may be less sensitive to the loss of large particles since i) it is an ensemble method (as opposed to a counting method) and ii) large particles have a smaller diffusion coefficient and therefore, take more time to enter the detection zone.

It is noteworthy to mention that since less volume is recovered over time as deposition progresses, the volume of the final fraction was often significantly smaller than that of the first or middle fractions. In the case of batches 1 and 2, the final fraction was too small to be analyzed by DLS (Figure 4.11b). Also, due to the smaller volume, the PDF of the final fraction of *NPT-F40* analyzed by Coulter Counter is less smooth than the first and middle fractions (Figure 4.11a). Indeed, the signal to noise ratio (SNR) is only 6 for the final fraction compared to 11, 44 and 160 for middle fraction, first fraction and reference dispersion, respectively.

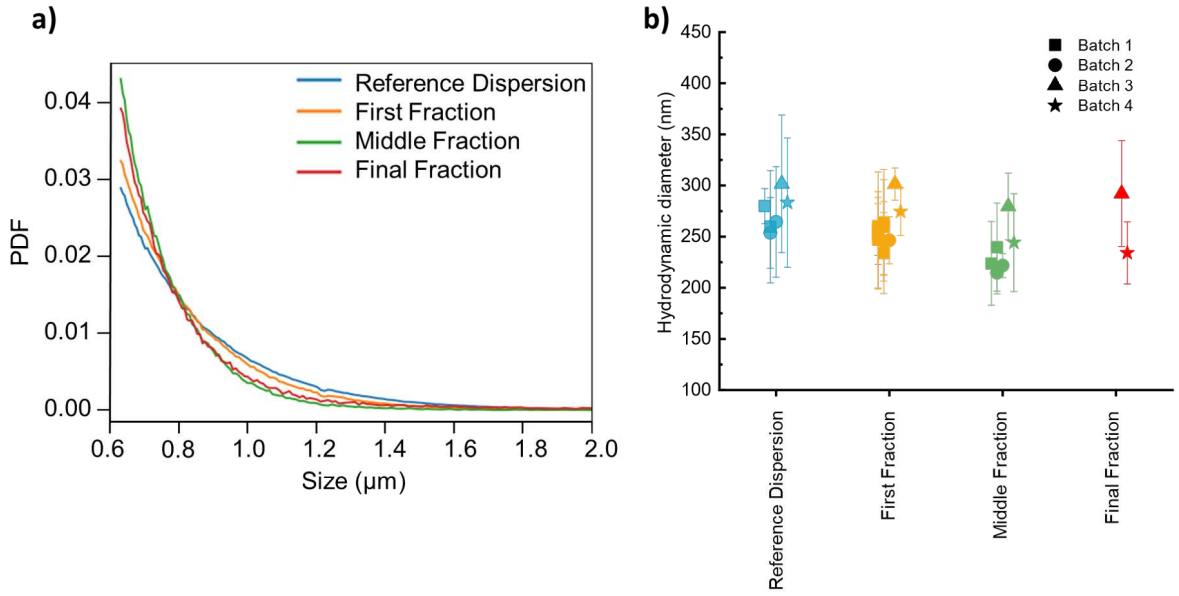


*Figure 4.11: Evolution of a) the tail-end of NPT-F40 size distribution (Batch 3) b) $d_{zH}$ of NPT-F40, as a function of advancement of deposition in porous media. The whiskers indicate width (standard deviation) of the $d_{zH}$ size distributions. The reference dispersion = initial NPT-F40 dispersion. First fraction = NPT-F40 recovered at flow rate > 25 µL $min^{-1}$. Middle fraction = NPT-F40 recovered at flow rates around 15 µL $min^{-1}$. Final fraction = NPT-F40 recovered at flow rates < 10 µL $min^{-1}$.*

The *NPT-F3* dispersions have less pronounced changes in size as they become deposited in the porous media compared to *NPT-F40* (Figure 4.12). Indeed, there is a loss of particles with sizes ranging between 800 and 1500 nm observed for the middle fraction (Figure 4.12a) and only a slight decrease in $d_{zH}$ (Figure 4.12b). The Coulter Counter analysis shows that the middle fraction has a stronger decrease in sizes compared to the final fraction. This is only due to the noisier signal of the final fraction since the SNRs are 88, 85, 18, and 4 for the PDFs of the reference dispersion, first, middle and final fractions, respectively. Globally, the less pronounced change in size of *NPT-F3* compared to *NPT-F40* is due to the filtering out of larger particles. This is illustrated by the stronger inflexion of the *NPT-F3* PDF towards small sizes (Figure 4.12a) compared to *NPT-F40* (Figure 4.11a) and the smaller $d_{zH}$ (approximately 225nm or *NPT-F3* and 275 nm for *NPT-F40*, Figures 4.12b and 4.11b, respectively). Therefore, the micrometric particles deposited in the porous media form a smaller fraction of the total particles and cause a less pronounced shift in sizes.

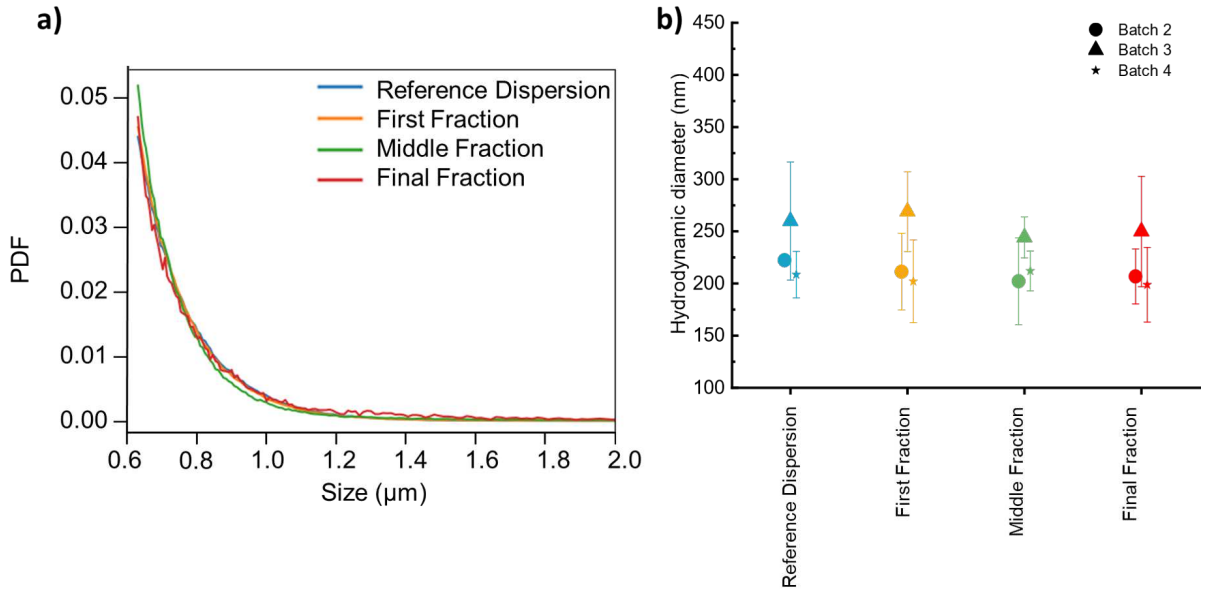


*Figure 4.12: Evolution of a) the tail-end NPT-F3 size distribution (Batch 3) and b) $d_{zH}$ of NPT-F3 as a function of advancement of deposition in porous media. The whiskers indicate width (standard deviation) of the $d_{zH}$ size distributions. The reference dispersion = initial NPT-F3 dispersion. First fraction = NPT-F3 recovered at flow rate > 25 $\mu L\ min^{-1}$. Middle fraction = NPT-F3 recovered at flow rates around 15 $\mu L\ min^{-1}$. Final fraction = NPT-F3 recovered at flow rates < 10 $\mu L\ min^{-1}$.*

The preferential deposition of large particles is supported by *NPT-F40* and *NPT-F3* changes in concentration (Figure 4.10) and changes in size (Figures 4.11 and 4.12) at the outlet of the porous media. Indeed, the relative concentration at which clogging is complete (flow rate < 5 $\mu$L min$^{-1}$) is the same (0.82) for both particles. The loss of large particles in the tail-end size distribution suggests that the decreases in concentration is more likely to due to the loss of a few large particles rather than a loss of 18% of all particles. Indeed, as can be seen in Figure 4.13, *NPT* dispersions that contain more large particles have a stronger absorbance of light. This is due to the fact that large particles cause multiple scattering, which deflects light in all directions and decreases transmission of light to the absorbance detector. So, the decrease in concentration at the outlet indicates that large particles are significantly deposited, but cannot give indication concerning the extent to which small *NPT* particles are retained (Figure 4.10).

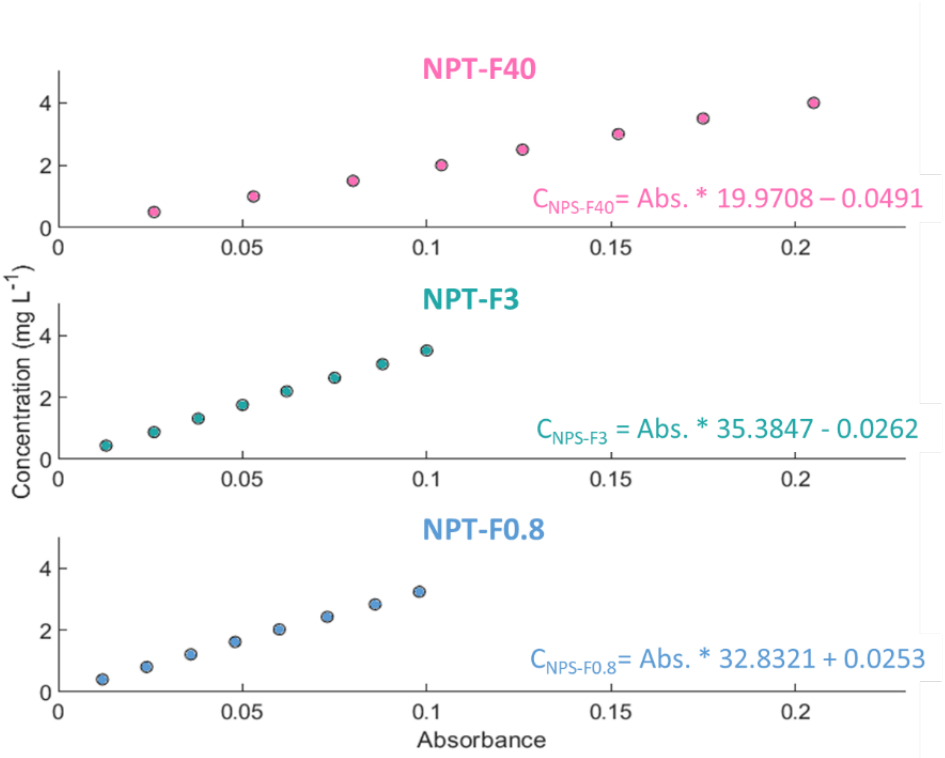


*Figure 4.13: Calibration curves of NPT concentration as a function of absorbance at $\lambda$ = 226 nm for dispersions filtered at 40 $\mu$m, 3 $\mu$m and 0.8 $\mu$m*

Assuming that in Chapter 3 only particles <0.8 $\mu$m are eluted from the sand column, applying a correction to the breakthrough curves would yield a plateau of $C/C_0$ equal to 0.50 instead of 0.30 for *NPT 350-P* and 0.17 instead of 0.10 for *NPT-460-P*. This would mean that *NPT* are globally less deposited in the porous media but still significantly more than PSL spheres (cf: Section 3.3)

*NPT-F40* and *NPT-F3* deposits observed at different depths of the porous media show that, after clogging, most of the deposits are present at the entrance of the porous media. In the middle of the porous media, only some lines of clogged pores are observed, and no deposited particles are observed at the outlet (Figure 4.14. Similar types of deposition were observed for different batches of *NPT*. This trend towards a decrease in deposition as a function of depth of the porous media is common and deserves to be better quantified and compared with other experiments (Molnar et al. 2015 and references therein). When the whole medium is clogged, a continuous line of dense particle deposits runs across the entire width of the porous medium. This clog line prevents redistribution of particles into adjacent pores. The position of this line in the porous medium shown in Figure 4.15 for *NPT-F40* and *NPT-F3* and follows the deposition trend observed on the images (Figure 4.14).

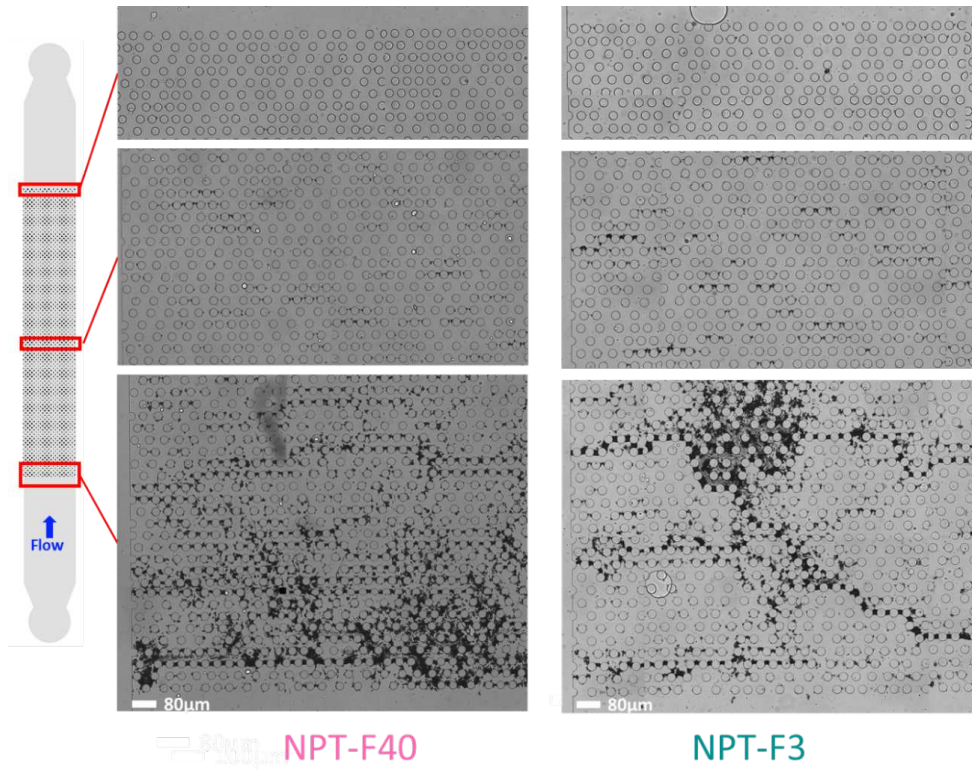


*Figure 4.14: Microscopy images of NPT-F40 (Batch 4) and NPT-F3 (Batch 3) deposits observed at different depths of the porous media after clogging.*

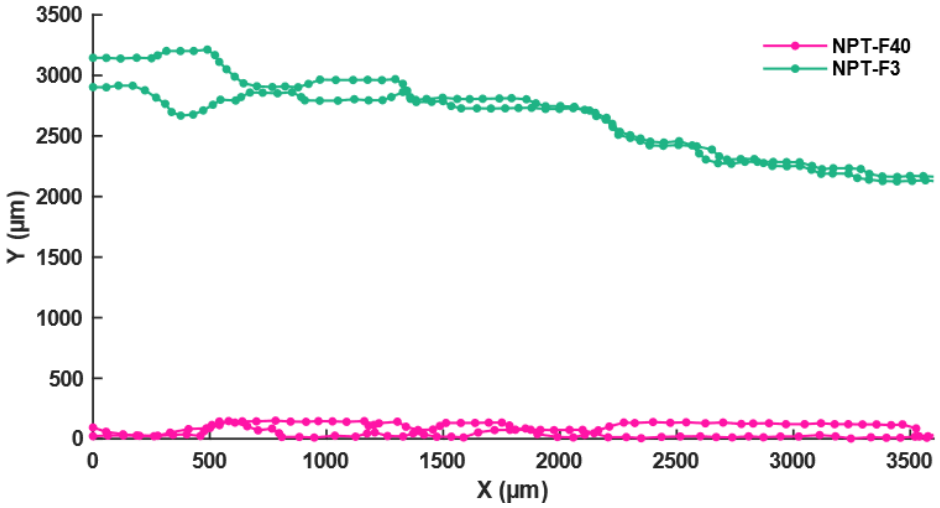


*Figure 4.15: Position of the clog line of for two replicates of NPT-F40 (Batch 4) and NPT-F3 (Batch 4), with X the width of the channel and Y the depth.*

*NPT-F40*, which contains more micrometric particles, forms a clog line as soon as they enter the porous medium. However, *NPT-F3* form a clog line located up to 3mm after the first pores (Figure 4.15). This position is dependent on the size distribution:

large objects have a higher probability of capture than small ones because of their size and will be preferentially captured as soon as they encounter collectors (i.e.: pillars). By removing these large objects, *NPT-F3* dispersions are transported further into the porous medium before being captured. As is the case for the single pores, the first deposited particles cause the subsequent deposition of inflowing particles. Therefore, the clog line forms deeper in the porous media. For *NPT-F3*, clogging is delayed since i) there are fewer large particles to deposit and ii) the clog line is positioned deeper in the porous media allows objects to be captured on the first collectors upstream from the clog line (in the first 3 millimeters in the case of Figure 4.15).

**Transport in porous media: Effect of natural organic matter (NOM)**

The transport and deposition of *NPT-F40* was compared to that of *NPT-F40* in the presence of either 30 mg $L^{-1}$ HA or 50 mg $L^{-1}$ SA, for the same batch (Figure 4.16). These NOM concentrations are higher than those expected in natural waters. For example, concentrations of dissolved organic matter in surface sea water is around 1 mg $L^{-1}$ (Benner 2002), while concentrations in sediments and soils can be more variable, ranging from a few mg $L^{-1}$ to 100s of mg $L^{-1}$ (Burdige 2002). However, since the *NPT* concentration is relatively high (8 mg $L^{-1}$) it is necessary to increase the concentration of NOM in order to keep a realistic proportion of *NPT* and NOM. Furthermore, these concentrations were selected since 30 mg $L^{-1}$ HA and 50 mg $L^{-1}$ SA were able to strongly stabilize *NPT* by steric and electrostatic repulsion at high ionic strength ($>$ 50 mmol $L^{-1}$ NaCl) (Pradel, Ferreres, et al. 2021).

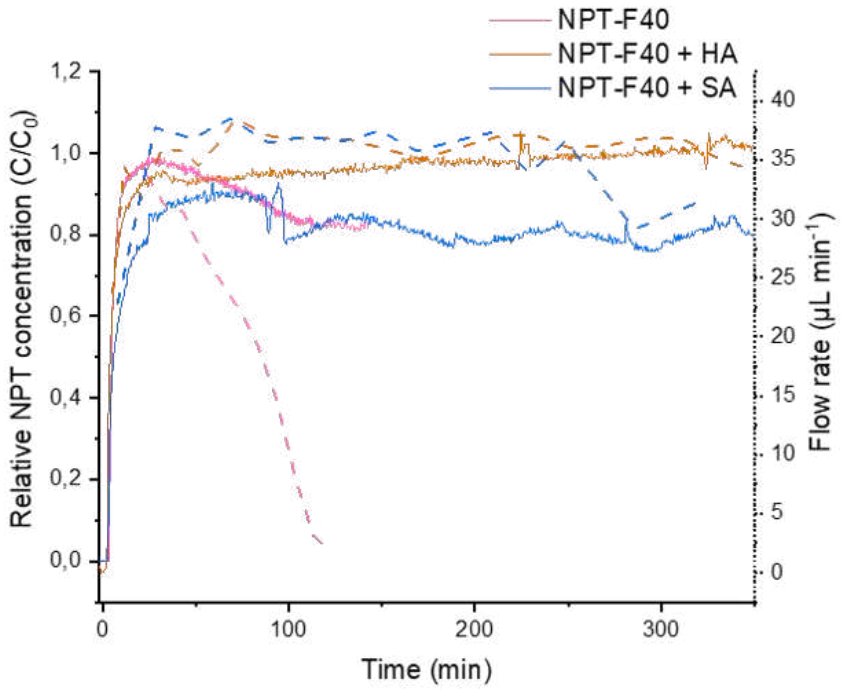


*Figure 4.16: Evolution of relative particle concentration (full lines, left axis) and flow rate (dashed lines, right axis) over time for NPT-F40, NPT-F40 + HA and NPT-F40 + SA (Batch 3).*

While *NPT-F40* clog the porous media, the addition of HA or SA inhibits or delays such clogging (Figure 4.16). With HA, the concentrations remain relatively constant, increasing from 0.95 to 1.02 over the course of 350 minutes (5.8 hours). The flow rate also remains relatively constant, around 37 $\mu$L min$^{-1}$. However, with SA the relative concentration decreases from 0.90 to 0.80 over the same time period. This is accompanied by a more pronounced decrease in flow rate, from 37 to 30 $\mu$L min$^{-1}$. For other batches of *NPT-F40*, NOM also delays or impeded clogging of the porous media (Table 4.2).

*Table 4.2: Time (min) required for flow rate to become inferior to 5 $\mu L\ min^{-1}$ for different batches of NPT-F40 alone or with either 30 mg $L^{-1}$ HA or 50 mg $L^{-1}$ SA. Each number corresponds to a separate experiment.*

| | *NPT-F40* | *NPT-F40* + HA | *NPT-F40* +SA |
|---|---|---|---|
| Batch 1 | 65 | > 600 | |
| | 80 | | |
| | 83 | | |
| Batch 2 | 40 | 335 | 230 |
| | 30 | 330 | 250 |
| | 35 | | |
| | 40 | | |
| | 42 | | |
| Batch 3 | 110 | >414 | > 357 |
| | 86 | >437 | |
| | 90 | | |
| Batch 4 | 50 | 520 | |
| | 57 | 430 | |

When *NPT-F40* were transported with NOM, changes in size could always be characterized by DLS and Coulter Counter since large volumes of *NPT-F40* + NOM were recovered due to the absent or delayed clogging. Indeed, all final fractions were measured by DLS and the SNR was > 50 for all Coulter Counter analysis. On one hand, with HA the size of *NPT-F40* eluted from the porous media does not vary over time (Figure 4.17). Indeed, all PDF obtained by Coulter Counter are superimposed for batch 3 (Figure 4.17a) and the $d_{zH}$ do no decrease as a function of time (Figure 4.17b). On the other hand, with SA, *NPT-F40* eluted from the porous media (first, middle and final fractions) all show a decrease in the proportion of micrometric particles, compared to the reference dispersion (Figure 4.17c). The $d_{zH}$ of eluted dispersions of *NPT-F40* with SA, are slightly, but not significantly, smaller than the $d_{zH}$ of reference dispersions (Figure 4.17d). This suggests that HA inhibits the preferential deposition of micrometric *NPT*, while with SA large particles are still deposited, but only initially, and their deposition does not continue over time. For batches 2 and 4 of *NPT-F40*, the presence of NOM only delayed clogging but did not inhibit it (Table 4.2). In these cases, larger particles (800 to 1500 nm) were preferentially deposited, as is the case for *NPT-F40* experiments (Figure 4.11). This shows that the mechanism of clogging is the same in the presence NOM, but that NOM delays this clogging.

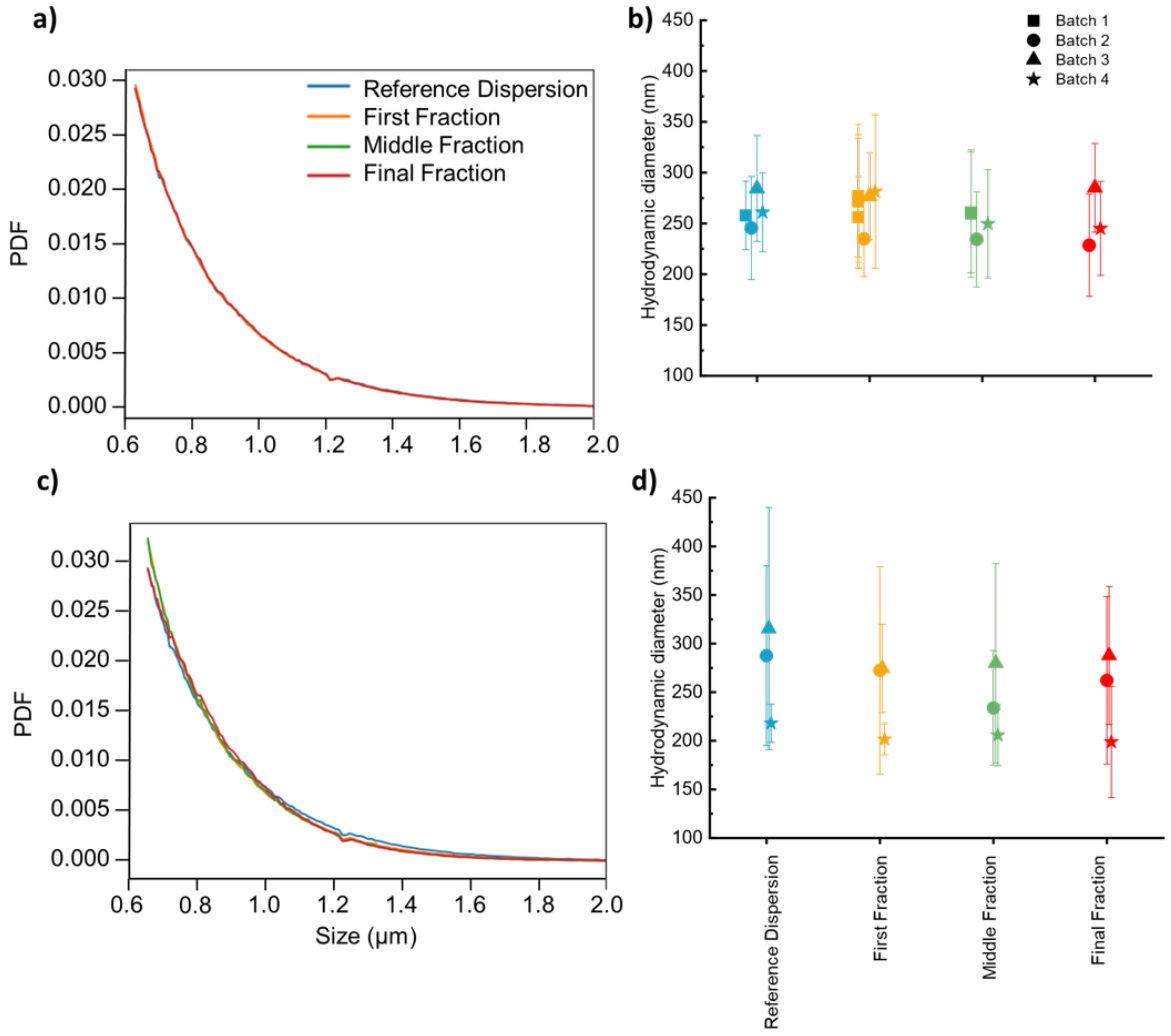


*Figure 4.17: Evolution of a) the tail-end of NPT-F40 + HA and c) of NPT-F40 + SA size distributions (Batch 3) and of b) $d_{zH}$ of NPT-F40 + HA and d) $d_{zH}$ of NPT-F40 + SA as a function of advancement of deposition in porous media. The whiskers indicate width (standard deviation) of the $d_{zH}$ size distributions. The reference dispersion = initial NPT-F40 + HA or SA dispersion. First fraction = 1st 20 minutes. Middle fraction ≈ 200 minutes. Final fraction ≈ 400 minutes.*

Microscopy images show that in the presence of NOM particles are still deposited (Figure 14.18). These images were obtained from batches 2 and 4 of *NPT* and NOM, which have entirely clogged the porous media (Table 4.2). However, similar deposits were observed in Batch 3. Compared to deposits formed from NOM-free dispersions of *NPT-F40*, in the presence of both HA and SA, *NPT-F40* deposits are also predominantly located at the entrance of the porous media (Figure 4.18). However, the density of deposits and the clog line needs to be better quantified.

Since all experiments with NOM were performed at low ionic strength ($< 5$ mmol $L^{-1}$) the NOM is not expected to significantly increase the electrostatic repulsion. However,

it can cause steric repulsion between deposited particles and inflowing particles. This would have the effect of increasing the porosity of deposits and delaying clogging.

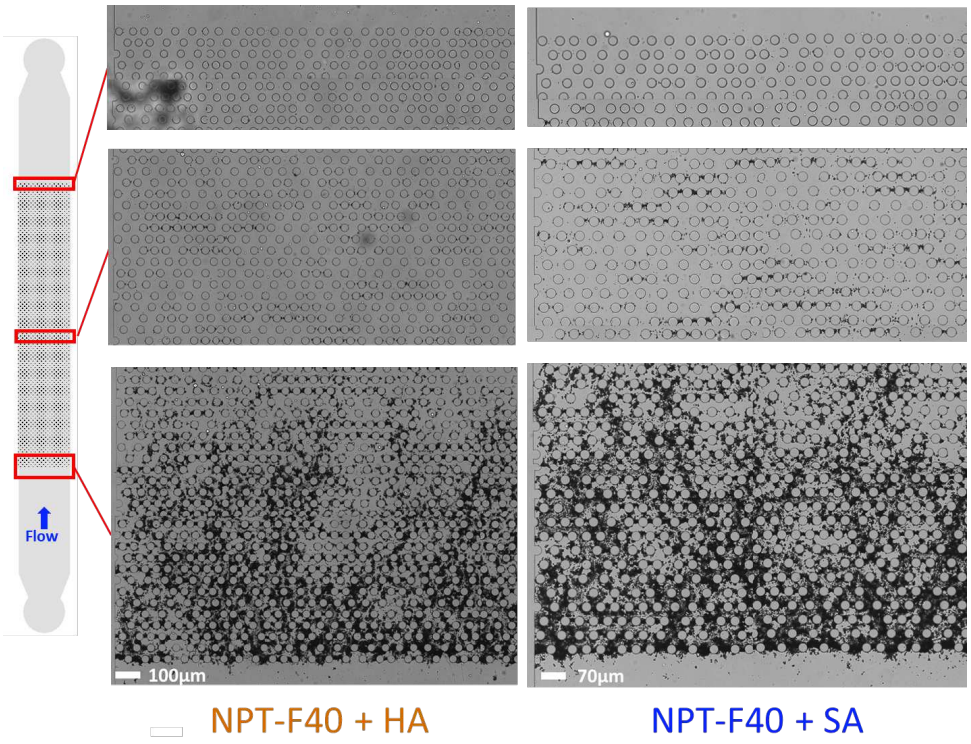


*Figure 4.18: Microscopy images of NPT-F40 + HA (Batch 4) and NPT-F3 + SA (Batch 2) deposits observed at different depths of the porous media after clogging.*

## 4.4 Conclusion

Plastics are abundant in terrestrial systems and environmental factors (e.g.: irradiation, abrasion etc.) are expected to fragment plastics to colloidal sizes. However, the study of nanoplastics transport in porous media has disproportionally focused on spherical PSL particles and there is little understanding of the processes which may cause environmentally relevant nanoplastics to be retained. This study explores how fragmental nanoplastic dispersions may be deposited in porous media thanks to the use of microfluidic channels with controlled geometries, microscopic observations and systematic characterization of size and concentration.

The fragmental nanoplastic dispersions have a characteristically large size polydispersity (PDI $> 0.1$). In experiments conducted at a constant pressure, by filtering out many of the micrometric particles ($> 3$ $\mu$m) fragmental nanoplastics were less deposited and took longer to clog a porous medium compared to dispersions that were only filtered at 40 $\mu$m. Entirely filtering out micrometric particles ($> 0.8$ $\mu$m) inhibited clogging. These

observations, coupled to analysis of variations in size and concentration, revealed that the larger size-fraction of nanoplastic dispersions is most rapidly deposited and triggers clogging of porous media. This is confirmed by the fact that that the larger size fraction (800 to 1500 nm) is preferentially retained in the porous media when particles are strongly deposited. In the presence of NOM particles are still deposited however, steric repulsion between particles is suspected to create more porous deposits which delays clogging.

This study highlights the importance of choosing environmentally relevant nanoplastic models to study the fate of these particles. Furthermore, NOM will control the extent to which nanoplastics are retained in porous media, such as soils, sediments and aquifers. However, natural porous media also contain other naturally occurring species, such as clays, hydrous iron oxides, as well as biological activity. These species and organisms are also likely to affect the transport and deposition rate of nanoplastic particles, which warrants further investigation.

**Acknowledgements:**

The authors would like to thank Véronique Vié for AFM observations performed at 2CBioMIF (ScanMAT, UMS 2001 CNRS - University of Rennes 1) which received a financial support from the Région Bretagne and European Union(CPER-FEDER 2007-2014, Présage n°39126 and Présage n°37339), as well as Sunniva Pinnabel for analysis of samples with the Coulter Counter.

# References


Baalousha, M. and J. R. Lead (June 2012). "Rationalizing Nanomaterial Sizes Measured by Atomic Force Microscopy, Flow Field-Flow Fractionation, and Dynamic Light Scattering: Sample Preparation, Polydispersity, and Particle Structure". en. In: *Environmental Science & Technology* 46.11, pp. 6134–6142. ISSN: 0013-936X, 1520-5851. DOI: 10.1021/es301167x.

Benner, Ronald (Jan. 2002). "Chapter 3 - Chemical Composition and Reactivity". In: *Biogeochemistry of Marine Dissolved Organic Matter*. Ed. by Dennis A. Hansell and Craig A. Carlson. San Diego: Academic Press, pp. 59–90. ISBN: 978-0-12-323841-2. DOI: 10.1016/B978-012323841-2/50005-1.

Bradford, Scott A. and Feike J. Leij (Dec. 2018). "Modeling the Transport and Retention of Polydispersed Colloidal Suspensions in Porous Media". In: *Chemical Engineering Science* 192, pp. 972–980. ISSN: 00092509. DOI: 10.1016/j.ces.2018.08.037.

Burdige, David J. (Jan. 2002). "Chapter 13 - Sediment Pore Waters". In: *Biogeochemistry of Marine Dissolved Organic Matter*. Ed. by Dennis A. Hansell and Craig A. Carlson. San Diego: Academic Press, pp. 611–663. ISBN: 978-0-12-323841-2. DOI: 10.1016/B978-012323841-2/50015-4.

Chen, Kai Loon and Menachem Elimelech (Oct. 2008). "Interaction of Fullerene ($C_{60}$) Nanoparticles with Humic Acid and Alginate Coated Silica Surfaces: Measurements, Mechanisms, and Environmental Implications". In: *Environmental Science & Technology* 42.20, pp. 7607–7614. ISSN: 0013-936X, 1520-5851. DOI: 10.1021/es8012062.

Delouche, N., A. B. Schofield, and H. Tabuteau (2020). "Dynamics of Progressive Pore Clogging by Colloidal Aggregates". en. In: *Soft Matter*, 10.1039.D0SM01403F. ISSN: 1744-683X, 1744-6848. DOI: 10.1039/D0SM01403F.

El Hadri, Hind, Julien Gigault, Benoit Maxit, Bruno Grassl, and Stéphanie Reynaud (2020). "Nanoplastic from Mechanically Degraded Primary and Secondary Microplastics for Environmental Assessments". In: *NanoImpact*, p. 100206. ISSN: 2452-0748. DOI: 10.1016/j.impact.2019.100206.

Espinasse, Benjamin, Ernest M. Hotze, and Mark R. Wiesner (Nov. 2007). "Transport and Retention of Colloidal Aggregates of $C_{60}$ in Porous Media: Effects of Organic Macromolecules, Ionic Composition, and Preparation Method". en. In: *Environmental Science & Technology* 41.21, pp. 7396–7402. ISSN: 0013-936X, 1520-5851. DOI: 10.1021/es0708767.

He, Lei, Haifeng Rong, Dan Wu, Meng Li, Chengyi Wang, and Meiping Tong (Apr. 2020). "Influence of Biofilm on the Transport and Deposition Behaviors of Nano- and Micro-Plastic Particles in Quartz Sand". en. In: *Water Research*, p. 115808. ISSN: 00431354. DOI: 10.1016/j.watres.2020.115808.

Molnar, Ian L., William P. Johnson, Jason I. Gerhard, Clinton S. Willson, and Denis M. O'Carroll (Sept. 2015). "Predicting Colloid Transport through Saturated Porous Media: A Critical Review". en. In: *Water Resources Research* 51.9, pp. 6804–6845. ISSN: 00431397. DOI: 10.1002/2015WR017318.

Pelley, Andrew J. and Nathalie Tufenkji (May 2008). "Effect of Particle Size and Natural Organic Matter on the Migration of Nano- and Microscale Latex Particles in Saturated Porous Media". en. In: *Journal of Colloid and Interface Science* 321.1, pp. 74–83. ISSN: 00219797. DOI: 10.1016/j.jcis.2008.01.046.

Pradel, Alice, Séléna Ferreres, Cloé Veclin, Hind El Hadri, Maud Gautier, Bruno Grassl, and Julien Gigault (Mar. 2021). "Stabilization of Fragmental Polystyrene Nanoplastic by Natural Organic Matter: Insight into Mechanisms". en. In: *ACS ES&T Water*, acsestwater.0c00283. ISSN: 2690-0637. DOI: 10.1021/acsestwater.0c00283.

Pradel, Alice, Hind el Hadri, Cloé Desmet, Jessica Ponti, Stéphanie Reynaud, Bruno Grassl, and Julien Gigault (Apr. 2020). "Deposition of Environmentally Relevant Nanoplastic Models in Sand during Transport Experiments". en. In: *Chemosphere*, p. 126912. ISSN: 00456535. DOI: 10.1016/j.chemosphere.2020.126912.

The previous chapters have studied nanoplastics' transfer in porous media to elucidate their behavior in terrestrial environments. While plastic debris is an anthropic contaminant, it can be transported over long distances. Therefore, its presence in remote areas (removed from anthropic activity) is highly probable and must not be overlooked. Evidence from ocean and atmospheric circulation models suggests that plastic debris will accumulate in the Arctic Ocean. Recent efforts to sample and characterize microplastics in Arctic seawater and sea ice confirmed these predictions. However, little is known about the behavior of nanoplastics in this environmental system. Experimental setups provide the opportunity to better understand the processes that dictate plastic particles' fate at the surface of the Arctic Ocean since they can simplify the inherent complexity of Arctic environmental conditions (i.e.: variability of weather, currents, biological activity, etc.). Therefore, a novel experimental setup has been developed to study the transfer of micro- and nanoplastic model particles between saltwater and a growing front of ice. This Chapter is an article that has been published in *Environmental Science: Processes & Impacts* in September 2021, which explores, for the first time, the behavior of nanoplastics at the interface between saltwater and saline ice.

**Cite as:** Pradel A., Gautier M., Bavay D., Gigault J., Micro- and nanoplastics' transfer in freezing saltwater: Implications for their fate in polar waters, *Environ. Sci.: Processes Impacts* (2021), doi: https://dx.doi.org/10.1039/d1em00280e

# Chapter 5

# Micro- and nanoplastics' transfer in freezing saltwater: Implications for their fate in polar waters

Pradel Alice[a,b], Gautier Maud[a], Bavay Dominique[a], Gigault Julien[a,b]

[a] Univ Rennes, CNRS, Géosciences Rennes - UMR 6118, 35000 Rennes, France

[b] TAKUVIK, CNRS, Université Laval UMI 3376, Quebec, Canada

**Abstract:** Plastic debris accumulate in the Arctic by way of oceanic and atmospheric circulation. High concentrations of microplastics (1$\mu$m to 5 mm) have been measured and nanoplastics (<1$\mu$m) are expected to be abundant as well. However, little is known about the mobility of micro- and nanoplastics at the seawater/ice interface. This study investigates the fate of micro- and nanoplastics during sea ice formation. A novel experimental approach simulates growth of sea ice by progressively freezing a saline solution. After different durations of freezing, the concentration of different NaCl, natural organic matter, microplastics and nanoplastics was measured in the ice and liquid. Micro- and nanoplastics' distribution coefficient between saltwater and ice was determined, reflecting their behavior during congelation sea ice growth. The results show that microplastics are retained in ice while nanoplastics are expulsed from it. Furthermore, natural organic matter plays a crucial role in stabilizing nanoplastics at this interface. These results raise new questions concerning the impact of micro- and nanoplastics in fragile polar environments and the analytical strategy that needs to be developed to detect them.

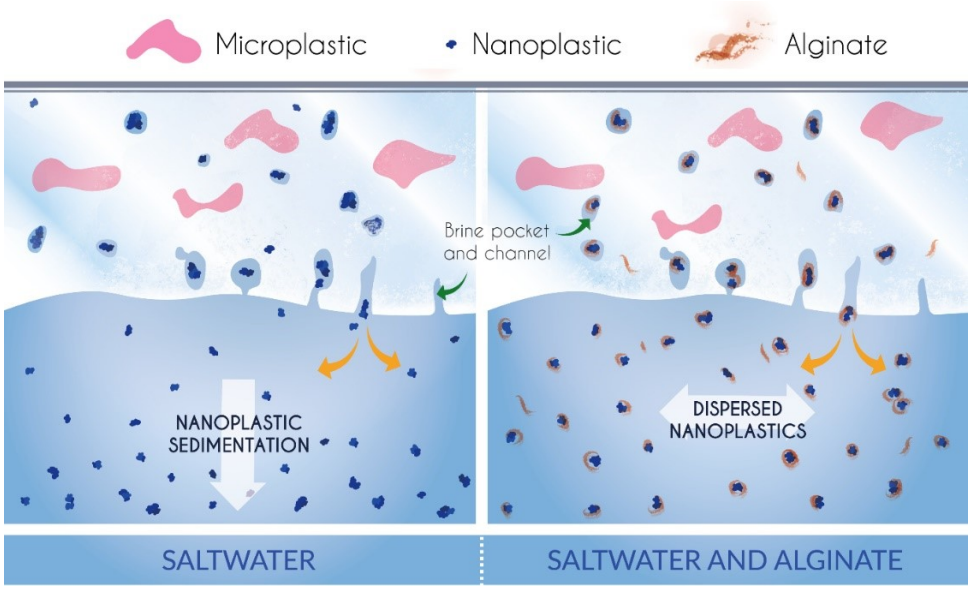


**Keywords:** Plastic debris, Arctic, Cryosphere, Pollution, Sea ice, Transfer, Natural Organic Matter

**Environmental Significance:**While microplastics are trapped in saline ice, nanoplastics are expulsed along with salts. Natural organic matter, such as alginate, stabilizes nanoplastics against aggregation during freezing.

## 5.1 Introduction

Plastic debris is globally recognized as an urgent and multi-faceted issue(GESAMP 2015; SAPEA, Science Advice for Policy by European Academies 2019; Programme 2018). More than half of all of the total plastic produced on Earth has been discarded (Geyer, Jenna R. Jambeck, and Kara Lavender Law 2017) and due to mismanagement, it is estimated that over 25% of all the plastic produced makes its way into the environment( (Alimi, Farner Budarz, et al. 2018). Microplastics (1$\mu$m to 5 mm) have already contaminated all of the Earth's compartments, from freshwater and terrestrial systems (Horton et al. 2017) to more remote areas such as the Arctic Ocean (Amélineau et al. 2016; Bergmann, Wirzberger, et al. 2017; Andrés Cózar et al. 2017; Kanhai, Gårdfeldt, et al. 2018; Kanhai, Gardfeldt, et al. 2020; S.-K. Kim et al. 2021; Lusher et al. 2015; Morgana et al. 2018; Mu et al. 2019; Obbard et al. 2014; Peeken et al. 2018; Tekman et al. 2020; Ross et al. 2021; Yakushev et al. 2021). Indeed, microplastics were ubiquitous throughout Arctic waters and sediments, with surface water concentrations ranging from 1.1 x $10^2$ to 1.3 x $10^3$ particles per $m^3$ (Tekman et al. 2020). Although comparing microplastic concentrations from different studies is difficult due to the diversity of sampling and characterization methods, several studies suggest that Arctic concentrations are close to those reported in populated areas and accumulation zones (Amélineau et al. 2016; Bergmann, Wirzberger, et al. 2017; Andrés Cózar et al. 2017; Kanhai, Gårdfeldt, et al. 2018; Kanhai, Gardfeldt, et al. 2020; S.-K. Kim et al. 2021; Lusher et al. 2015; Morgana et al. 2018; Mu et al. 2019; Tekman et al. 2020; Ross et al. 2021; Yakushev et al. 2021)). Indeed, average concentrations in surface waters of the Arctic Ocean of 0.34 $\pm$ 0.31 particles per $m^3$ are in the same order of magnitude as those reported at the surface of the North Pacific and North Atlantic subtropical gyres (Lusher et al. 2015). Other studies found lower (Yakushev et al. 2021) similar(Amélineau et al. 2016; Kanhai, Gårdfeldt, et al. 2018; Kanhai, Gardfeldt, et al. 2020; Morgana et al. 2018; Mu et al. 2019) or higher (Kanhai, Gårdfeldt, et al. 2018; Kanhai, Gardfeldt, et al. 2020; Tekman et al. 2020; Ross et al. 2021) surface and subsurface concentrations of microplastics. Another study has concluded that while maximal concentrations are still higher in subtropical gyres compared to the Arctic Ocean, median concentrations are similar (Andrés Cózar et al. 2017). As for other anthropogenic contaminants, long-distance transport of microplastic by atmospheric and oceanic currents is responsible for their high concentration in the Arctic Ocean, where the direct human impact is low (Obbard 2018; van Sebille, England, and Froyland 2012). Indeed, Atlantic waters were identified as the primary source of microplastics, followed by Siberian river waters (Yakushev et al. 2021). Analysis of fibers' surface chemistry revealed that particles found in the western Arctic were increasingly weathered, suggesting

that inputs from the Atlantic Ocean or atmospheric deposition were important sources (Yakushev et al. 2021). The number of microplastics in Arctic sediments are three orders of magnitude higher than in surface and subsurface waters, corroborating that sediments are one of the potential sinks of microplastics in the Arctic(Tekman et al. 2020).

Sea ice is particularly impacted by microplastic contamination, since microplastics accumulate in sea ice compared to seawater. Only one study simultaneously sampled microplastics in both sea ice and the underlying seawater during the same expedition. In the Arctic Central Basin, they found that the majority of microplastics detected were fibers and their concentrations were approximately 3 orders of magnitude higher in sea ice than seawater (Kanhai, Gardfeldt, et al. 2020). Similar enrichment of microplastic in Antarctic sea ice was reported with average concentrations of 3.1 x $10^{-2}$ particles per $m^3$ in surface water and 1.2 x $10^4$ in sea ice(Kelly et al. 2020). Furthermore, concentrations of microplastics in sea ice were significantly higher than in accumulation zones such as the Pacific Gyre (S.-K. Kim et al. 2021; Obbard et al. 2014; Peeken et al. 2018). When studying sea ice cores, snow, and meltwater in the Western Arctic, the snow had a limited contribution to the overall sea ice load of microplastics, suggesting instead that incorporation of microplastics dispersed in seawater is the dominant pathway for accumulation in sea ice (S.-K. Kim et al. 2021). After their accumulation in sea ice, microplastics can be transported by sea ice drift and redistributed during sea ice melt (Kanhai, Gardfeldt, et al. 2020; Peeken et al. 2018). Indeed, a thorough investigation of microplastic concentrations in polar waters and sediments found that the highest concentration of their study (which was conducted during one expedition, using the same sampling and analysis methods) was (1.3 x $10^3$ particles per $m^3$) at the marginal ice zone in the surface waters of the Greenland Sea (Tekman et al. 2020). Therefore, it is crucial to better understand how plastic debris transfer between seawater and sea ice, in order to determine their distribution, transport, and accumulation in polar regions. This is especially critical since sea ice is a habitat that supports large communities of algae, which form the base of the food web (Popova et al. 2012; Thomas and Dieckmann 2003). Furthermore, due to climate change, sea ice is shifting from multi-year ice to thinner annual ice, making it especially important to understand the mobility of plastic debris during sea ice growth (Stroeve and Notz 2018).

Since quantifying microplastics and nanoplastics in polar environments is highly challenging and since particles' mobility between seawater and ice is a complex process, experimental modeling must be used to understand and predict the fate of plastic debris (Kanhai, Gardfeldt, et al. 2020). Indeed, on top of analytical challenges, sampling microplastics and nanoplastics within sea ice and polar waters presents additional challenges such as the variability of natural features (e.g.: ice structure, temperature, biological ac-

tivity, etc.), seasonality, and lack of infrastructure. Furthermore, the processes by which dissolved or particulate material is either rejected from sea ice or captured in sea ice are complex (Dumont et al. 2009; Eicken 2003). When water freezes, it rejects impurities from its crystalline structure. A well-known example of this is the rejection of brine from sea ice, which causes the sinking of cold and dense water, in turn driving thermohaline circulation (Aagaard, Coachman, and Carmack 1981; Worster and Jones 2015). However, many of these dissolved species accumulate in localized areas of the sea ice, which leads to the formation of bubbles (when gas' solubility limits are exceeded) and brine pockets (as salts lower the freezing temperature of the liquid)(Eicken 2003; Lake and E. L. Lewis 1970). Different processes lead to the accumulation of particulate species in sea ice. High enrichment of particulate matter occurs during the growth of frazil ice in turbulent waters, which can lead to the production of dirty ice enriched in sediments (Ito et al. 2019; Nürnberg et al. 1994; Reimnitz et al. 1993). Also, particles can be captured in thick sea ice during congelation freezing in calmer waters. At this point, buoyant particles can become entrapped in sea ice given a sufficient speed of advancement of the freezing front (Eicken 2003; Janssens et al. 2016; Bronstein, Itkin, and Ishkov 1981; Yemmou, Brierre, and Azouni 1991). Globally, the capture of impurities in sea ice depends on parameters such as particle size and density (Grossmann and Gleitz 1993; Janssens et al. 2016; Reimnitz et al. 1993), the speed at which the freezing front advances (Bronstein, Itkin, and Ishkov 1981; Yemmou, Brierre, and Azouni 1991; Hullar and Anastasio 2016; Kao, Golovin, and Davis 2009), water turbulence (Ito et al. 2019; Nürnberg et al. 1994) as well as compatibility of the impurity with solid water (Janssens et al. 2016). For example, larger and denser sediments require more turbulence to become suspended and entrapped in frazil ice crystals(Reimnitz et al. 1993). For congelation growth, larger particles can be entrapped at a lower speed of advancement of the freezing front, compared to smaller particles (Kao, Golovin, and Davis 2009; Yemmou, Brierre, and Azouni 1991). Since many processes co-occur, it is necessary to understand how these separately affect the mobility of microplastics and nanoplastics. Recently, a mesocosm experiment has studied the incorporation of microplastics during sea ice growth (Geilfus et al. 2019). They found that microplastics were enriched in sea ice relative to the underlying seawater. In particular, concentrations were highest at the surface of ice, suggesting efficient incorporation during initial sea ice formation and slower accumulation rates during subsequent ice growth. However, to date, no experimental study has focused on nanoplastics' flux between seawater and ice.

This study aims to quantify microplastics and nanoplastics' flux between saltwater and a freezing front in non-turbulent conditions. A novel lab-scale freezing reactor simulates the seawater/ice interface and allowed the quantification of microplastic and nanoplastic

transfer between liquid water and a growing ice front. This freezing reactor has more controlled freezing conditions than previous mesoscale studies (Geilfus et al. 2019), allowing a more mechanistic understanding of plastic particles' fate. Nanoplastics' stability at this interface was assessed in light of their physical properties (size, surface, shape) and the presence of relevant natural organic matter (NOM).

## 5.2 Materials and Methods

### 5.2.1 Materials

All solutions and colloidal dispersions were prepared with deionized (DI) water (Millipore, 18.2 MΩ). A stock solution of NaCl (solid, LabKem ExtraPure) was prepared at a concentration of 100 g $kg^{-1}$. The sodium alginate (SA) stock solution was prepared by adding SA (solid, Acros Organics) in DI water and agitating at 400 rpm for 12 hours. The stock solutions had concentrations of approximately 1 g $kg^{-1}$ as determined with a Total Carbon Analyzer (TOC-V CSH, Shimadzu, Japan). According to the SA's molecular composition, 1 mg $kg^{-1}$ of organic carbon was converted to 2.8 mg $kg^{-1}$ SA.

The two spherical models studied, *nPSL-200* and *nPSL-350* were purchased from Polysciences© (Polybead® Carboxylate Orange Dyed Microspheres 0.20 $\mu$m and Polybead® Carboxylate Microspheres 0.3 $\mu$m, Warrington USA). Stock dispersions at a concentration of 100 mg $kg^{-1}$ were prepared. The nanoplastic model with irregular shapes and polydisperse sizes (*nPS-360*) was produced by mechanical abrasion of industrial-grade polystyrene (PS) pellets (Total, Paris, France) with the method described by El Hadri et al. 2020. Stock solutions had a concentration of around 40 mg $kg^{-1}$. The PS pellets did not contain additives and were not aged. The microplastic model ($\mu$PS) was obtained by grinding these same PS pellets in a coffee grinder for 3 minutes, with interruptions to avoid overheating, and then keeping the particles retained between sieves of 125 and 400 $\mu$m. In all experiments, nanoplastic and microplastic concentrations were 10 mg $kg^{-1}$ and 4.25 g $kg^{-1}$, respectively. These concentrations are higher than those expected in the environment (Lenz, Enders, and Nielsen 2016), but were necessary to remain within instruments' detection limits. All solutions' pH was fixed at 8 during 1 hour, using a pH-meter (F20, Mettler-Toledo, Schwerzenbach, Switzerland) and 0.1 mol $kg^{-1}$ solutions of NaOH (Fisher Scientific, Analytical Grade).

### 5.2.2 Methods

The effect of freezing on the nanoplastic dispersions was studied in two setups: i) bulk freezing and ii) partial and progressive freezing in a freezing reactor.

For bulk freezing, glass vials were filled with 3.5 mL of solution with varying concentrations of NaCl (5 to 55 g $kg^{-1}$) and SA (1 to 100 mg $kg^{-1}$) and were either frozen at -22 °C for 3 hours and thawed, or kept at 24 °C . Each experimental condition was performed in triplicate. Bulk freezing was used to study the effect of varying concentrations of NaCl and SA on the colloidal stability of nanoplastics. This stability was assessed by measuring changes in size and concentration between the nanoplastic dispersions that underwent a cycle of freeze/thaw and those that remained at room temperature. For the partial and progressive freezing experiments, the experimental protocol is thoroughly illustrated in Figure 5.1. Briefly, 12 mL of solution was inserted in a vessel, which had a capacity of 22 mL. At the end of the experiment, the part of the solution that remained liquid was recovered, then the bottom of the vessel was then rinsed, and finally, the thawed ice was recovered. Once the solutions returned to room temperature, the mass of each phase was weighed, and the solutions were characterized by measuring pH, the concentrations of NaCl, micro- and nanoplastics and SA, and the size of nanoplastics. The freezing reactors' vessel and the cold finger were composed of glass with thicknesses between 1.8 and 2 mm. The cold finger contains a cooling liquid in constant circulation through a thermostat (Ecoline RE106 Lauda, Delran, USA). Two reactors were set up in parallel to obtain duplicate experiments.

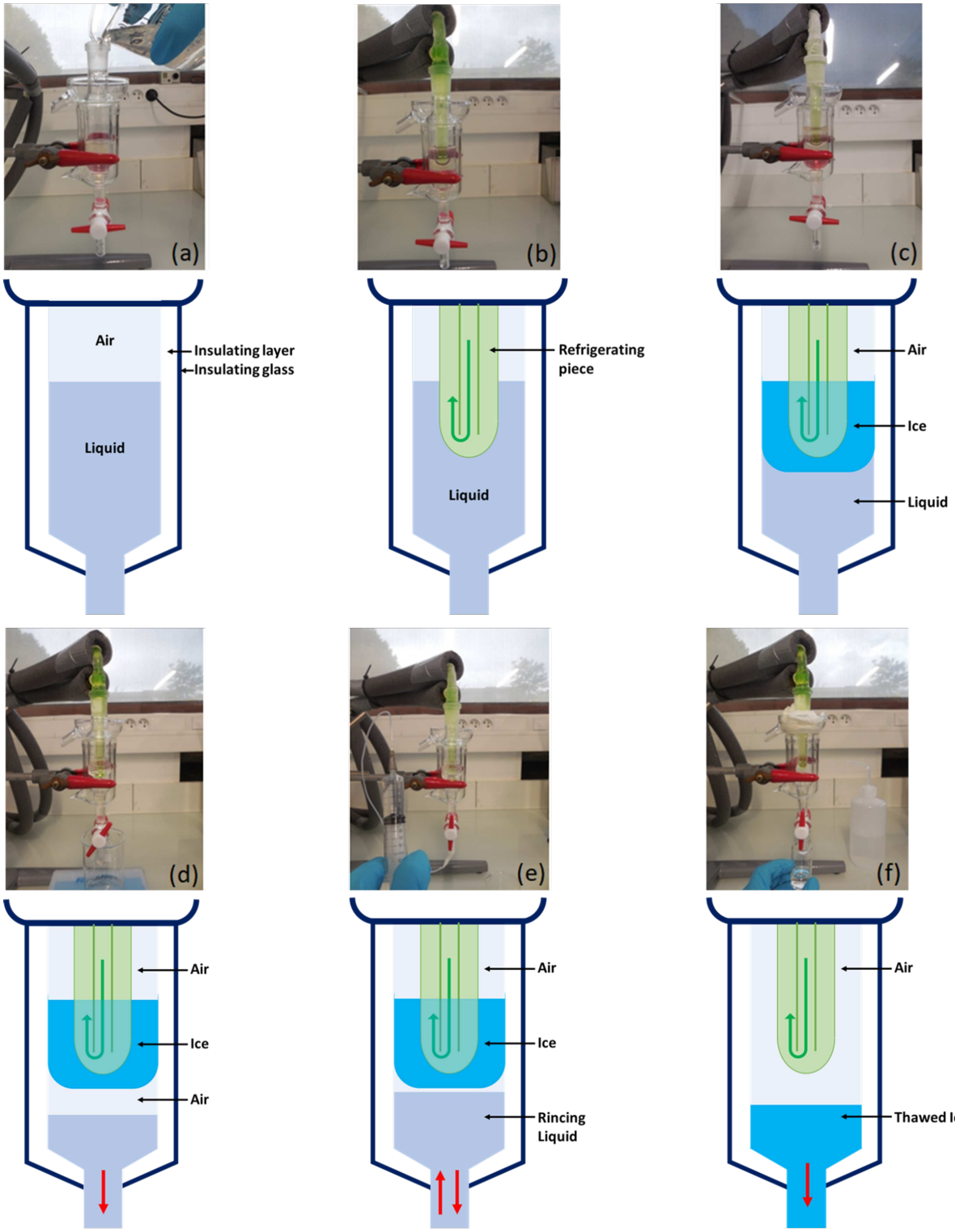


*Figure 5.1: Steps of the progressive and partial freezing protocol in images above and corresponding diagrams below: a) insertion of the solution in the freezing reactor, b) insertion of the cold finger, c) solidification of the liquid, d) recovery of the liquid phase, e) rinsing of the bottom of the vessel, f) recovery of thawed ice.*

The internal temperature of the cold finger was -6.7 ± 0.6 °C. Ice formation was described by time-lapse photography (Figure 5.2). The first ice was observed after 7 minutes in DI water and after 9 minutes in 35 g $kg^{-1}$ NaCl. The maximum speed of the freezing front was 8 $\mu$m $s^{-1}$ in DI and 4 $\mu$m $s^{-1}$ in NaCl. In DI, the ice grows first parallel to the sides of the refrigerating piece. Upon attaining the walls of the vessel (at 20 to 25 minutes), the ice then grows vertically and stabilizes after 3 hours. In NaCl, freezing follows the same dynamic, except the ice i) has a more rounded shape, ii) reaches the walls of the vessel after 25 to 30 minutes, and finally, iii) the underneath of the ice, in contact with the liquid, systematically thaws after approximately 1.5 hours, after which the ice volume stabilizes. The volume of ice formed in DI is 35 % superior to that formed in NaCl.

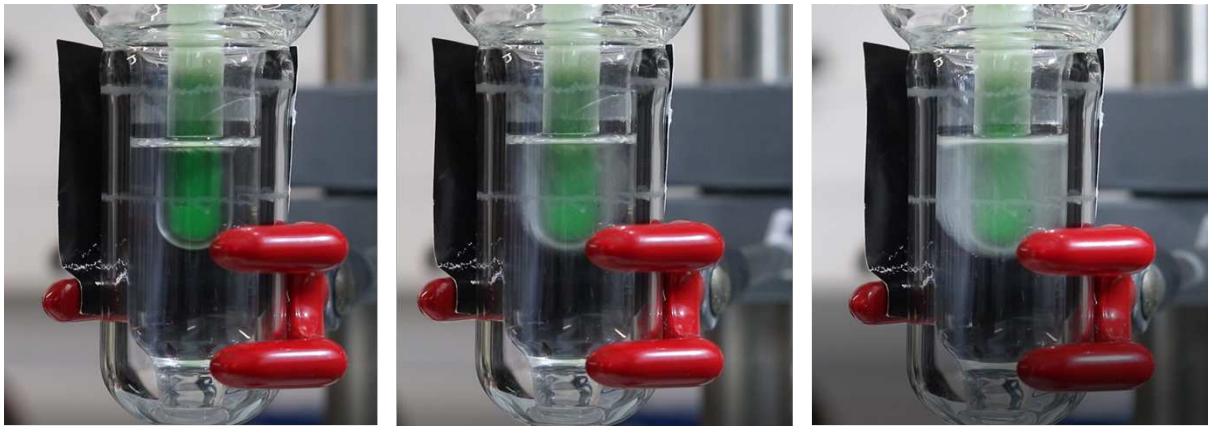

*Figure 5.2: Examples of time-lapse photography, used to calculate speed and shape of freezing at 0 minutes, approximately 15 minutes and 40 minutes (35 g $kg^{-1}$ NaCl)*

The z-average hydrodynamic diameters ($d_{zH}$) were determined by a dynamic light scattering (DLS) probe (Vasco-Flex, Cordouan Technologies, Pessac, France). The backscattered light is collected at a geometric angle of 170° with respect to the incident beam direction. Each measurement was obtained from an average of five correlation functions that were accumulated for 60 seconds. $d_{zH}$ is obtained by fitting a monomodal, normal distribution to the raw data (Cumulant algorithm ISO 22412:2008). Nanoplastic concentrations were measured by absorbance at a wavelength of 226 nm (UV-2600 UV-Visible Spectrophotometer, Shimadzu, Japan). Alginate concentrations were measured by Total Carbon Analyzer (TOC-V CSH, Shimadzu, Japan). The ionic strengths and pHs were measured with a conductivity meter and pH meter (F30 and F20, Mettler-Toledo, Schwerzenbach, Switzerland). The surface potential of the nanoplastics was assessed using a Wallis zetameter (Cordouan Technologies, Pessac, France). The zetameter measures the electrophoretic mobility by laser Doppler electrophoresis and applies the Smoluchowski model to determine the zeta potential. Mass balances were calculated with the mass

of initial solution ($M_{Init}$), and liquid ($M_{Liq}$) and ice ($M_{Ice}$) solutions recovered from the freezing reactor, as well as the SA or particle concentrations measured in the initial solution ($C_{Init}$), and in the liquid ($C_{Liq}$) and ice ($C_{Ice}$) solutions recovered from the freezing reactor. Mass balance of liquid lost was calculated as:

$$\frac{M_{Init} - (M_{Liq} + M_{Ice})}{M_{Init}} \tag{5.1}$$

A positive (negative) value indicates a loss (gain) of mass. The distribution of initial SA or particle masses between liquid and ice were calculated as:

$$\frac{C_{Liq} \cdot C_{Liq}}{C_{Init} \cdot C_{Init}} \tag{5.2}$$

for the liquid phase, and as:

$$\frac{C_{Ice} \cdot C_{Ice}}{C_{Init} \cdot C_{Init}} \tag{5.3}$$

for the solid phases. Losses of SA or particle masses were calculated as 1- (Proportion in Liquid + Ice). Percent variations in concentration (C) and sizes ($d_{zH}$) were given by the following equations:

$$\frac{(C_{final} - C_{initial})}{C_{final}} * 100 \tag{5.4}$$

and

$$\frac{(d_{zH,final} - d_{zH,initial})}{d_{zH,final}} * 100 \tag{5.5}$$

## 5.3 Results and Discussion

Freezing reactors were designed to partially and progressively freeze aqueous solutions, simulating growing sea ice (Figures 5.1, 5.2 5.3a and 5.4a). These were composed of vessels containing a solution of 35 g $kg^{-1}$ NaCl at pH 8 and a cold finger that was inserted in the solution (t = 0). The evolution of the ice and liquid's physical and chemical properties (water mass, ionic strength, and pH) were investigated (Figure 5.3b, 5.4b and 5.4c). The water mass balance (the difference between the initial water mass and the sum of liquid and ice masses recovered) is generally well conserved. Indeed, as can be seen in the Supplementary Data (page 217), throughout the 64 data points, most had a final mass balance within ± 6 % of the initial mass. 78 % of data points have a positive mass balance indicating a loss of water mass. This can be explained by liquid retained on the surfaces of the freezing reactor vessel and in the faucet by capillary action. On the other hand, gain of mass can be explained by condensation of water vapor in the air due to the cold temperatures (either during the experiment or when recovering liquid and ice).

Only on 6 occasions, the mass balance was superior to ± 6 %, with a loss of 7 %, 7 %, 8 %, and 22 % and two gains of 18 %.

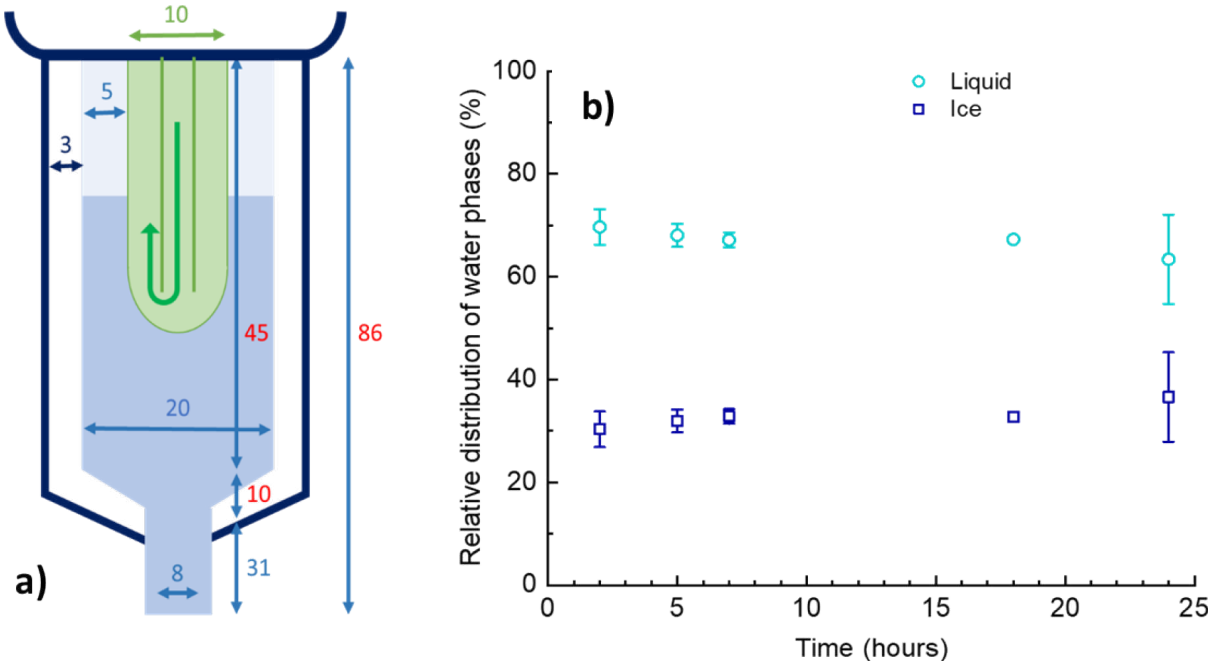


*Figure 5.3: a) Dimensions of the system in mm (not to scale). From the exterior to the interior: the insulating layer of glass (dark blue), the inner vessel containing liquid (blue) and air (light blue), the refrigerating piece (green) with the direction of flow of the cooling liquid (bright green). Numbers in red represent dimensions that differed between the duplicate systems, with 86, 45 and 10 mm corresponding to 90, 52 and 7 mm, respectively. b) Evolution of the relative proportion of liquid and solid phases (m/m) for the 35 g kg$^{-1}$ NaCl solution.*

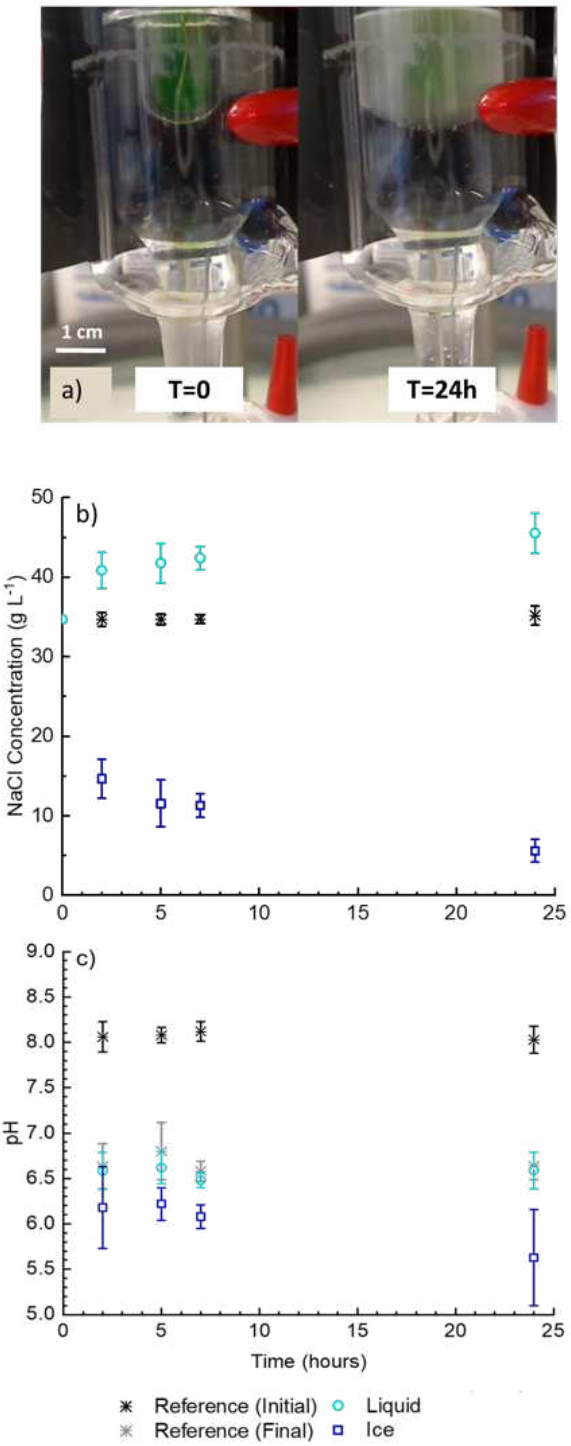


*Figure 5.4: a) Freezing reactor at the beginning of freezing (T = 0) and after 24 hours of freezing (T = 24h) of 35 g $kg^{-1}$ NaCl. Evolution of (b) NaCl concentrations and (c) pH of the liquid, thawed ice, and reference solution, for initial solutions containing 35 g $kg^{-1}$ NaCl at pH 8 frozen in the freezing reactor. (n = 40, i.e.: duplicates of 20 different solutions; whiskers represent standard deviation).*

The initial NaCl concentration is 35 g $kg^{-1}$ which is typical of the Atlantic sector of the Arctic Ocean and areas below 80 °N (Boyer et al. 2012). During freezing, NaCl segregates between liquid and ice: its concentration decreases in ice and increases proportionally in the liquid phase, reaching 40 g $kg^{-1}$ (Figure 5.4b). This is due to freeze-exclusion, the mechanism by which impurities such as ions are expulsed from the crystalline structure of ice. Some of the NaCl is not expulsed out of the ice structure but is incorporated in it, forming the brine channels and pockets (Crabeck et al. 2015; Hullar and Anastasio 2016). These zones remain liquid since the accumulation of salt lowers the freezing point of brine. Hence, in ice, substantial heterogeneity in NaCl concentrations is expected. Nonetheless, the average salinity of ice decreases from 14.6 g $kg^{-1}$ at 2 hours, which is typical of the early stages of freezing (Hare et al. 2013; Crabeck et al. 2015) to 5.6 g $kg^{-1}$ at 24 hours, which is typical for first year ice (Kowalik and Matthews 1983; Worster and Jones 2015). The mass balance of salts was also generally conserved. Although the amount of NaCl losses (7.6 ± 3.3 %) was superior to the mass of water losses (2.0 ± 5.6 %) it was less variable. There is only a slight positive correlation between mass of water lost and mass of NaCl lost ($R^2 = 0.19$). There is no correlation between mass of particles or alginate lost and mass of NaCl lost ($R^2 = 0.08$) (Supplementary Data page 217). The loss of NaCl cannot be attributed to precipitation since NaCl is soluble at these temperature and concentrations. However, since conductivity is positively correlated to temperature, this loss of NaCl could be a deviation caused by measurements of conductivity at temperatures slightly lower than the ambient temperature, despite the care in waiting for samples to return to ambient temperature.

Freezing is known to produce changes in pH (Hare et al. 2013; Thomas and Dieckmann 2003) and nanoplastics are sensitive to pH changes when they contain surface functional groups such as carboxylic acids (which is the case for *nPSL-200* and *nPSL-350*)(Alimi, Farner Budarz, et al. 2018). Therefore, the pH changes during freezing were investigated. Initially, the pH of all solutions studied are fixed at 8.07 ± 0.05, as illustrated by Reference (Initial) in Figure 5.4c. During the experiment, a part of this initial solution is kept at room temperature and its pH decreases by 1.42 ± 0.12 pH units, as illustrated by Reference (final) (Figure 5.4c). This is due to the reaction of atmospheric $CO_2$ with hydroxide ions which forms carbonates. The pH of the liquid and thawed ice recovered from the freezing reactors, were measured at room temperature. In the liquid phase, the decrease in pH is not significantly different from that of the same solution kept at room temperature (-1.50 ± 0.29 pH units). However, the thawed ice is systematically more acidified: with a decrease of 2.04 ± 0.25 pH units. This is due to the higher solubility of $CO_2$ at lower temperatures, which causes the transfer of aqueous $CO_2$ to the colder section of liquid in the freezing reactor. This is supported by the fact that there is no enhanced

acidification after complete (bulk) freeze/thaw experiments, compared to a solution that remained at room temperature. This evolution of pH typical of that of sea ice without photosynthetic activity, since in natural sea ice, the excess $CO_2$ in ice is consumed by photosynthetic organisms (Hare et al. 2013).

Model nanoplastics and microplastics were used to study the segregation of these particles at a growing freezing front. Their properties are summarized in Table 5.1 and images are presented in Figure 5.6. Concerning nanoplastics, two spherical polystyrene latex (PSL) particles with monodisperse sizes of 200 nm (*nPSL-200*) and 350 nm (*nPSL-350*) and a more environmentally relevant nanoplastic model (*nPS-360*) were studied. *nPSL-200* contain trace amounts of surfactants whereas *nPSL-350* was purified. Finally, *nPS-360* is produced by mechanical abrasion of polystyrene (PS) pellets. Due to the synthesis method, *nPS-360* are surfactant-free and have an irregular, asymmetrical shape and polydisperse sizes. Nanoplastics' behavior was assessed in the presence of sodium alginate (SA). SA is a natural organic matter (NOM) that serves as a proxy for exopolymeric substances (EPS)(Flemming and Wingender 2010) which are abundant in sea ice (Krembs et al. 2002). The zeta-potential of *nPSL-200* and *nPSL-350*, -50.5 ± 5.5 mV and -43.7 ± 5.1 mV, respectively, are more negatively charged than *nPS-360*, which has a zeta-potential of -28.1 ± 5.6 mV. This also contributes to making *nPS-360* a more environmentally relevant particle. The presence of SA did not significantly modify the surface potential of nanoplastics (Figure 5.5). Finally, a microplastic model ($\mu$PS) was produced using the same PS pellets as for *nPS-360*.

Nanoplastics are sensitive to concentrations of NaCl and SA due to their colloidal properties. Indeed, on the one hand, NaCl may cause rapid aggregation and sedimentation by screening the electrostatic repulsion between particles. On the other hand, SA prevents this destabilization by electrostatic and steric repulsion (Pradel, Ferreres, et al. 2021). The ice growth in the freezing reactor produces gradients of NaCl and SA (the latter will be discussed below). Therefore, the stability of nanoplastics subject to a cycle of freeze/thaw was assessed in varying concentrations of SA and NaCl. Before experiments conducted in the freezing reactor, nanoplastics were studied in bulk experiments by entirely freezing solutions at -20°C and thawing them at 24 °C.

*Table 5.1: Characteristics of the nanoplastic (nP) and microplastic (μP) models studied*

| Name | Synthesis Method | Particle Dimensions[a] | PDI[b] | Morphology | Natural Organic Matter | Envirmtal. Relevance |
|---|---|---|---|---|---|---|
| *nPSL-200* | Emulsion polymerizat° | 0.168 | 0.0261 | Spherical | No | - |
| *nPSL-200* +SA | Emulsion polymerizat° | 0.168 | 0.0261 | Spherical | SA<br>SA | +<br>+ |
| *nPSL-350* +SA | Emulsion polymerizat° Surfactant-free | 0.337 | 0.089 | Spherical | SA | ++ |
| *nPS-360* +SA | Mechanical abrasion of PS pellets | 0.364 | 0.102 | Asymmetrical and irregular | SA | +++ |
| μPS +SA | Mechanical abrasion of PS pellets | 125 to 400 | NA | Asymmetrical and irregular | | ++ |

[a] *z-average hydrodynamic diameter ($d_{zH}$) or Sieve Mesh Size (μm);* [b] *Polydispersity index (PDI), defined as the variance of the Gaussian-fitted size distribution.*

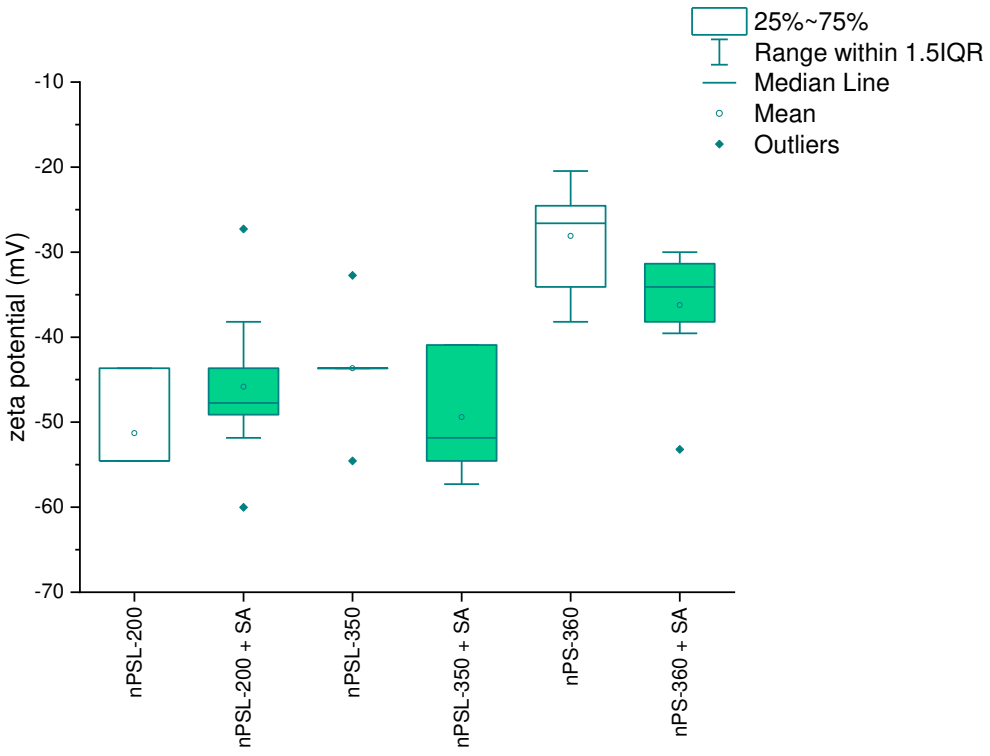


*Figure 5.5: Zeta potential of 10 mg $kg^{-1}$ of nanoplastic (nP) models in 4 mmol $kg^{-1}$ NaCl, alone and with 50 mg $kg^{-1}$ SA. Results are composed of 10 measurements in medium resolution mode*

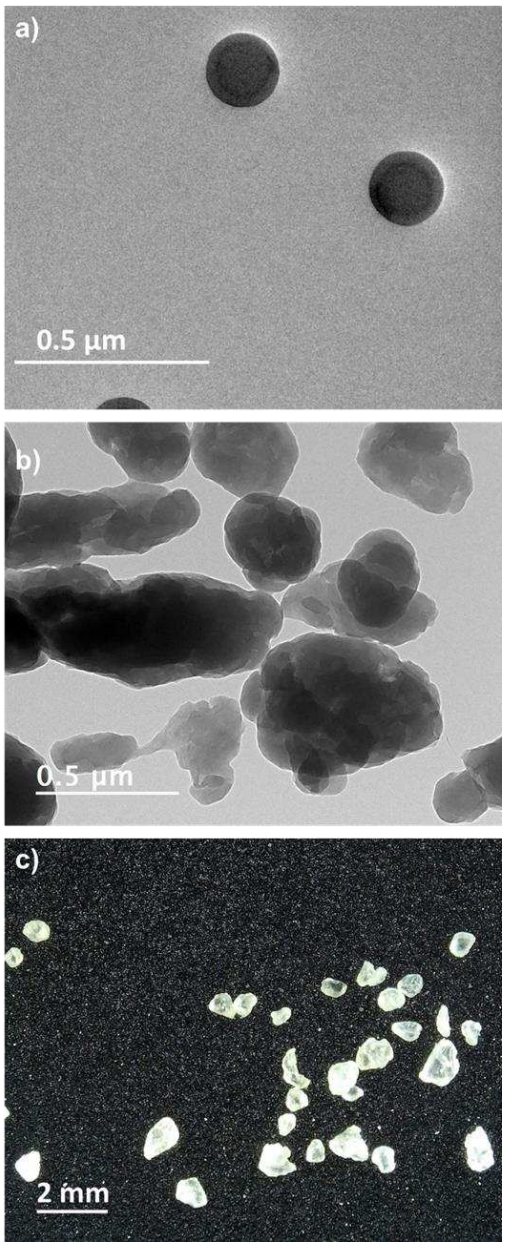


*Figure 5.6: TEM images of a) nPSL-200 and b) nPS-360. c) Digital photography of µPS.*

After bulk freeze/thaw *nPSL-200* formed aggregates independently of NaCl and SA concentrations (Figure 5.7). As solidifying water rejects particles from its crystalline structure, their concentration increases at the freezing front, which increases the possibility of collision and induces aggregation (S. Deville 2008). Indeed, freezing is known to destabilize colloidal dispersions such as biopolymers (e.g.: milk) and solid colloids (e.g.: latex paints, nanoplastics) (Alimi, Farner, and Tufenkji 2021; Barb and Mikucki 1959; S. Deville 2008). In pure water (without NaCl), the aggregation is more likely due to the strong mechanical stress caused by the growth of the homogenous crystalline structure

of ice (Chou et al. 2014). However, with NaCl, the ice structure is more porous, causing less mechanical stress. In this case locally high concentrations of NaCl are more likely to cause aggregation.

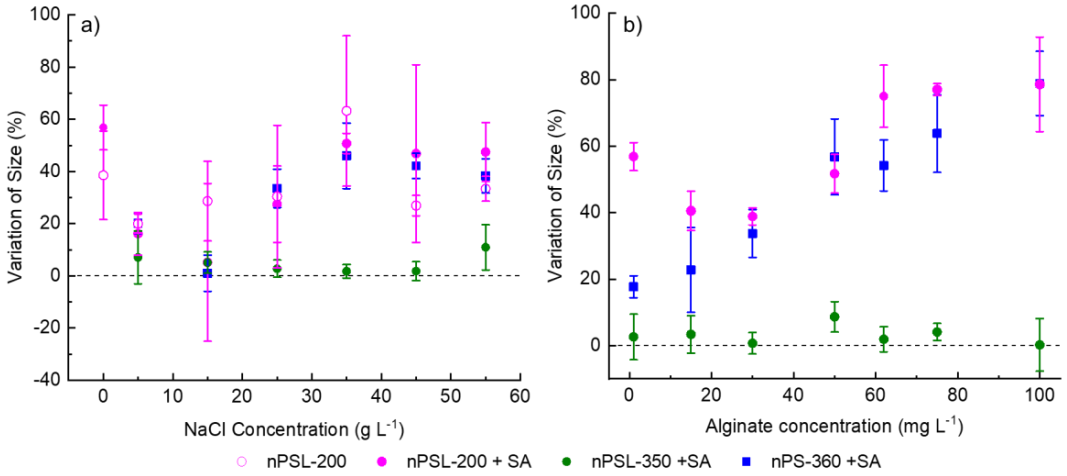


*Figure 5.7: Variations of size of nanoplastics (nPs) after bulk freeze/thaw a) as a function of NaCl concentration (keeping SA at 50 mg kg$^{-1}$, if present) and b) as a function SA (keeping NaCl at 35 g kg$^{-1}$ NaCl).*

When *nPSL-200* are frozen in NaCl without SA, the large aggregates sediment, causing a 22 to 41% decrease in concentrations compared to particles that remained at room temperature (Figure 5.8a). However, with 50 mg kg$^{-1}$ SA the aggregates formed did not sediment (Figure 5.8a). SA also successfully stabilized *nPSL-350* and *nPS-360* after one freeze/thaw cycle with up to 55 g kg$^{-1}$ NaCl (Figure 5.8a). At 35 g kg$^{-1}$ NaCl, even low concentrations of SA (15 mg kg$^{-1}$) are sufficient to stabilize all particles (Figure 5.8b). This demonstrates that the association of SA with nanoplastics prevents their destabilization during freezing. Since naturally occurring organic matter is expected to be more abundant than nanoplastics (Benner 2002; Lenz, Enders, and Nielsen 2016) and to study nanoplastics that retained their colloidal behavior during freezing, the initial concentration of SA in the freezing reactor was set at 50 mg kg$^{-1}$ (for an initial concentration of nanoplastics of 10 mg kg$^{-1}$).

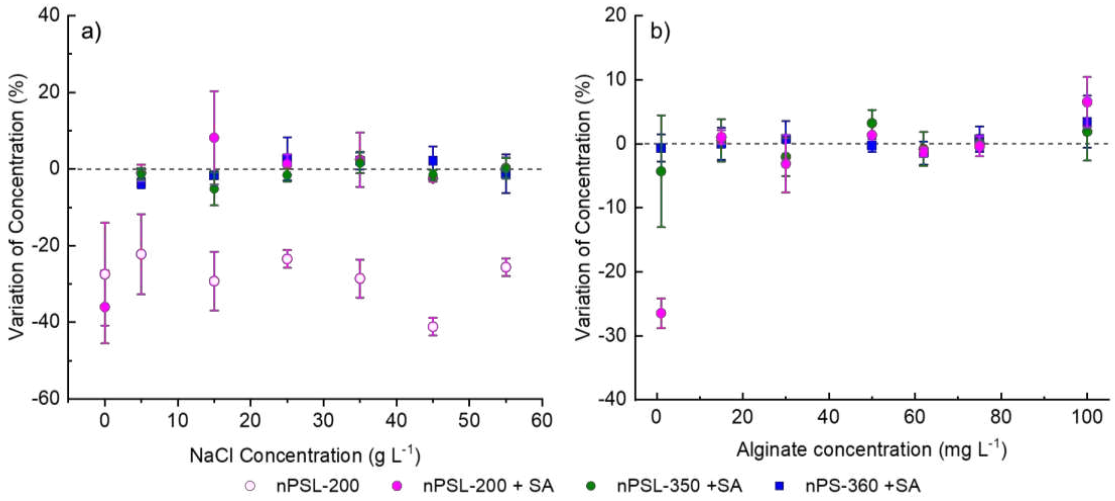


*Figure 5.8: Variations of concentration of nanoplastics (nPS) after bulk freeze/thaw a) as a function of NaCl concentration (keeping SA at 50 mg kg $^{-1}$, if present) and b) as a function SA (keeping NaCl at 35 g kg$^{-1}$ NaCl).*

When solutions are frozen in the freezing reactor, nanoplastics and SA can separate between liquid and solid phases, mimicking their mobility during sea ice growth in polar waters. Figure 5.9 shows the relative distribution of SA (Figure 5.9a) and *nPSL-200* (Figure 5.9b) between water and ice, in de-ionized water and in 35 g kg$^{-1}$ NaCl. All concentrations of species that were frozen in the reactor are presented in Supplementary Data page 217. Both species are expulsed from ice to water, akin to NaCl. For both SA and *nPSL-200*, the expulsion from ice to water is less pronounced when NaCl is involved (Figure 5.9 and Figure 5.10). Similar to bulk experiments, in the freezing reactor losses of SA and *nPSL-200* mass are higher in deionized water (12 ± 10% for SA and 30 ± 7% for *nPSL-200*) than in 35 g kg$^{-1}$ NaCl (-1 ± 4% for SA and 27 ± 16% for *nPSL-200*). The growth of pure water crystals without the porous areas formed by brine physically forces alginate molecules and *nPSL-200* particles together (Alimi, Farner, and Tufenkji 2021; Chou et al. 2014). When frozen in NaCl, they are subject to less shear strength in the brine pockets than between the pure ice crystals of deionized water. Therefore, SA and *nPSL-200* frozen in deionized water aggregate and either are not recovered from the faucet of the freezing reactor or, if recovered, sediment out of solution due to their large size. In both cases, this fraction was not measured by absorbance or total organic carbon measurements, which leads to losses in the mass balance. The loss of SA and *nPSL-200* when frozen in deionized water as well as the increased proportion of SA and *nPSL-200* present in ice when frozen in 35 g kg$^{-1}$ NaCl strongly suggests that SA and *nPSL-200* are trapped in brine pockets. Indeed, the accumulation of NOM in brine pockets has already been established (Dumont et al. 2009; Giannelli et al. 2001).

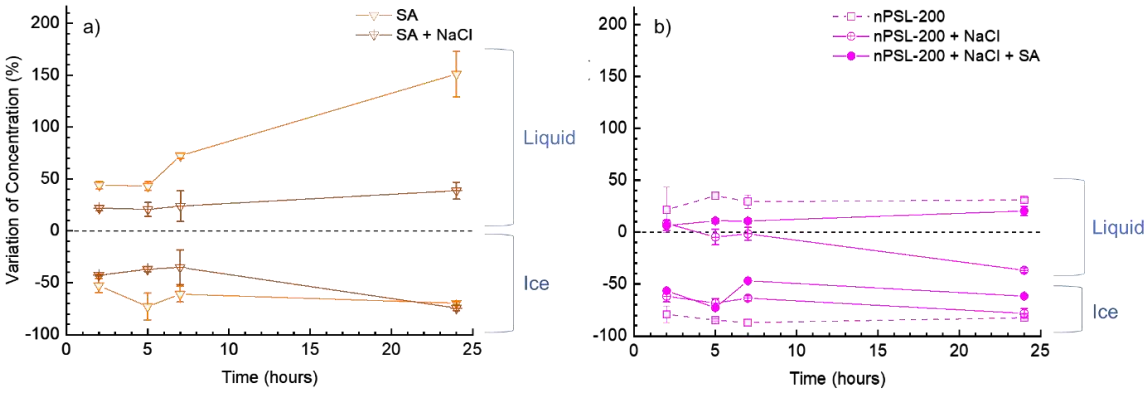


*Figure 5.9: Variation of the concentration of a) SA and b) nPSL-200 in liquid and ice, as a function of the duration of freezing in the reactor. The empty symbols represent de-ionized water at pH 8. Symbols with a cross represent 35 g $kg^{-1}$ NaCl at pH 8. For nPSL-200, the full symbol represents a dispersion in 35 g $kg^{-1}$ NaCl and 50 mg $kg^{-1}$ SA at pH 8.*

When *nPSL-200* is dispersed in NaCl without SA, their concentration decreases in both liquid and ice, indicating a global loss of mass (Figure 5.9b). Indeed, losses amount to 10 ± 2%, 29 ± 5%, 24 ± 0%, 52 ± 3% of the total mass at 2, 5, 7 and 24 hours (Supplementary Data page 217). This is due to aggregation followed by sedimentation in the liquid, as predicted by bulk experiments (Figure 5.8a), and confirmed by size measurements (discussed below). SA significantly reduced the loss of nanoplastics by sedimentation in 35 g $kg^{-1}$ NaCl with losses equal to 9 ± 7%, 6 ± 2%, 7 ± 7%, 13 ± 7% of total mass at 2, 5, 7 and 24 hours (Supplementary Data page 217). These losses show no time-dependency which confirms that SA has a stabilizing role, since aggregation is time-dependent. Similarly, losses of *nPSL-350* and *nPS-360* in NaCl and SA did not show time-dependency and were of the same magnitude (11 ± 3% and 8 ± 3% averaged over the four freezing durations, for *nPSL-350* and *nPS-360*, respectively cf : Supplementary Data page 217 ).

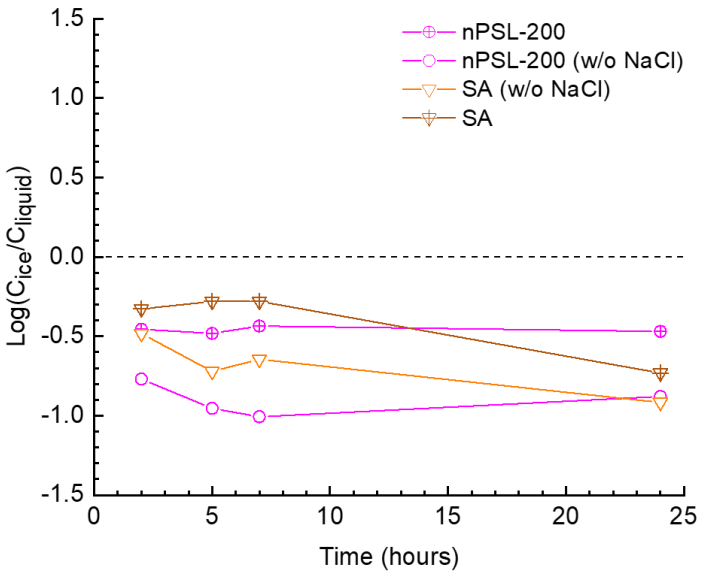


*Figure 5.10: Logarithm of the partition coefficient between ice and liquid phase ($C_{ice}/C_{liquid}$) of nanoplastic nPSL-200 and SA, dispersed in deionized water at pH 8 or NaCl 35 g $kg^{-1}$ pH 8, as a function of duration of the freezing experiment*

All nanoplastic models (*nPSL-200*, *nPSL-350*, and *nPS-360*) show the same global behavior in the presence of NaCl and SA (Figure 5.11). Their concentration increases in the liquid and decreases in the ice over time, following a similar trend as that of NaCl and SA (Figure 5.12). In ice, *nPSL-200* concentration is reduced by 47 to 53%, while the concentrations of *nPSL-350* and *nPS-360* decrease continually (-45% to -63% and -38% to -90%, respectively). The larger *nPSL-350* is more slowly expulsed from ice than its smaller counterparts (*nPSL-200* and *nPS-360*). Indeed, due to the high polydispersity of *nPS-360*'s size distribution (PDI = 0.102) most particles are actually smaller than their hydrodynamic diameter ($d_{zH}$ = 360 nm). This is due to the fact that the scattered light (used to determine $d_{zH}$) is dominated by the larger particles (M. Baalousha and Lead 2012; R. Xu 2006). The diffusion coefficient drives the rate of expulsion from ice to saltwater, as expected theoretically (Asthana and Tewari 1993; Körber 1988). Indeed NaCl, which diffuses most rapidly, has a stronger expulsion rate (Figure 5.12). However, SA is slowly expulsed from ice due to its linear structure which prevents it from diffusing like salts or colloids (Figure 5.9 and Figure 5.12) (Dumont et al. 2009; Krembs et al. 2002). Even though *nPS-360* has many particles that are similar in size to *nPSL-200*, they are not expulsed from the ice at the same rate. Since particles are likely to aggregate in ice and since nanoplastics are particularly sensitive to aggregation, differences in nanoplastic retention in ice during freezing could be attributed to differences in aggregation states.

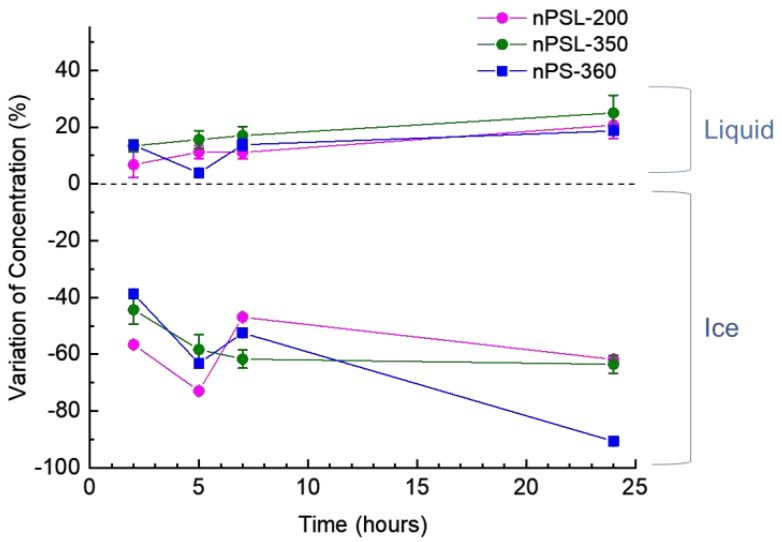


*Figure 5.11: Variation of the concentration of nanoplastics (nPs) in the liquid and ice, as a function of the duration of the freezing in the reactor. Nanoplastics were dispersed in 35 g $kg^{-1}$ NaCl and 50 mg $kg^{-1}$ SA at pH 8.*

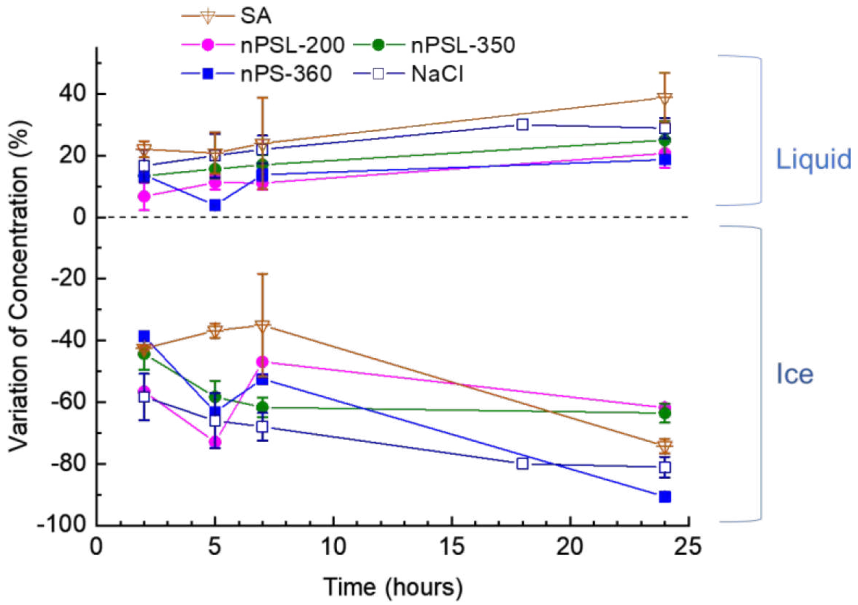


*Figure 5.12: Variation of the concentrations of different species in liquid and ice, as a function of the duration of the freezing in the reactor. All experiments were conducted with 35 g $kg^{-1}$ NaCl and 50 mg $kg^{-1}$ SA at pH 8.*

To understand differences in nanoplastic retention in ice, variations of nanoplastics' sizes recovered in liquid and ice were investigated (Figure 5.13). With NaCl and SA no aggregation is observed, and all nanoplastics (*nPSL-200*, *nPSL-350* and *nPS-360*) remain stable in both saltwater and ice. SA stabilizes nanoplastics at high ionic strength

by wrapping the particles and providing electrostatic and steric repulsion between the particles (Pradel, Ferreres, et al. 2021). So, the differences in expulsion between different types of nanoplastic cannot be attributed to differences in aggregation state. Without SA, *nPSL-200* that remained in ice aggregate, whereas they do not in the liquid. In the liquid, aggregated *nPSL-200* can sediment and leave the suspension during the experiment, as illustrated by the significant losses of *nPSL-200* in these conditions (Supplementary Data page 217). However, in ice, *nPSL-200* are trapped at high concentrations in brine pockets and channels. They aggregate due to higher collision rates and favorable collisions (screened the electrostatic repulsion), as observed in bulk freezing experiments and cannot sediment out of the ice (Figure 5.7).

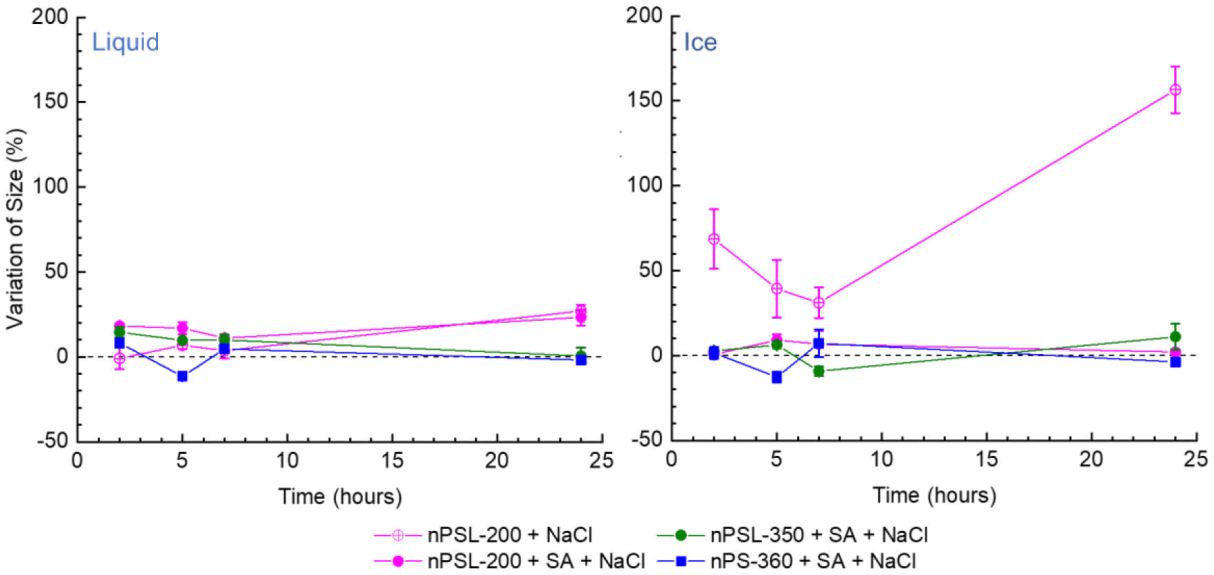


*Figure 5.13: Variation of the hydrodynamic radius ($d_{zH}$) of different nanoplastic particles dispersed in 35 g $kg^{-1}$ NaCl and recovered from liquid (left) and ice (right) after different durations of freezing in the reactor.*

Due to their larger size and buoyancy, microplastics' showed an opposite behavior compared to nanoplastics (Figure 5.14). The proportion of microplastics located in the ice was 68 ± 10% after 2 hours of freezing, 76 ± 9% after 5 hours, 69 ± 10% after 7 hours and 77 ± 4% after 24 hours. Total losses of microplastics are not time-dependent and were generally higher and more variable than for nanoplastics (14 ± 8% and 9 ± 4% for microplastics and nanoplastics, respectively, Supplementary Data page 217). Contrary to nanoplastics or others colloidal materials, microplastics are not a homogenous dispersion. Therefore, small losses of water mass can lead to large losses of microplastic particles. Also, due to their larger size, it is more likely that microplastics be retained in the vessel.

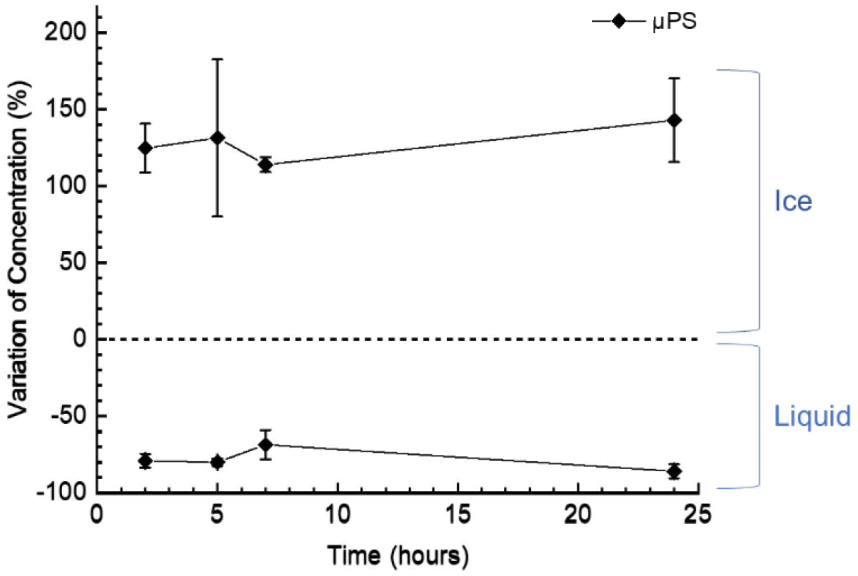


*Figure 5.14: Variation of the concentration of polystyrene microplastics (μPS) dispersed in 35 g $kg^{-1}$ NaCl at pH 8, and recovered in liquid and ice, as a function of the duration of freezing in the reactor*

Microplastics' incorporation in ice depends on their location at the moment of freezing. Since all microplastic particles studied here are buoyant, they were preferentially entrapped in the ice which grows from top to bottom. Since the volume of microplastics in ice are much higher than volume of brine pockets and channels it is expected that these particles are not solely trapped in brine pockets and channels (as are nanoplastics), but rather entrapped by the growing ice crystals. Microplastics' buoyancy is attributed to their density and to their hydrophobicity. Microplastics' density of 1055 kg $m^{-3}$ is relatively close to that of a solution of 35 g $kg^{-1}$ NaCl (1020 kg $m^{-3}$). Also, microplastics were hydrophobic since they were produced from pure PS which was mechanically degraded but not oxidized. Due to their hydrophobicity, a large part is attracted to the air/water interface due to the surface tension of water (Z. T. Anderson et al. 2018), similar to accumulation of microplastic at sea surface microlayer (Y. K. Song, Hong, Jang, et al. 2014). Mesocosm experiments also showed that during the initial stages of freezing, ice crystals preferentially trap low-density microplastics (Geilfus et al. 2019).

The use of initial microplastic mass concentrations that are higher than nanoplastic concentrations could lead to differences in the morphology and speed of the freezing front, and therefore to their microplastics' distribution between liquid and ice (Asthana and Tewari 1993; Tyagi, Monteux, and Sylvain Deville 2021). However, we observed no differences in the speed of advancement of the freezing front, in the proportion of liquid and ice formed, nor in the distribution of NaCl between liquid and ice. High particle concentrations can also lead to entrapped of multiple particles at a time which could lead to higher enrichment rate in ice (Tyagi, Monteux, and Sylvain Deville 2021). However,

this is a minor effect compared to the importance of the speed and morphology of the freezing front (Asthana and Tewari 1993; Körber 1988; Tyagi, Monteux, and Sylvain Deville 2021). Therefore, our conclusions about nanoplastics and microplastics behavior in saltwater remain valid despite our use of concentrations that are significantly higher than concentrations measured or estimated in the environment (Lenz, Enders, and Nielsen 2016).

Due to their large size, microplastics' movement is solely affected by gravity and water advection. In this experimental setup, there is only water convection caused by differences in salinity and temperature, which is minimal compared to the water flow expected in the Arctic Ocean. So, while we show that micrometric fragments of PS will be trapped by ice if they are in the vicinity of the ice front, processes are expected to be more complex in the environment. First of all, water turbulence can move microplastics into the sea ice matrix, comparable to microplastic transport in porous media. Secondly, differences in behavior can be expected depending on microplastic composition and shape. Microplastics in polar waters have a wide array of compositions (polyethylene, polyethylyene terephthalate, etc) and some studies suggest that the majority are fibers (Kanhai, Gardfeldt, et al. 2020; S.-K. Kim et al. 2021; Mu et al. 2019; Obbard et al. 2014; Ross et al. 2021). Finally, microplastics in the Arctic Ocean are mostly expected to come from distant areas. Therefore, their surface is expected to be highly oxidized and covered with an eco-corona. Due to this surface aging, they may be less hydrophobic and have less affinity for the air/water interface.

Based on this experimental work, we propose, for the first time, a distribution coefficient of nanoplastics and microplastics between ice and saltwater: $\log(\frac{C_{ice}}{C_{liquid}})$, illustrated in Figure 5.15 according to the freezing duration. This experimental work shows that plastic debris has size-dependent behavior at this saltwater/ice interface. This is expected from previous experiments and field studies concerned with the distribution of natural particles between saltwater and ice(Asthana and Tewari 1993; Dumont et al. 2009; Janssens et al. 2016; Kao, Golovin, and Davis 2009; Körber 1988; Tyagi, Monteux, and Sylvain Deville 2021). Indeed, the distribution coefficient is negative for nanoplastics (ranging from -0.27 to -1.10) and positive for microplastic (0.85 to 1.26). For both the microplastics and nanoplastics, except *nPS-360*, no clear evolution of the distribution coefficient is observed over time, showing the importance of the first stage of ice formation on the segregations of plastic debris according to their size. The continued expulsion of *nPS-360* in ice at 24 hours, should be further explored. These distribution coefficients can be used to inform numerical models of plastic debris' fate in the Arctic (Mountford and Morales Maqueda 2021).

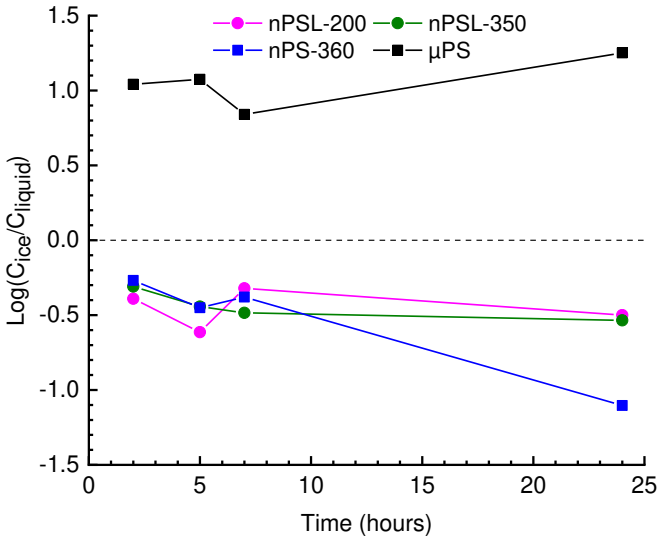


*Figure 5.15: Logarithm of nanoplastics' and microplastics' distribution between ice and liquid phase ($C_{ice}/C_{liquid}$) as a function of the duration of freezing in the freezing reactor. Experiments were conducted with 35 g $kg^{-1}$ NaCl and 50 mg $kg^{-1}$ SA.*

## 5.4 Conclusion

The different behaviors of micro- and nanoplastics expected during congelation growth of sea ice are summarized in Figure 5.16. Due to their colloidal nature, most nanoplastics are rapidly expulsed from ice, whether formed from freshwater (left) or saltwater (middle and right). The nanoplastics retained in freshwater ice may be strongly aggregated by the shear stress of growing ice crystals (aggregates not shown). Nanoplastics frozen in saltwater can accumulate in the brine pockets of sea ice. The growing ice front entraps non-colloidal plastics (microplastics). In saltwater, SA stabilized nanoplastics during freezing (right), suggesting that native NOM with high polysaccharide content will cause nanoplastics to remain suspended under sea ice. However, this saltwater/ice interface is also rich in sinking materials of chemical and biological origin such as gypsum and algae, which will propel nanoplastics down the water column to sediments (Hare et al. 2013; Thomas and Dieckmann 2003). So, while sea ice acts as a medium to short-term sink for microplastics, it may accelerate nanoplastics' sedimentation. This highlights the fact that sub-micrometric plastic debris cannot be lumped into the same category as microplastics (Gigault, El Hadri, Nguyen, et al. 2021).

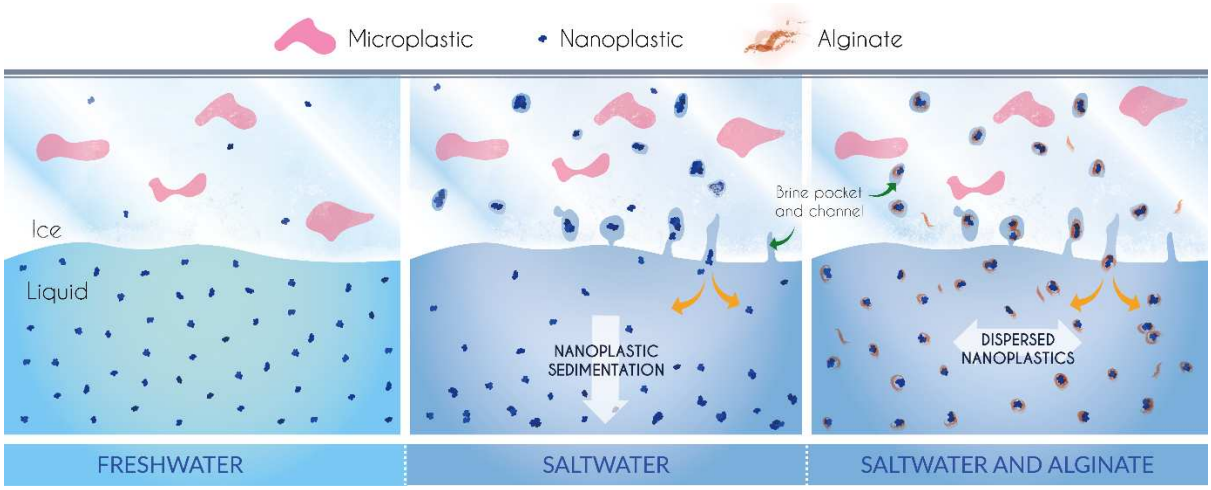


*Figure 5.16: Summary of nanoplastics' and microplastics' behaviors at the water/ice interface as a function of water composition*

## 5.5 Supplementary Data

*Summary of mass of initial solution ($M_{Init}$), liquid ($M_{Liq}$) and ice ($M_{Ice}$) solutions recovered from the freezing reactor, losses of liquid or NaCl recovered, SA or particle concentrations measured in the initial solution ($C_{Init}$), and in the Liquid ($C_{Liq}$) and Ice ($C_{Ice}$) solutions recovered from the freezing reactor; and proportion of initial SA or particle masses recovered in liquid and in ice.*
*Since SA is stable when frozen in NaCl (mass balance of -1 ± 4%), for mixtures containing plastics and SA in NaCl, for simplicity we only showed the concentrations and mass balances of particles. For nPSL-200 and nPS-360 with NaCl and SA, concentrations in ice are the average of ice recovered in the two duplicate experiments.*

| | Freezing duration | Mass of solution (g) | | | | NaCl Losses | Alginate Concentration (mg kg$^{-1}$) | | | Distribution of Initial Alginate Mass between | | |
|---|---|---|---|---|---|---|---|---|---|---|---|---|
| | (hours) | Initial | Liquid | Ice | Losses | | Initial | Liquid | Ice | Liquid | Ice | Losses |
| SA | 2 | 12.04 | 6.09 | 5.93 | 0% | | 21.49 | 31.57 | 11.20 | 74% | 26% | 0% |
| | 2 | 12.01 | 5.50 | 6.75 | -2% | | 21.49 | 30.45 | 9.13 | 65% | 24% | 11% |
| | 5 | 12.01 | 5.75 | 6.08 | 1% | | 21.70 | 31.78 | 3.87 | 70% | 9% | 21% |
| | 5 | 12.03 | 6.13 | 6.11 | -2% | | 21.70 | 30.49 | 7.83 | 72% | 18% | 10% |
| | 7 | 12.03 | 5.38 | 6.82 | -1% | | 28.71 | 50.04 | 9.64 | 78% | 19% | 3% |
| | 7 | 12.03 | 3.57 | 7.92 | 5% | | 28.71 | 48.99 | 12.69 | 51% | 29% | 20% |
| | 24 | 12.02 | 4.82 | 6.63 | 5% | | 20.67 | 29.82 | 6.14 | 58% | 16% | 26% |
| | 24 | 12.04 | 3.95 | 7.34 | 6% | | 20.67 | 49.26 | 6.56 | 78% | 19% | 2% |
| SA + NaCl | 2 | 12.02 | 7.22 | 4.20 | 5% | 8% | 20.38 | 25.29 | 11.65 | 74% | 27% | -1% |
| | 2 | 12.00 | 8.00 | 3.65 | 3% | 5% | 20.38 | 24.52 | 11.84 | 80% | 22% | -2% |
| | 5 | 12.05 | 7.69 | 3.97 | 3% | 9% | 25.03 | 28.98 | 15.37 | 74% | 27% | -1% |
| | 5 | 12.01 | 7.59 | 4.09 | 3% | 9% | 25.03 | 31.36 | 16.19 | 79% | 28% | -7% |
| | 7 | 12.01 | 8.22 | 4.21 | -3% | 3% | 25.54 | 26.57 | 12.42 | 71% | 24% | 5% |
| | 7 | 12.00 | 7.83 | 3.94 | 2% | 4% | 25.54 | 31.48 | 15.96 | 80% | 26% | -6% |
| | 24 | 12.01 | 7.48 | 3.84 | 6% | 9% | 20.56 | 29.73 | 5.00 | 90% | 9% | 1% |
| | 24 | 12.00 | 7.87 | 3.54 | 5% | 10% | 20.56 | 27.40 | 5.69 | 87% | 9% | 3% |
| | Freezing duration | Mass of solution (g) | | | | NaCl Losses | Particle Concentration (mg kg$^{-1}$) | | | Distribution of Initial Particle Mass between | | |
| | (hours) | Initial | Liquid | Ice | Losses | | Initial | Liquid | Ice | Liquid | Ice | Losses |
| nPSL-200 | 2 | 12.00 | 6.29 | 4.71 | 8% | | 10.18 | 13.93 | 1.46 | 72% | 6% | 23% |
| | 2 | 12.00 | 4.23 | 5.13 | 22% | | 10.18 | 10.81 | 2.68 | 37% | 32% | 31% |
| | 5 | 12.04 | 5.10 | 6.15 | 7% | | 10.90 | 14.43 | 1.74 | 56% | 8% | 36% |
| | 5 | 12.03 | 4.46 | 7.00 | 5% | | 10.90 | 14.99 | 1.61 | 51% | 9% | 40% |
| | 7 | 12.02 | 6.09 | 6.08 | -1% | | 10.95 | 13.75 | 1.38 | 64% | 6% | 30% |
| | 7 | 12.02 | 5.17 | 6.39 | 4% | | 10.95 | 14.70 | 1.35 | 58% | 7% | 36% |
| | 24 | 12.02 | 6.29 | 6.01 | -2% | | 14.08 | 18.33 | 2.44 | 68% | 9% | 23% |
| | 24 | 12.03 | 6.12 | 5.51 | 3% | | 14.08 | 18.84 | 2.52 | 68% | 8% | 24% |
| nPSL-200 + NaCl | 2 | 10.31 | 8.17 | 1.99 | 2% | 4% | 9.16 | 9.77 | 3.19 | 85% | 7% | 9% |
| | 2 | 12.11 | 8.21 | 3.83 | 1% | 4% | 9.16 | 10.19 | 3.89 | 75% | 13% | 11% |
| | 5 | 12.02 | 7.51 | 4.14 | 3% | 6% | 9.24 | 9.25 | 3.21 | 63% | 12% | 25% |
| | 5 | 12.03 | 7.94 | 3.69 | 3% | 12% | 9.24 | 8.28 | 2.67 | 59% | 9% | 32% |
| | 7 | 12.01 | 7.60 | 3.70 | 6% | 8% | 8.01 | 8.25 | 2.75 | 65% | 11% | 24% |
| | 7 | 12.01 | 8.26 | 3.42 | 3% | 6% | 8.01 | 7.54 | 3.01 | 65% | 11% | 25% |
| | 24 | 12.02 | 7.39 | 3.88 | 6% | 12% | 8.76 | 5.74 | 1.63 | 40% | 6% | 54% |
| | 24 | 12.02 | 8.33 | 3.38 | 3% | 9% | 8.76 | 5.50 | 2.14 | 44% | 7% | 50% |

| | Freezing duration | Mass of solution (g) | | | | NaCl Losses | Particle Concentration (mg kg$^{-1}$) | | | Distribution of Initial Particle Mass between | | |
|---|---|---|---|---|---|---|---|---|---|---|---|---|
| | (hours) | Initial | Liquid | Ice | Losses | | Initial | Liquid | Ice | Liquid | Ice | Losses |
| nPSL-200 + NaCl + SA | 2 | 10.30 | 7.46 | 2.56 | 3% | 11% | 8.87 | 9.21 | 3.86 | 75% | 11% | 14% |
| | 2 | 11.19 | 8.34 | 3.29 | -4% | 5% | 8.87 | 9.83 | 3.86 | 83% | 13% | 5% |
| | 5 | 11.13 | 7.79 | 3.30 | 0% | 7% | 8.95 | 9.83 | 4.78 | 77% | 16% | 7% |
| | 5 | 11.63 | 8.36 | 3.27 | 0% | 5% | 8.95 | 10.06 | 4.78 | 81% | 15% | 4% |
| | 7 | 10.88 | 7.56 | 3.28 | 0% | 8% | 8.96 | 9.87 | 3.32 | 77% | 11% | 12% |
| | 7 | 12.01 | 8.67 | 5.48 | -18% | 3% | 8.96 | 10.10 | 3.32 | 81% | 17% | 2% |
| | 24 | 12.59 | 7.72 | 4.12 | 6% | 15% | 8.71 | 10.28 | 2.41 | 72% | 9% | 19% |
| | 24 | 11.15 | 7.51 | 3.38 | 2% | 6% | 8.71 | 10.79 | 2.41 | 83% | 8% | 8% |
| nPS-360 + NaCl + SA | 2 | 11.08 | 7.58 | 3.23 | 2% | 11% | 8.78 | 10.04 | 5.39 | 78% | 18% | 4% |
| | 2 | 11.85 | 7.79 | 3.64 | 4% | 10% | 8.78 | 10.01 | 5.39 | 75% | 19% | 6% |
| | 5 | 11.34 | 8.20 | 5.16 | -18% | 6% | 10.25 | 10.81 | 3.79 | 76% | 17% | 7% |
| | 5 | 10.80 | 8.66 | 2.66 | -5% | 6% | 10.25 | 10.62 | 3.79 | 83% | 9% | 8% |
| | 7 | 11.51 | 7.88 | 3.52 | 1% | 8% | 10.93 | 12.28 | 5.18 | 77% | 14% | 9% |
| | 7 | 12.27 | 8.01 | 4.14 | 1% | 8% | 10.93 | 12.59 | 5.18 | 75% | 16% | 9% |
| | 24 | 9.94 | 7.76 | 2.26 | -1% | 1% | 10.68 | 12.62 | 1.00 | 92% | 2% | 6% |
| | 24 | 10.76 | 7.65 | 2.56 | 5% | 14% | 10.68 | 12.78 | 1.00 | 85% | 2% | 13% |
| nPSL-350 + NaCl + SA | 2 | 12.04 | 6.96 | 4.21 | 7% | 11% | 9.73 | 11.17 | 5.78 | 66% | 21% | 13% |
| | 2 | 12.03 | 8.00 | 3.43 | 5% | 7% | 9.73 | 10.92 | 5.12 | 75% | 15% | 10% |
| | 5 | 12.05 | 7.36 | 4.29 | 3% | 6% | 9.64 | 11.30 | 4.36 | 72% | 16% | 12% |
| | 5 | 12.02 | 7.99 | 3.83 | 2% | 4% | 9.64 | 10.92 | 3.62 | 75% | 12% | 13% |
| | 7 | 12.03 | 7.44 | 4.05 | 4% | 9% | 9.39 | 11.21 | 3.78 | 74% | 14% | 13% |
| | 7 | 12.01 | 7.86 | 3.84 | 3% | 6% | 9.39 | 10.72 | 3.37 | 75% | 11% | 14% |
| | 24 | 12.02 | 7.78 | 3.76 | 4% | 10% | 9.60 | 12.40 | 3.71 | 84% | 12% | 4% |
| | 24 | 12.03 | 8.22 | 3.45 | 3% | 9% | 9.60 | 11.53 | 3.33 | 82% | 10% | 8% |
| µPS + NaCl + SA | 2 | 12.00 | 7.93 | 3.77 | 3% | 8% | 4351 | 756 | 10396 | 11% | 75% | 14% |
| | 2 | 12.00 | 8.28 | 3.38 | 3% | 7% | 4382 | 1063 | 9446 | 17% | 61% | 23% |
| | 5 | 12.01 | 8.33 | 4.25 | -5% | 5% | 4075 | 712 | 8016 | 12% | 70% | 18% |
| | 5 | 12.01 | 8.83 | 3.67 | -4% | -1% | 4103 | 862 | 10948 | 15% | 82% | 3% |
| | 7 | 12.02 | 8.09 | 3.40 | 4% | 14% | 4141 | 1065 | 9037 | 17% | 62% | 21% |
| | 7 | 12.00 | 7.91 | 4.43 | -3% | 12% | 4340 | 1545 | 8952 | 23% | 76% | 0% |
| | 24 | 12.03 | 7.23 | 4.32 | 4% | NA | 4451 | 427 | 9859 | 6% | 80% | 15% |
| | 24 | 12.02 | 8.00 | 3.43 | 5% | 6% | 4443 | 707 | 11621 | 11% | 75% | 15% |

# References


Aagaard, Knut, L.K. Coachman, and Eddy Carmack (June 1981). "On the Halocline of the Arctic Ocean". en. In: *Deep Sea Research Part A. Oceanographic Research Papers* 28.6, pp. 529–545. ISSN: 01980149. DOI: 10.1016/0198-0149(81)90115-1.

Alimi, Olubukola S., Jeffrey M. Farner, and Nathalie Tufenkji (Feb. 2021). "Exposure of Nanoplastics to Freeze-Thaw Leads to Aggregation and Reduced Transport in Model Groundwater Environments". en. In: *Water Research* 189, p. 116533. ISSN: 00431354. DOI: 10.1016/j.watres.2020.116533.

Alimi, Olubukola S., Jeffrey Farner Budarz, Laura M. Hernandez, and Nathalie Tufenkji (Feb. 2018). "Microplastics and Nanoplastics in Aquatic Environments: Aggregation, Deposition, and Enhanced Contaminant Transport". en. In: *Environmental Science & Technology* 52.4, pp. 1704–1724. ISSN: 0013-936X, 1520-5851. DOI: 10.1021/acs.est.7b05559.

Amélineau, F., D. Bonnet, O. Heitz, V. Mortreux, A.M.A. Harding, N. Karnovsky, W. Walkusz, J. Fort, and D. Grémillet (Dec. 2016). "Microplastic Pollution in the Greenland Sea: Background Levels and Selective Contamination of Planktivorous Diving Seabirds". en. In: *Environmental Pollution* 219, pp. 1131–1139. ISSN: 02697491. DOI: 10.1016/j.envpol.2016.09.017.

Anderson, Zachary T., Andrew B. Cundy, Ian W. Croudace, Phillip E. Warwick, Omar Celis-Hernandez, and Jessica L. Stead (Dec. 2018). "A Rapid Method for Assessing the Accumulation of Microplastics in the Sea Surface Microlayer (SML) of Estuarine Systems". en. In: *Scientific Reports* 8.1, p. 9428. ISSN: 2045-2322. DOI: 10.1038/s41598-018-27612-w.

Asthana, R. and S. N. Tewari (Oct. 1993). "The Engulfment of Foreign Particles by a Freezing Interface". en. In: *Journal of Materials Science* 28.20, pp. 5414–5425. ISSN: 0022-2461, 1573-4803. DOI: 10.1007/BF00367810.

Baalousha, M. and J. R. Lead (June 2012). "Rationalizing Nanomaterial Sizes Measured by Atomic Force Microscopy, Flow Field-Flow Fractionation, and Dynamic Light Scattering: Sample Preparation, Polydispersity, and Particle Structure". en. In: *Environmental Science & Technology* 46.11, pp. 6134–6142. ISSN: 0013-936X, 1520-5851. DOI: 10.1021/es301167x.

Barb, W. G. and W. Mikucki (1959). "On the Coagulation of Polymer Latices by Freezing and Thawing". In: *Journal of Polymer Science* 37.132, pp. 499–514. DOI: 10.1002/pol.1959.1203713219. eprint: https://onlinelibrary.wiley.com/doi/pdf/10.1002/pol.1959.1203713219.

Benner, Ronald (Jan. 2002). "Chapter 3 - Chemical Composition and Reactivity". In: *Biogeochemistry of Marine Dissolved Organic Matter*. Ed. by Dennis A. Hansell and Craig A. Carlson. San Diego: Academic Press, pp. 59–90. ISBN: 978-0-12-323841-2. DOI: 10.1016/B978-012323841-2/50005-1.

Bergmann, Melanie, Vanessa Wirzberger, Thomas Krumpen, Claudia Lorenz, Sebastian Primpke, Mine B. Tekman, and Gunnar Gerdts (Oct. 2017). "High Quantities of Microplastic in Arctic Deep-Sea Sediments from the HAUSGARTEN Observatory". en. In: *Environmental Science & Technology* 51.19, pp. 11000–11010. ISSN: 0013-936X, 1520-5851. DOI: 10.1021/acs.est.7b03331.

Boyer, T. P., O.K. Baranova, M. Biddle, D.R. Johnson, A.V. Mishonov, C. Paver, D Seidov, and M Zweng (2012). "Arctic Regional Climatology, Regional Climatology Team, NOAA/NODC". In: DOI: doi:10.7289/V5QC01J0.

Bronstein, V.L., Y.A. Itkin, and G.S. Ishkov (Apr. 1981). "Rejection and Capture of Cells by Ice Crystals on Freezing Aqueous Solutions". In: *Journal of Crystal Growth* 52, pp. 345–349. ISSN: 00220248. DOI: 10.1016/0022-0248(81)90216-5.

Chou, Kan-Sen, Hsuan-Liang Liu, Li-Hsing Kao, Chi-Ming Yang, and Shu-Hao Huang (Apr. 2014). "A Quick and Simple Method to Test Silica Colloids' Ability to Resist Aggregation". en. In: *Colloids and Surfaces A: Physicochemical and Engineering Aspects* 448, pp. 115–118. ISSN: 09277757. DOI: 10.1016/j.colsurfa.2014.02.020.

Cózar, Andrés, Elisa Martí, Carlos M. Duarte, Juan García-de-Lomas, Erik van Sebille, Thomas J. Ballatore, Victor M. Eguíluz, J. Ignacio González-Gordillo, Maria L. Pedrotti, Fidel Echevarría, Romain Troublè, and Xabier Irigoien (Apr. 2017). "The Arctic Ocean as a Dead End for Floating Plastics in the North Atlantic Branch of the Thermohaline Circulation". In: *Science Advances* 3.4, e1600582. DOI: 10.1126/sciadv.1600582.

Crabeck, O, R J Galley, B Delille, and B G T Else (2015). "Imaging Air Volume Fraction in Sea Ice Using Non-Destructive X-Ray Tomography". en. In: *Discussion Paper*, p. 49.

Deville, S. (Mar. 2008). "Freeze-Casting of Porous Ceramics: A Review of Current Achievements and Issues". en. In: *Advanced Engineering Materials* 10.3, pp. 155–169. ISSN: 14381656, 15272648. DOI: 10.1002/adem.200700270.

Dumont, I., V. Schoemann, D. Lannuzel, L. Chou, J.-L. Tison, and S. Becquevort (May 2009). "Distribution and Characterization of Dissolved and Particulate Organic Matter in Antarctic Pack Ice". en. In: *Polar Biology* 32.5, pp. 733–750. ISSN: 0722-4060, 1432-2056. DOI: 10.1007/s00300-008-0577-y.

Eicken, Hajo (May 2003). "From the Microscopic, to the Macroscopic, to the Regional Scale: Growth, Microstructure and Properties of Sea Ice". en. In: *Sea Ice*. Ed. by David N. Thomas and Gerhard S. Dieckmann. Oxford, UK: Blackwell Science Ltd, pp. 22–81. ISBN: 978-0-470-75716-1 978-0-632-05808-2. DOI: 10.1002/9780470757161.ch2.

El Hadri, Hind, Julien Gigault, Benoit Maxit, Bruno Grassl, and Stéphanie Reynaud (2020). "Nanoplastic from Mechanically Degraded Primary and Secondary Microplastics for Environmental Assessments". In: *NanoImpact*, p. 100206. ISSN: 2452-0748. DOI: 10.1016/j.impact.2019.100206.

Flemming, Hans-Curt and Jost Wingender (Sept. 2010). "The Biofilm Matrix". en. In: *Nature Reviews Microbiology* 8.9, pp. 623–633. ISSN: 1740-1526, 1740-1534. DOI: 10.1038/nrmicro2415.

Geilfus, N.-X., K.M. Munson, J. Sousa, Y. Germanov, S. Bhugaloo, D. Babb, and F. Wang (Aug. 2019). "Distribution and Impacts of Microplastic Incorporation within Sea Ice". en. In: *Marine Pollution Bulletin* 145, pp. 463–473. ISSN: 0025326X. DOI: 10.1016/j.marpolbul.2019.06.029.

GESAMP (2015). *Sources, Fate and Effects of Microplastics in the Marine Environment: A Global Assessment*. English. Ed. by PJ Kershaw. GESAMP Reports & Studies Series 90. GESAMP (Group of Experts on the Scientific Aspects of Marine Environmental Protection). ISBN: 1020-4873.

Geyer, Roland, Jenna R. Jambeck, and Kara Lavender Law (July 2017). "Production, Use, and Fate of All Plastics Ever Made". en. In: *Science Advances* 3.7, e1700782. ISSN: 2375-2548. DOI: 10.1126/sciadv.1700782.

Giannelli, Virginia, David N. Thomas, Christian Haas, Gerhard Kattner, Hilary Kennedy, and Gerhard S. Dieckmann (2001). "Behaviour of Dissolved Organic Matter and Inorganic Nutrients during Experimental Sea-Ice Formation". en. In: *Annals of Glaciology* 33, pp. 317–321. ISSN: 0260-3055, 1727-5644. DOI: 10.3189/172756401781818572.

Gigault, Julien, Hind El Hadri, Brian Nguyen, Bruno Grassl, Laura Rowenczyk, Nathalie Tufenkji, Siyuan Feng, and Mark Wiesner (May 2021). "Nanoplastics Are Neither Microplastics nor Engineered Nanoparticles". In: *Nature Nanotechnology* 16.5, pp. 501–507. ISSN: 1748-3395. DOI: 10.1038/s41565-021-00886-4.

Grossmann, Sönnke and Markus Gleitz (Nov. 1993). "Microbial Responses to Experimental Sea-Ice Formation: Implications for the Establishment of Antarctic Sea-Ice Communities". en. In: *Journal of Experimental Marine Biology and Ecology* 173.2, pp. 273–289. ISSN: 00220981. DOI: 10.1016/0022-0981(93)90058-V.

Hare, A.A., F. Wang, D. Barber, N.-X. Geilfus, R.J. Galley, and S. Rysgaard (Aug. 2013). "pH Evolution in Sea Ice Grown at an Outdoor Experimental Facility". en. In: *Marine Chemistry* 154, pp. 46–54. ISSN: 03044203. DOI: 10.1016/j.marchem.2013.04.007.

Horton, Alice A., Alexander Walton, David J. Spurgeon, Elma Lahive, and Claus Svendsen (May 2017). "Microplastics in Freshwater and Terrestrial Environments: Evaluating the Current Understanding to Identify the Knowledge Gaps and Future Research Priorities". en. In: *Science of The Total Environment* 586, pp. 127–141. ISSN: 00489697. DOI: 10.1016/j.scitotenv.2017.01.190.

Hullar, Ted and Cort Anastasio (Sept. 2016). "Direct Visualization of Solute Locations in Laboratory Ice Samples". en. In: *The Cryosphere* 10.5, pp. 2057–2068. ISSN: 1994-0424. DOI: 10.5194/tc-10-2057-2016.

Ito, Masato, Kay I. Ohshima, Yasushi Fukamachi, Daisuke Hirano, Andrew R. Mahoney, Joshua Jones, Toru Takatsuka, and Hajo Eicken (Dec. 2019). "Favorable Conditions for Suspension Freezing in an Arctic Coastal Polynya". en. In: *Journal of Geophysical Research: Oceans* 124.12, pp. 8701–8719. ISSN: 2169-9275, 2169-9291. DOI: 10.1029/2019JC015536.

Janssens, Julie, Klaus M. Meiners, Jean-Louis Tison, Gerhard Dieckmann, Bruno Delille, and Delphine Lannuzel (Aug. 2016). "Incorporation of Iron and Organic Matter into Young Antarctic Sea Ice during Its Initial Growth Stages". en. In: *Elem Sci Anth* 4.0, p. 000123. ISSN: 2325-1026. DOI: 10.12952/journal.elementa.000123.

Kanhai, La Daana K., Katarina Gardfeldt, Thomas Krumpen, Richard C. Thompson, and Ian O'Connor (Dec. 2020). "Microplastics in Sea Ice and Seawater beneath Ice Floes from the Arctic Ocean". en. In: *Scientific Reports* 10.1, p. 5004. ISSN: 2045-2322. DOI: 10.1038/s41598-020-61948-6.

Kanhai, La Daana K., Katarina Gårdfeldt, Olga Lyashevska, Martin Hassellöv, Richard C. Thompson, and Ian O'Connor (May 2018). "Microplastics in Sub-Surface Waters of the Arctic Central Basin". en. In: *Marine Pollution Bulletin* 130, pp. 8–18. ISSN: 0025326X. DOI: 10.1016/j.marpolbul.2018.03.011.

Kao, Justin C. T., Alexander A. Golovin, and Stephen H. Davis (Apr. 2009). "Particle Capture in Binary Solidification". en. In: *Journal of Fluid Mechanics* 625, pp. 299–320. ISSN: 0022-1120, 1469-7645. DOI: 10.1017/S0022112008005570.

Kelly, A., D. Lannuzel, T. Rodemann, K.M. Meiners, and H.J. Auman (May 2020). "Microplastic Contamination in East Antarctic Sea Ice". en. In: *Marine Pollution Bulletin* 154, p. 111130. ISSN: 0025326X. DOI: 10.1016/j.marpolbul.2020.111130.

Kim, Seung-Kyu, Hee-Jee Lee, Ji-Su Kim, Sung-Ho Kang, Eun-Jin Yang, Kyoung-Ho Cho, Zhexi Tian, and Anthony Andrady (May 2021). "Importance of Seasonal Sea Ice in the Western Arctic Ocean to the Arctic and Global Microplastic Budgets". In: *Journal of Hazardous Materials*, p. 125971. ISSN: 0304-3894. DOI: 10.1016/j.jhazmat.2021.125971.

Körber, Christoph (May 1988). "Phenomena at the Advancing IceLiquid Interface: Solutes, Particles and Biological Cells". en. In: *Quarterly Reviews of Biophysics* 21.2, pp. 229–298. ISSN: 0033-5835, 1469-8994. DOI: 10.1017/S0033583500004303.

Kowalik, Zygmunt and J. B. Matthews (Mar. 1983). "Numerical Study of the Water Movement Driven by Brine Rejection from Nearshore Arctic Ice". In: *Journal of*

*Geophysical Research: Oceans* 88.C5, pp. 2953–2958. ISSN: 0148-0227. DOI: 10.1029/JC088iC05p02953.

Krembs, C, H Eicken, K Junge, and J.W Deming (Dec. 2002). "High Concentrations of Exopolymeric Substances in Arctic Winter Sea Ice: Implications for the Polar Ocean Carbon Cycle and Cryoprotection of Diatoms". In: *Deep Sea Research Part I: Oceanographic Research Papers* 49.12, pp. 2163–2181. ISSN: 0967-0637. DOI: 10.1016/S0967-0637(02)00122-X.

Lake, R. A. and E. L. Lewis (Jan. 1970). "Salt Rejection by Sea Ice during Growth". en. In: *Journal of Geophysical Research* 75.3, pp. 583–597. ISSN: 01480227. DOI: 10.1029/JC075i003p00583.

Lenz, Robin, Kristina Enders, and Torkel Gissel Nielsen (July 2016). "Microplastic Exposure Studies Should Be Environmentally Realistic". en. In: *Proceedings of the National Academy of Sciences* 113.29, E4121–E4122. ISSN: 0027-8424, 1091-6490. DOI: 10.1073/pnas.1606615113.

Lusher, Amy L., Valentina Tirelli, Ian O'Connor, and Rick Officer (Oct. 2015). "Microplastics in Arctic Polar Waters: The First Reported Values of Particles in Surface and Sub-Surface Samples". In: *Scientific Reports* 5.1, p. 14947. ISSN: 2045-2322. DOI: 10.1038/srep14947.

Morgana, Silvia, Laura Ghigliotti, Noelia Estévez-Calvar, Roberto Stifanese, Alina Wieckzorek, Tom Doyle, Jørgen S. Christiansen, Marco Faimali, and Francesca Garaventa (Nov. 2018). "Microplastics in the Arctic: A Case Study with Sub-Surface Water and Fish Samples off Northeast Greenland". en. In: *Environmental Pollution* 242, pp. 1078–1086. ISSN: 02697491. DOI: 10.1016/j.envpol.2018.08.001.

Mountford, A. S. and M. A. Morales Maqueda (Feb. 2021). "Modeling the Accumulation and Transport of Microplastics by Sea Ice". en. In: *Journal of Geophysical Research: Oceans* 126.2. ISSN: 2169-9275, 2169-9291. DOI: 10.1029/2020JC016826.

Mu, Jingli, Shoufeng Zhang, Ling Qu, Fei Jin, Chao Fang, Xindong Ma, Weiwei Zhang, and Juying Wang (June 2019). "Microplastics Abundance and Characteristics in Surface Waters from the Northwest Pacific, the Bering Sea, and the Chukchi Sea". en. In: *Marine Pollution Bulletin* 143, pp. 58–65. ISSN: 0025326X. DOI: 10.1016/j.marpolbul.2019.04.023.

Nürnberg, D., I. Wollenburg, D. Dethleff, H. Eicken, H. Kassens, T. Letzig, E. Reimnitz, and J. Thiede (July 1994). "Sediments in Arctic Sea Ice: Implications for Entrainment, Transport and Release". en. In: *Marine Geology* 119.3-4, pp. 185–214. ISSN: 00253227. DOI: 10.1016/0025-3227(94)90181-3.

Obbard, Rachel W. (Feb. 2018). "Microplastics in Polar Regions: The Role of Long Range Transport". en. In: *Current Opinion in Environmental Science & Health* 1, pp. 24–29. ISSN: 24685844. DOI: 10.1016/j.coesh.2017.10.004.

Obbard, Rachel W., Saeed Sadri, Ying Qi Wong, Alexandra A. Khitun, Ian Baker, and Richard C. Thompson (June 2014). "Global Warming Releases Microplastic Legacy Frozen in Arctic Sea Ice". en. In: *Earth's Future* 2.6, pp. 315–320. ISSN: 23284277. DOI: 10.1002/2014EF000240.

Peeken, Ilka, Sebastian Primpke, Birte Beyer, Julia Gütermann, Christian Katlein, Thomas Krumpen, Melanie Bergmann, Laura Hehemann, and Gunnar Gerdts (Dec. 2018). "Arctic Sea Ice Is an Important Temporal Sink and Means of Transport for Microplastic". en. In: *Nature Communications* 9.1. ISSN: 2041-1723. DOI: 10.1038/s41467-018-03825-5.

Popova, Ekaterina E., Andrew Yool, Andrew C. Coward, Frederic Dupont, Clara Deal, Scott Elliott, Elizabeth Hunke, Meibing Jin, Mike Steele, and Jinlun Zhang (Aug. 2012). "What Controls Primary Production in the Arctic Ocean? Results from an Intercomparison of Five General Circulation Models with Biogeochemistry: PRIMARY PRODUCTION IN THE ARCTIC OCEAN". en. In: *Journal of Geophysical Research: Oceans* 117.C8, n/a–n/a. ISSN: 01480227. DOI: 10.1029/2011JC007112.

Pradel, Alice, Séléna Ferreres, Cloé Veclin, Hind El Hadri, Maud Gautier, Bruno Grassl, and Julien Gigault (Mar. 2021). "Stabilization of Fragmental Polystyrene Nanoplastic by Natural Organic Matter: Insight into Mechanisms". en. In: *ACS ES&T Water*, acsestwater.0c00283. ISSN: 2690-0637. DOI: 10.1021/acsestwater.0c00283.

Programme, UN Environment (June 2018). *The State of Plastics*. Tech. rep., p. 20.

Reimnitz, Erk, J.R. Clayton, E.W. Kempema, J.R. Payne, and W.S. Weber (1993). "Interaction of Rising Frazil with Suspended Particles: Tank Experiments with Applications to Nature". In: *Cold Regions Science and Technology* 21.2, pp. 117–135. ISSN: 0165-232X. DOI: 10.1016/0165-232X(93)90002-P.

Ross, Peter S., Stephen Chastain, Ekaterina Vassilenko, Anahita Etemadifar, Sarah Zimmermann, Sarah-Ann Quesnel, Jane Eert, Eric Solomon, Shreyas Patankar, Anna M. Posacka, and Bill Williams (Dec. 2021). "Pervasive Distribution of Polyester Fibres in the Arctic Ocean Is Driven by Atlantic Inputs". In: *Nature Communications* 12.1, p. 106. ISSN: 2041-1723. DOI: 10.1038/s41467-020-20347-1.

SAPEA, Science Advice for Policy by European Academies (2019). *A Scientific Perspective on Microplastics in Nature and Society*. en. Berlin: SAPEA. ISBN: 978-3-9820301-0-4.

Song, Young Kyoung, Sang Hee Hong, Mi Jang, Jung-Hoon Kang, Oh Youn Kwon, Gi Myung Han, and Won Joon Shim (Aug. 2014). "Large Accumulation of Micro-Sized Synthetic Polymer Particles in the Sea Surface Microlayer". en. In: *Environmental Science & Technology*

48.16, pp. 9014–9021. ISSN: 0013-936X, 1520-5851. DOI: 10.1021/es501757s.

Stroeve, Julienne and Dirk Notz (Sept. 2018). "Changing State of Arctic Sea Ice across All Seasons". en. In: *Environmental Research Letters* 13.10, p. 103001. ISSN: 1748-9326. DOI: 10.1088/1748-9326/aade56.

Tekman, Mine B., Claudia Wekerle, Claudia Lorenz, Sebastian Primpke, Christiane Hasemann, Gunnar Gerdts, and Melanie Bergmann (Apr. 2020). "Tying up Loose Ends of Microplastic Pollution in the Arctic: Distribution from the Sea Surface through the Water Column to Deep-Sea Sediments at the HAUSGARTEN Observatory". en. In: *Environmental Science & Technology* 54.7, pp. 4079–4090. ISSN: 0013-936X, 1520-5851. DOI: 10.1021/acs.est.9b06981.

Thomas, David N. and Gerhard Dieckmann (2003). *Sea Ice: An Introduction to Its Physics, Chemistry, Biology, and Geology*. en. Oxford, UK ; Malden, MA, USA: Blackwell Science. ISBN: 978-0-632-05808-2.

Tyagi, Sidhanth, Cécile Monteux, and Sylvain Deville (Dec. 2021). "Multiple Objects Interacting with a Solidification Front". en. In: *Scientific Reports* 11.1, p. 3513. ISSN: 2045-2322. DOI: 10.1038/s41598-021-82713-3.

van Sebille, Erik, Matthew H England, and Gary Froyland (Dec. 2012). "Origin, Dynamics and Evolution of Ocean Garbage Patches from Observed Surface Drifters". en. In: *Environmental Research Letters* 7.4, p. 044040. ISSN: 1748-9326. DOI: 10.1088/1748-9326/7/4/044040.

Worster, M. Grae and David W. Rees Jones (2015). "Sea-Ice Thermodynamics and Brine Drainage". In: *Philosophical Transactions of the Royal Society A: Mathematical, Physical and Engineering Sciences* 373.2045, p. 20140166.

Xu, R. (2006). *Particle Characterization: Light Scattering Methods*. Springer Netherlands. ISBN: 978-0-306-47124-7.

Yakushev, Evgeniy, Anna Gebruk, Alexander Osadchiev, Svetlana Pakhomova, Amy Lusher, Anfisa Berezina, Bert van Bavel, Elena Vorozheikina, Denis Chernykh, Glafira Kolbasova, Ilia Razgon, and Igor Semiletov (Dec. 2021). "Microplastics Distribution in the Eurasian Arctic Is Affected by Atlantic Waters and Siberian Rivers". In: *Communications Earth & Environment* 2.1, p. 23. ISSN: 2662-4435. DOI: 10.1038/s43247-021-00091-0.

Yemmou, M., A. Brierre, and M.A. Azouni (Jan. 1991). "Rejection and Capture of Solid Particles by Ice". In: *Advances in Space Research* 11.7, pp. 327–330. ISSN: 02731177. DOI: 10.1016/0273-1177(91)90302-Z.

# Chapter 6

# Conclusion and Perspectives

This work has improved our understanding of nanoplastics' potential environmental fate by using more environmentally relevant nanoplastic models and by focusing on environmental interfaces through which nanoplastics are expected to transit. Model nanoplastic particles produced from the mechanical fragmentation of polystyrene pellets had non-spherical, irregular shapes, polydisperse sizes, and a moderate negative charge. Due to these different physicochemical properties, they had a different behavior compared to the commercial polystyrene latex size-standard particles (spherical, monodisperse, and with strong surface charges).

Differences in behavior between these nanoplastic models were assessed by modeling environmental interfaces in simplified lab conditions. Solution chemistry was simplified by using i) only monovalent salts that do not form surface complexes (i.e.: sodium chloride) as electrolytes, ii) purified NOMs (humic and alginic acids), and iii) no other particulate matter. The properties of terrestrial interfaces were also simplified by conceptualizing these as porous media. Indeed, the porosity of terrestrial interfaces can arise from other geometries than homogenously dispersed pores, such as, for example, networks of fissures and fractures. Furthermore, the porous media used had homogenous chemical composition (quartz sand or a silicone polymer), whereas soils, sediments, and aquifers, like aqueous solutions, have heterogeneous and complex compositions. Finally, modeling the interface between seawater and ice also required substantial simplifications. Once again, the solution composition was simplified to obtain create an ionic strength equivalent to the ionic strength of seawater, without all the multivalent ions, dissolved or particulate matter. Also, the sea ice was produced by freezing the solution at a constant temperature in non-turbulent conditions, which is an idealized condition. A further limitation of all studies is that they focus only on abiotic processes, while biotic processes occur in all environmental systems.

Mimicking these environmental systems with highly simplified experimental condi-

tions revealed differences in nanoplastic models' behavior was attributable to differences in shape and surface properties (i.e.: charge, roughness, and surface tension), which modified their hydrodynamic behavior and interaction energies. Compared to the commonly-used commercial polystyrene latex (PSL) size-standard particles, fragmental polystyrene particles were more sensitive to aggregation caused by the screening of electrostatic repulsion. This suggests that nanoplastics dispersed in natural waters are more likely to settle in the sediments of lakes, rivers, but mostly in the sediments of oceans, compared to initial predictions made with PSL. Fragmental polystyrene was also more likely to be deposited and retained in porous media, pointing towards an accumulation in soils, aquifers, and sediments. However, concerning the interface between seawater and sea ice, all nanoplastic models showed similar behavior: they were mainly expulsed into the underlying water column during the growth of saline ice and partly accumulated in the brine pockets of ice.

In each of these scenarios (i.e.: aggregation, deposition, expulsion from saline ice), the presence of NOM significantly modified the behavior of fragmental nanoplastics. Both humic and alginic acids stabilized fragmental nanoplastics against aggregation at high ionic strength, albeit with different mechanisms. These two NOMs also reduced their rate of deposition in porous media. Furthermore, alginic acid also stabilized nanoplastics at the interface between saltwater and saline ice. This suggests that the concentration and type of NOM in environmental systems strongly impact nanoplastics' fate. For example, nanoplastics may be more abundant in the water column of mesotrophic lakes than oligotrophic lakes. Nanoplastics may also have longer residence periods in polar surface waters with high biological activity and high microbial and algal exudates, compared to polar surface waters with low biological activity.

However, this progress in understanding how nanoplastics may behave in the environment must be completed by further investigations. In particular, studies can be improved by using other types of environmentally relevant nanoplastic models and more complex and realistic solution compositions and environmental interfaces. Also, numerical models that incorporate results from experimental models should be developed to gain insight into nanoplastics' accumulation zones. It is also essential to verify the hypothesis put forward by characterizing nanoplastics in environmental samples. Finally, contamination by nanoplastics should always be assessed in light of the multiple and interconnected environmental stressors, such as climate change, loss of biodiversity, etc.

1. Environmentally relevant nanoplastic models

   The fragmental nanoplastic models used during this thesis were produced by mechanical abrasion of polystyrene. However, different types of plastics and degradation processes can be used to produce nanoplastic models for experiments. For the

scientific community to efficiently address the issue of contamination by nanoplastics, it is essential to determine i) which types of plastics are most likely to degrade into nanoplastics and ii) which processes and are most likely to produce nanoplastics. Resolving this could allow us to produce, characterize, and then study nanoplastic models in experimental setups that are most representative of environmental nanoplastics, and therefore to draw more accurate conclusions about their environmental behavior.

Most of the research concerning nanoplastics has studied PS nanoplastic. However, nanoplastic models composed of other polymers inherently have different physicochemical properties. For example, PP are much more hydrophobic than polyamides (e.g.: nylons)(Min, Cuiffi, and Mathers 2020). Therefore, we can expect PP particles to have a stronger affinity for hydrophobic surfaces and to be more rapidly coated by hydrophobic or amphiphilic NOM than polyamides. Also, when subject to a specific degradation process, different polymers age differently. For example, when subject to mechanical degradation, PE produced smaller particles than PS (El Hadri et al. 2020). A wide diversity of compositions and shapes of nanoplastics can be formed because plastics' properties depend not only on the chemical structure of a polymer but also on the type of additives it contains and the type of manufacturing process it has undergone. For example, commercial plastic objects that were subject to the same process of mechanical abrasion were degraded into different shapes. Low-density PE garbage bags degraded into elongated particles, single-use PS plates were quickly embrittled into crumbs, single-use PP cups formed rectangular shapes, and expanded PS insulation sheets had spheroidal shapes (Efimova et al. 2018). This illustrates the diversity of shapes that can be expected for plastic objects subject to only one degradation mechanism.

Furthermore, a wide array of types and combinations of degradation processes exist, each of which produce different particle properties. For example, photo-oxidation can be expected to induce the formation of more electronegative particles than mechanical degradation. Indeed, the reactive functional groups produced by photo-oxidation of plastic surfaces are often negatively charged in water.

Since nanoplastics can have a myriad of properties, constraining which nanoplastic models are environmentally relevant is a complex task. Therefore, another approach to study environmentally relevant nanoplastics models is to extract nanoplastics from the weathered surfaces of plastic debris that has aged in the environment. This can produce nanoplastic models representative of specific contamination zones, as has recently been done with marine debris (Blancho et al. 2021).

2. Environmentally realistic solutions chemistries and interfaces.

   To further advance our global understanding of nanoplastics' fate in the environment, it is necessary to assess their behavior in environmentally realistic solution chemistries and interfaces. Based on the knowledge that I have acquired during my doctoral thesis, the following directions for future research seem promising:

   First, the effect of particulate matter on nanoplastics' stability must be better assessed. Indeed, so far, the few studies that have studied this topic have revealed that nanoplastics rapidly hetero-aggregate with particulate matter. The speed at which this hetero-aggregation causes settling must be assessed to determine which ecosystems are at risk. Furthermore, there is the possibility that the incorporation of large quantities of nanoplastics may modify the density of aggregates, in turn reducing or increasing their speed of sedimentation.

   Second, it is unrealistic to test all possible combinations of solution chemistries and environmental interfaces. Therefore, an efficient strategy (and one that has already been proposed for nanomaterials) would consist in assessing nanoplastics behavior in a selected number of standardized solutions and environmental interfaces(Hendren et al. 2015). For example, artificial seawaters and freshwaters with a few different degrees of water hardness can be easily recreated in laboratory experiments. However, particulate matter and dissolved organic matter are not prescribed in these artificial solutions. Due to these species' impact on nanoplastics' aggregation rate and their abundance in natural waters, it would be advisable to amend standardized solutions with types and concentrations of particulate matter and dissolved organic matter that are similar to those present in natural waters.

   Finally, studying environmental interfaces has proven to be an efficient way to determine potential accumulation zones for nanoplastics. Similar to the study of solution chemistries, the study of nanoplastics transfer through environmental interfaces, such as porous media, estuaries, seawater/sea ice interfaces, surface/air interfaces, etc., can benefit from the complementary approaches of assessing mechanisms in simplified systems and then, evaluating realistic scenarios in a select subset of more complex systems.

3. Numerical modeling and characterization of environmental samples

   Experimental models effectively identify and quantify physicochemical processes that can lead to nanoplastic accumulation in specific environmental systems. However, nanoplastic concentrations must be quantified in environmental systems to verify the validity of experimental results and conclusions. Quantifying nanoplastics

in environmental matrices is inherently complicated since nanoplastics are carbon-based particles and natural environments are carbon-rich. Indeed, nanoplastics have recently been detected in the North Atlantic Ocean (Ter Halle et al. 2017) and soils (Wahl et al. 2021) but have not been quantified.

To facilitate this endeavor, many analytical methods are being developed that allow the characterization and quantification of increasingly small and diluted plastic particles, as has been reviewed recently (Ivleva 2021; Schwaferts et al. 2019). Besides improving analytical methods, it is also advisable to analyze environmental samples that are expected to be highly contaminated to facilitate quantification. In this respect, numerical models can help predict which environmental compartments are most likely to accumulate nanoplastics. For example, numerical models, can predict the fate of plastic particles by modeling their advection by water currents and attachment efficiency ($\alpha$) to natural particles (Besseling et al. 2017). These can help predict where nanoplastics accumulate if $\alpha$ has been determined with environmentally relevant nanoplastics and natural species models. Therefore, to characterize the risk posed by this emerging contaminant, coming to grasps with nanoplastics' environmental fate requires the joint effort of scientists from many disciplines: analytical chemistry, mathematics, physics, and environmental engineers, etc.

4. Nanoplastics as one of multiple environmental stressors

   Finally, assessing nanoplastics fate in the environment must take into account the fact that environmental issues are interrelated with one another (Arp et al. 2021). Indeed, environmental systems are subject to multiple stressors, such as a variety of chemical pollutants, climate change, loss of biodiversity, soil erosion, ocean acidification, etc., which are interlinked and can have compounded, unforeseen effects, with unknown repercussions on Earth-system processes (Rockström et al. 2009; Villarrubia-Gómez, Cornell, and Fabres 2018). For example, in polar systems plastic contamination is only one one of multiple stressors, such as accumulation of anthropic contaminants (Muir and de Wit 2010), spreading of invasive species (Barnes and Milner 2005), and the more pronounced effects of climate change and water acidification compared to temperate environments (Stocker et al. 2018; Stroeve and Notz 2018; Qi et al. 2017). These issues are interconnected. For example, ocean acidification, by dissolving carbonates, may diminish the rate of nanoplastics and microplastics' hetero-aggregation and settling (L. Galgani and S. Loiselle 2019). Also, invasive species could be more resistant to ingestion of plastic debris compared to native species, which would further aggravate biodiversity loss. On a

global scale, the extent to which plastic debris is either mineralized (into $CO_2$ and elemental building blocks) or incorporated into sediments as larger objects or particles, will impact Earth's greenhouse gas budget. Addressing these issues inevitably requires interdisciplinary collaboration.

# References


Arp, Hans Peter H., Dana Kühnel, Christoph Rummel, Matthew MacLeod, Annegret Potthoff, Sophia Reichelt, Elisa Rojo-Nieto, Mechthild Schmitt-Jansen, Johanna Sonnenberg, Erik Toorman, and Annika Jahnke (May 2021). "Weathering Plastics as a Planetary Boundary Threat: Exposure, Fate, and Hazards". en. In: *Environmental Science & Technology*, acs.est.1c01512. ISSN: 0013-936X, 1520-5851. DOI: 10.1021/acs.est.1c01512.

Barnes, D. K. A. and P. Milner (Mar. 2005). "Drifting Plastic and Its Consequences for Sessile Organism Dispersal in the Atlantic Ocean". In: *Marine Biology* 146.4, pp. 815–825. ISSN: 1432-1793. DOI: 10.1007/s00227-004-1474-8.

Besseling, Ellen, Joris T.K. Quik, Muzhi Sun, and Albert A. Koelmans (Jan. 2017). "Fate of Nano- and Microplastic in Freshwater Systems: A Modeling Study". en. In: *Environmental Pollution* 220, pp. 540–548. ISSN: 02697491. DOI: 10.1016/j.envpol.2016.10.001.

Blancho, Florent, Mélanie Davranche, Francesco Fumagalli, Giacomo Ceccone, and Julien Gigault (2021). "A Reliable Procedure to Obtain Environmentally Relevant Nanoplastic Proxies". In: *Environmental Science: Nano* Accepted.

Efimova, Irina, Margarita Bagaeva, Andrei Bagaev, Alexander Kileso, and Irina P. Chubarenko (Sept. 2018). "Secondary Microplastics Generation in the Sea Swash Zone With Coarse Bottom Sediments: Laboratory Experiments". en. In: *Frontiers in Marine Science* 5, p. 313. ISSN: 2296-7745. DOI: 10.3389/fmars.2018.00313.

El Hadri, Hind, Julien Gigault, Benoit Maxit, Bruno Grassl, and Stéphanie Reynaud (2020). "Nanoplastic from Mechanically Degraded Primary and Secondary Microplastics for Environmental Assessments". In: *NanoImpact*, p. 100206. ISSN: 2452-0748. DOI: 10.1016/j.impact.2019.100206.

Galgani, Luisa and Steven Loiselle (Jan. 2019). "Plastic Accumulation in the Sea Surface Microlayer: An Experiment-Based Perspective for Future Studies". en. In: *Geosciences* 9.2, p. 66. ISSN: 2076-3263. DOI: 10.3390/geosciences9020066.

Hendren, Christine Ogilvie, Gregory V. Lowry, Jason M. Unrine, and Mark R. Wiesner (Dec. 2015). "A Functional Assay-Based Strategy for Nanomaterial Risk Forecasting". en. In: *Science of The Total Environment* 536, pp. 1029–1037. ISSN: 00489697. DOI: 10.1016/j.scitotenv.2015.06.100.

Ivleva, Natalia P. (Aug. 2021). "Chemical Analysis of Microplastics and Nanoplastics: Challenges Advanced Methods, and Perspectives". In: *Chemical Reviews*. ISSN: 0009-2665. DOI: 10.1021/acs.chemrev.1c00178.

Min, Kyungjun, Joseph D. Cuiffi, and Robert T. Mathers (Dec. 2020). "Ranking Environmental Degradation Trends of Plastic Marine Debris Based on Physical Properties and Molecular Structure". en. In: *Nature Communications* 11.1, p. 727. ISSN: 2041-1723. DOI: 10.1038/s41467-020-14538-z.

Muir, Derek C.G. and Cynthia A. de Wit (July 2010). "Trends of Legacy and New Persistent Organic Pollutants in the Circumpolar Arctic: Overview, Conclusions, and Recommendations". en. In: *Science of The Total Environment* 408.15, pp. 3044–3051. ISSN: 00489697. DOI: 10.1016/j.scitotenv.2009.11.032.

Qi, Di, Liqi Chen, Baoshan Chen, Zhongyong Gao, Wenli Zhong, Richard A. Feely, Leif G. Anderson, Heng Sun, Jianfang Chen, Min Chen, Liyang Zhan, Yuanhui Zhang, and Wei-Jun Cai (Mar. 2017). "Increase in Acidifying Water in the Western Arctic Ocean". en. In: *Nature Climate Change* 7.3, pp. 195–199. ISSN: 1758-678X, 1758-6798. DOI: 10.1038/nclimate3228.

Rockström, Johan, Will Steffen, Kevin Noone, Åsa Persson, F. Stuart Chapin, Eric F. Lambin, Timothy M. Lenton, Marten Scheffer, Carl Folke, Hans Joachim Schellnhuber, Björn Nykvist, Cynthia A. de Wit, Terry Hughes, Sander van der Leeuw, Henning Rodhe, Sverker Sörlin, Peter K. Snyder, Robert Costanza, Uno Svedin, Malin Falkenmark, Louise Karlberg, Robert W. Corell, Victoria J. Fabry, James Hansen, Brian Walker, Diana Liverman, Katherine Richardson, Paul Crutzen, and Jonathan A. Foley (Sept. 2009). "A Safe Operating Space for Humanity". en. In: *Nature* 461.7263, pp. 472–475. ISSN: 0028-0836, 1476-4687. DOI: 10.1038/461472a.

Schwaferts, Christian, Reinhard Niessner, Martin Elsner, and Natalia P. Ivleva (Mar. 2019). "Methods for the Analysis of Submicrometer- and Nanoplastic Particles in the Environment". en. In: *TrAC Trends in Analytical Chemistry* 112, pp. 52–65. ISSN: 01659936. DOI: 10.1016/j.trac.2018.12.014.

Stocker, T.F., D Qin, G.-K. Plattner, Melinda M. B. Tignor, Simon K. Allen, Judith Boschung, Alexander Nauels, Yu Xia, Vincent Bex, and Pauline M. Midgley (2018). *Climate Change 2013: The Physical Science Basis. Contribution of Working Group I to the Fifth Assessment Report of the Intergovernmental Panel on Climate Change*.

Stroeve, Julienne and Dirk Notz (Sept. 2018). "Changing State of Arctic Sea Ice across All Seasons". en. In: *Environmental Research Letters* 13.10, p. 103001. ISSN: 1748-9326. DOI: 10.1088/1748-9326/aade56.

Ter Halle, Alexandra, Laurent Jeanneau, Marion Martignac, Emilie Jardé, Boris Pedrono, Laurent Brach, and Julien Gigault (Dec. 2017). "Nanoplastic in the North Atlantic Subtropical Gyre". en. In: *Environmental Science & Technology* 51.23, pp. 13689–13697. ISSN: 0013-936X, 1520-5851. DOI: 10.1021/acs.est.7b03667.

Villarrubia-Gómez, Patricia, Sarah E. Cornell, and Joan Fabres (Oct. 2018). "Marine Plastic Pollution as a Planetary Boundary Threat  The Drifting Piece in the Sustainability Puzzle". en. In: *Marine Policy* 96, pp. 213–220. ISSN: 0308597X. DOI: 10.1016/j.marpol.2017.11.035.

Wahl, Aurélie, Corentin Le Juge, Mélanie Davranche, Hind El Hadri, Bruno Grassl, Stéphanie Reynaud, and Julien Gigault (Jan. 2021). "Nanoplastic Occurrence in a Soil Amended with Plastic Debris". en. In: *Chemosphere* 262, p. 127784. ISSN: 00456535. DOI: 10.1016/j.chemosphere.2020.127784.

# Résume Français

## Introduction

Le plastique est le troisième matériau le plus produit sur Terre. Mais en raison de la mauvaise gestion des déchets et du vieillissement des matières plastiques dans l'environnement, une proportion considérable (>25 %) se déverse dans les habitats naturels. Pour évaluer les risques que cette contamination engendre, il est nécessaire de comprendre les sources, les voies de transport et les zones potentielles d'accumulation des débris de plastique. Cet objectif est un vrai enjeu sociétal mais surtout scientifique puisque de nombreux processus abiotiques et biotiques, encore mal compris, transforment les objets plastiques en particules trop petites pour être échantillonnées et quantifiées (Figure 1).

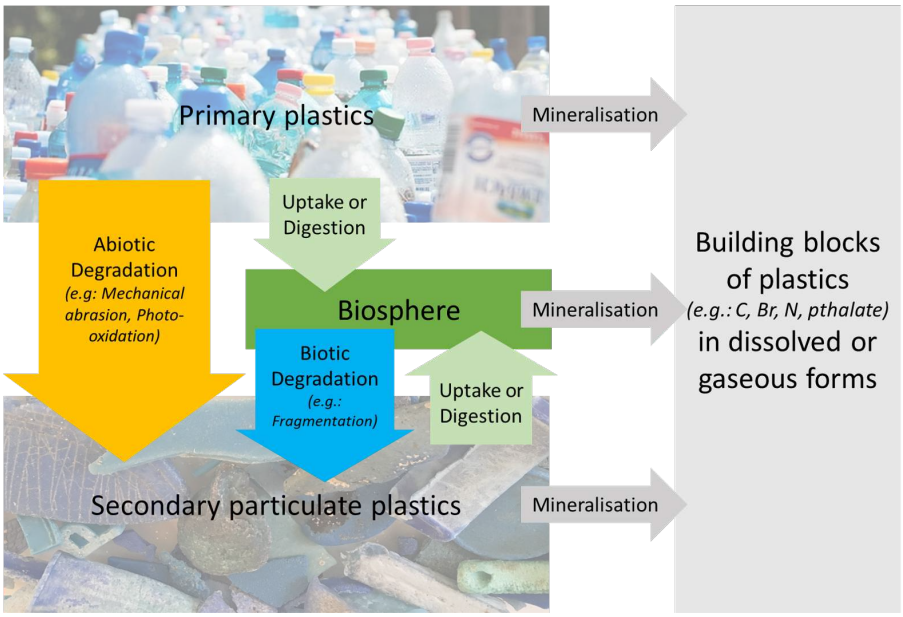


*Figure 1: Schémas des stocks de plastique primaires (produits intentionnellement) et des processus qui mènent à la production et à l'élimination de plastiques secondaires (produits inintentionnellement) dans l'environnement*

Les nanoplastiques sont des particules de plastique produits inintentionnellement, de tailles inférieures à 1 $\mu$m et qui ont un comportement colloïdal (mouvement Brown-

ien, forte surface spécifique, etc.). Les données obtenues à partir de prélèvements dans différents écosystèmes et de modèles expérimentaux et numériques, suggèrent que les nanoplastiques constituent une fraction importante de la quantité totale des débris plastiques sur Terre.

Dans ce **contexte**, l'objectif principal de ces travaux est de comprendre les voies de transports et d'accumulation des nanoplastiques dans l'environnement.

L'**approche** vise à modéliser expérimentalement les processus de diffusion et d'advection des dispersions aqueuses de nanoplastiques dans certains écosystèmes et les milieux à l'interface de ceux-ci. Ces interfaces sont des zones où les caractéristiques physiques et biogéochimiques du système environnemental changent brusquement dans l'espace et/ou dans le temps. Elles sont caractérisées par de forts gradients physicochimiques qui modifient le comportement et le trajet des colloïdes. Par conséquent, une des hypothèses de cette thèse est, qu'en se concentrant sur ces interfaces, il nous sera possible de mieux identifier les zones potentielles d'accumulation des nanoplastiques. Parmi les différentes interfaces, nous nous sommes intéressés aux milieux poreux (qui représentent de manière simplifiée les sols, les sédiments et les aquifères) et à l'interface entre un liquide salé et un front de congélation (comme substitut pour l'interface eau de mer/banquise).

Plus spécifiquement, cette étude permet d'apporter de premières informations sur l'impact des processus physicochimiques sur le transport et l'accumulation des nanoplastiques dans l'environnement. Comme l'illustre la Figure 2, de nombreux processus naturels ont une incidence sur le devenir des colloïdes et donc potentiellement sur les nanoplastiques. Le processus d'agrégation des nanoplastiques est le paramètre clé à étudier puisque :

i) les colloïdes sont sensibles à l'agrégation dans l'eau,

i) leur état d'agrégation a un impact sur leur sédimentation, leur transfert dans les sols, leur assimilation par les organismes, etc.

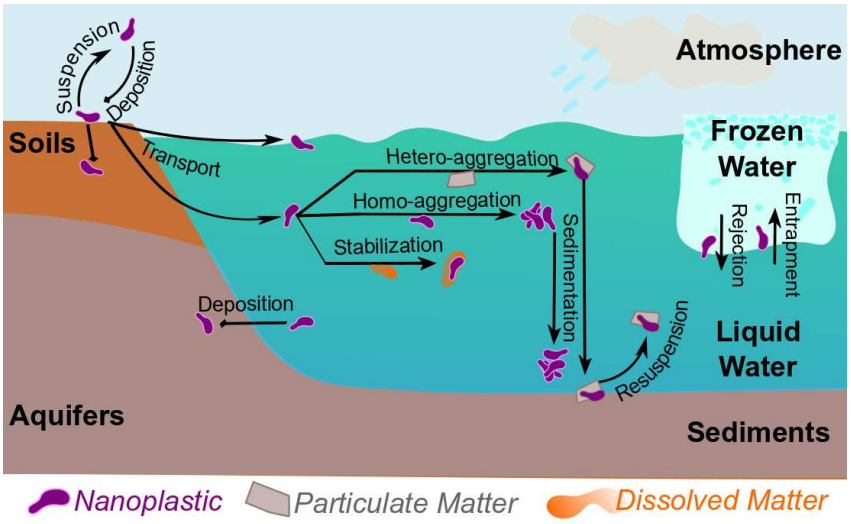


*Figure 2: Schémas des principaux processus abiotiques qui contrôlent le devenir environnemental des nanoplastiques*

# Résultats

Le Chapitre 1 *"Déterminer le devenir environnemental des nanoplastiques : Analyse bibliographique critique des processus d'agrégation", page 5*) est une analyse bibliographique autour des questions scientifiques définissant les objectifs de la thèse. Le but principal est de présenter comment les propriétés des nanoplastiques peuvent contrôler leur agrégation dans des systèmes expérimentaux.

Étant donné que les nanoplastiques sont difficiles à détecter dans les échantillons naturels, leur devenir doit être étudié en utilisant des particules modèles de nanoplastique en laboratoire. Par conséquent, pour évaluer correctement le devenir environnemental des nanoplastiques, il faut étudier des particules qui sont représentatives des nanoplastiques présents dans l'environnement.

Comme l'illustre la Figure 3, les études actuelles ont utilisé principalement des modèles de nanoplastiques qui sont des sphères de latex, que nous jugeons non représentatifs des nanoplastiques environnementaux. En effet, ces sphères de latex ont des surfaces lisses et sont synthétisées par des méthodes bottom-up de polymérisation en émulsion (Figure 3a), loin des processus de dégradation susceptibles de se produire dans l'environnement (top-down). Ces particules sphériques sont composées de polystyrène (PS), alors que ce polymère n'est ni fréquemment rejeté dans l'environnement ou ni fréquemment observé dans les échantillons environnementaux. (Figure 3b). De plus, le procédé de synthèse de ces nanoparticules sphériques implique l'utilisation de tensioactifs et autres additifs (Figure 3c). Enfin, les particules modèles ont différentes propriétés chimiques de surface, tel que des groupes fonctionnels carboxyliques (COOH), amine (NH2) ou sulfonate (SO3),

ou encore l'absence de groupe fonctionnel (NF) (Figure 3d). Nous estimons que certaines surfaces (par ex: COOH) sont plus environnementalement pertinentes que d'autres (par ex: NF, NH2, SO3).

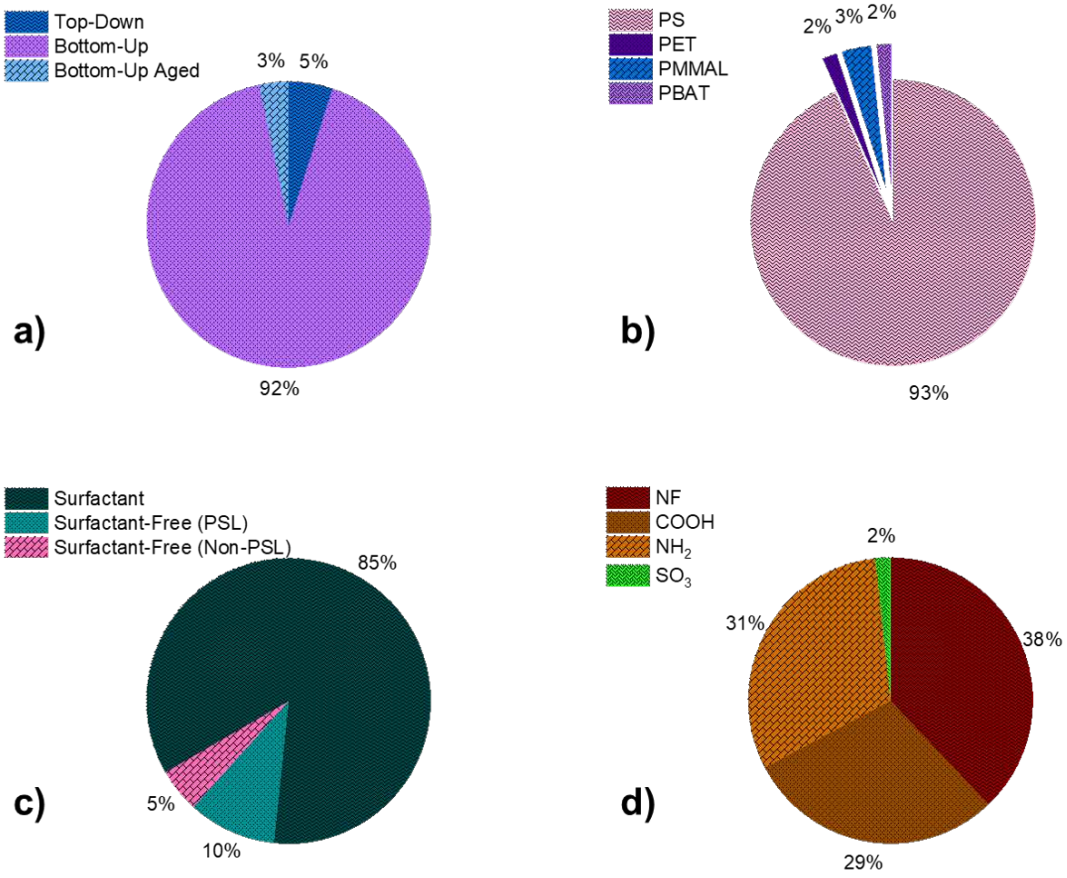


*Figure 3: Part des modèles nanoplastiques étudiés selon a) la méthode de production/synthèse, b) la composition avec PS = polystyrène, PET = polyéthylène téréphtalate, PMMAL = polyméthylméthacrylate et PBAT = polybutyrate adipate-co-téréphtalate, c) présence de surfactant et d) présence et type de groupe fonctionnel de surface avec NF = non-fonctionnalisé, COOH = carboxylique, NH2 = amine et SO3 = sulfonate. (Nombre de particules = 60)*

L'analyse bibliographique a permis de révéler des enjeux et verrous importants à lever pour évaluer la stabilité des nanoplastiques, c'est-à-dire, leur capacité à éviter l'agrégation et rester dispersés :

- Les sphères de latex de PS (PSL) avec des groupements fonctionnels aminés (PSL-NH2) sont plus stables que les PSL-carboxyliques (PSL COOH) ou non-fonctionnalisés (PSL NF). *Quelle est l'influence de la composition chimique de la surface sur le comportement des nanoplastiques ?*

- Les nanoplastiques modèles produits à partir de processus top-down tel que la fragmentation ou l'ablation d'objets plastiques, ont des comportements plus variables et sont généralement moins stables. *Quelle est l'influence de leurs propriétés (par ex: formes irrégulières et non-sphériques, tailles polydisperses, compositions, etc.) sur leur stabilité?*
- L'ajout de matière organique naturelle (MON) peut soit provoquer ou réduire l'agrégation des particules par des processus antagonistes en fonction de la nature de la MON, de la composition ionique de la solution et des propriétés des nanoplastiques. *Quelle est l'influence de différentes MON sur le comportement de nanoplastiques, en particulier des modèles produits par des processus top down ?*
- L'ajout de matières particulaires (non-dissoutes) déstabilise les nanoplastiques par hétéro-agrégation (agrégation d'un type de particule avec un autre type de particule). *Quelle est l'influence de cette hétéro-agrégation sur le devenir des nanoplastiques dans l'environnement ?*

Ces principales questions ont permis de définir les objectifs de ce travail de thèse. Celle-ci est composée de différents chapitres qui ont comme point commun l'utilisation et la comparaison de modèles de nanoplastiques variées et plus ou moins pertinents par rapport aux particules de plastiques observés dans l'environnement. Une attention particulière a été accordée à l'étude de nouveaux modèles de nanoplastiques nommés *NPT*. Ceux-ci ont été produits à partir de granules de PS fragmentés dispersés dans de l'eau ultra pure et filtrés à 40 $\mu$m, en utilisant la méthode d' El Hadri et al. 2020. Les *NPT* présentent des formes non sphériques et irrégulières, des tailles polydisperses et une charge modérément négative, ce qui les rend plus pertinent que les PSL qui sont largement utilisés dans la littérature (Tableau 1).

*Table 1: Caractéristiques du PSL COOH et du NPT*

| *Nom* | $d_{zH}$ *(nm) | PDI + | Rapport de Forme | Polarité (mJ $m^{-2}$) | Potentiel zêta (mV) dans 5 mmol $L^{-1}$ NaCl | | |
|---|---|---|---|---|---|---|---|
| | | | | | pH 5 | pH 6.5 | pH 8 |
| *PSL COOH* | 197 ± 2 | 0.03 ± 0.01 | 1.02 ± 0.05 | 33.91 | -37.69 ± 1.91 | -38.65 ± 2.23 | -42.80 ± 2.98 |
| *NPT-P* | 339 ± 7 | 0.18 ± 0.03 | 1.70 ± 0.57 | 31.82 | -31.67 ± 1.01 | -33.54 ± 2.72 | -35.14 ± 2.13 |

* $d_{zH}$ *= diametre hydrodynamique moyen;* + *PDI = indice de polydispersité, soit la variance de la disribution* $d_{zH}$*; Rapport de forme = rapport de l'axe majeur à l'axe mineur d'une particule; La polarité est la composante polaire de l'énergie de surface caractérisée avec la méthode de Valsesia et al. 2018; Le potentiel zêta représente la charge de la particule.*

La morphologie des *NPT* a été caractérisée par microscopie électronique à balayage (MEB), à transmission (MET) et à force atomique (AFM) (Figures 4, 5 et 6, respec-

tivement). Les images MEB illustrent les différentes formes des *NPT*: sphéroïdes (flèche orange dans la Figure 4), bâtonnets (flèche violette) et paillettes (flèches bleues). La surface de certaines particules est rugueuse, ce qui suggère que des morceaux de la particule ont été ablatés de la surface (flèches rouges à la figure 4b). Des observations similaires ont été faites à partir des images obtenues par MET (Figure 5). En effet, certaines particules sphéroïdales ont des densités de couleur homogènes qui indiquent une densité de matière homogène (flèches bleues Figure 5a), tandis que d'autres non. Les zones de densité plus faibles sont caractéristiques d'une ablation d'un morceau de la surface (flèches rouges dans Figure 5b). Cette diversité de formes s'explique par la friabilité du polystyrène vis-à-vis du processus d'abrasion mécanique par broyage utilisé pour les produire.

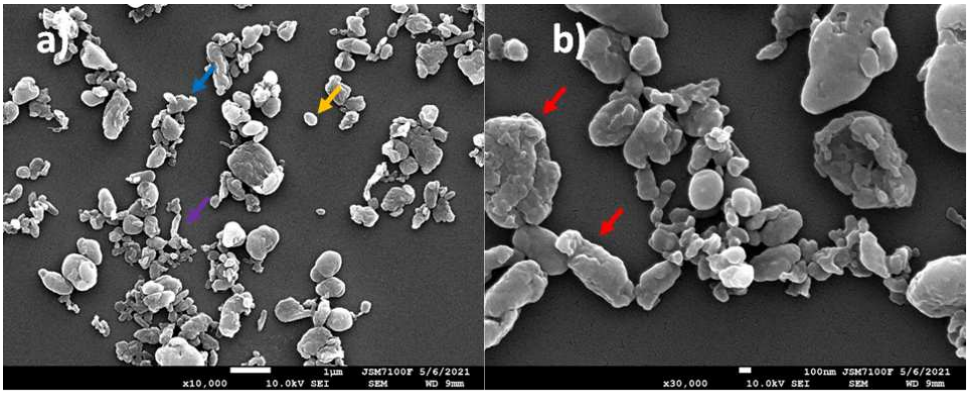


*Figure 4: Images de microscopie électronique à balayage (MEB) de NPT à a) 1 µm et b) grossissement de 100 nm.*

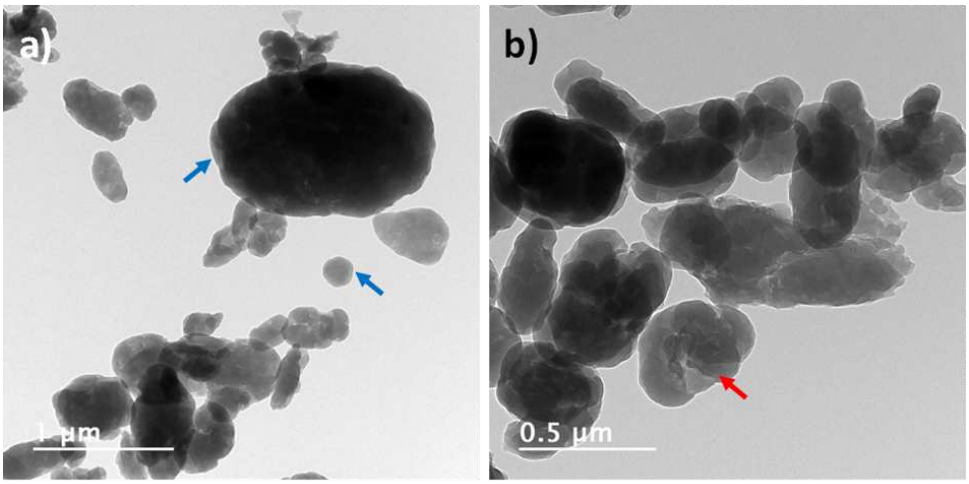


*Figure 5: Images de microscopie électronique de transmission (MET) du NPT à a) 1 µm et b) grossissement de 500 nm*

Tandis le MEB et le MET permettent d'obtenir une image en 2 dimensions des particules, l'AFM permet d'analyser la topographie des particules (Figure 6). Les images

AFM confirment la présence de i) particules en forme de paillettes de taille ≈1 $\mu$m de large et 50-80 nm de haut (Figure 6a et 6b) et ii) particules sphéroïdales, plus ou moins allongées (Figure 6c et 6d). Les rugosités à la surface des particules mesurent quelques dizaines de nanomètres (Figure 6d), ce qui correspond à l'épaisseur des paillettes de *NPT*, corroborant ainsi l'hypothèse que ces particules en forme de paillettes sont éliminées des particules sphéroïdales plus grandes.

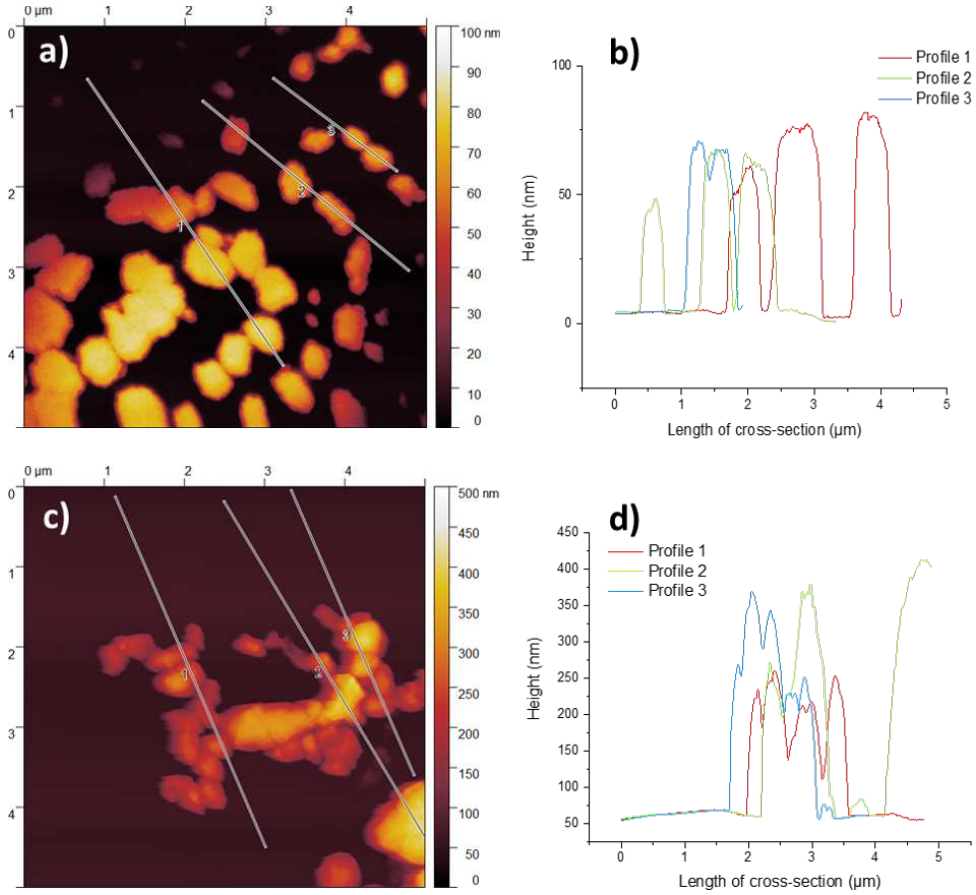


*Figure 6: Images de microscopie à force atomique (AFM) du NPT montrant a) une carte des hauteurs des particules en forme de paillettes et b) le profil de hauteur correspondant aux transects de l'image a ; et c) une carte des hauteurs des particules sphéroïdales, ainsi que d) les profils de hauteur correspondants des transects de l'image c*

La Figure 7 compare les diamètres des *NPT* déterminés par TEM (basés sur une aire de surface équivalente) et le diamètre hydrodynamique moyen ($d_{zH}$) obtenu par diffusion de lumière dynamique (DLS). La taille moyenne déterminée par DLS est plus grande que celle observée par TEM. L'intensité de la lumière diffusée est une fonction puissance de la taille des particules alors que le MET permet une détermination nominale du nombre de particules observées sur une image. Il faut donc comparer avec précaution les distributions de taille obtenues par ces différentes techniques. Ici, les deux distributions (MET et DLS) suggèrent que quelques particules micrométriques sont présentes dans la

dispersion aqueuse de nanoplastiques. Cette présence s'explique par la dernière étape de préparation des *NPT* qui consiste à filtrer à 40 $\mu$m la dispersion pour minimiser les pertes de nanoparticules sur les filtres de porosité plus faible (par ex : 0.2 à 1.2 $\mu$m). Le compteur Coulter est utilisé pour mesurer des particules de taille supérieure à 650 nm (ligne rouge dans la Figure 7). Cela permet de compléter la distribution de taille des *NPT* en analysant la fin de la distribution. Les diamètres (basés sur un volume équivalent) déterminés par compteur Coulter confirment qu'une fraction mineure (non-quantifiée) des dispersions de *NPT* contient des particules de diamètres supérieures à 1 $\mu$m.

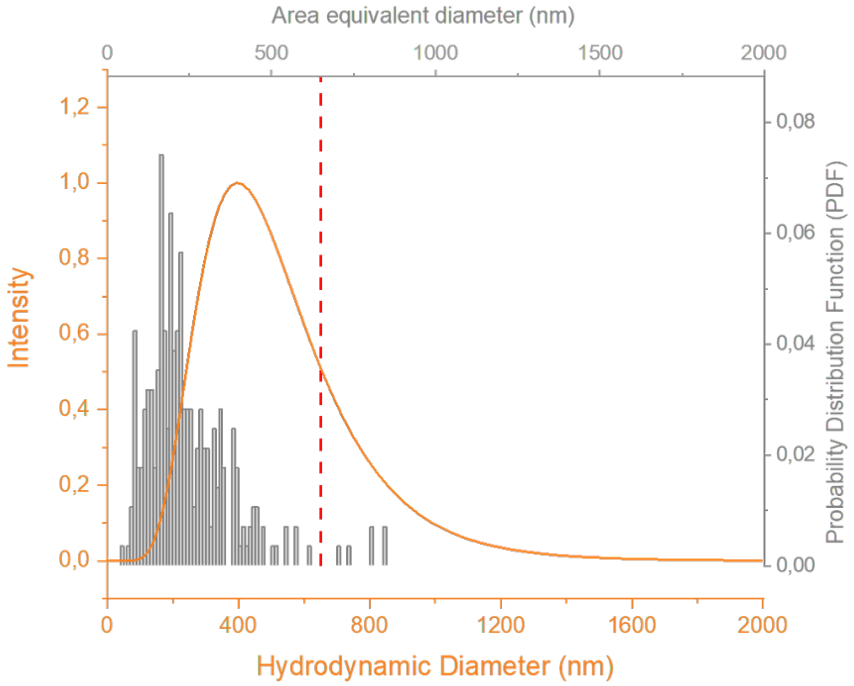


*Figure 7: Dimensions des NPT déterminées à partir de la distribution de diamètres hydrodynamiques moyens ($d_{zH}$) en orange et des diamètres basés sur une aire de surface équivalente des particules imagées par TEM (283 particules). La ligne rouge à 650 nm correspond à la limite de quantification des tailles du compteur Coulter.*

Le Chapitre 2 *"Stabilisation du nanoplastique polystyrène fragmenté par la matière organique naturelle : aperçu des mécanismes", page 93* compare l'agrégation des deux nanoplastiques modèles présentés dans le Tableau 1. La stabilité est évaluée dans une solution simple de NaCl, où seul l'écrantage des forces électrostatique à lieu. La Figure 8 illustre l'évolution des tailles des nanoplastiques en fonction du temps (la cinétique d'agrégation) à deux forces ioniques caractéristiques : 5 mmol $L^{-1}$ pour représenter des eaux douces et 600 mmol $L^{-1}$ pour des conditions marines. Il apparaît que la taille des deux modèles de nanoplastiques n'évolue pas en fonction du temps (signifiant qu'ils ne s'agrègent pas et restent stables) à de faibles forces ioniques (5 mmol $L^{-1}$). A l'opposé,

lorsque la force ionique augmente à 600 mmol $L^{-1}$, les nanoplastiques ont des comportement divergent : les *PSL COOH* ne s'agrègent pas, contrairement aux *NPT* dont la taille ($d_{zH}$) croît de 359 à 623 nm en 60 minutes. Ces tendances sont identiques dans la gamme de pH des environnements aqueux naturels (pH compris entre 5 et 8). Selon la théorie XDLVO, les énergies d'interaction entre *NPT* et *PSL COOH* sont du même ordre de grandeur. Cela suggère que la taille, la charge de surface et l'hydrophobicité, qui sont utilisées pour calculer l'énergie d'interaction, ne sont pas les propriétés des nanoplastiques permettant d'expliquer leur stabilité. Donc, les morphologies non-sphériques et irrégulières des *NPT*, leur polydispersité, ainsi que l'absence de tensioactifs dans la dispersion, sont responsables de la forte agrégation observée.

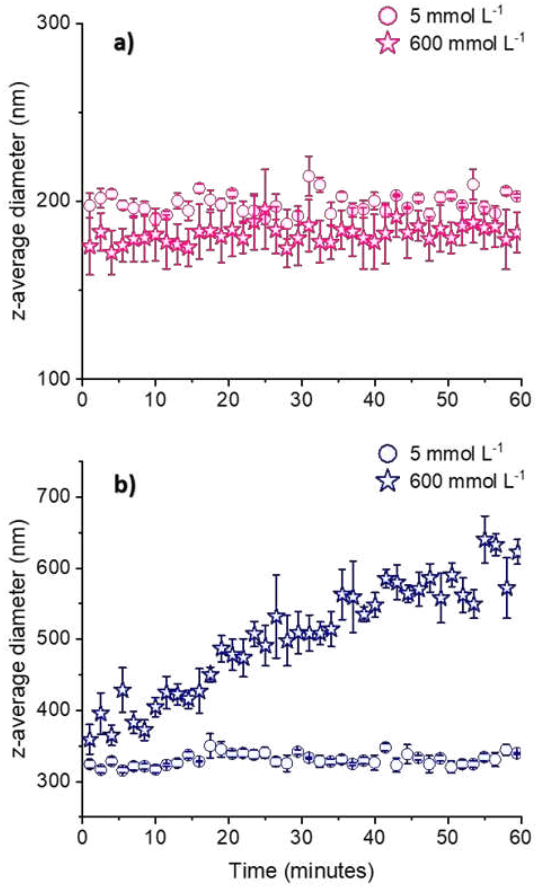


*Figure 8: Cinétique d'agrégation de 4 mg $L^{-1}$ a) PSL COOH et b) NPT dans 5 mmol $L^{-1}$ ou 600 mmol $L^{-1}$ de NaCl à pH 6,5. (Barre d'erreur = écart-type, n=3)*

Les *NPT* n'étant pas stables à des forces ioniques élevées, l'effet stabilisateur de deux MON différentes a été étudié. L'acide humique (HA) a des propriétés amphiphiles et a été choisi pour représenter la matière organique terrestre. L'alginate de sodium (SA) est un polysaccharide extrait d'algues marines qui représente la MON marine et qui est un com-

posant des substances polymériques extracellulaires produites par des micro-organismes. Leur effet sur le *NPT* a été évalué à l'aide de deux méthodes optiques complémentaires : la DLS et le fractionnement par couplage flux-force (A4F) couplé à la diffusion multi-angle de la lumière (SLS). Les résultats montrent que les deux MONs stabilisent les *NPT* à des forces ioniques élevées. Cependant, elles ont des mécanismes de stabilisation différents. La Figure 9 montre qu'en présence de SA, le $d_{zH}$ des *NPT* augmente d'abord puis atteint un plateau et qu'en présence de HA, le $d_{zH}$ de la *NPT* reste stable. Les HA induisent une répulsion électrostatique et un encombrement stérique (surtout pour les tailles les plus importantes) entre les particules. L'alginate de sodium semble s'adsorber sur les particules individuelles et sur des petits agrégats de nanoplastiques. Les particules recouvertes sont stabilisées par les répulsions stériques entre les molécules de SA. Ces résultats soulignent qu'il est important de prendre en compte les propriétés des MONs lors de l'évaluation du comportement des nanoplastiques dans l'environnement.

Cette étude a fait l'objet d'une publication dans la revue *ACS Environmental Science and Technology Water en Mars 2021* (Pradel, Ferreres, et al. 2021). Ils contribuent à notre évaluation du transport des nanoplastiques dans les milieux poreux (Chapitre 4) et de leur mobilité dans les eaux polaires (Chapitre 5).

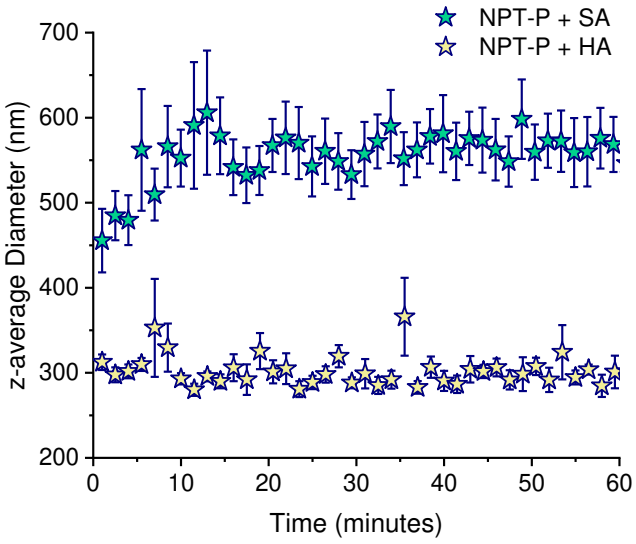


*Figure 9: Cinétique d'agrégation de 4.0 mg $L^{-1}$ de NPT, dans 600 mmol $L^{-1}$ de NaCl, avec 57 mg $L^{-1}$ d'alginate de sodium (SA) at pH 8 et 30 mg $L^{-1}$ d'acide humique (HA).*

Les chapitres suivants étudient deux interfaces environnementales : les milieux poreux et un front de congélation d'eau saline. La Figure 10 illustre certains gradients physico-chimiques dans ces systèmes environnementaux. Par exemple, les milieux poreux sont caractérisés par des gradients de vitesse (Figure 10a), mais peuvent également contenir

des gradients de charge et d'hydrophobicité sur la matrice solide. L'interface entre l'eau de mer et la banquise est caractérisée par des gradients de salinité (Figure 10b), ainsi que des gradients de température et de vitesse d'écoulement, entre autres.

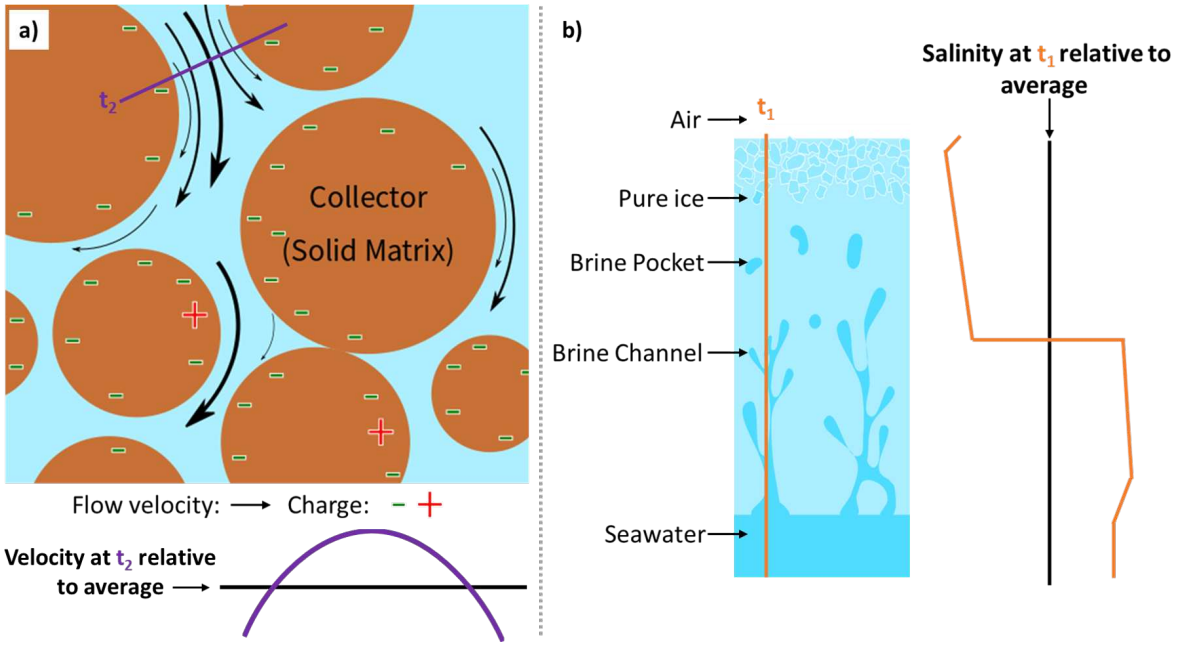


*Figure 10: Schémas de a) interfaces solides/liquides terrestres, montrant diverses charges et gradients de vitesse et b) interfaces solide/liquide d'eau de mer polaire montrant les gradients de salinité (non à l'échelle).*

Le Chapitre 3 *"Dépôt nanoplastiques modèles environnementalement pertinents dans un sable pendant des expériences de transport", page 131* a pour objectif de comparer la dynamique des nanoplastiques modèles pendant leur transport par advection dans un milieu poreux. Leur transport a été étudié dans une colonne de sable à faible force ionique, créant ainsi des conditions de répulsion électrostatique entre les particules et le sable. Chaque nanoplastique modèle présente une taille, une composition et une forme spécifique qui permet d'étudier l'effet de chacune de ces propriétés sur le taux de déposition des particules dans le milieu. La Figure 11a présente les courbes de percée (BTC), c'est-à-dire la concentration (C) de particules éluées du milieu poreux normalisée par la concentration initiale ($C_0$). La courbe de percée des *PSL COOH* de 200 nm de diamètre est similaire à celle du traceur KBr avec 92 ± 5 % des *PSL COOH* récupérés en sortie de colonne. Ceci indique un transport avec un dépôt négligeable dans le sable. Le *PSL COOH* de 430 nm de diamètre est davantage déposé, car seulement 67 ± 1 % de la masse injectée est récupéré en sortie de colonne. Enfin, les *NPT* sont les plus déposés, avec un recouvrement de seulement 28 % des *NPT* dont le $d_{zH}$ est de 350nm, et 10 % de *NPT* ayant un $d_{zH}$ de 460 nm. La comparaison de nanoplastiques modèles qui ont des formes similaires révèle que l'augmentation de la taille des particules entraîne une augmentation du taux de dépôt.

Notons aussi que dans le cas des *PSL COOH*, le transport plus élevé des plus petites particules ($d_{zH}$ = 200 nm) peut s'expliquer partiellement par la présence de tensioactifs dans la dispersion. D'après les BTC, il semble que le taux de dépôt augmente fortement lorsque les particules on tune forme irrégulière et asymétrique. D'après l'évolution des tailles en sortie de la colonne de sable, la part des *NPT* ayant des plus grandes tailles seraient davantage retenue dans le milieu poreux (Figure 11b). Donc, à taille plus faible, les *NPT* sont significativement plus déposés que les *PSL COOH*.

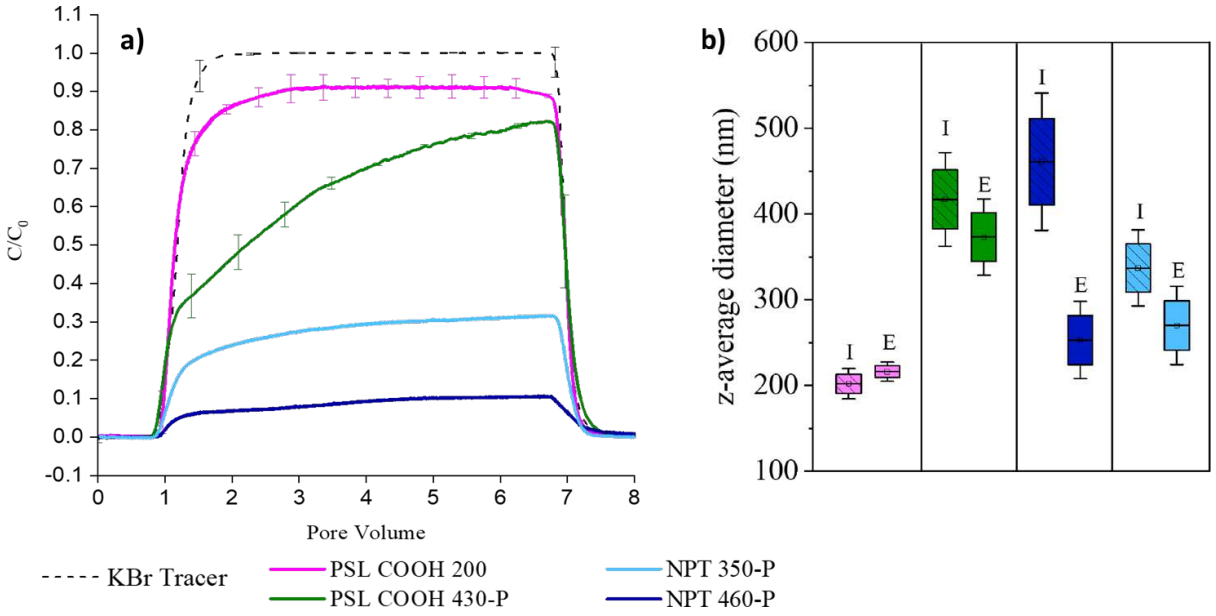


*Figure 11: a) Courbes de percée du traceur KCl et des nanoplastiques modèles injectés durant 6 volumes de pores à une concentration initiale ($C_0$) de 5.0 mg $L^{-1}$ dans 5.0 mmol $L^{-1}$ NaCl à pH 6.5 (barres d'erreur = écart-type, n = 2), b) $d_{zH}$ des nanoparticules plastiques injectées (I) et éluées (E) de la colonne de sable (n=6, barres d'erreur = $PDI^{0.5}$).*

Cette étude a été publiée dans la revue *Chemosphere* en Avril 2020 (Pradel, Hadri, et al. 2020). Bien qu'elle ait démontré que les nanoplastiques fragmentés (*NPT*) se déposent davantage dans les milieux poreux, des incertitudes subsistent sur les mécanismes responsables du dépôt important en raison :

i) des géométries complexes des colonnes de sable (ex : surfaces rugueuses, tailles de pores variables, zones de débit réduit, etc.) ;

ii) de l'impossibilité de quantifier les profils de dépôt des *NPT* puisqu'ils n'ont pas pu être observés *in-situ* ni quantifiés *ex-situ*.

Pour lever ces incertitudes une étude en cours, présentée dans le Chapitre 4 *"Dépôt de nanoplastiques: Les rôles de la polydispersité en tailles et de la matière organique naturelle" page 159*) vise à comprendre les mécanismes de dépôt des *NPT* en fonction

de leur polydispersité en tailles. Pour cela, des canaux de microfludique ont été utilisés pour créer des milieux poreux à géométrie contrôlée. Les résultats suggèrent que la faible fraction de particules micrométriques sont davantage déposées dans le milieu poreux, et entrainent le dépôt de plus petits *NPT*. De plus la présence MON, tel que le HA ou SA, réduiraient le taux de dépôt des *NPT*.

Les chapitres précédents se focalisent sur le comportement des nanoplastiques dans les environnements terrestres en étudiant leur transport dans des milieux poreux. Cependant, les nanoplastiques peuvent être présents dans des zones non exposées directement aux activités anthropiques. En effet, les modèles de circulation océanique et atmosphérique suggèrent que les débris plastiques s'accumulent dans l'océan Arctique. L'échantillonnage et la caractérisation de microplastiques (1 $\mu$m à 5mm) dans l'Arctique confirme ces prédictions. Cependant, même si la présence de nanoplastiques n'a toujours pas été démontré, il semble primordial d'anticiper et d'évaluer le comportement et l'impact des nanoplastiques dans cet écosystème.

Le 5ème et dernier Chapitre de ce travail *"Transfert des micro- et nanoplastiques lors de la congélation d'eau salée : Implications pour leur devenir dans les eaux polaires" page 189* ) utilise un nouveau dispositif expérimental pour étudier le transfert des micro- et nanoplastiques entre l'eau salée et un front de congélation. Ce dispositif expérimental simule la croissance de la glace en congelant progressivement une solution saline, comme l'illustre la Figure 12a. Après différentes durées de congélation (2, 5, 7 et 24 heures), la concentration de chlorure de sodium, de SA, de microplastiques (125 à 400 $\mu$m), et de nanoplastiques a été mesurée dans la glace décongelée et dans le liquide.

Il est admis et connu que le chlorure de sodium est expulsé de la glace quand celle-ci se forme. Ceci est dû au fait que lorsque l'eau se congèle elle tend à expulser toutes les impuretés qui peuvent gêner la cristallisation des molécules d'eau. Au contraire, les microplastiques sont retenus et capturés dans la glace. Ceci s'explique par la mobilité des microplastiques qui est régie par leur densité. En effet, contrairement aux solutés, ils n'ont pas un coefficient de diffusion significatif. Par conséquent, les microplastiques qui sont situés à proximité d'un front de congélation qui approche et auxquels ils ne peuvent pas échapper par advection, sont incorporés dans la glace. Contrairement aux microplastiques et aux idées préconçues, pour la première fois, nous avons montré que les nanoplastiques et le SA ont eu un comportement similaire à celui des sels. Ils sont expulsés de la glace et retenus dans les poches et canaux de saumure de la glace (*Brine pocket* dans le jargon océanographique). Néanmoins, la présence de SA est primordiale pour stabiliser les nanoplastiques à cette interface, en accord avec l'étude présentée dans le Chapitre 2. Ceci soulève de nombreuses questions sur l'impact de la productivité primaire sur le devenir des nanoplastiques dans les eaux polaires.

Ce travail a permis de calculer un coefficient de distribution des micro et nanoplastiques entre l'eau salée et la glace : $\log(C_{glace}/C_{liquide})$ (Figure 12b). Ce coefficient est un outil pour normaliser le comportement des particules plastiques pour que les résultats soient comparables avec d'éventuelles futures études. Ces différences de comportement soulignent le fait que les nanoplastiques ne peuvent pas être simplement catégorisé comme des petits microplastiques. Cette étude a été publiée dans la revue *Environmental Science : Processes & Impacts* en septembre 2021 (Pradel, Gautier, et al. 2021).

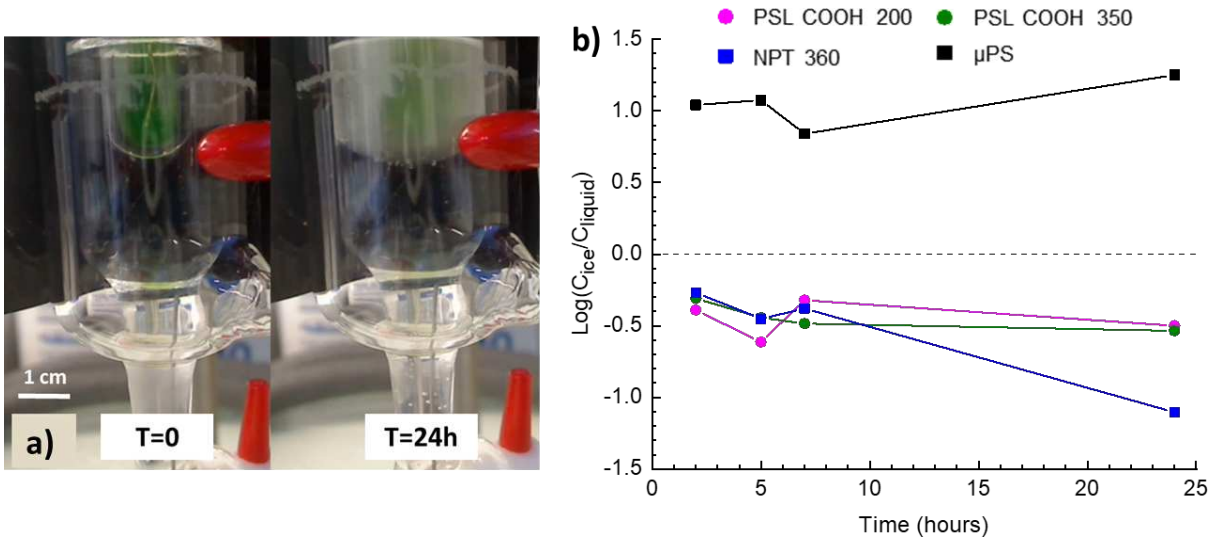


*Figure 12: a) Dispositif expérimental de congélation au début de la congélation (T = 0) et après 24 heures de congélation (T = 24h) de 35 g $kg^{-1}$ NaCl montrant un doigt froid (en vert) autour duquel la solution congèle et b) Logarithme de la distribution des nanoplastiques (PSL et NPT) et microplastiques (µP) entre la glace (ice) et le liquide ($C_{ice}/C_{liquid}$) en fonction de la durée de congélation dans 35 g $kg^{-1}$ NaCl et 50 mg $kg^{-1}$ SA.*

# Conclusion et Perspectives

En conclusion, ce travail a apporté de nouvelles connaissances sur le devenir environnemental des nanoplastiques en utilisant des modèles pertinents et en se concentrant sur les interfaces à travers lesquelles ils peuvent transiter.

Les comportements des différents nanoplastiques modèles ont été comparés en modélisant expérimentalement les interfaces environnementales dans des conditions simplifiées. Ces simplifications étaient nécessaires pour comprendre les mécanismes, mais s'avèrent limitées en termes de représentativité environnementale. Les limitations concernent notamment l'utilisation :

i) uniquement de sels monovalents qui ne forment pas de complexes de surface (ex. : chlorure de sodium),

ii) des matières organiques purifiées, et

iii) d'aucune autre matière particulaire.

De plus, les interfaces terrestres ont été conceptualisées comme des milieux poreux de composition chimique homogène (sable de quartz ou polymère de silicone). Enfin, l'interface entre l'eau de mer et la banquise a été simplifiée en utilisant une solution simple sans ions multivalents, ni matière naturelle particulaire, et en congelant la solution à une température constante dans des conditions non turbulentes. Une autre limite de toutes ces études est qu'elles se concentrent uniquement sur les processus abiotiques, alors que les processus biotiques (ex : sécrétion d'exsudats, digestion, etc.) peuvent avoir des effets sur le devenir environnemental des nanoplastiques.

Ce travail montre que les différents comportements des nanoplastiques sont liés à leurs formes et propriétés de surface (ex : charge, rugosité et tension superficielle) qui modifient leurs comportements hydrodynamiques et leurs énergies d'interaction entre eux et les surfaces. Comparées aux latex de polystyrène (PSL) couramment utilisées, les particules de polystyrène fragmenté ($NPT$) sont plus sensibles à l'agrégation causée par l'écrantage de la répulsion électrostatique. Cela suggère que les nanoplastiques dispersés dans les eaux naturelles s'accumuleront plus que prévus dans les sédiments des lacs, des rivières, mais surtout des océans. Ce $NPT$ semble être déposé préférentiellement dans les milieux poreux, ce qui indique une accumulation dans les sols, les aquifères et les sédiments. Cependant, concernant l'interface entre l'eau de mer et la banquise, tous les nanoplastiques présentent un comportement similaire dans ce dispositif experimental. Ils sont expulsés lors de la croissance de la glace dans la colonne d'eau sous-jacente et partiellement accumulés dans les poches de saumure de la glace.

Dans chacun de ces scénarios (agrégation, dépôt et expulsion de la glace saline), la présence de MON modifie de façon significative le comportement des nanoplastiques. La MON stabilise les nanoplastiques à une force ionique élevée et réduisent leur taux de colmatage dans les milieux poreux. De plus, le SA stabilise les nanoplastiques à l'interface entre l'eau salée et la glace. Cela suggère que la concentration et le type de MON dans les systèmes environnementaux ont un effet important sur le devenir des nanoplastiques. Par exemple, les nanoplastiques seront plus abondants dans la colonne d'eau des lacs mésotrophes que des lacs oligotrophes. De même, les nanoplastiques auront des temps de résidence plus longs dans les eaux de surface polaires qui ont une forte activité biologique (présence d'exsudats microbiens et algaux), par rapport aux eaux de surface polaires avec une faible activité biologique.

Ces progrès dans la compréhension du comportement des nanoplastiques dans l'environnement doivent être complétés par d'autres investigations. En particulier, les études peuvent être améliorées en utilisant d'autres types de nanoplastiques modèles pertinents

et des solutions et interfaces environnementales plus réalistes. De même, des modèles numériques qui intègrent les résultats expérimentaux devraient être développés pour mieux évaluer les zones potentielles d'accumulation des nanoplastiques. Il est essentiel de vérifier les hypothèses émises en caractérisant les nanoplastiques dans des échantillons environnementaux. Enfin, la problématique de la contamination environnementale par les nanoplastiques n'est qu'une problématique environnementale parmi d'autres. Le comportement des déchets plastiques dans l'environnement doit donc être évaluée en prenant en compte les autres, multiples, problématiques environnementales, tels que le changement climatique, la perte de biodiversité, etc., ainsi que leurs ramifications sociétales.

# References


El Hadri, Hind, Julien Gigault, Benoit Maxit, Bruno Grassl, and Stéphanie Reynaud (2020). "Nanoplastic from Mechanically Degraded Primary and Secondary Microplastics for Environmental Assessments". In: *NanoImpact*, p. 100206. ISSN: 2452-0748. DOI: 10.1016/j.impact.2019.100206.

Pradel, Alice, Séléna Ferreres, Cloé Veclin, Hind El Hadri, Maud Gautier, Bruno Grassl, and Julien Gigault (Mar. 2021). "Stabilization of Fragmental Polystyrene Nanoplastic by Natural Organic Matter: Insight into Mechanisms". en. In: *ACS ES&T Water*, acsestwater.0c00283. ISSN: 2690-0637. DOI: 10.1021/acsestwater.0c00283.

Pradel, Alice, Maud Gautier, Dominique Bavay, and Julien Gigault (2021). "Micro- and Nanoplastics' Transfer in Freezing Saltwater: Implications for Their Fate in Polar Waters". In: *Environmental Science: Processes & Impacts*. ISSN: 2050-7887. DOI: 10.1039/D1EM00280E.

Pradel, Alice, Hind el Hadri, Cloé Desmet, Jessica Ponti, Stéphanie Reynaud, Bruno Grassl, and Julien Gigault (Apr. 2020). "Deposition of Environmentally Relevant Nanoplastic Models in Sand during Transport Experiments". en. In: *Chemosphere*, p. 126912. ISSN: 00456535. DOI: 10.1016/j.chemosphere.2020.126912.

Valsesia, Andrea, Cloé Desmet, Isaac Ojea-Jiménez, Arianna Oddo, Robin Capomaccio, François Rossi, and Pascal Colpo (Dec. 2018). "Direct Quantification of Nanoparticle Surface Hydrophobicity". en. In: *Communications Chemistry* 1.1, p. 53. ISSN: 2399-3669. DOI: 10.1038/s42004-018-0054-7.

# List of Figures

# List of Tables

UNIVERSITÉ DE RENNES 1

**Titre :** Comportement et devenir environnemental des nanoplastiques : Quels processus physico-chimiques ?

**Mots clés :** Contamination, Colloïde, Transport, Transfert, Matière organique

**Résumé :** Les plastiques sont le troisième matériau le plus produit sur Terre et une importante fraction (>25%) se retrouve dans l'environnement. Pour évaluer les risques liés aux débris plastiques, il est nécessaire de comprendre les sources, et les mécanismes de transport et d'accumulation des débris plastiques dans l'environnement. Ceci s'avère difficile car le plastique se dégrade en particules qui sont trop petites pour être échantillonnées et quantifiées. En particulier, les nanoplastiques (< 1 µm), qui sont des particules colloïdales, pourraient constituer une fraction importante du budget global de débris plastiques.
L'objectif de ce travail est d'examiner les possibles lieux d'accumulation des nanoplastiques en étudiant des processus physicochimiques lors d'expérimentations. Une attention particulière a été accordée à la pertinence environnementale des modèles de nanoplastiques utilisés.
D'abord, l'agrégation des nanoplastiques est étudiée car c'est un processus clé dans le transport des colloïdes. Ensuite, ce travail se focalise sur le transfert des nanoplastiques à travers deux interfaces environnementales. Celles-ci présentent des gradients physico-chimiques soupçonnés de contrôler le devenir des nanoplastiques : les milieux poreux (qui représentent des sols, sédiments et aquifères) et l'interface entre l'eau salée et la glace (qui représente l'interface eau de mer/banquise). Cette étude montre que les différents comportements des nanoplastiques modèles sont principalement attribuables à leurs tailles, formes et propriétés de surface qui influencent leurs comportements hydrodynamiques et leurs énergies d'interaction.

**Title :** Environmental fate and behavior of nanoplastics : Implication of physico-chemical processes

**Keywords :** Contamination, Colloid, Transport, Transfer, Organic Matter

**Abstract :** Plastics are the third most-produced material on Earth and a significant proportion (>25%) ends up in the environment. To elucidate the risks that this contamination can cause, it is necessary to track the sources, transport pathways, and sinks of plastic debris in the environment. This has proven difficult since plastic degrades into particles that are too small to sample and quantify. In particular, nanoplastics (<1µm), which are colloidal particles, could form a substantial fraction of the global budget of plastic debris.
Therefore, the goal of this was to investigate where nanoplastics may accumulate, by studying physicochemical processes in lab experiments. Throughout this work, special attention has been devoted to the environmental relevance of the nanoplastic models used.
First, nanoplastics' aggregation dynamics was investigated since it impacts downstream transport processes. Then, this work studied nanoplastics' transfer through two environmental interfaces. These have physicochemical gradients suspected to control nanoplastics' fate: porous media (as a proxy for soils, sediments and aquifers) and the interface between saltwater and ice (as a proxy for seawater/sea ice interfaces). This study shows that the different behaviors of the nanoplastic model are attributable to their sizes, shapes and surface properties that modify their hydrodynamic behaviors and interaction energies.